# HIGH MASS ACCURACY COUPLED TO SPATIALLY-DIRECTED PROTEOMICS FOR IMPROVED PROTEIN IDENTIFICATIONS IN IMAGING MASS SPECTROMETRY EXPERIMENTS

By

David Geoffrey Rizzo

Dissertation

Submitted to the Faculty of the

Graduate School of Vanderbilt University

in partial fulfillment of the requirements

for the degree of

DOCTOR OF PHILOSOPHY

in

Chemistry

August, 2016

Nashville, Tennessee

Approved:

Richard M. Caprioli, Ph.D.

Kevin L. Schey, Ph.D.

John A. McLean, Ph.D.

Michael P. Stone, Ph.D.

*This work is dedicated to my family and friends, who have shown nothing but support for me in all of life's endeavors.*

# ACKNOWLEDGEMENTS

Gessel, Joshua Nicklay, Glenn Harris, Jeffrey Spraggins, and Boone Prentice have all been vital to my development as a scientist, acting as soundboards for ideas and encouraging me to enjoy successes and learn from failures. Whenever I needed to vent about science or life, they were there to listen. The fellow graduate students in lab who have seen me through this journey have left a lasting impression on me as well. They have always been there to lend a hand and I will truly miss seeing them in lab every day.

None of this would be possible without support from my family and friends. My mother, Robin, and father, Joe, encouraged me to pursue my love of science from an early age, even if that meant driving to enrichment programs early Saturday mornings. They taught me how to be a hard worker and independent person, but to never forget that no man is an island. Success and humility should never be mutually exclusive. My brother, Joey, and my sister, Meghan, continue to encourage me every day in everything that I do. Meghan has listened to the recap of my current state of life at day's end, and for that, I am eternally grateful. I cannot forget Rebecca Rosenberg, who has been a part of our family since the first grade. We have grown up together and will always be there to ground each other, no matter how far apart we are. My dogs, Marco and Polo, are the first things I see when I wake up and the last things I see when I go to bed. They've made the roughest days better, always showing excitement and affection when I get home (no matter how late that may be). Lastly, I would like to thank my entire extended family, including all of my aunts, uncles, and cousins. Though my grandparents could not be here to see this achievement, I know they would all be proud of such an accomplishment.

# TABLE OF CONTENTS

Page

# TECHNICAL ABBREVIATIONS

2-NPG: 2-nitrophloroglucinol

9AA: 9-aminoacridine

ANOVA: analysis of variance

ACN: acetonitrile

ccRCC: clear cell renal cell carcinoma

CHCA: α-cyano-4-hydroxycinnamic acid

CID: collision induced dissociation

CMBT: 5-chloro-2-mercaptobenzothiazole

CT: computed tomography

Da: Dalton

DAN: 1,5-Diaminonapthalene

df: degrees of freedom

DHA: 2,5-dihydroxyacetophenone

DHB: 2,5-dihydroxybenzoic acid

ESI: electrospray ionization

ETD: electron-transfer dissociation

FID: free induction decay

FTICR: Fourier transform ion cyclotron resonance

H&E: hemotoxylin and eosin

HPLC: high-performance liquid chromatography

IHC: immunohistochemistry

IMS: imaging mass spectrometry

ITO: indium-tin-oxide

LC: liquid chromatographic

LCM: laser capture microdissection

MALDI: matrix-assisted laser desorption/ionization

MRI: magnetic resonance imaging

MS: mass spectrometry

MS/MS: tandem MS

$M_r$: molecular mass

*m/z*: mass-to-charge ratio

Nd:YAG: neodymium-doped yttrium aluminum garnet

Nd:YLF: neodymium-doped yttrium lithium garnet

ppm: parts per million

RF: radio frequency

RP: resolving power

SA: sinapinic acid

S/N: signal-to-noise ratio

THAP: 2′,4′,6′-trihydroxyacetophenone

TOF: time-of-flight

TOF/TOF: time-of-flight/time-of-flight

UV: ultraviolet

# LIST OF TABLES

# LIST OF FIGURES

# CHAPTER I

# INTRODUCTION

## Matrix-Assisted Laser Desorption/Ionization Mass Spectrometry

Mass spectrometry (MS) is a powerful technology that allows for the simultaneous measurement of multiple molecular species, with no *a priori* knowledge about the analyte required. Detection by MS is achieved by measuring an analyte's mass-to-charge ratio (*m/z*), thus requiring the analyte to be ionized and have a charge. One such method of ionization is matrix-assisted laser desorption/ionization (MALDI) MS. First developed in the 1980s,[1, 2] MALDI is achieved by applying a matrix that absorbs at the wavelength of a laser and facilitates molecular desorption and ionization.[3] Both UV and IR lasers have been shown to be successful in MALDI experiments,[4, 5] though most current commercial instruments utilize UV lasers. Solid state lasers, such as frequency-tripled Nd:YAG and Nd:YLF, and nitrogen ($N_2$) lasers are by far the most common lasers used in MALDI experiments.

The mechanism(s) of ionization during the MALDI process are still being investigated and debated, with evidence to support both the lucky survivor and gas phase protonation models.[6] Briefly, the lucky survivor model stipulates that analytes are incorporated into the matrix crystals with their respective charge states preserved from solution. The gas phase protonation model describes neutral analyte molecules undergoing gas phase collisions with charged matrix ions, leading to charge transfer and ionized analyte species. More extensive reviews can be found elsewhere for greater detail and empirical evidence.[6, 7]

1

There are a wide variety of matrices available that have shown to be effective in the analysis of different classes of biomolecules (Figure 1.1), such as dihydroxybenzoic acid (DHB) for lipids,[8, 9] α-cyano-4-hydroxycinnamic acid (CHCA) for peptides,[10, 11] and sinapinic acid (SA) for proteins.[12, 13] Novel matrices are continuing to be discovered and synthesized to improve sensitivity and selectivity.[14, 15] While most are small organic molecules, unconventional matrices, such as graphite,[1, 16] nanoparticles,[17, 18] and ionic liquids[19-21] have also been utilized for specific analytes.
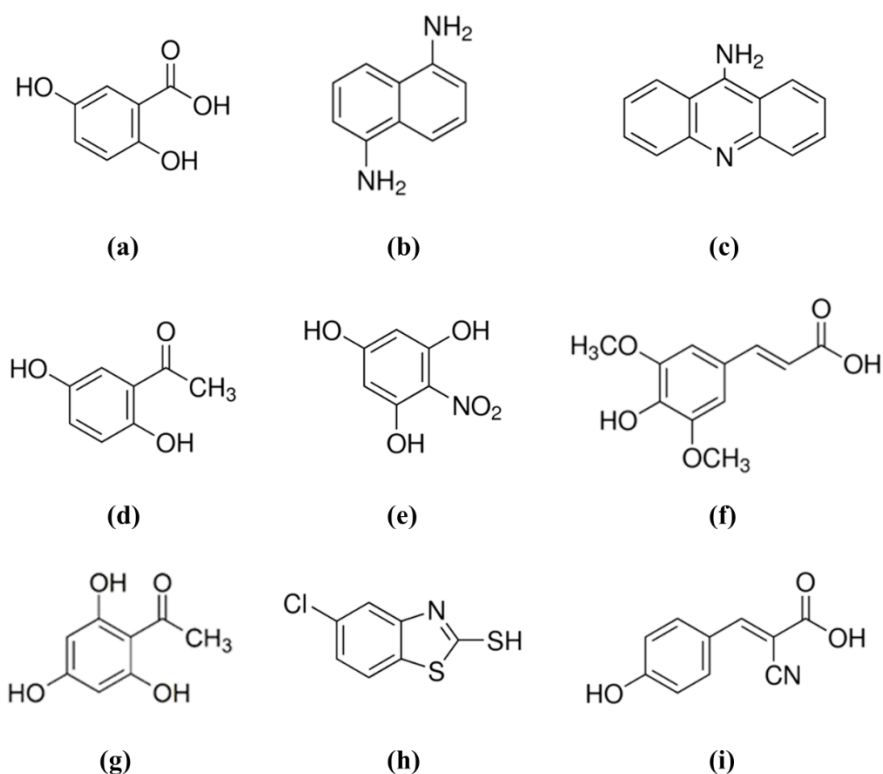


**Figure 1.1.** Structures of common MALDI matrices.(a) 2,5-dihydroxybenzoic acid – DHB; (b) 1,5-diaminonaphthalene – DAN; (c) 9-aminoacridine – 9AA; (d) 2,5-dihydroxyacetophenone – DHA; (e) 2-nitrophloroglucinol – 2-NPG; (f) 3,5-dimethoxy-4-hydroxycinnamic acid, or sinapinic acid – SA; (g) 2′,4′,6′-trihydroxyacetophenone – THAP; (h) 5-chloro-2-mercaptobenzothiazole – CMBT; (i) α-cyano-4-hydroxycinnamic acid – CHCA.

## Imaging Mass Spectrometry

MALDI imaging mass spectrometry (IMS) enables the visualization of biomolecules in tissue by combining the sensitivity and selectivity of mass spectrometry with the spatially descriptive characteristics of classic histology. Originally described by Caprioli et al.,[22] the technology has been applied to the analysis of a variety of analyte classes, including pharmaceuticals,[23, 24] metabolites,[25] lipids,[26] peptides,[11, 27] and proteins.[28, 29]

Briefly, MALDI IMS experiments are performed by cutting fresh frozen or fixed tissue into thin sections and flat-mounting them onto a target. The sample is then coated with a MALDI matrix. This can be achieved by acoustically spotting matrix in discrete regions,[30, 31] spraying matrix onto the sample surface manually or robotically,[28, 32] or by employing dry coating techniques such as sublimation.[9, 33]

During acquisition, virtually defined regions of the tissue are irradiated by a laser in an array of discrete points generating a mass spectrum at each x,y coordinate. Typically, image spatial resolution is defined by the size of the laser spot on target and the spacing between the points in the array. Spectral intensities for a given ion are then plotted across the array, creating ion images that can be compared with stained images of the tissue providing an additional molecular dimension to classical histologic analysis (Figure 1.1).[34]

MALDI IMS of intact proteins is of particular interest because in a single experiment it has the potential to spatially describe the many endogenous proteoforms of a given protein, the various molecular forms which a protein product of a single gene can take (e.g., genetic variations and post-translational modifications).[35] However, protein imaging experiments have been hindered by the inability to structurally identify observed peaks, inhibiting the contextualization of IMS results with biological processes.
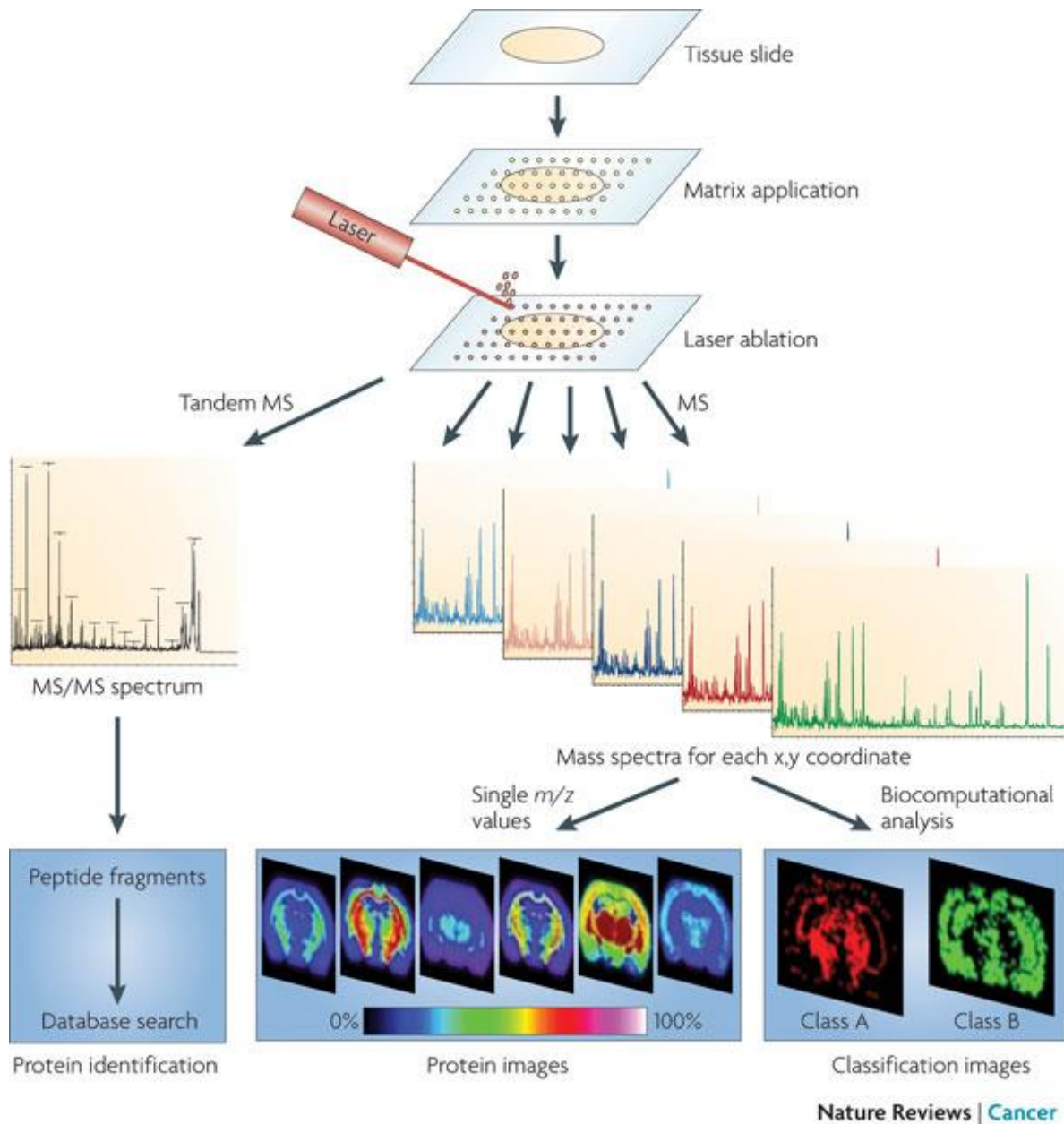
**Figure 1.2.** Schematic outline of a typical IMS workflow for fresh frozen tissue samples. Sample pretreatment steps include cutting and mounting the tissue section on a conductive target. Matrix is applied in an ordered array across the tissue section and mass spectra are generated at each x,y coordinate for protein analysis or tandem MS (MS/MS) spectra for protein identification. Reproduced from Ref. 32 with permission from Nature Reviews Cancer.[34]

**Fourier Transform Ion Cyclotron Resonance Mass Spectrometry**

First, the definitions of mass resolution and mass resolving power must be established. Mass resolution refers to the separation (typically in Daltons) between two peaks in a mass spectrum. In figure 1.3a, this is represented by $\Delta m_{50\%}$, the peak full-width at half-maximum of the peak height. Mass resolving power factors in the specific *m/z* of the peak, calculated by $(m/z)/\Delta m_{50\%}$.[36] The superior resolving power of the Fourier transform ion cyclotron resonance (FTICR) mass spectrometers has been used to investigate drugs and metabolites,[37] lipids,[38] and peptides[39] in biological tissue samples, where near-isobaric species are able to be differentiated.
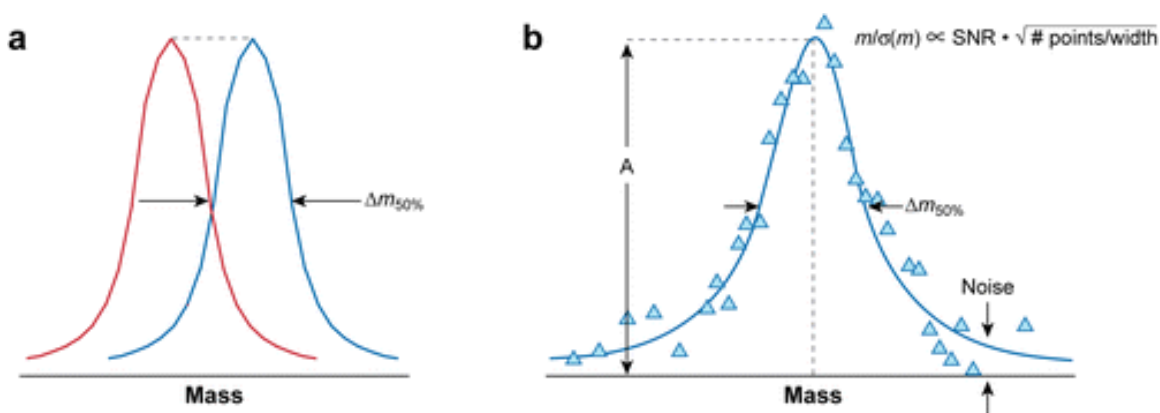


Marshall AG, Hendrickson CL. 2008.
Annu. Rev. Anal. Chem. 1:579–99.

**Figure 1.3**. Defining mass resolution and mass-measurement precision. (a) Two equal-magnitude mass spectral peaks of equal width, separated by one peak width at half-maximum peak height, $\Delta m_{50\%}$. Mass resolution is typically defined as $\Delta m_{50\%}$, whereas mass-resolving power is typically defined as $m/\Delta m_{50\%}$. (b) Relation between the mass-measurement precision predicted for the average of many measurements, and the signal-to-noise ratio and number of data points per peak width for a single mass spectrum. Reproduced from Ref. 34 with permission from the Annual Review of Analytical Chemistry.[36]

Additional figures of merit include mass precision and mass accuracy. Mass imprecision, denoted as $\sigma(m)$, accounts for the deviation of many mass measurements in a root-mean-squared

fashion. The mass precision is therefore the inverse of this value, or $1/\sigma(m)$. Mass precision can be practically calculated for most instruments by:

$$mass\ precision = c(\frac{S}{N})\sqrt{number\ of\ data\ points\ per\ peak\ width}$$

where c is a constant that is determined by the peak shape. For FT instruments, the spectral baseline noise is independent of the signal.[40] A prediction of precision can therefore be made, using the S/N and sampling of individual measurements (Figure 1.3b). The last figure of merit discussed is mass accuracy. Mass accuracy describes the exact molecular mass of a particular analyte and how well the instrument is able to measure that exact mass.[41] Internal and external calibrations ensure minimal deviations from the expected measured value.[42]

Fourier transform ion cyclotron resonance (FTICR) mass spectrometers are examples of instruments with high figures of merit that have become more prevalent in the realm of MALDI MS over the past few decades.[43-45] These analyzers have remarkably high resolving power ($10^5$ -$10^6$) and high mass accuracy, typically on the order of low to single digit ppm errors.[46] Though the fundamentals are critical to fully understanding the power and scope of the instrument, they have been covered elsewhere at length.[36, 46, 47] Therefore, only the key concepts will be discussed and how they pertain to imaging mass spectrometry in particular.

Two essential components of the FTICR are a strong, fixed magnetic field and a cell that traps ions within this field. Ions will adopt a circular trajectory when they come into contact with the magnetic field, orbiting within the cell. This can be explained by centripetal and centrifugal forces for a given magnetic field ($B$) and an ion velocity ($v$):

$$\text{Centripetal force:} \quad F = qvB$$

$$\text{Centrifugal force:} \, F' = \frac{mv^2}{r}$$

The forces will eventually balance, stabilizing the trajectory:

$$qvB = \frac{mv^2}{r}$$

$$qB = \frac{mv}{r}$$

Once the ion completes a full rotation, in a circular trajectory of $2\pi r$ with a frequency

$$v = \frac{v}{2\pi r}$$

Therefore the angular velocity, $\omega$, is equal to:

$$\omega = 2\pi v = \frac{v}{r} = \frac{q}{m}B$$

Now simplified, the frequency and angular velocity depend on the ratio of $(q/m)B$.[47] This rotation, or non-coherent cyclotron motion, occurs within an ICR cell consisting of three sets of plates positioned opposite of each other: two excitation, two trapping, and two detection plates. As their names imply, the trapping plates are meant to keep the ions within the ICR cell during the analysis. The two excitation plates lying in parallel to the magnetic field apply a radio frequency (RF) current to the cell to excite the ions and cause them to coalesce into coherent ion packets with wider radii.[48] The ions do not collide with the detection plates, as seen in other mass analyzers, but rather induce a charge as they pass by, allowing for many measurements of the same packet(s) of ions (Figure 1.4a). The resulting readout is in a time-domain signal (Figure 1.4b), and a fast Fourier transform is performed to convert it into a frequency-domain (Figure

1.4c). Finally, a calibration of frequency-to *m/z* produces a mass spectrum with mass-to-charge

ratios being plotted (Figure 1.4d).



**a**

Differential
amplifier

**b** Bovine ubiquitin

Image current

0

80    240    400
Time (ms)

FT

**c**

10⁺
9⁺
8⁺
11⁺
7⁺  12⁺

100   150   200   250
Frequency (kHz)

$m/z = A/\nu + B/\nu^2$

**d**

10⁺
9⁺
8⁺
11⁺
12⁺  7⁺

1071   1072
*m/z*

600   1000   1400   1800
*m/z*
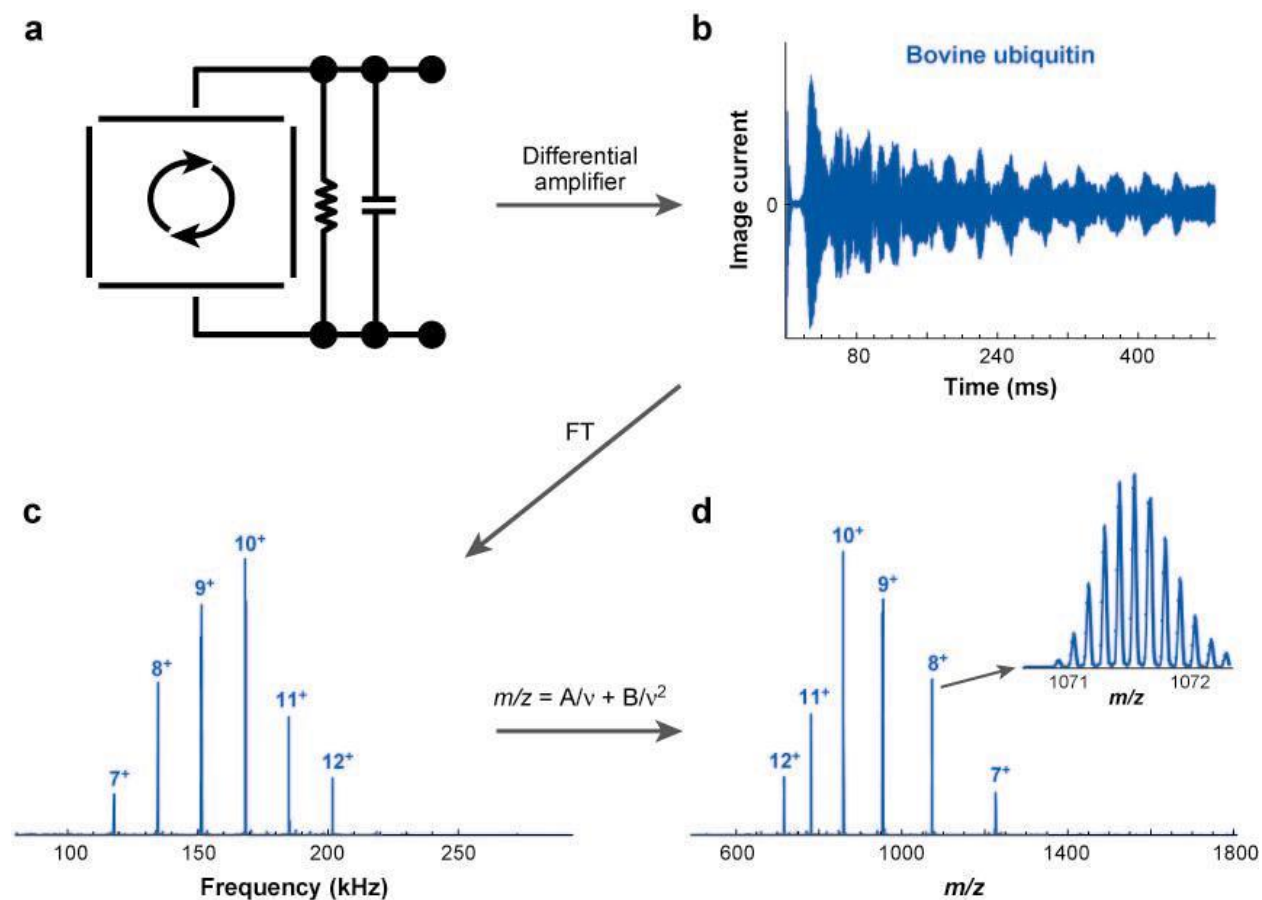
Marshall AG, Hendrickson CL. 2008.
Annu. Rev. Anal. Chem. 1:579–99.

**Figure 1.4.** Fourier transform ion cyclotron resonance (FTICR) MS signal detection process. (a) Schematic representation of excited ion cyclotron rotation, (b) time-domain image-current signal from opposed detection electrodes, (c) frequency-domain spectrum obtained by fast Fourier transform of the digitized time-domain signal, and (d) Fourier transform–ion cyclotron resistance *m/z* spectrum obtained by calibrated frequency-to-*m/z* conversion. Reproduced from Ref. 34 with permission from the Annual Review of Analytical Chemistry.[36]

## Spatially-Directed Tissue Collection Methods

Successful tissue-based proteomics experiments require the adequate extraction of proteins from very complex biological matrices. Traditionally, this has achieved by homogenizing the tissue and performing solution-based extraction or enrichment prior to an LC-based separation.[49-51] This approach is very comprehensive in terms of total number of analytes detected, but any spatial component to the tissue is lost in the homogenization process. Furthermore, the dynamic range of proteins can span nearly seven orders of magnitude, while most modern mass spectrometers can only achieve up to four orders of magnitude in untargeted methods.[52] Proteins in high abundance will overshadow lower abundance species if not adequately separated, causing missed protein identifications.

One method used to provide a spatial component to the collection process is laser capture microdissection (LCM). Samples are observed through a microscope and regions of interest are marked for collection. These can be large regions of tissue, individual cells, or even intercellular components.[53-55] A finely-focused laser is used to then perforate the tissue region, then defocused to catapult the tissue into a collection device for down-stream analysis.[56] Figure 1.5 shows a schematic of this process as well as the very precise nature of collection achieved. The main disadvantage of this technology is the potential cost for equipment and upkeep. The required number of cells for a particular experiment is variable depending on the analyte, with rather large cell counts needed to successfully detect certain protein classes. [57]

Liquid-based collection strategies have also been developed to maintain spatial localizations during extraction. Manual microextractions have been used to target substructures within kidney and brain sections, using common lab materials such as pipettes and gel-loading tips. [58,59] Liquid extraction surface analysis (LESA) and liquid microjunction surface sampling

are similar approaches that utilize droplet contact to robotically extract analytes from the surface.[60-62] Most applications of the technology have spatial limitations of around 1mm, though this a major focus for future development.[63]
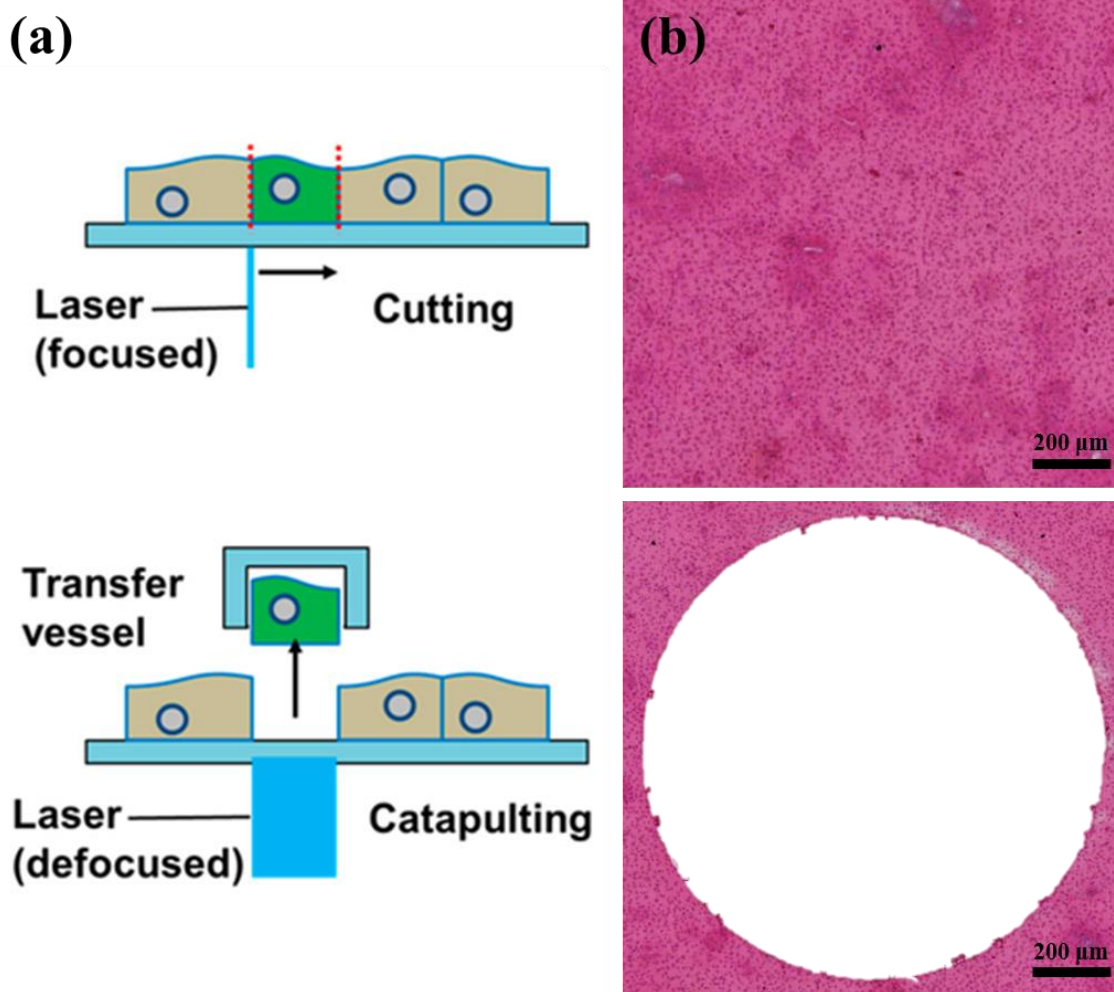


**Figure 1.5.** Implementation of laser capture microdissection (LCM). (a) Schematic of LCM collecting single cells from a tissue section. (b) Top – H&E stained section of tissue prior to LCM collection; Bottom – Same area post-LCM collection of 1.2 mm diameter circular region. Scale bar for (b) and (c) is 200 µm. 1.5a was reproduced from Ref. 51 with permission from the International Journal of Molecular Sciences.[56]

The recent development of gel-based extraction methods have shown success from many biological tissues, both fresh frozen and formalin-fixed, paraffin-embedded.[64, 65] The polymers serve a dual purpose, both delivering reagents to the specific regions of tissue and extracting analytes for off-line analysis. The targeted digestion and extraction has even identified modified integral membrane proteins from brain sections.[66] Current fabrication methods create hydrogels with diameters of 1-3 mm, similar to both the manual and robotic liquid extraction methods.[67] A reduction of size while maintaining the high caliber of proteomic results would greatly improve the applicability of this approach in both the academic and clinical fields.

**Traditional Protein Identification Approaches for IMS Experiments**

Protein identification strategies fall into three general categories; bottom-up, top-down, and indirect identification (Figure 1.6).[68] Bottom-up experiments involve enzymatic digestion of the protein mixture prior to analysis by mass spectrometry.[69] For imaging experiments, proteins are digested on tissue by applying an enzyme and performing hydrolysis in a way that preserves the spatial integrity of the proteins. Matrix is then applied, and both MS and MS/MS analyses are performed directly from tissue.[70, 71] Because MALDI ions tend to be singly charged, collision induced dissociation (CID) is often the method used for fragmentation. This approach can be advantageous because it extends the mass range of observable proteins by enzymatic digestion. Further, for most anatomic pathology examinations of biopsies, the tissue has been formalin fixed and paraffin embedded for preservation, and so bottom-up proteomics is the preferred procedure for analysis. The downside is that in practice, fragmenting peptides from tissue is hindered by the inability to effectively isolate ions from the considerable background signal and low fragmentation efficiencies for singly-charged peptides. Additionally, performing bottom-up

experiments in general may miss information regarding post-translational modifications (PTMs) if the modified peptide is not detected.
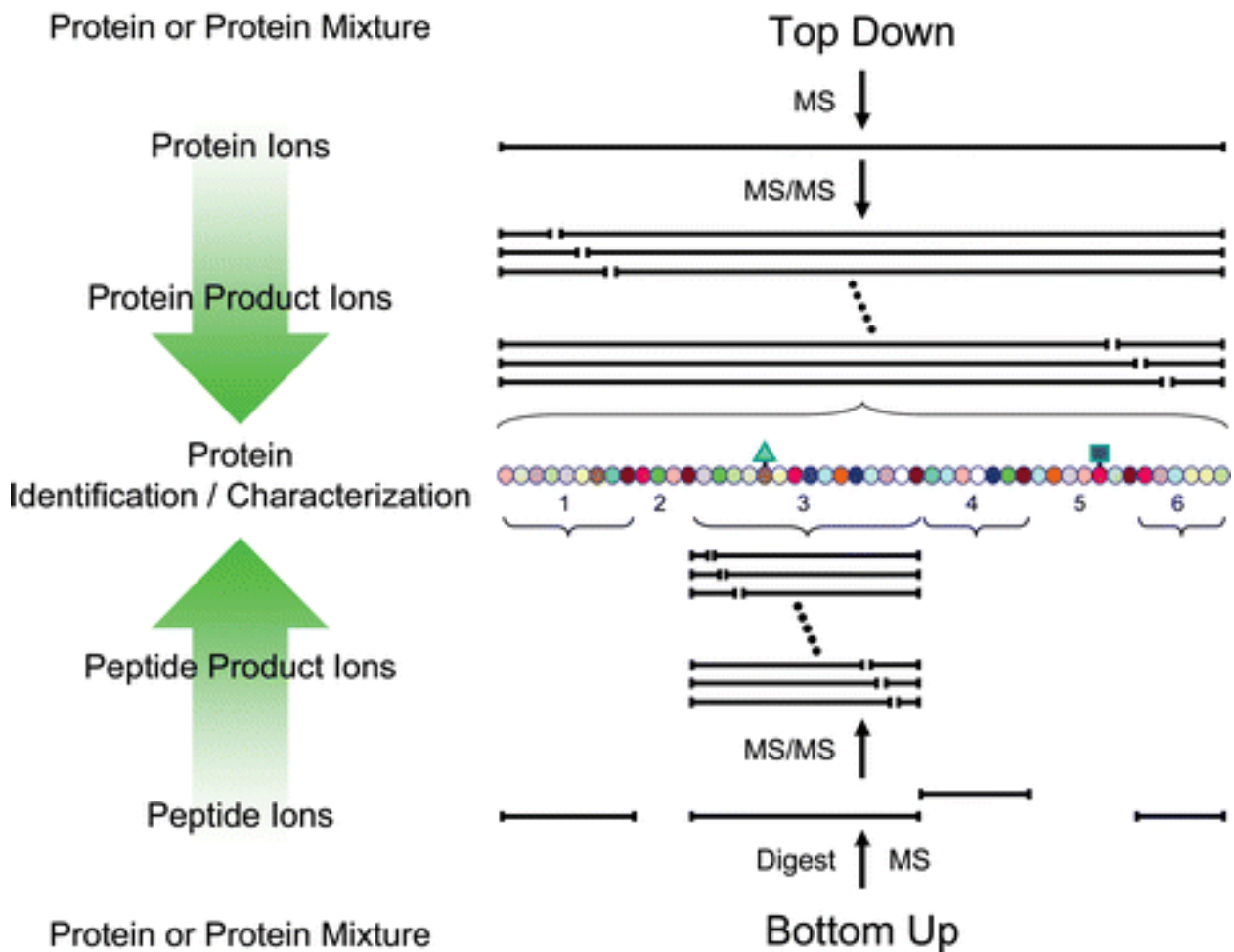


**Figure 1.6.** Schematic overview of 'bottom-up' and 'top-down' approaches employed for tandem mass spectrometry-based protein identification and characterization. The colored circles represent the amino acids of a protein, while the colored triangle and rectangle represent post-translational modifications. Reproduced from Ref. 47 with permission from the Royal Society of Chemistry.[68]

Top-down strategies[72] provide another approach for protein identification in IMS experiments. Here identifications are made through measurements of intact proteins followed by on-tissue MS/MS analysis. This approach is ideal for spatially describing the different proteoforms of endogenous proteins. However, similar to bottom-up experiments, on-tissue fragmentation of intact proteins is restricted by poor fragmentation efficiency for singly-charged proteins. Moreover, because most ions produced by MALDI have low charge states, electron-based fragmentation mechanisms (e.g., electron transfer dissociation) are often ineffective. Although work has been done to increase the charge state of ions generated from standards and tissue through matrix spotting approaches,[73] supercharging matrices[74, 75] or "ESI-like" surface analysis techniques[76-80] (e.g., LAESI, DESI, and MALDESI), further development is needed to improve image quality and sensitivity.

Indirect identification is an alternative approach that uses secondary information such as mass accuracy and spatial localization to link separate IMS and proteomics experiments. Because differences in preferential ionization between ESI and MALDI often lead to different peptides being detected, a direct link can be made between the two experiments by performing the analysis on intact proteins. Typically, protein images are collected using a linear time-of-flight (TOF) MS to accommodate for the relatively high $m/z$ range. Then, with a serial section, proteins are extracted and analyzed using either top-down or bottom-up LC-ESI MS/MS based identification strategies. Protein extraction can be performed by homogenizing the entire section[81, 82] or by using spatially directed extraction technologies.[83] A major advantage of indirect identification is that it allows both the imaging and proteomics experiments to be operated under optimal conditions maximizing the sensitivity of both technologies. However, protein imaging using MALDI TOF MS does not provide the resolving power and mass accuracy

13

necessary to correlate imaging data to proteomics experiments with high confidence. Mass accuracies for MALDI TOF measurements are particularly skewed when collecting data directly from tissue, which introduces sample height differences and can promote surface charging attributable to the insulating nature of many tissues. In practice, the mass accuracy of a MALDI TOF protein imaging experiment is limited to 20–100 ppm, making identification based on mass accuracy unachievable. These negative sample surface effects on spectral quality are minimized when using decoupled mass analyzers such as FTICR, Orbitrap, and orthogonal TOF mass spectrometers.

## Summary and Research Objectives

The objectives of this dissertation are to develop robust analytical methods of MALDI FTICR IMS, both or peptides and intact proteins. This will be achieved through sample preparation and instrumentation improvements. The proper combination of matrix and solvent can be pivotal to improving signal from imaging experiments. An added benefit of the FTICR is that the source is at reduced pressure, meaning that volatile matrices that have shown promise on other platforms would be perfectly suited for the FTICR. There is a much lower risk of matrix subliming off of the sample and the ion optics are situated in a way that matrix accumulation would not interfere with the signal for longer acquisition time imaging runs. By incorporating high mass resolution and accuracy into a protein imaging platform, new biology can be investigated by looking at overlapping proteoforms or post-translationally modified species. Though traditionally mass-limited, the FTICR mass spectrometer has the capability of unambiguous protein identification by accurate mass when used in tandem with accurate mass fragmentation information. Additionally, the implementation of spatially-localized extraction

methods for protein identification has shown promise from previous iterations, but needs to be thoroughly evaluated and characterized before being incorporated into a routine assay. Hydrogel technologies are currently much larger than is required to accurately target many biological features. By improving the formulations, enzyme concentrations, and other factors within the hydrogel process, they will be able to be used in true histology-direct workflow with minimal interferences from surrounding regions of tissue.

**Objective 1:** Develop methods for direct tissue analysis of proteins on high-performance instrumentation such as FTICR mass spectrometers.

**Objective 2:** Assess the current methods of IMS-based protein identification by top-down and bottom-up methodologies, and improve identification confidence by incorporating spatially-driven proteomics.

**Objective 3:** Develop advanced hydrogel technologies capable of achieving sub-millimeter diameters while maintaining robust proteomic signal.

# CHAPTER II

## MALDI FTICR IMS OF INTACT PROTEINS: USING MASS ACCURACY

## TO LINK PROTEIN IMAGES WITH PROTEOMICS DATA

### Introduction

Large portions of this section were adapted from J. M. Spraggins et al., *Journal of the American Society for Mass Spectrometry*, Copyright 2015 Springer[84] and J. M. Spraggins et al., *Proteomics*, Copyright 2016 John Wiley & Sons, Ltd.[85]

Fourier transform mass spectrometers, such as Fourier transform ion cyclotron resonance (FTICR)[47] and orbital trapping (Orbitrap),[86, 87] provide the highest mass resolution and accuracy of all mass analyzers. For imaging experiments, these high performance instruments routinely produce ion images with mass resolving powers greater than 50,000 ($m/\Delta m$ $_{50\%}$) and mass accuracies better than 5 ppm.[25, 37, 88] These instruments are extremely valuable for tissue analysis where high resolving power is necessary to distinguish endogenous nominal isobars and high mass accuracy allows for more robust identification. Recently, accurate mass measurements (<5 ppm) have been shown to greatly increase the reliability of peptide identification by dramatically reducing the number of false positive identifications for IMS experiments using indirect identification strategies.[89, 90] FT-based IMS in combination with LC-ESI MS/MS has also proven to be useful for small molecule[91] and lipid analysis.[88] Neither FTICR nor Orbitrap platforms have traditionally been used for MALDI IMS of intact proteins because FT-based platforms have been *m/z* range limited. However, modern instrumentation (source ion optics) and access to

higher magnetic fields has dramatically improved the sensitivity and throughput of FTICR platforms at higher mass ranges.

## Methodologies for MALDI FTICR IMS and Identification of Intact Proteins

*Tissue Preparation*

Fresh frozen rat brains and human clear cell renal cell carcinoma (ccRCC) samples were investigated due to the extensive literature surrounding protein IMS of these tissues using other mass analyzers and platforms.[92-95] Frozen tissue was sectioned to 10-12 microns and mounted onto conductive Indium-tin-oxide (ITO) coated slides (Delta Technologies, Loveland, CO, USA). Tissues were washed to remove interfering lipids and salts in sequential washes of 70% ethanol (30 seconds), 100% ethanol (30 seconds), Carnoy fluid (6:3:1 ethanol: chloroform: acetic acid) (2 minutes), 100% ethanol (30 seconds), ddH$_2$O (30 seconds), and 100% ethanol (30 seconds).[96]

*Matrix Application*

Matrix was applied using a TM Sprayer (HTX Technologies, Carrboro, NC, USA) with 15 mg/mL DHA in 9:1 ACN:ddH$_2$O with 0.2% TFA. Sprayer conditions include a flow rate 0.1 mL/min, nitrogen flow of 10 psi, spray temperature of 80°C, a spray velocity of 1,100 mm/min, 4 passes with offsets and rotations, and 9:1 ACN:ddH$_2$O as the pushing solvent. Samples were rehydrated as previously described [97] at 37°C for 3 minutes with 1 mL of 50 mM acetic acid as the rehydration solvent. This aids in the extraction of analytes into the matrix layer as the matrix recrystallizes.

*MALDI FTICR IMS*

High mass resolution imaging experiments were performed using a 15T Bruker MALDI FTICR mass spectrometer (Bruker Daltonics, Billerica, MA, USA). The instrument is equipped with an Apollo II dual MALDI/ESI ion source and a Smartbeam II 2kHz Nd:YAG (355nm) laser. Data were collected from *m/z* 1,100 – 25,000 with a data size of 1MB per spectrum. Special tuning of the Funnel RF amplitude (250 Vpp), accumulation hexapole (1.4 MHz, 1950 Vpp), transfer optics (1 MHz, 380 Vpp), time of flight delay (2.8 ms), and ICR cell (Sweep excitation power: 48%) were required for high *m/z* analysis. Although all parameters play a role in improving ion transmission through the source ion optics, tuning of the accumulation hexapole had the greatest impact on ion signal for high mass ions. External calibration was performed prior to analysis using CsI clusters. Ion images consisted of 13,596 pixels and 14,632 pixels for rat brain and ccRCC samples respectively. All protein identifications were made using mass accuracy (<5 ppm) of the highest intensity isotope by comparing MALDI FTICR IMS data to previously reported results or the compiled MSiMass database .[98]

*Histology*

Immediately following MALDI IMS experiments, matrix was removed from samples using 100% ethanol and samples were hydrated through graded ethanol to ddH$_2$O prior to using the Masson's Trichrome stain kit. Briefly, samples were incubated in a mordant solution, and then immersed in a Weigert's hematoxylin solution to stain cell nuclear contents black. A Biebrich Scarlet-Acid Fuchsin solution was used to stain acidophilic tissue components such as keratin and intercellular fiber red, and an aniline blue solution was used to stain collagen and

mucus blue. Optical images of stained tissue sections were obtained at 20x magnification using a Leica SCN400 Brightfield Slide Scanner.

*Protein Purification for Identification*

Rat brain was sectioned on a Leica cryostat and cerebrum was separated from cerebellum by a chilled razor blade. The cerebellum and cerebrum tissue sections were collected into corresponding pre-weighed Eppendorf tubes. At least 10 sections were combined into each tube before extraction was performed. An extraction solution composed of 25mM Tris (pH7.4), 50mM NaCl, and 0.25mM EDTA was made and approximately 350 μL was pipetted into each tube. An ice-chilled homogenizer was used to homogenize the tissues, with 15–20 homogenization strokes used to liquefy the samples. A 150 μL aliquot of each homogenate was taken and 1.53 μL of acetic acid and TFA were added. The samples were homogenized again using the tissue homogenizer and set on ice for 30min with intermittent vortexing to avoid sample aggregation. Homogenates were spun down at 20,000×g for 15 min and the supernatants collected. A Bradford assay (Thermo Scientific Pierce, Rockford, IL, USA) was used to quantify total protein concentration from each sample and the concentrations were adjusted to 2 μg/μL with 0.1% formic acid for subsequent LC analysis.

*LC-Coupled Tandem Mass Spectrometry* (ETD)

Rat brain homogenate extracts were loaded onto a reversed phase capillary trap column using a helium-pressurized cell (pressure bomb). The trap column was packed with $C_8$ reverse phase material. Once the sample was loaded, the trap column was connected to a capillary analytical column equipped with a laser-pulled emitter tip and packed with 15 cm of $C_8$ material.

Using an Eksigent NanoLC Ultra HPLC, proteins were gradient-eluted at a flow rate of 500 nL/min, and the mobile phase solvents consisted of 0.1% formic acid, 99.9% water (solvent A) and 0.1% formic acid, 99.9% acetonitrile (solvent B). The gradient consisted of 5%–50% B in 55 min, followed by 50%–95% B in 8 min. Upon gradient-elution, proteins were mass analyzed on an ETD-enabled LTQ Orbitrap Velos mass spectrometer, equipped with a nanoelectrospray ionization source (Thermo Scientific, San Jose, CA, USA). The instrument was operated using a data-dependent method. Full scan spectra of $m/z$ 400– 2,000 (resolving power: 60,000 at $m/z$ 200) were acquired as the initial scan event per duty cycle. For data-dependent scan events, the four most abundant ions in each MS scan were selected for fragmentation using ETD in the Velos ion trap. Dynamic exclusion was enabled allowing a repeat count of 1 within 20 seconds. ETD tandem mass spectra were acquired sequentially using the LTQ Velos ion trap followed by the Orbitrap (RP: 15,000 at $m/z$ 200) for mass analysis. An isolation width of 3 Da and an ETD reaction time of 80 ms were used for MS/MS spectra. The $MS^n$ AGC target value in the ion trap was set to $2 \times 10^4$, the $MS^n$ AGC target for Orbitrap scan events was $8 \times 10^5$, and the ETD reagent ion (fluoranthene) AGC target was set to $1 \times 10^5$.

*Data Analysis*

Fragmentation spectra were *de novo* sequenced using Thermo Fisher Scientific Xcalibur™ Software and searched using BLAST databases. Once confident identifications were made, theoretical fragment ions produced from MS-Product within Protein Prospector (University of California at San Francisco) were matched to observed fragment ions within the spectra.
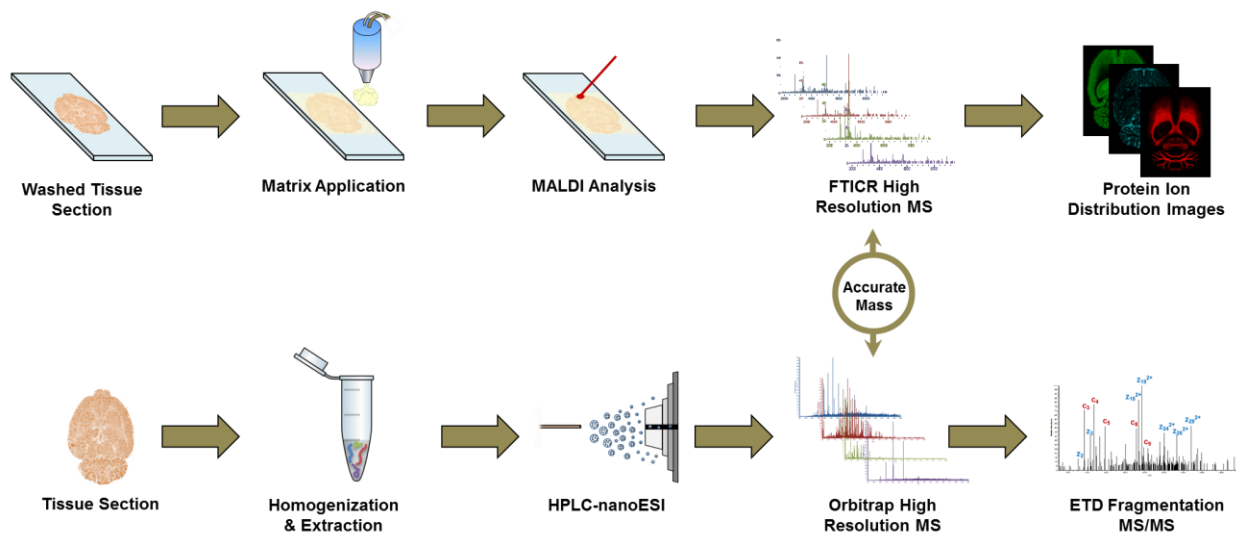
**Figure 2.1.** General sample preparation workflow for MALDI FTICR protein IMS and subsequent identification strategies using ETD fragmentation.

### MALDI FTICR IMS of Rat Brain as a Model System for Protein Imaging

For MALDI IMS, protein identification has traditionally been limited by poor sensitivity and fragmentation efficiency for on-tissue analysis or inadequate mass accuracy to effectively correlate imaging data with proteomics experiments using indirect identification strategies. As shown in Figure 2.2, MALDI FTICR IMS is capable of overcoming these challenges by producing imaging data of intact proteins with high mass resolution and accuracy. Initial analysis of rat brain tissue provided rich data with good sensitivity for ions up to $m/z$ ~12,000 (Figure 2.2a). The presented data, which are plotted as the overall average from the entire imaging experiment, were collected with a resolving power of ~40,000 at $m/z$ 5,000 resulting in 2,123 peaks between $m/z$ 2,000 and 12,000 with S/N > 20. Expanding the intensity scale (Figure 2.2b) shows the overall complexity and quality of the data.

MALDI FTICR IMS provides the mass resolution necessary to distinguish protein charge states and overlapping isotopic distributions from neighboring ions (Figure 2.2c). The resolving

21

power of the experiment is more than sufficient to resolve the isotopic envelope for a given protein, enabling unambiguous assignment of charge state as demonstrated by the difference in isotope spacing between the singly charged ion labeled 1 (spacing: ~1.00 Da) and the doubly charged ions labeled 2 and 3 (spacing: ~0.501 Da). Although not all of the isotopic patterns were fully resolved, at least 10 different species can be discerned from the MALDI FTICR IMS results in just the 70 Da window spanning *m/z* 5,630–5,700. It should be noted that, although at lower signal intensity, the singly charged ions of the proteins observed as doubly charged in this mass range were detected with *m/z* values >10,000.
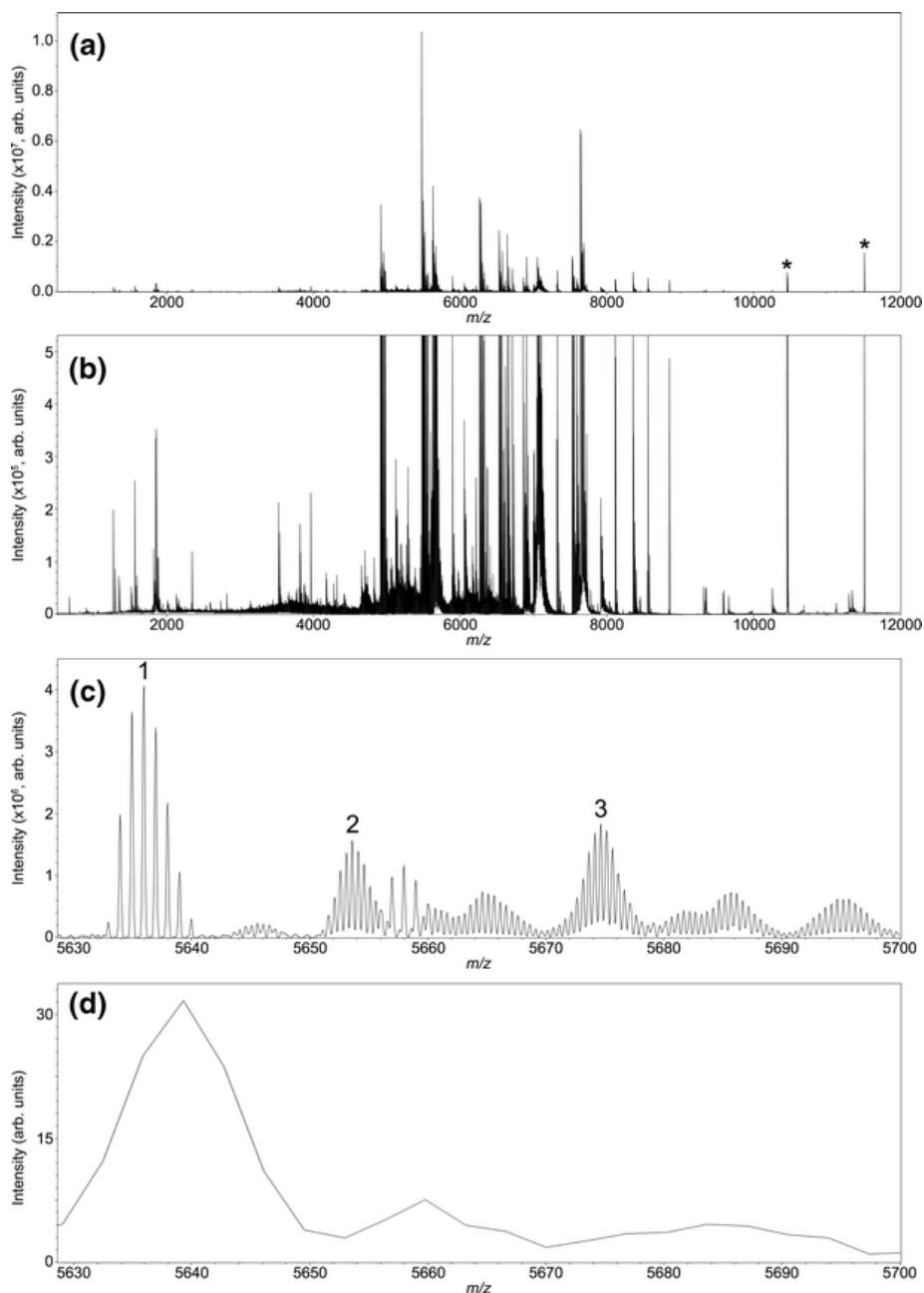
**Figure 2.2.** MALDI FTICR IMS average spectra of intact proteins from transversally sectioned rat brain tissue. The average spectrum of the entire imaging data set is shown in (**a**). Expanding the intensity scale (**b**) highlights the overall complexity and quality of the data with singly and doubly charged protein signals detected between *m/z* 1,000 and 12,000. Data were collected with a resolving power of ~40,000 at *m/z* 5,000 providing isotopic resolution and allowing ions of different charge states and modifications to be distinguished (**c**). The ion labeled 1 is singly charged and ions labeled 2 and 3 are examples of doubly charged ions. For comparison, MALDI TOF IMS data set collected in linear mode from a serial tissue section is displayed in (**d**). Electronic noise peaks are labeled (*)

23

Figure 2.2d represents the average spectrum from a serial tissue section using MALDI TOF IMS in linear mode. These data are typical of most protein imaging experiments and clearly demonstrate the difficulty in making accurate identifications using low mass resolution IMS. Although reflectron TOF can provide higher mass resolution, at the expense of sensitivity due to the propensity for post-source decay,[99] linear MALDI TOF analysis was unable to resolve the complex mixture of overlapping proteoforms and proteins of differing charge states detected from rat brain tissue in this same *m/z* window (*m/z* 5,630–5,700).

Additionally, peak shifts and broadening, likely due to surface charging or varying sample height, are clearly observed. MALDI FTICR platforms are not subject to adverse effects related to surface characteristics because the mass analyzer is decoupled from the ion source. However, TOF analyzers have a dramatic throughput advantage over FT-based platforms because pixel acquisition rates for FT instruments are generally limited by the scan time of the detection event. Although tunable, to maintain relatively high mass resolving powers, images are typically collected with scan times ranging from 0.5 to 2 s, limiting acquisition rates to ~2 pixel/s. TOF mass analyzers equipped with high repetition rate lasers, on the other hand, are limited by ion flight times that range from ~10 to 200 μs and are able to rapidly produce ion images with acquisition rates that approach 10–30 pixel/s.[100-102] FTICR instruments can also suffer from space charge effects, limiting the observable dynamic range. This can be overcome using front-end accumulation techniques such as continuous accumulation of selected ions (CASI).[103] Both platforms have specific advantages for IMS experiments, but the ability of MALDI FTICR MS to produce ion images with high mass resolution and accuracy is ideal for imaging and identifying proteins from biological tissues.
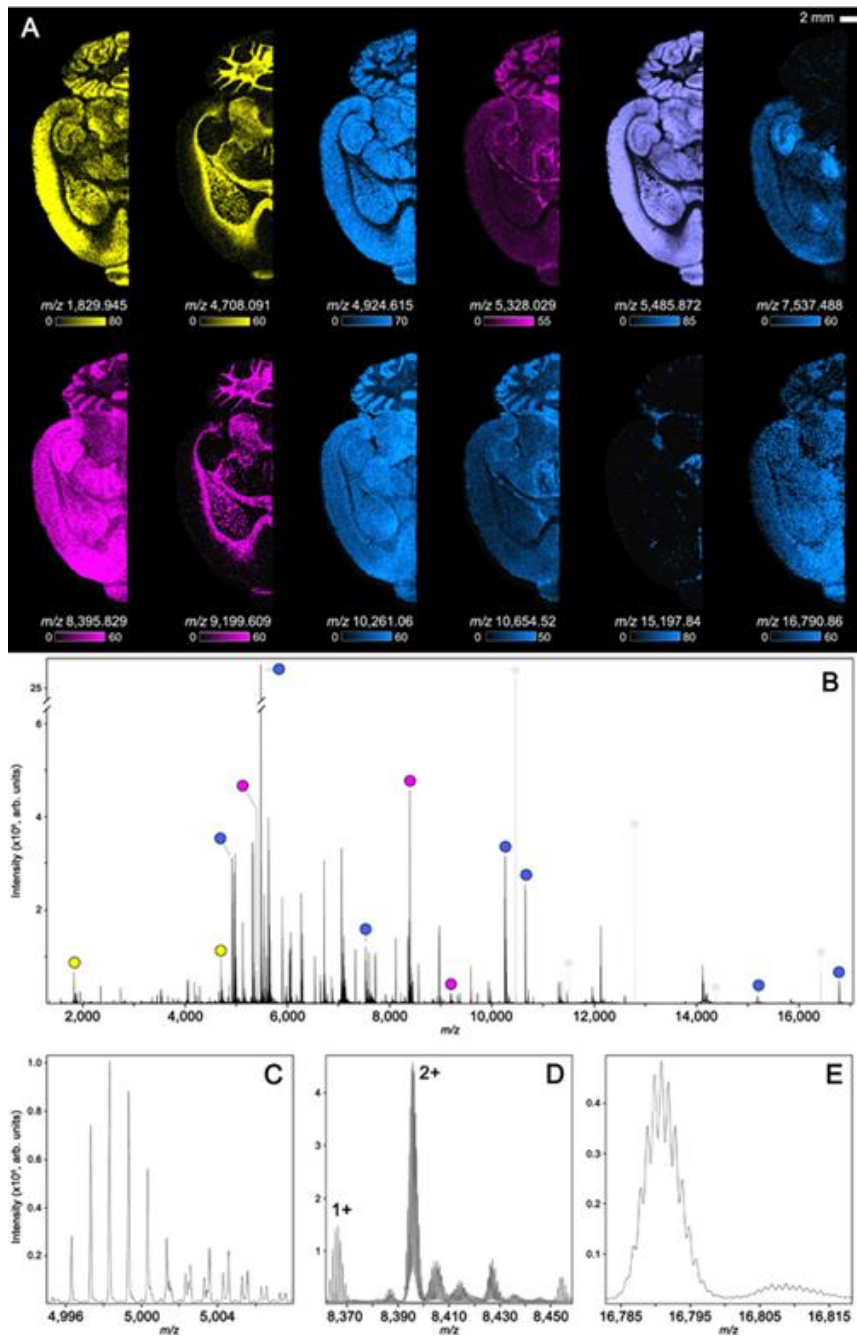
**Figure 2.3.** MALDI FTICR IMS data collected from transversally sectioned rat brain tissue. Selected ion images (A) are color-coordinated based on charge state (Blue: 1+, Pink: 2+ and Yellow: 3+). The overall average spectrum for the 100 μm imaging experiment is shown in (B) highlighting each peak used to generate the selected ion images (A). Expanded *m/z* windows (C–E) highlight the ability to detect proteins up to roughly *m/z* 17,000 while providing the mass resolving power necessary to differentiate overlapping isotopic envelopes and determine protein

charge states. Electronic noise peaks have been greyed and marked (*) to simplify the spectrum (B).

Figure 2.3 shows the capabilities of MALDI FTICR MS for protein imaging experiments. The analysis of rat brain tissue using MALDI FTICR IMS provided rich data with good sensitivity for ions up to $m/z$ ~17 000 and proteins approaching 20 kDa (Figure 2.3a). The spectral data (Figure 2.3b–e), which are plotted as the overall average from the entire imaging experiment, were collected with a resolving power of ~70,000 at $m/z$ 5,000, resulting in 2,695 peaks between $m/z$ 1,100–17,000 with S/N > 20. These data represent the largest ions detected from tissue using MALDI FTICR IMS with an $m/z$ increase of ~5,000 compared to previously reported results.[84] It is noted that this resolving power is not the theoretical limit of the spectral performance for MALDI FTICR protein imaging. For all experiments, resolving power is tuned to provide the performance necessary to resolve the target analytes but maintain the practicality of collecting imaging data. To achieve a resolving power of 70,000 at $m/z$ 5,000, a time-domain signal of ~2 s is required. Although detection events can be extended to increase resolving power further, the throughput of the experiment can become prohibitive for collecting ion images with large number of pixels.

The peak for each of the selected ion images is highlighted by the colored dots overlaid on the full-scan spectrum (Fig. 2.3b). Expanding the $m/z$ scale (Figure 2.3c-e) shows the overall complexity and quality of the data. MALDI FTICR IMS provides the mass resolution necessary to distinguish overlapping isotopic distributions from neighboring ions (Figure 2.3c and d) and protein charge states (Figure 2.3d). The resolving power of the experiment is more than sufficient to resolve the isotopic envelope for a given protein, enabling unambiguous assignment of charge states as demonstrated by the difference in isotope spacing between the singly charged ion labeled 1+ (spacing: $m/z$ ~1.0) and the doubly charged ion labeled 2+ (spacing: $m/z$ ~0.5

Da). The same is true for higher *m/z* ions. Although not fully resolved, MALDI FTICR IMS can resolve the isotopic envelope even for a protein detected at *m/z* 16,790.86 (Fig. 2.3e). Selected ion images are color-coordinated based on charge state (Blue: 1+, Pink: 2+ and Yellow: 3+).

Although protein identification was not the goal of this particular experiment, high-performance MALDI FTICR IMS also improves the ability to identify proteins observed in imaging experiments. High mass resolution IMS enables the differentiation between different proteoforms and provides the mass accuracy (<5 ppm) needed to link imaging data to orthogonal LC-based proteomics experiments and databases of previously identified biomolecules.[84] For example, the largest ion detected in this experiment was *m/z* 16,790.864 (highest intensity isotope). Based on previously reported protein identifications from rat brain in imaging experiments,[104] it is most likely calmodulin (theoretical *m/z* 16,790.847, ~1 ppm mass accuracy). Calmodulin is a $Ca^{2+}$-binding protein that activates several intracellular enzymes (e.g. kinases, phosphates and adenyl cyclases) in cells.[105] In the brain, $Ca^{2+}$/calmodulin signaling is involved in processes such as neurotransmitter release, transcriptional regulation, and cell death.[106, 107]
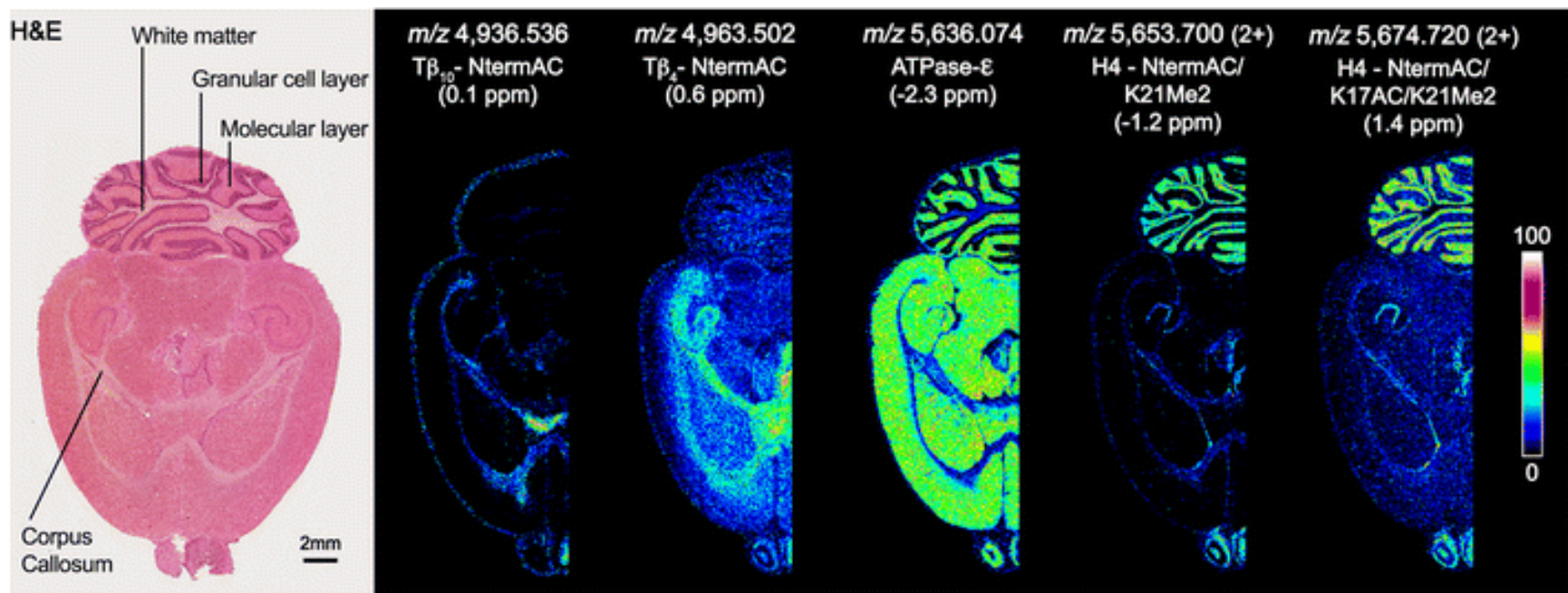
**Figure 2.4.** Selected ion images of identified intact proteins from rat brain tissue collected using MALDI FTICR IMS. Ions were identified using mass accuracy to correlate imaging results with separate top-down proteomics experiments. For comparison, the tissue was H&E stained following IMS analysis. Doubly charged ions are indicated in parentheses.

Figure 2.4 shows selected ion images at $m/z$ 4,936.536 ([M + H]$^{1+}$), $m/z$ 4,963.502 ([M + H]$^{1+}$), $m/z$ 5,636.074 ([M + H]$^{1+}$), $m/z$ 5,653.700 ([M + 2H]$^{2+}$, 11.3kDa), and $m/z$ 5,674.720 ([M + 2H]$^{2+}$, 11.4kDa). Imaging data were collected at a spatial resolution of 75 μm (pixel spacing) with ~38,000 total pixels. Even at this modest spatial resolution, substructures within the cerebellum (white matter, granular cell layer, and molecular layer) are clearly resolved. To minimize interference from overlapping isotopic patterns, images were plotted by selecting only the highest intensity isotope for each protein. Each of the presented ion images has a distinct spatial distribution within rat brain tissue. The ion at $m/z$ 5,636.074 is detected throughout the brain; however, within the cerebellum it can be found at higher intensities in the molecular layer. Ions at $m/z$ 5,653.700 and $m/z$ 5,674.720 are both found to be enriched in the granular cell layer of the cerebellum and proteins detected at $m/z$ 4,936.536 and $m/z$ 4,963.502 are absent from the cerebellum and primarily observed to be localized to the corpus callosum. For comparison, the tissue was stained by H&E following IMS analysis. All of the ion distributions are consistent with observed structures in the microscopy image.

Proteins highlighted in Figure 2.4 were identified using mass accuracy as the link between MALDI FTICR IMS data and LC-ESI top-down proteomics results. All top-down experiments were performed in high mass resolution mode (resolving power: ~60,000 at $m/z$ 200) using standard identification strategies. The protein detected at $m/z$ 4,963.502 by MALDI FTICR IMS was identified as N-terminally acetylated thymosin β4 (Tβ4-NtermAC, 0.1ppm). Top-down ETD data for the [M + 8H]$^{8+}$ charge state of Tβ4-NtermAC ($m/z$ 621.4440, 0.13ppm) can be found in Figure 2.5. The protein was determined to be acetylated on the N-terminus based on the observed mass shift of ~42.01 for all observed c ions. The ion at $m/z$ 4,936.536 was determined to be N-terminally acetylated thymosin β10 (Tβ10-NtermAC,

0.1ppm – Figure 2.6). Thymosin β4 and β10 are known to bind monomeric actin (G-actin) and regulate actin polymerization (F-actin). Controlled actin polymerization is essential for normal cytoskeletal function.[108, 109] The protein detected by MALDI FTICR IMS at *m/z* 5,636.074 was identified as mitochondrial ATP synthase subunit ε (ATPase-ε, –2.3ppm Figure 2.7). ATPase-ε is a subunit of the F1 complex of ATP synthase, a 500kDa protein found in mitochondria that is critical for production of ATP.[110, 111] The MALDI ions detected at *m/z* 5,653.700 and *m/z* 5,674.720 are both doubly charged proteoforms of histone H4; the first of which, *m/z* 5,653.700, is acetylated at the N-terminus and the amino acid residue lysine 21 hypothesized to be dimethylated,[112] though the MS/MS data was unable to confirm this due to poor fragment ion peak signals (H4-NtermAC/K21Me2*, -1.2ppm Figure 2.8). The ion at *m/z* 5,674.720 is similar but has an additional acetylation of the lysine at position 17 (H4-NtermAC/K17AC/K21Me2 Figure 2.9). These fragmentation spectra were able to confirm the location of the dimethylation, corroborated with previously observed PTM locations in the Uniprot database. Histone H4 is one of five primary histone proteins that act as the structural core of nucleosomes. Histone H4 is known to undergo extensive acetylation and methylation, which is thought to control gene expression.[113, 114] MALDI FTICR IMS provides the mass resolution and accuracy needed to differentiate the complex mixture of proteins and their associated proteoforms while enabling identifications to be made with greater confidence than with traditional MALDI TOF experiments.
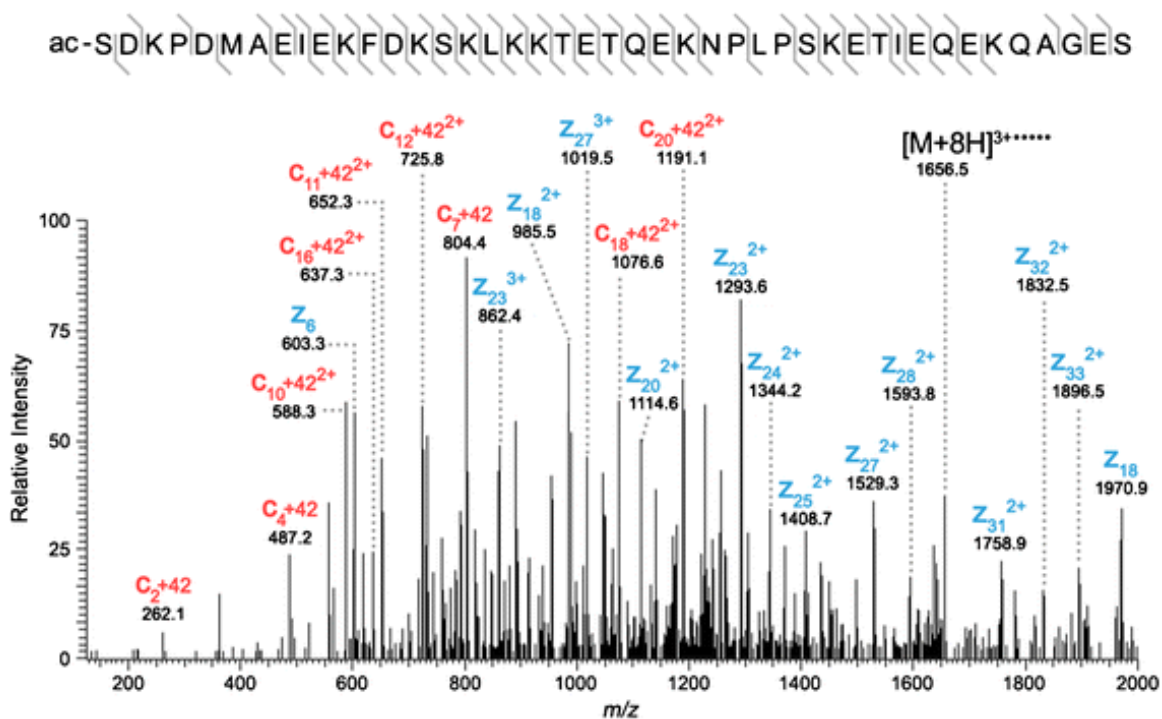
**Figure 2.5.** High mass resolution top-down ETD for the [M + 8H]$^{8+}$ charge state of thymosin β4. Selected c (red) and z (blue) ions are labeled clearly showing acetylation on the N-terminus. The amino acid sequence highlighting the fragmentation coverage is also provided.
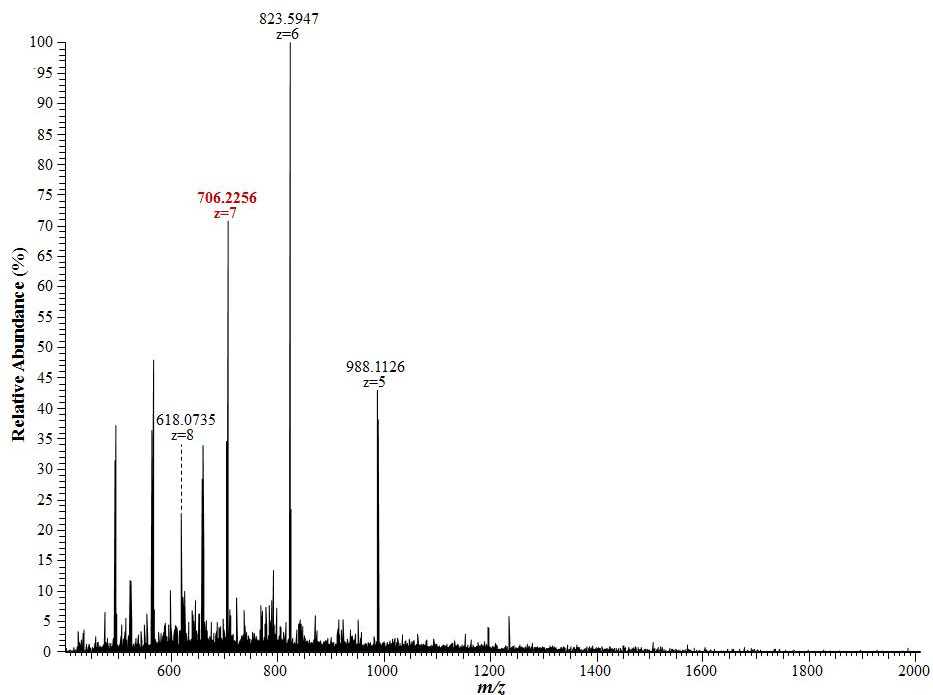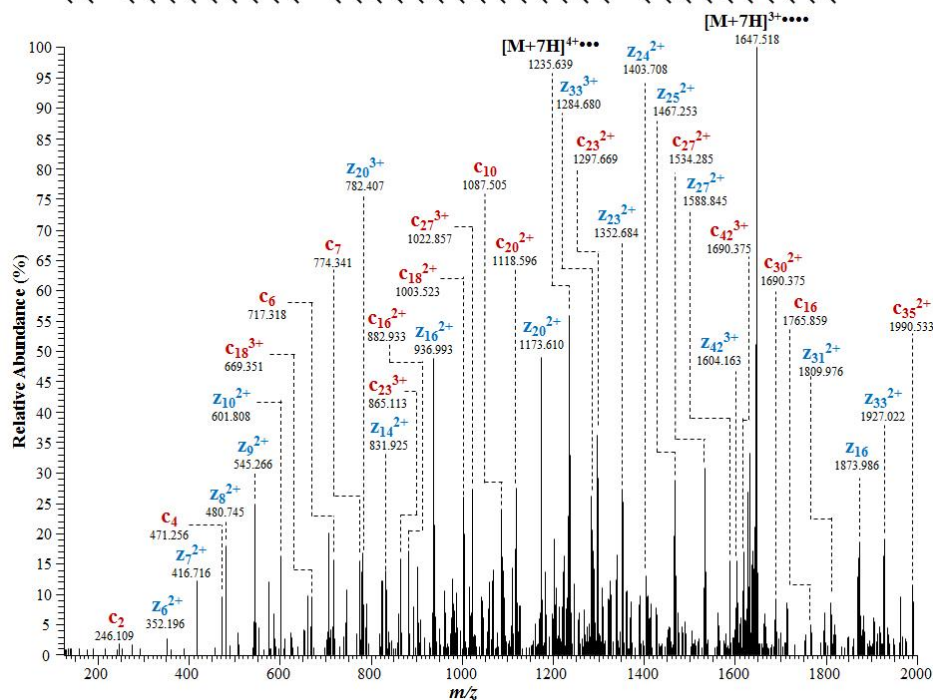
**Figure 2.6.** ETD LC-MS/MS data for N-terminally acetylated thymosin β₁₀. The charge state distribution is shown in the top panel with the specific charge state selected for MS/MS highlighted in red. ETD fragmentation data is shown in the bottom panel including selected c (red) and z (blue) ion annotations. A summary of the observed fragments and sequence coverage is also included.
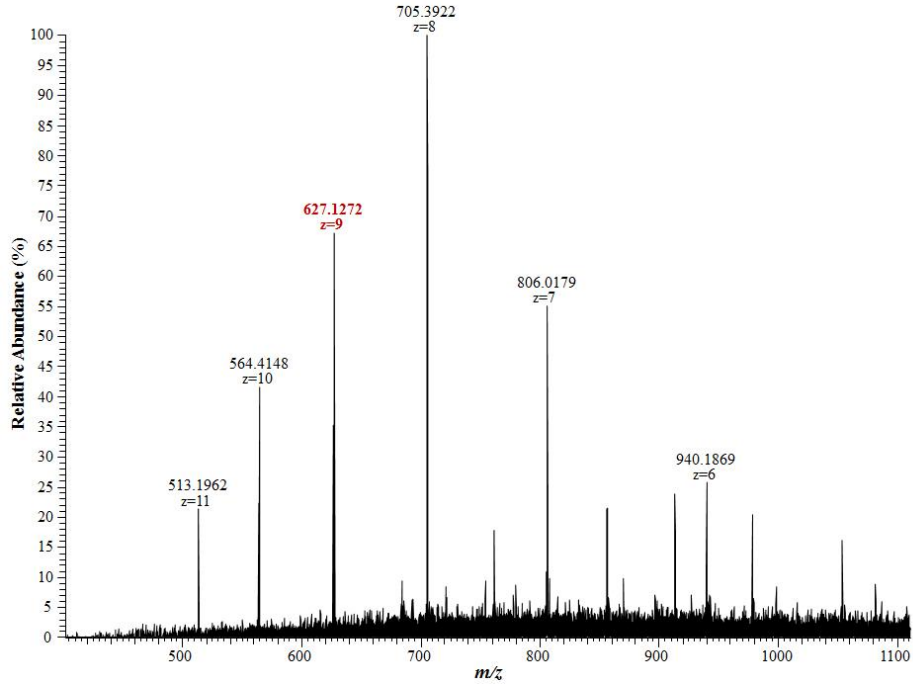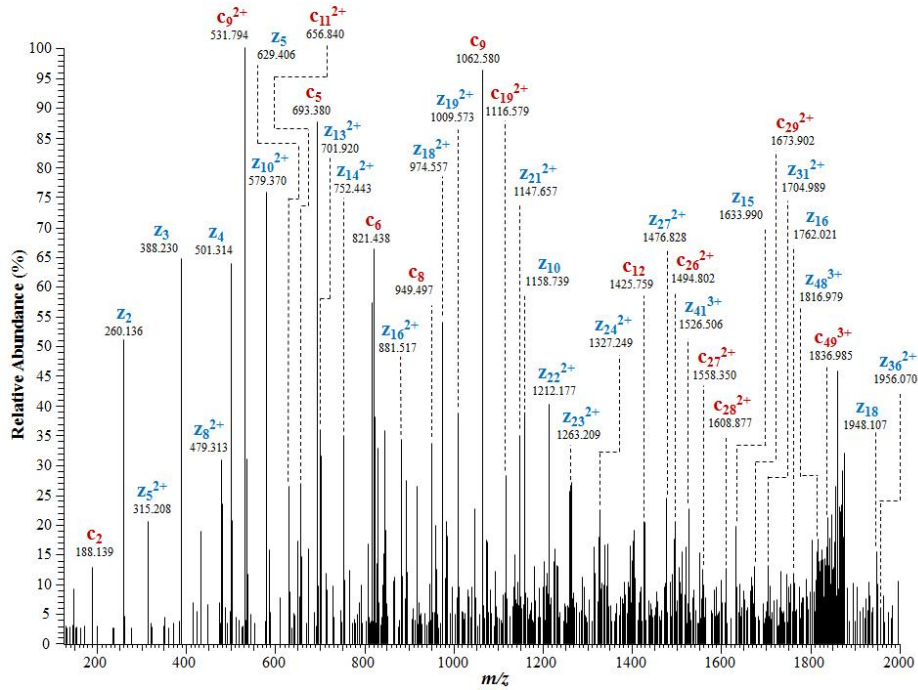
**Figure 2.7.** ETD LC-MS/MS data for ATP synthase subunit epsilon. The charge state distribution is shown in the top panel with the specific charge state selected for MS/MS highlighted in red. ETD fragmentation data is shown in the bottom panel including selected c (red) and z (blue) ion annotations. A summary of the observed fragments and sequence coverage is also included.
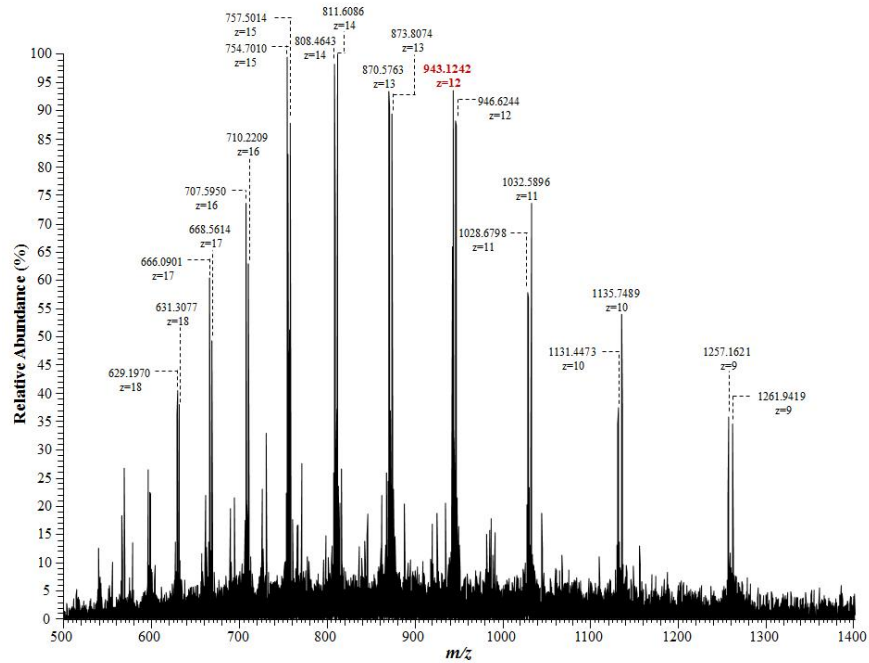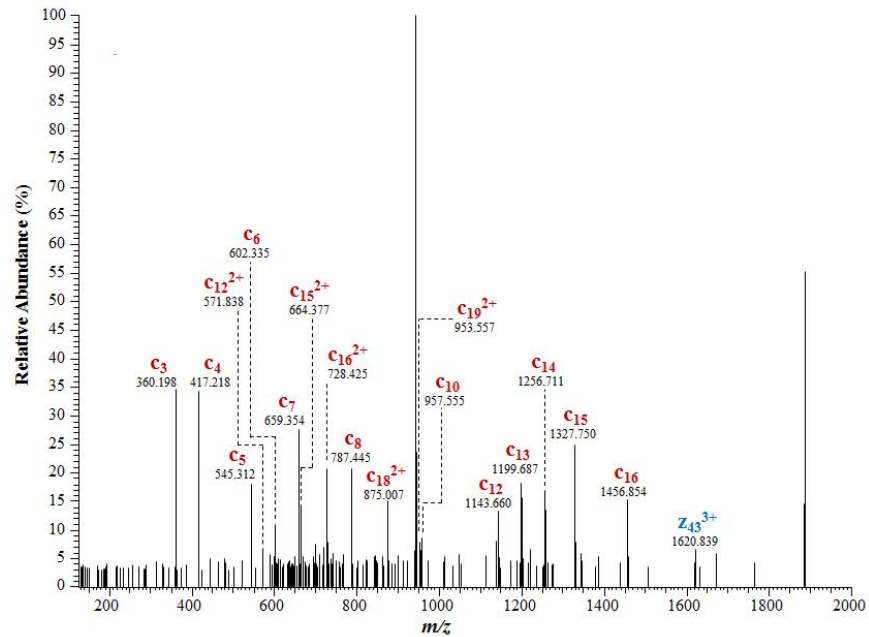
**Figure 2.8.** ETD LC-MS/MS data for Histone H4 (N-acetylated, K21 dimethylated*). The charge state distribution is shown in the top panel with the specific charge state selected for MS/MS highlighted in red. ETD fragmentation data is shown in the bottom panel including selected c (red) and z (blue) ion annotations. A summary of the observed fragments and sequence coverage is also included.*: hypothesized PTM location based on previous literature.[112]
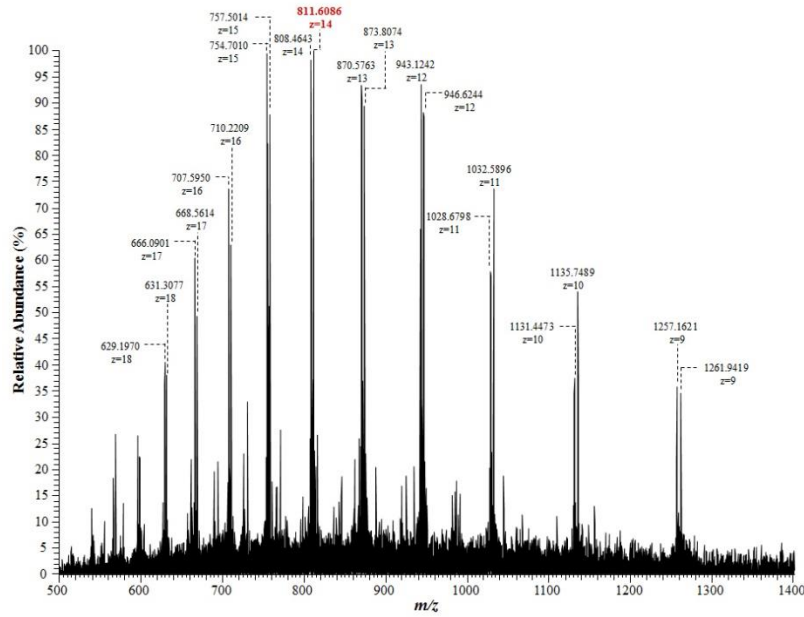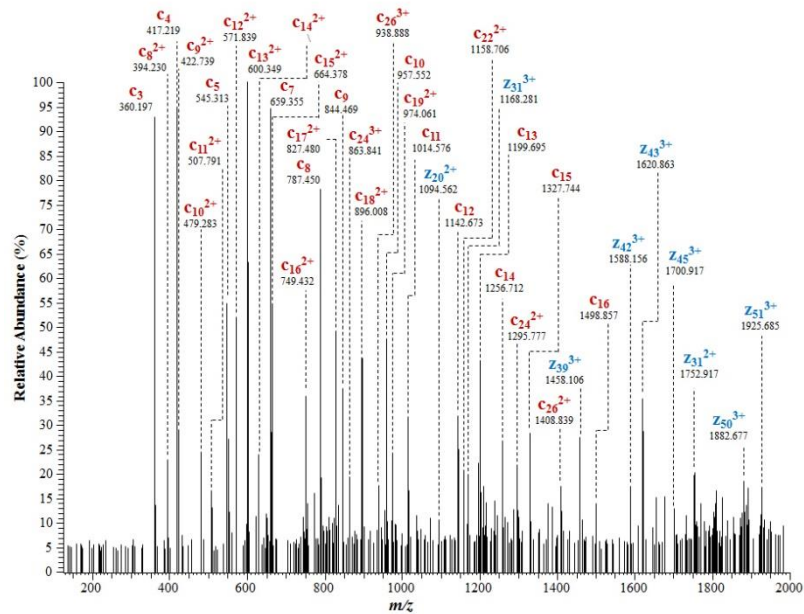
**Figure 2.9.** ETD LC-MS/MS data for Histone H4 (N-acetylated, K17 acetylated, K21 dimethylated). The charge state distribution is shown in the top panel with the specific charge state selected for MS/MS highlighted in red. ETD fragmentation data is shown in the bottom panel including selected c (red) and z (blue) ion annotations. A summary of the observed fragments and sequence coverage is also included.

## Observed Protein Expression in clear cell Renal Cell Carcinoma (ccRCC)

Cancer diagnoses of the kidney and renal pelvis are estimated to reach over 61,000 people in the United States in 2015, with roughly a 23% mortality rate.[115] Over 90% of these diagnoses will be of renal cell carcinoma, of which the majority will be clear cell renal cell carcinoma (ccRCC).[115] Detection and imaging of these tumors have typically been performed through computed tomography (CT) and magnetic resonance imaging (MRI),[116] though immunological and biomarker assays have become more prevalent in diagnostics.[117] Many ccRCC tumors are resistant to chemotherapy and radiation therapy, so nephrectomies still remain the gold standard of treatment with a greatly improved prognosis if the tumor is completely removed.[118] Unfortunately, visual and histological assessments of tumor margins can prove insufficient, with incomplete resections leading to disease recurrence.[119] Molecular localization patterns in and around the tumor can provide insight into the tumor microenvironment and aid in defining the molecular margin.[94]

MALDI FTICR IMS protein data collected from human ccRCC tissue is shown in Fig. 2.10. These data have similar figures of merit to the previously discussed rat brain FTICR IMS analysis. The average spectrum from the entire imaging experiment shows ions detected with good sensitivity up $m/z$ ~16,000 (Fig. 2.10b). The data were collected with a resolving power of ~75,000 at $m/z$ 5,000 resulting in 4,051 peaks detected between $m/z$ 2,000–16,000 with S/N > 20. An overlay of the proteins detected at $m/z$ 5,653.732, $m/z$ 4,936.521 and $m/z$ 7,934.107 show good correlation to tissue substructures visualized by histological staining (Fig. 2.10a). Hemoglobin subunit beta was detected at $m/z$ 7,934.107 (HBB, $[M+2H]^{2+}$, 4.7 ppm) and was observed throughout the kidney with regions of highest intensities near the tumor regions. Normal kidney functions include removing excess organic molecules from the blood through

small filtration units called glomeruli. However, renal cell carcinoma, like many other tumors, utilizes the process of angiogenesis to promote vascularization in and around the developing tumor. This in turn supplies the tumor with blood rich in nutrients for growth and proliferation.[120] Localization of hemoglobin to these regions likely corresponds to a highly vascularized carcinoma.

The ion observed at *m/z* 4,936.521 was found to be N-terminally acetylated thymosin β10 (Thyβ10-AC, $[M+H]^{1+}$, 3.0 ppm) and was localized specifically to the tumor region, with relatively low abundance in surrounding normal tissue. Thymosin β10 organizes the cytoskeleton between cells by regulating the formation of actin polymers. The relative abundances have been shown to rapidly increase during the development of various cancers, including renal cell carcinoma.[121] Histones are core components of the nucleosome and regulate DNA repair and replication. They have been shown to have many post-translational modifications, effectively altering their function within biological systems. Histone H4 has been observed in relatively lower abundance in cancerous regions compared to normal tissue,[122] however recent work has shown that renal cell carcinoma and many other cancers can alter histone modification pathways, changing the post-translational modifications that are expressed.[123] The image of *m/z* 5,653.732, determined to be histone H4 with an acetylation and dimethylation (HH4-AC/2Me, $[M+2H]^{2+}$, -4.4 ppm), shows an increased abundance in the adjacent normal tissue, with significantly lower signal in the tumor region.

A unique aspect of performing protein imaging experiments using MALDI FTICR IMS is the ability to both generate multiply charged ions using MALDI matrices such as DHA and then accurately determine the charge state of highly charged ions. Figure 2.10c-f show the ion images and isotopic distributions for the $[M+H]^{1+}$, $[M+2H]^{2+}$, $[M+3H]^{3+}$, and $[M+6H]^{6+}$ charge states of
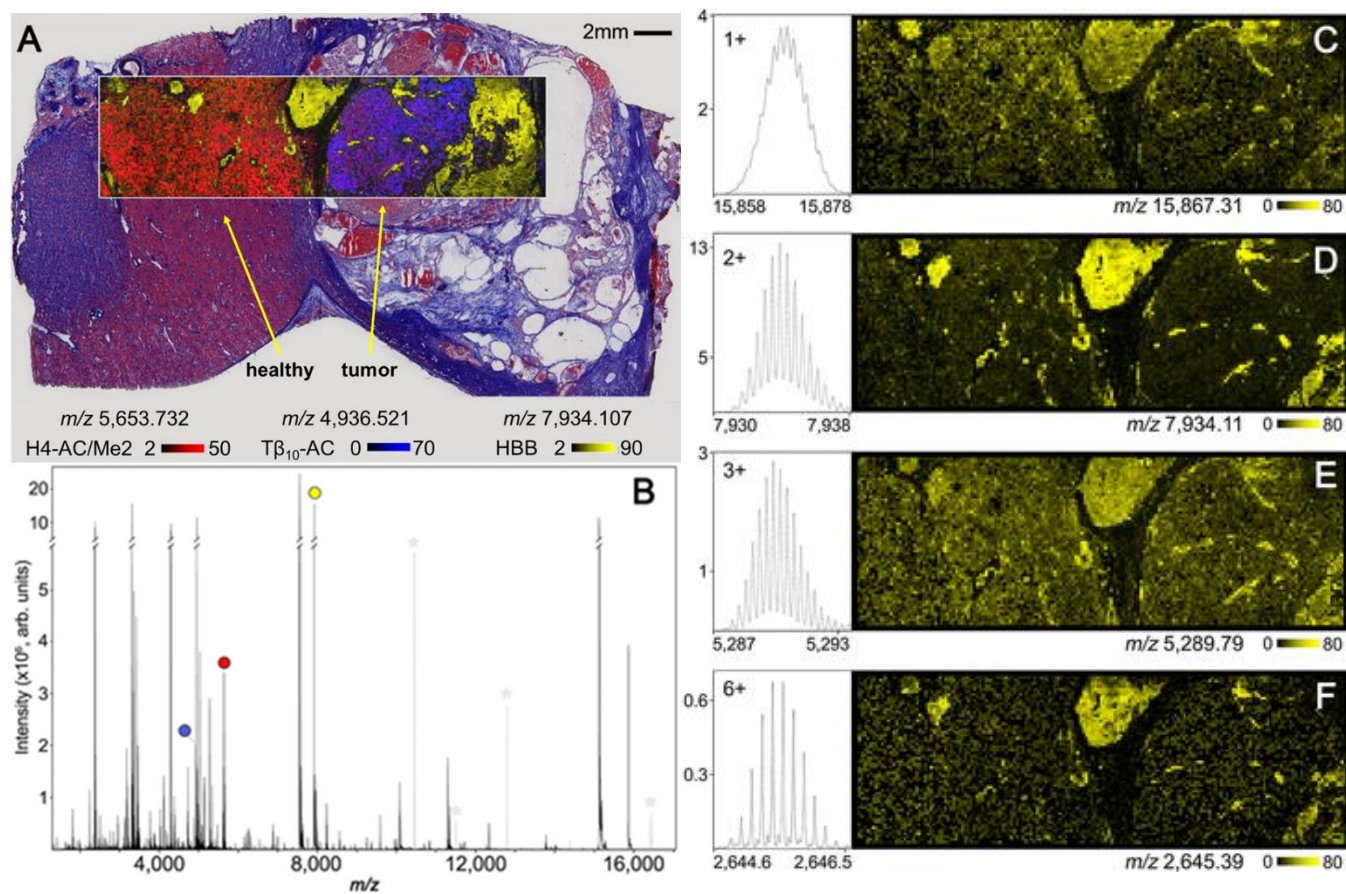
**Figure 2.10**. Selected ion images of identified intact proteins from human clear cell renal cell carcinoma collected using MALDI FTICR IMS. Observed substructures in the overlaid 30 μm ion image of $m/z$ 5,653.732 (HH4-AC/2Me, $[M+2H]^{2+}$, red), $m/z$ 4,936.521 (Thyβ10-AC, $[M+H]^{1+}$, blue), and $m/z$ 7,934.107 (HBB, $[M+2H]^{2+}$, yellow), were consistent with the trichrome staining following IMS acquisition (A). The overall average spectrum for the 100 μm imaging experiment is shown in B highlighting each peak used to generate the selected ion images (A). Ion images and isotopic distributions for the $[M+H]^{1+}$, $[M+2H]^{2+}$, $[M+3H]^{3+}$, and $[M+6H]^{6+}$ charge states of hemoglobin subunit beta are shown in (C–F). Electronic noise peaks have been greyed and marked (*) to simplify the spectrum (B).

hemoglobin subunit beta. Although the 2+ charge state is detected with much greater intensity, the other ions are still detected with good sensitivity. The generation of multiply charged ions using low mass resolution instruments can complicate spectral interpretation, particularly for complex samples such as biological tissues. However, the ability to produce highly charged ions using high resolving power instrumentation that can differentiate overlapping isotopic patterns to simplify interpretation is advantageous in moving larger proteins into the effective *m/z* range of the instrument. This potentially improves the capability of top-down fragmentation experiments directly from tissue.

**Conclusions**

Imaging mass spectrometry is a highly sensitive and efficient discovery tool used to enhance classic histologic analysis by providing specific molecular detail. However, identification of detected proteins remains a significant challenge. Indirect identification is one of the most effective strategies for identifying molecules of interest in IMS experiments. By separately performing MALDI IMS and LC-MS/MS, each can be operated optimally for their individual tasks. Previously, this strategy has lacked sufficient mass accuracy in the imaging data to correlate the two approaches with high confidence. MALDI FTICR MS is now capable of overcoming this challenge by producing ion images with high mass resolution (~75,000 at *m/z* 5,000) and accuracy (<5 ppm) for proteins up to and beyond 16,000 Da. This has been achieved by carefully optimizing sample preparation methods as well as tuning instrument parameters to increase signal of higher molecular weight species. Analysis of control rat brain tissue and human kidney tumor tissue showed that protein charge states and complex mixtures of proteoforms were able to be distinguished, making identification more feasible and allowing these tissues to be studied with unprecedented molecular detail.

# CHAPTER III


## SPATIALLY-TARGETED EXTRACTIONS TO IMPROVE PEPTIDE

## IDENTIFICATIONS FROM MALDI FTICR IMS EXPERIMENTS


### Introduction

While top-down proteomic approaches now provide a method for the identification of intact molecular species from tissue, many improvements still need to be made. Functional top-down databases are still relatively new,[124, 125] and have not had decades of curation as seen by larger genomic databases.[126, 127] Protein databases may not have all of the isoforms, splice variants, or post-translationally modified forms of the protein listed, as many are still unknown.[128] Additionally, many clinical samples are stored in tissue banks after formalin fixation and paraffin embedding. This process chemically cross-links the proteins within the sample, maintaining cellular histology and stabilizing them for long-term storage.[129] This process is irreversible, meaning that accessing proteins for proteomics or MALDI IMS requires an alternate approach.

Bottom-up approaches to proteomics rely on the enzymatic digestion of proteins into peptide components, bypassing the cross-linked nature of the formalin-fixed sample.[130, 131] Extensive literature exists on optimizing enzymatic digestion for specific samples, but it has been focused largely on in-solution digestions.[132-134] These strategies traditionally use homogenization to aid in the extraction of analytes, thus resulting in the loss of any spatial information from the sample. The procedures are effective, resulting in rich datasets for identifications but process can be extensive and require a relatively large amount of sample.

The introduction of *in situ* digestion of tissue samples has allowed for spatial information to be maintained while still providing peptide signatures for protein identification.[11, 135] Trypsin or other enzymes can be applied directly to the tissue, then the peptides can be analyzed by MALDI IMS or extracted for bottom-up identifications. The use of hydrogel technologies for this approach will be discussed in greater detail in Chapter IV. Regardless of the method, the goal of identifying peptides from specific regions of biological samples remains the same.

For MALDI peptide IMS experiments, time-of-flight (TOF) mass spectrometers have commonly been used due to the high sensitivity and dynamic range, large practical mass range, reasonable molecular specificity, and high throughput of the TOF analyzer.[136] Complex samples such as tissue provide many interferences, and the resolving power of TOF instruments can prove insufficient. Additionally, inherent mass accuracy differences between TOF imaging platforms and high performance LC-ESI-MS/MS require wide mass windows to match IMS spectral peaks to corresponding LC-MS/MS peaks for potential identification. By incorporating higher-performing instruments, such as FTICRs, into peptide imaging workflows, accurate mass measurements can be achieved.[137, 138]

**Methodologies for Trypsin Application, *in situ* Digestion, Incubation and MALDI IMS for Peptides**

*Tissue Preparation*

Fresh frozen rat brains and human clear cell renal cell carcinoma (ccRCC) samples were investigated because protein localization patterns were already investigated in Chapter II. Frozen tissue was sectioned to 10-12 microns and mounted onto conductive Indium-tin-oxide

(ITO)-coated slides. Tissues were washed to remove interfering lipids and salts as with the protein analysis. [96]

*Trypsin Digestion*

Trypsin was applied to the tissue sections using a modified TM Sprayer, which allowed for lower rate applications. Matrix application flow rates are typically on the order of 0.1-0.5 mL/min, while the trypsin methods call for 7.5 µL/min to allow for a relatively dry coating. This minimizes delocalization or enzyme "pooling" on the tissue surface. Samples were placed in an incubation chamber[39, 96] containing 100 mM ammonium bicarbonate, sealed with lab tape, and incubated at 37°C for 14 hrs. After incubation, samples were removed from the incubation chamber and dried in a desiccator prior to matrix application.

*Matrix Application*

Matrix was applied using a TM Sprayer with 15 mg/mL DHA in 9:1 ACN:ddH$_2$O with 0.2% TFA. Sprayer conditions include a flow rate 0.1 mL/min, nitrogen flow of 10 psi, spray temperature of 80°C, a spray velocity of 1,100 mm/min, 4 passes with offsets and rotations, and 9:1 ACN:ddH$_2$O as the pushing solvent. This is the same method that was used to successfully image proteins by MALDI FTICR and therefore was chosen because of the robust signal. Samples were rehydrated as previously described [97] at 37°C for 3 minutes with 1 mL of 50 mM acetic acid as the rehydration solvent.

*MALDI FTICR IMS*

High mass resolution imaging experiments were performed using a 15T Bruker MALDI FTICR mass spectrometer, as in Chapter II. Instrument tuning was performed in a similar fashion as before, though the mass range was limited to *m/z* 5,000-8,000 to minimize the detection of electronic interferences. DHA provided robust peptide signal from tissue samples and resolving power was adjusted to maximize signal intensity and minimize unresolved peaks. External calibration was performed prior to analysis using CsI clusters and protein standards.

*Peptide Extraction from Tissue*

Microextractions were performed for both proteins and peptides using 20% acetonitrile and a gel-loading pipette tip as previously described.[83] A 1 µL solution was pipetted onto the tissue and repeated aspirated then withdrawn. This was repeated 3x and collected into 2 µL of 20% acetonitrile.

*LC-Coupled Tandem Mass Spectrometry*

Microextracts were loaded onto a reversed phase capillary trap column using a helium-pressurized cell (pressure bomb). The trap column was packed with C18 reverse phase material. Using an Eksigent NanoLC Ultra HPLC, proteins were gradient-eluted at a flow rate of 500 nL/min, and the mobile phase solvents consisted of 0.1% formic acid, 99.9% water (solvent A) and 0.1% formic acid, 99.9% acetonitrile (solvent B). The gradient consisted of 5%–50% B in 55 min, followed by 50%–95% B in 8 min. Upon gradient-elution, peptides were mass analyzed on a Thermo Q Exactive mass spectrometer, equipped with a nanoelectrospray ionization source. HCD tandem mass spectra were acquired in a top 20 data-dependent manner.

*Data Analysis*

Tandem mass spectra were searched using SEQUEST software against the corresponding *Rattus norvegicus* or *Homo sapien* Uniprot database. Identified peptides were matched to their corresponding proteins and assembled in Scaffold 4.0 software. Confident identifications were made with protein identification probabilities of ≥ 99%, protein identification probabilities of ≥ 95%, and a minimum of 2 distinct peptides per protein.
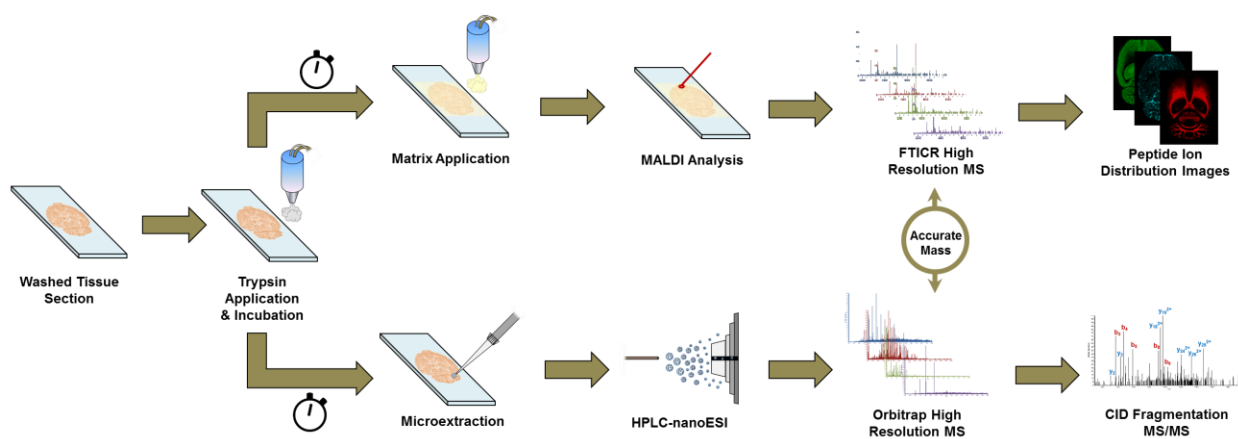


**Figure 3.1.** General sample preparation workflow for MALDI FTICR peptide IMS and subsequent identification strategies using HCD fragmentation.

**Optimizing Incubation Conditions to Maximize Digestion and Minimize Delocalization**

Though a great deal of research has focused on trypsin digestion, traditional approaches utilize in-solution digests, where the sample is dissolved into a solution containing the enzyme.[133, 134] The digestions conditions, such as buffer pH and concentration of enzyme present in-solution, can be easily maintained. These conditions become much more challenging for *in situ* trypsin digestion because digestion efficiency must be balanced with analyte localization.[139, 140] If analytes become delocalized in the tissue, then the spatial component is lost, thus negating the usefulness of such a technique. Discrete application of enzymes has proven successful

previously, minimizing the area analytes are able to delocalize within.[11, 141] However, delocalization can occur not only during the enzyme application step, but also during the incubation process. Efforts to minimize incubation times have proven successful with the introduction of microwave-assisted digestion.[67, 142] Alternatively, incubation chambers can be used to provide a humid environment for the tissue, and by extension the trypsin, to remain hydrated.[39] Since these are typically home-built, there is a great deal of variation that can be observed from method to method. To assess analyte delocalization during the incubation process, four serial rat brain sections were used. Each tissue was washed in an identical manner prior to trypsin application, and trypsin was applied to all four sections simultaneously using a TM Sprayer. The only difference in the four conditions was the amount of ammonium bicarbonate present in the incubation chambers.

After an over-night incubation, matrix was applied to all four sections at the same time and they were analyzed on a MALDI FTICR as one image to account for any normalization or visualization discrepancies that could occur. Figure 3.2 shows selected ion images of different peptides for each incubation condition. There are a few noticeable trends from this experiment that shed light onto the incubation process. The sample incubated with 50 μL of 100 mM ammonium bicarbonate appeared to have the least amount of delocalization, when comparing the ion images to the histology of the rat brain. As the volume of ammonium bicarbonate in the incubation chamber increased, the localization patterns seem to degrade fairly rapidly. Conversely, there were peaks observed in the higher-volume ammonium bicarbonate incubations that showed little or no intensity in the 50 or 100 μL conditions. This is most likely due to the fact that higher ammonium bicarbonate volumes led to a more humid environment in the incubation chambers. As these vapors condensed back down onto the tissue, this allowed for

optimal trypsin digestion to occur on the tissue surface. The lower volumes would not have provided the same level of moisture in the chambers, so therefore the efficiency of the digestion would have suffered, potentially leading to inactive trypsin or incomplete digestion. To balance digestion conditions and localization, incubation volumes of 50-100 µL were chosen for subsequent experiments.
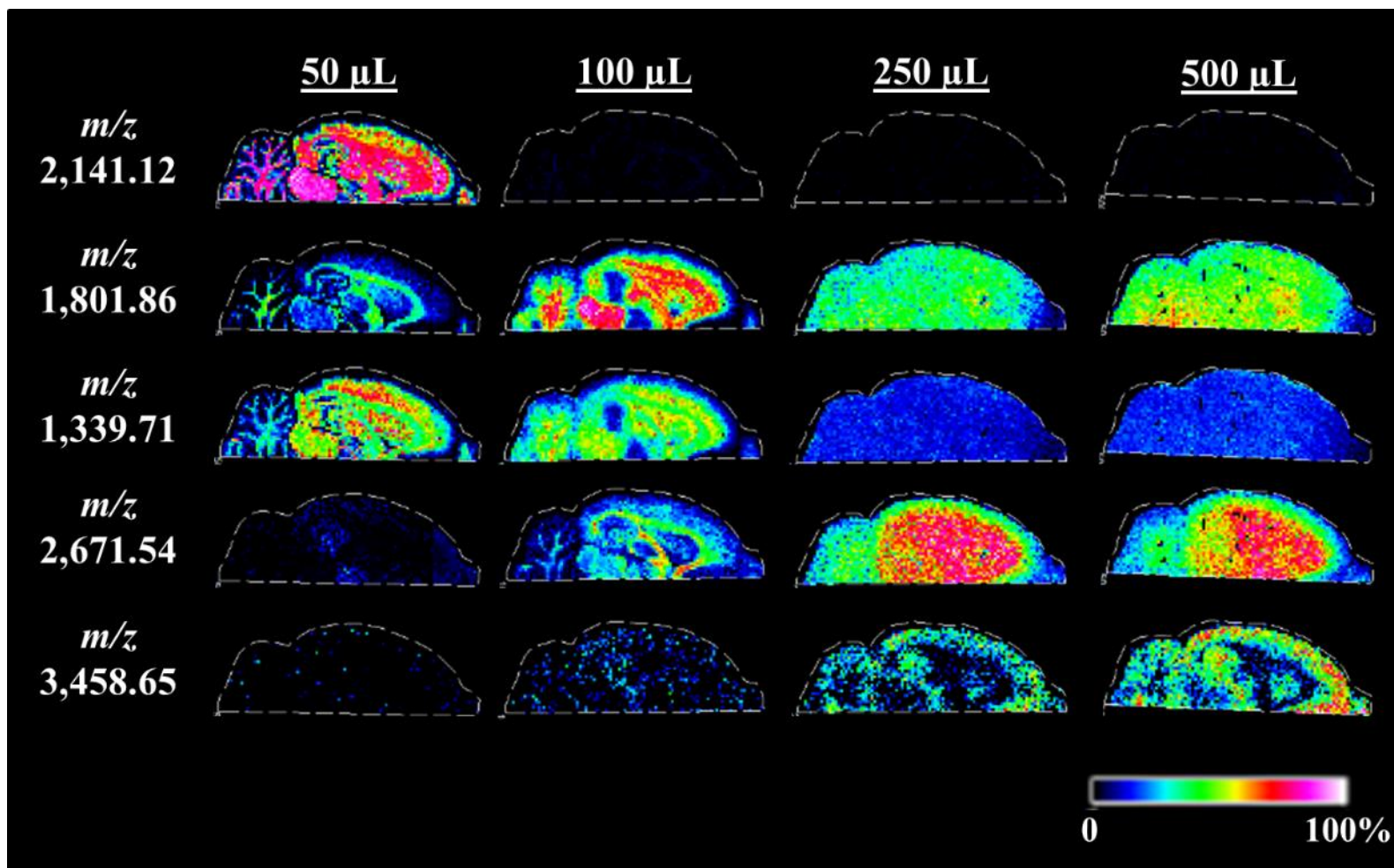
**Figure 3.2.** Utilizing MALDI IMS to aid in the assessment of enzymatic incubation conditions. Tissues were prepared and imaged in an identical manner, with only the volume of 100 mM ammonium bicarbonate in the incubation chamber being varied.

**MALDI FTICR IMS and Localized Peptide Analysis of Biological Samples**

To properly assess on-tissue digestion efficiencies or presence of miscleavages, peptide identifications must be established. On-tissue fragmentation of peptides has been used in many instances with great success.[92, 143] However, throughput for this process is very low, and many instruments can be limited, either by the inherent nature of the instrument or low signal intensities. As discussed previously, indirect identification methods have proven to be very successful because each analysis is run with optimal conditions.

Traditionally, peptide identification has been achieved using homogenization and in-solution digestion.[132] This can add a level of variability though, because the digestion conditions would be different from an on-tissue digest. To minimize differences in peptides observed from MALDI IMS and LC-ESI-MS/MS approaches, the digestion should remain the same for both. This means performing the digestion *in situ*, then extracting peptides for subsequent LC analysis. Microextracts have already been shown to provide robust signal from localized regions of tissue,[83] and this approach was used to extract peptides from three different regions of rat brain post-digestion. The extracts were analyzed independently and compared to a traditional homogenization approach. Figure 3.3 shows the three regions that were chosen for extraction on the H&E section. When comparing the peptide and protein overlap between the regions, there are distinct analytes from each region that are not found in the other two. Table 3.1 shows the identities of these unique proteins from each region. This highlights the strength of a spatially-directed approach, focusing identification strategies only on the region of interest, rather than the tissue as a whole.
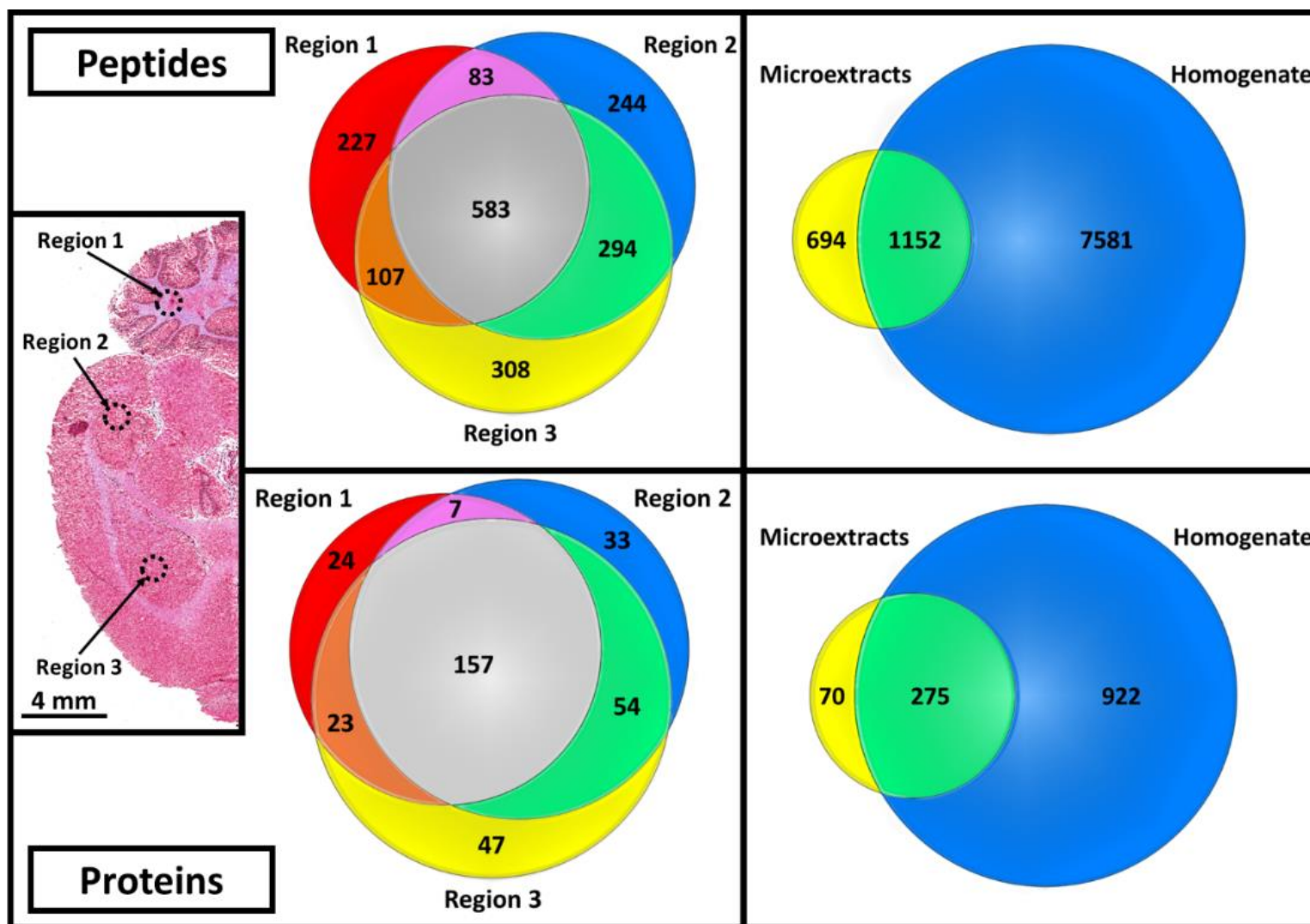
**Figure 3.3.** LC-MS/MS analysis of rat brain regions sampled by microextraction and tissue homogenization. Identifications were considered confident within Scaffold Proteome Viewing software when they had a 99.9% Protein Threshold, a 95% Peptide Threshold, and a minimum of 2 peptides.

| 70 Protein Identifications Unique to the "Microextracts": | | | | |
|---|---|---|---|---|
| *Description* | *Accession* | *Region 1* | *Region 2* | *Region 3* |
| 40S ribosomal protein S16 | sp\|P62250\|RS16_RAT | X | | X |
| 40S ribosomal protein S18 | sp\|P62271\|RS18_RAT | X | X | X |
| 40S ribosomal protein S25 | sp\|P62853\|RS25_RAT | | | X |
| 60S ribosomal protein L23a | sp\|P62752\|RL23A_RAT | | | X |
| 60S ribosomal protein L8 | sp\|P62919\|RL8_RAT | | X | |
| Adaptor protein complex AP-2, alpha 1 subunit (Predicted) | tr\|D3ZUY8\|D3ZUY8_RAT | | X | X |
| ADP/ATP translocase 2 | sp\|Q09073\|ADT2_RAT | X | | |
| ATPase, H+ transporting, V1 subunit D, isoform CRA_c | tr\|Q6P503\|Q6P503_RAT | | X | X |
| Brevican, isoform CRA_a | tr\|G3V8G4\|G3V8G4_RAT | | X | |
| Chaperonin subunit 8 (Theta) (Predicted), isoform CRA_a | tr\|D4ACB8\|D4ACB8_RAT | X | X | X |
| Creatine kinase, mitochondrial 1, ubiquitous | tr\|Q5BJT9\|Q5BJT9_RAT | X | X | X |
| Cytochrome b-c1 complex subunit 7 | tr\|B2RYS2\|B2RYS2_RAT | | X | |
| Disks large-associated protein 4 | sp\|P97839\|DLGP4_RAT | | X | |
| D-tyrosyl-tRNA(Tyr) deacylase | tr\|B0K014\|B0K014_RAT | | X | X |
| Epb4.9 protein | tr\|B2GUY4\|B2GUY4_RAT | | X | X |
| Erythrocyte protein band 4.1-like 3, isoform CRA_b | tr\|G3V874\|G3V874_RAT | X | X | X |
| Fusion, derived from t(1216) malignant liposarcoma (Human) | tr\|Q5PQK2\|Q5PQK2_RAT | X | | X |
| GTPase activating protein (SH3 domain) binding protein 2 | tr\|Q6AY21\|Q6AY21_RAT | | X | X |
| GTP-binding nuclear protein Ran, testis-specific isoform | sp\|Q8K586\|RANT_RAT | | | X |
| Heat shock 70 kDa protein 4L | tr\|B4F772\|B4F772_RAT | X | | X |
| Heat shock 70kDa protein 12A (Predicted), isoform CRA_a | tr\|D3ZC55\|D3ZC55_RAT | X | | X |
| Hemoglobin subunit beta-2 | sp\|P11517\|HBB2_RAT | X | X | X |
| Histone H1.5 | sp\|D3ZBN0\|H15_RAT | X | X | X |
| Histone H2A type 1 | sp\|P02262\|H2A1_RAT | X | | X |
| Histone H2B | tr\|D4A817\|D4A817_RAT | X | X | X |
| Histone H4 | sp\|P62804\|H4_RAT | X | | |
| Inositol polyphosphate-1-phosphatase | tr\|Q5RJK6\|Q5RJK6_RAT | X | | |
| Kinesin heavy chain isoform 5C (Fragment) | tr\|G3V6L4\|G3V6L4_RAT | | X | X |
| Lipid phosphate phosphatase-related protein type 4 | sp\|Q7TMB7\|LPPR4_RAT,tr\|G3V864\|G3V864_RAT | | X | |
| Microtubule-associated protein | tr\|F1MAQ5\|F1MAQ5_RAT | X | X | X |
| NADH dehydrogenase (Ubiquinone) 1 beta subcomplex, 7 (Predicted) | tr\|D3ZLT1\|D3ZLT1_RAT | X | X | X |
| NADH dehydrogenase (Ubiquinone) Fe-S protein 7 | tr\|Q5RJN0\|Q5RJN0_RAT | | X | |
| NADH dehydrogenase (Ubiquinone) flavoprotein 1 | tr\|Q5XIH3\|Q5XIH3_RAT | X | | X |
| Na-K-Cl cotransporter | tr\|Q9QX10\|Q9QX10_RAT | X | | |
| Ndufa4 protein | tr\|B2RZD6\|B2RZD6_RAT | | X | |
| Neurotrimin | tr\|G3V964\|G3V964_RAT | | | X |
| Neutral amino acid transporter ASCT1 | tr\|Q76GL9\|Q76GL9_RAT | X | | X |
| Phosphatase and actin regulator 1 | sp\|P62024\|PHAR1_RAT | | | X |
| Phosphorylase | tr\|B2GV03\|B2GV03_RAT,tr\|G3V6Y6\|G3V6Y6_RAT | X | X | X |
| Profilin | tr\|D3ZDU5\|D3ZDU5_RAT | X | X | |
| Protein Ank2 (Fragment) | tr\|F1M9N9\|F1M9N9_RAT | X | X | X |
| Protein Ankrd63 | tr\|D3ZKY6\|D3ZKY6_RAT | | | X |
| Protein Atp6v1a | tr\|D4A133\|D4A133_RAT | | X | X |
| Protein Cttn | tr\|D3ZGE6\|D3ZGE6_RAT,tr\|O70420\|O70420_RAT,tr\|Q66HL2\|Q66HL2_RAT | | X | |
| Protein Epb41l2 | tr\|D3ZM69\|D3ZM69_RAT | X | | |
| Protein Gprin3 | tr\|D3ZF21\|D3ZF21_RAT | | | X |
| Protein Icam5 | tr\|D4A435\|D4A435_RAT | | X | |
| Protein LOC684828 | tr\|M0R7B4\|M0R7B4_RAT | X | X | X |
| Protein Napg | tr\|D4A0E2\|D4A0E2_RAT | | X | X |
| Protein Ncam2 (Fragment) | tr\|F1M8G9\|F1M8G9_RAT | | | X |
| Protein Pcdh1 (Fragment) | tr\|F1M8K1\|F1M8K1_RAT | | X | |
| Protein Pcp2 | tr\|D3ZXP8\|D3ZXP8_RAT | X | | |
| Protein RGD1310819 (Fragment) | tr\|D3ZBU7\|D3ZBU7_RAT | | X | X |
| Protein Sptbn1 | tr\|G3V6S0\|G3V6S0_RAT,tr\|Q6XD99\|Q6XD99_RAT | X | X | X |
| Protein Srsf3 | tr\|Q0ZFS8\|Q0ZFS8_RAT | | | X |
| Protein Tceal5 | tr\|M0RDJ7\|M0RDJ7_RAT | | X | X |
| Protein Tppp | tr\|D3ZQL7\|D3ZQL7_RAT | X | X | X |
| Protein Tubb4a | tr\|B4F7C2\|B4F7C2_RAT | X | X | X |
| RAB10, member RAS oncogene family | tr\|Q5RKJ9\|Q5RKJ9_RAT | X | X | X |
| RAP1, GTPase activating protein 1, isoform CRA_a | tr\|F1LV89\|F1LV89_RAT | | | X |
| Rat apolipoprotein E protein | tr\|Q65ZS7\|Q65ZS7_RAT | | X | |
| Rat glutathione S-transferase | tr\|Q6LDP3\|Q6LDP3_RAT | | | X |
| RNA-binding motif protein, X chromosome retrogene-like | sp\|P84586\|RMXRL_RAT | X | X | X |
| Septin 5, isoform CRA_d | tr\|D3ZDH8\|D3ZDH8_RAT | | X | X |
| Septin 7 | tr\|A2VCW8\|A2VCW8_RAT | X | X | X |
| SP120 | tr\|Q63555\|Q63555_RAT,tr\|Q6IMY8\|Q6IMY8_RAT | | X | X |
| Transcription factor Pur-beta | tr\|F1LSL1\|F1LSL1_RAT | X | X | X |
| Tropomyosin alpha isoform | tr\|Q91XN7\|Q91XN7_RAT | X | X | X |
| Uncharacterized protein | tr\|E9PT22\|E9PT22_RAT,tr\|F1MAJ2\|F1MAJ2_RAT | | | X |
| Zero beta-globin (Fragment) | tr\|Q63011\|Q63011_RAT | X | X | X |

**Table 3.1.** Protein identifications from rat brain regions exclusively observed by microextraction analysis. Identifications were considered confident within Scaffold Proteome Viewing software when they had a 99.9% Protein Threshold, a 95% Peptide Threshold, and a minimum of 2 peptides.

While the rat brain does provide various substructures and spatial heterogeneity, a more complex sample was chosen to validate this approach. A human ccRCC tumor sample contained various stages of tumor progression, the adjacent normal tissue, and a margin in between these two regions. Performing a similar microextract and homogenate analysis, peptide and protein identifications were collected. There were much greater variations between identifications within the microextract regions, both at the peptide and protein level (Figure 3.4). This is supported by previous reports highlighting the very heterogeneous nature of molecules within these tumors.[94] A similar trend was observed for the microextract and homogenate comparison as was seen in the rat brain sample. Table 3.2 lists the identified proteins unique to the microextract analysis. Overall, the number of protein identifications was lower for the human ccRCC sample compared to the rat brain, most likely due to the fibrotic nature of the tumor. This was highlighted in the homogenization process, where extensive homogenization did not completely solubilize the tissue.
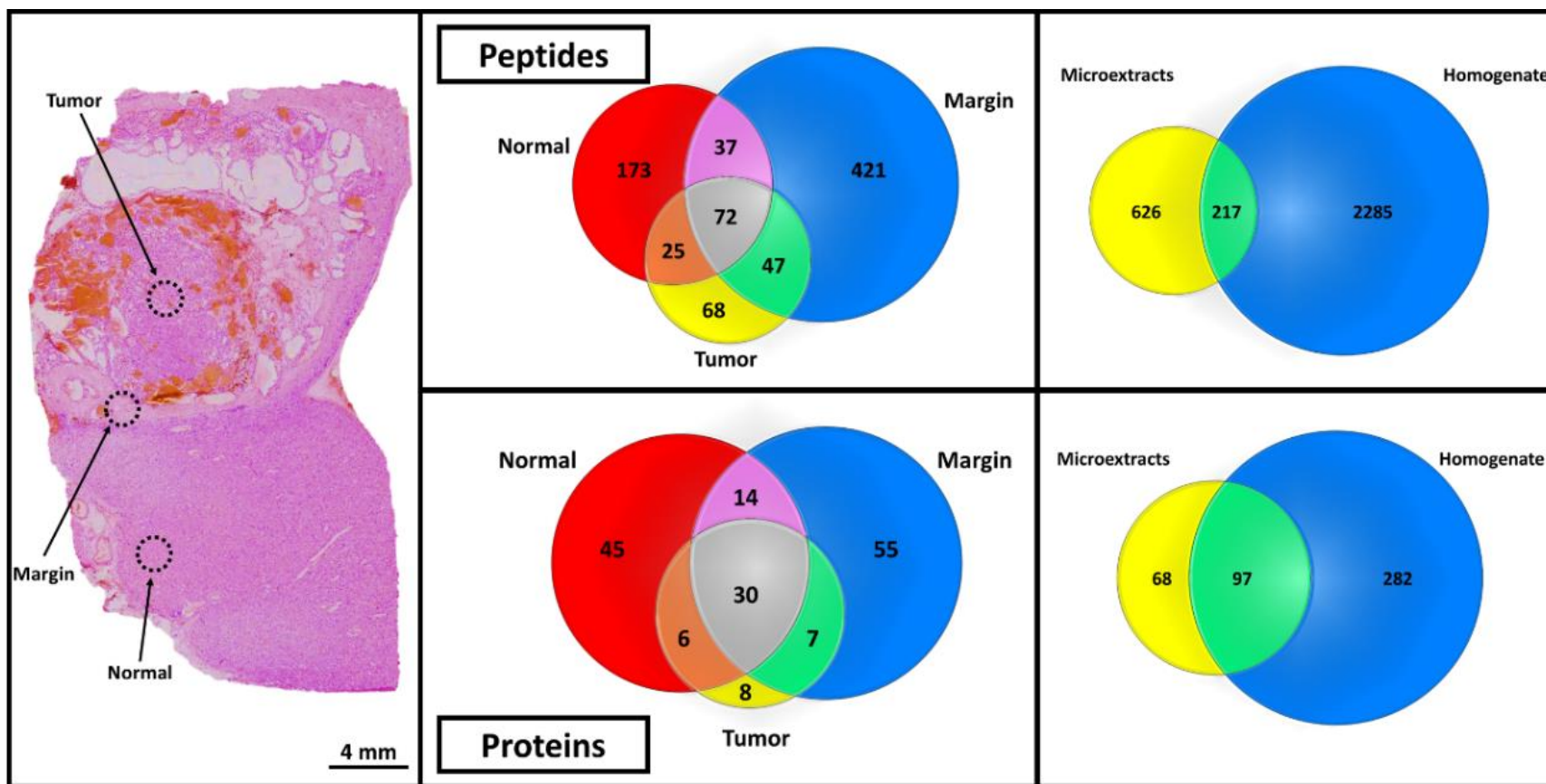
**Figure 3.4.** LC-MS/MS analysis of resected human ccRCC tumor regions sampled by microextraction and tissue homogenization. Identifications were considered confident within Scaffold Proteome Viewing software when they had a 99.9% Protein Threshold, a 95% Peptide Threshold, and a minimum of 2 peptides.

| 68 Protein Identifications Unique to the "Microextracts": | | | | |
|---|---|---|---|---|
| *Description* | *Accession* | *Normal* | *Margin* | *Tumor* |
| 14-3-3 protein beta/alpha | sp\|P31946\|1433B_HUMAN | X | X | X |
| 40S ribosomal protein S18 | sp\|P62269\|RS18_HUMAN | | X | |
| Actin, aortic smooth muscle | sp\|P62736\|ACTA_HUMAN,sp\|P68032\|ACTC_HUMAN | X | X | X |
| Acyl-CoA synthetase family member 2, mitochondrial | sp\|Q96CM8\|ACSF2_HUMAN | X | | |
| Adenosylhomocysteinase | sp\|P23526\|SAHH_HUMAN | X | | |
| Alcohol dehydrogenase [NADP(+)] | sp\|P14550\|AK1A1_HUMAN | X | X | |
| Alpha-actinin-1 | sp\|P12814\|ACTN1_HUMAN | | X | |
| Alpha-crystallin B chain | sp\|P02511\|CRYAB_HUMAN | | | X |
| Apolipoprotein E | sp\|P02649\|APOE_HUMAN | | X | |
| ATP synthase-coupling factor 6, mitochondrial | sp\|P18859\|ATP5J_HUMAN | X | | |
| Bifunctional ATP-dependent dihydroxyacetone kinase/FAD-AMP lyase (cyclizing) | sp\|Q3LXA3\|DHAK_HUMAN | X | | |
| Calponin-1 | sp\|P51911\|CNN1_HUMAN | | X | |
| Clusterin | sp\|P10909\|CLUS_HUMAN | | X | |
| Collagen alpha-1(VI) chain | sp\|P12109\|CO6A1_HUMAN | | X | |
| Collagen alpha-1(XVIII) chain | sp\|P39060\|COIA1_HUMAN | | X | |
| Collagen alpha-2(VI) chain | sp\|P12110\|CO6A2_HUMAN | | X | |
| Complement factor B | sp\|P00751\|CFAB_HUMAN | | X | X |
| Cysteine and glycine-rich protein 1 | sp\|P21291\|CSRP1_HUMAN | | X | |
| Cysteine and glycine-rich protein 2 | sp\|Q16527\|CSRP2_HUMAN | | X | |
| Cytochrome c oxidase subunit 5B, mitochondrial | sp\|P10606\|COX5B_HUMAN | X | | |
| Cytosol aminopeptidase | sp\|P28838\|AMPL_HUMAN | X | | |
| Delta-1-pyrroline-5-carboxylate dehydrogenase, mitochondrial | sp\|P30038\|AL4A1_HUMAN | X | | |
| Desmin | sp\|P17661\|DESM_HUMAN | | X | |
| Dihydropyrimidinase-related protein 3 | sp\|Q14195\|DPYL3_HUMAN | | X | |
| Disabled homolog 2 | sp\|P98082\|DAB2_HUMAN | X | | |
| Electron transfer flavoprotein subunit beta | sp\|P38117\|ETFB_HUMAN | X | | |
| Elongation factor Tu, mitochondrial | sp\|P49411\|EFTU_HUMAN | X | | |
| Enoyl-CoA hydratase, mitochondrial | sp\|P30084\|ECHM_HUMAN | X | | |
| Heat shock 70 kDa protein 1A/1B | sp\|P08107\|HSP71_HUMAN | X | X | X |
| Heat shock cognate 71 kDa protein | sp\|P11142\|HSP7C_HUMAN | X | X | X |
| Heterogeneous nuclear ribonucleoprotein A1 | sp\|P09651\|ROA1_HUMAN | | | X |
| Heterogeneous nuclear ribonucleoproteins A2/B1 | sp\|P22626\|ROA2_HUMAN | | X | X |
| Heterogeneous nuclear ribonucleoproteins C1/C2 | sp\|P07910\|HNRPC_HUMAN | X | | |
| Histone H1.0 | sp\|P07305\|H10_HUMAN | | X | |
| Histone H1.2 | sp\|P16403\|H12_HUMAN | X | X | X |
| Inter-alpha-trypsin inhibitor heavy chain H1 | sp\|P19827\|ITIH1_HUMAN | | X | |
| Ladinin-1 | sp\|O00515\|LAD1_HUMAN | X | | |
| Latent-transforming growth factor beta-binding protein 2 | sp\|Q14767\|LTBP2_HUMAN | | X | |
| LIM and SH3 domain protein 1 | sp\|Q14847\|LASP1_HUMAN | | X | |
| Lipoma-preferred partner | sp\|Q93052\|LPP_HUMAN | | X | |
| Lumican | sp\|P51884\|LUM_HUMAN | X | X | |
| Malate dehydrogenase, mitochondrial | sp\|P40926\|MDHM_HUMAN | X | | |
| Myosin light polypeptide 6 | sp\|P60660\|MYL6_HUMAN | | X | |
| Myosin regulatory light polypeptide 9 | sp\|P24844\|MYL9_HUMAN | | X | |
| Palladin | sp\|Q8WX93\|PALLD_HUMAN | | X | |
| PDZ and LIM domain protein 7 | sp\|Q9NR12\|PDLI7_HUMAN | | X | |
| Peptidyl-prolyl cis-trans isomerase A | sp\|P62937\|PPIA_HUMAN,sp\|PPIA_HUMAN\| | X | X | |
| Periostin | sp\|Q15063\|POSTN_HUMAN | | X | |
| Phosphoenolpyruvate carboxykinase [GTP], mitochondrial | sp\|Q16822\|PCKGM_HUMAN | X | | |
| Prelamin-A/C | sp\|P02545\|LMNA_HUMAN | | X | |
| Probable ATP-dependent RNA helicase DDX17 | sp\|Q92841\|DDX17_HUMAN | | | X |
| Profilin-1 | sp\|P07737\|PROF1_HUMAN | X | X | |
| Prolargin | sp\|P51888\|PRELP_HUMAN | | X | |
| Protein NDRG1 | sp\|Q92597\|NDRG1_HUMAN | X | | X |
| Rho GDP-dissociation inhibitor 1 | sp\|P52565\|GDIR1_HUMAN | X | X | X |
| Septin-9 | sp\|Q9UHD8\|SEPT9_HUMAN | | | X |
| Serum albumin | sp\|P02768\|ALBU_HUMAN | X | X | X |
| Sorbin and SH3 domain-containing protein 1 | sp\|Q9BX66\|SRBS1_HUMAN | | X | |
| Synaptopodin | sp\|Q8N3V7\|SYNPO_HUMAN | | X | |
| Synaptopodin-2 | sp\|Q9UMS6\|SYNP2_HUMAN | | X | |
| Tensin-1 | sp\|Q9HBL0\|TENS1_HUMAN | | X | |
| Thiosulfate sulfurtransferase | sp\|Q16762\|THTR_HUMAN | X | | |
| Transgelin-2 | sp\|P37802\|TAGL2_HUMAN | | X | |
| Transmembrane protein C19orf77 | sp\|O75264\|CS077_HUMAN | X | | |
| Tropomyosin alpha-1 chain | sp\|P09493\|TPM1_HUMAN | | X | |
| Tropomyosin alpha-4 chain | sp\|P67936\|TPM4_HUMAN | | X | |
| Tropomyosin beta chain | sp\|P07951\|TPM2_HUMAN | X | X | |
| Tubulin beta-4B chain | sp\|P68371\|TBB4B_HUMAN | X | X | |

**Table 3.2.** Protein identifications from resected human ccRCC tumor regions exclusively observed by microextraction analysis. Identifications were considered confident within Scaffold Proteome Viewing software when they had a 99.9% Protein Threshold, a 95% Peptide Threshold, and a minimum of 2 peptides.

When comparing to a homogenization strategy, the combined results of the microextracts provided roughly one third of the protein identifications. This was expected because there were many parts of the tissue that were not sampled by microextraction that would have contributed to the homogenate identifications. However, there were ~70 protein identifications made by the microextract workflow that were not observed in the homogenate (Tables 3.1 and 3.2). The sample complexity of a microextract is much less than that of an in-solution digest of a tissue homogenate. Therefore, it stands to reason that it is much less likely for analytes to be suppressed during the LC analysis. Data-dependent acquisitions rely on peak intensities and exclusion lists to sort through spectra in real time, and samples such as homogenates have much larger differences in analyte dynamic range. This is not to say that abundant peptides and proteins would not also be observed in microextract analyses, however by reducing the complexity of a sample can aid in observing species that may coelute with highly abundant species and otherwise go undetected.

With the high performance characteristics of the FTICR and Q Exactive, peptide identifications could be made using mass accuracy to link the data sets, in a similar manner as described in Chapter II. Peak lists were compared between the MALDI IMS data and the LC-based identification approaches. Identifications were made for peaks with less than 5 ppm mass errors relative to the peptide molecular weight. Figure 3.4 shows examples of ions that were identified using this strategy. To do a complete and thorough comparison, informatics and isotope modelling software would prove beneficial. As the molecular weight increases, the isotopic distribution shifts from the monoisotopic peak. For larger peptides, this means that the most abundant isotope, which provides the highest S/N ion image, would not match to the theoretical mass of the peptide in most databases. Incorporating mass tolerances and isotopic

information into comparisons would provide for more efficient searches and higher yields in terms of confident identifications.
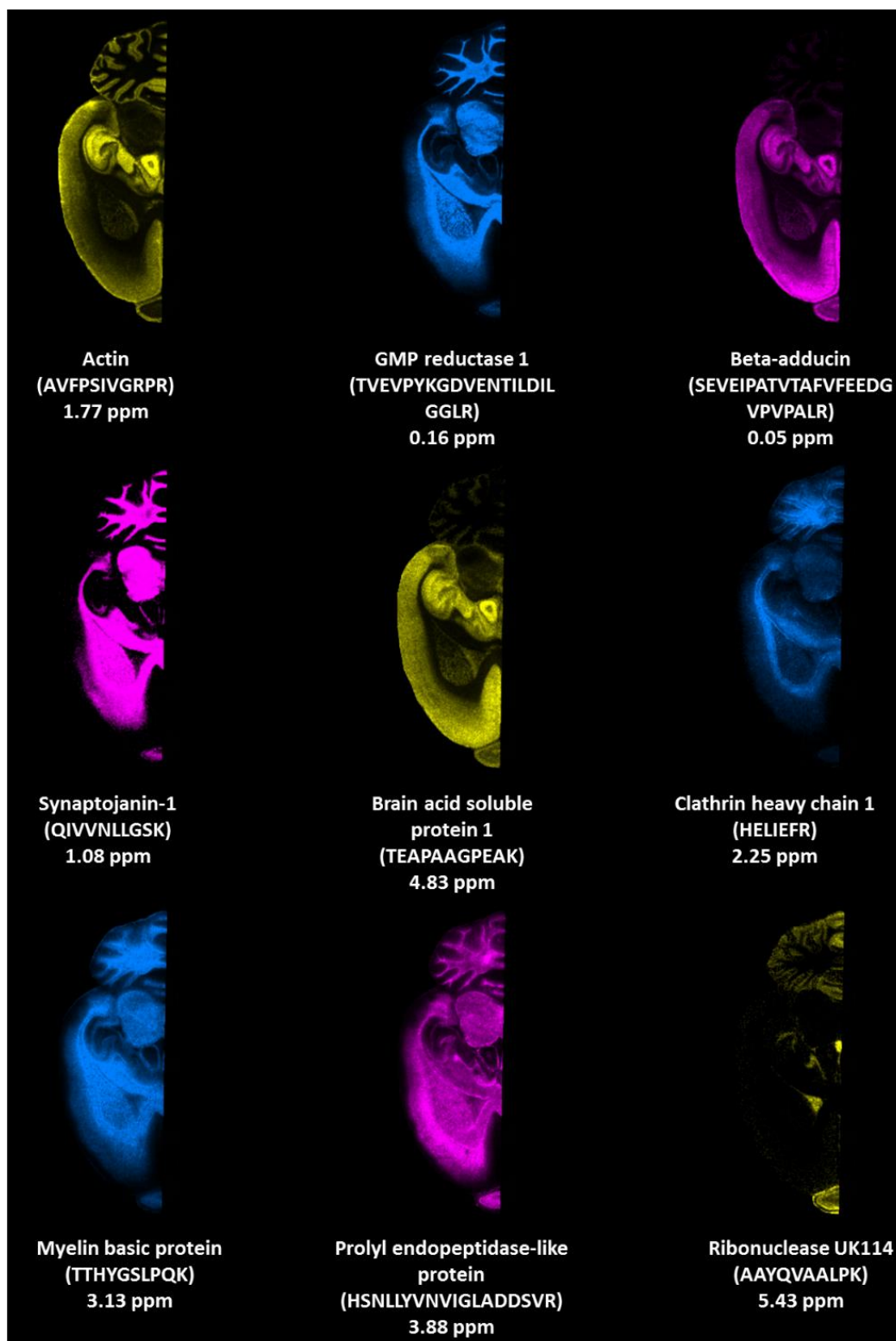
**Figure 3.5** MALDI FTICR IMS of rat brain peptides identified by localized extraction methods. Identifications were made by localized microextractions and verified with tissue homogenization methods. All peptide identifications had mass errors of ~5 ppm or less.

**Conclusions**

Peptide analysis by MALDI FTICR IMS have been improved by robust sample preparation methods, including incubation optimization and spatially localized extraction for identifications. The incorporation of methods previously used for protein analysis have also improved sensitivity from biological tissues, providing analyte-rich spectra. Small volumes of ammonium bicarbonate (50-100 μL) in the incubation chamber yielded the least amount of observed analyte delocalization while still producing spectra rich in peptide signals. The microextraction method allowed for bottom-up proteomic data to be analyzed on Q Exactive while still maintaining a 1 mm spatial area from within the tissue sections. In fact, roughly 70 protein identifications in each case study were only observed from the microextract analysis compared to a traditional homogenization approach. The high mass resolution and mass accuracy of these two instruments were used to correlate IMS and proteomic data for both rat brain and human ccRCC tumor samples. By utilizing the microextraction method to identify analytes by LC-MS/MS, identifications of peptides were made without the need for bulk tissue homogenization. These data showed the capabilities of MALDI FTICR IMS to provide the molecular specificity needed to overcome the challenges associated with direct tissue analysis.

# CHAPTER IV

## ADVANCED HYDROGEL TECHNOLOGIES FOR ENHANCED ON-TISSUE

## PROTEIN DIGESTION AND IMPROVED SPATIAL LOCALIZATION

### Introduction

Protein identification for IMS experiments has historically been performed by homogenizing pieces of tissue, performing protein fractionation and digestion, and then leveraging classical LC-MS/MS bottom-up proteomics methods.[144, 145] Protein peaks observed in the IMS experiment are then matched to those observed in the LC-MS/MS experiment.[146] In Chapter II, top-down proteomics was used to help match high mass accuracy MALDI protein imaging mass spectrometry data to LC-based identifications of intact proteins.[84, 85] While bulk tissue homogenization provides analyte-rich samples for downstream proteomics experiments, little to no spatial information is retained. This reduces the ability to confidently correlate protein signals from the IMS experiment to the protein identifications from the LC-MS/MS experiment.

One method that enables protein identification while still maintaining some level of spatial localization is laser capture microdissection (LCM), where sample regions are perforated with a laser and catapulted into a collection device for downstream analysis.[53-55] Depending on the focus of the laser and magnification power of the microscope, individual cells or cell types can be collected out of complex samples, such as tissue biopsies,[147] plants,[148] or even individual glomeruli.[149] Though ideal for targets smaller than a millimeter, LCM instrumentation can be cost-prohibitive, time-consuming, and require substrates compatible with the laser. Traditionally, large cell counts have been required to produce robust proteomics results.[57]

Within the last several years, several other extraction approaches have been developed to extract proteins from tissue sections while preserving localization. For example, liquid microextractions have proven successful for targeting distinct regions of tissue for a wide variety of analyte classes.[58,59] Approaches such as liquid extraction surface analysis (LESA) have the added benefit of automated sample extraction and processing[60], and can be coupled directly to the mass spectrometer for either top-down or bottom-up analyses.[62,150] In these types of experiments, the spatial limitation of the extraction is typically dictated by the physical characteristics of the liquid-sample interface, such as droplet diameter, contact angle, and surface tension.[151] Though research is ongoing to reduce the size of this effective footprint, most current applications have extraction diameters on the millimeter scale.

An alternative approach to direct liquid extractions or capture-based methods is the incorporation of hydrogel technologies into proteomic workflows.[64, 66] These polymer gels act as both a delivery system of reagents, such as enzymes, directly to the tissue sample, and a tool for localized analyte extraction. This allows for digestion and extraction to occur within one incubation period. Different iterations of hydrogels have been used in several biological applications, including both fresh frozen[64, 66, 152] and formalin-fixed, paraffin-embedded[65] (FFPE) samples. Hydrogels can be advantageous because of the relatively low-cost of the materials used in their preparation, straightforward use, and ability to perform diverse types of experiments in different areas of the same tissue section. Previous approaches have used hydrogels with diameters between 1-2 mm,[66, 152] which is similar in size to the areas sampled by liquid extractions.

**Methodologies for Hydrogel Comparisons & Analysis**

*Tissue Preparation and In-Solution Digests*

Fresh frozen rat livers were used because of their relatively large size compared to other organs, and due to the moderate homogeneity in terms of cell type and structure. As in chapters II and III, samples were sectioned at 12 µm and thaw-mounted onto microscope slides and dried in a desiccator for 30 minutes before washing with the Carnoy's solution protocol[96] to remove endogenous salts and lipids. For experiments utilizing discrete regions of tissue collected by biopsy punch for in-solution digests, tissues were cryostectioned in an identical manner as above. While the tissue section was still frozen in the cryostat, a 1.5 mm diameter biopsy punch was used to resect regions from the tissue, and the thin tissue punch was moved to an Eppendorf tube for in-solution digestion and analysis. For LCM collection, areas of washed tissue sections were collected in circular regions with diameters of 1.2 mm and 1.5 mm to equal the hydrogel and tissue punch diameters, respectively. Samples were collected into 20 µL of 100 mM ammonium bicarbonate in the cap of a PCR tube to ensure that the sample remained in the cap and did not fall back onto the surface.

Both LCM and tissue punch samples underwent in-solution digests modified from previous reports.[153] Briefly, the samples were suspended in solutions consisting of 10 µL TFE, 25 µL 0.1 µg/µL trypsin, and a total of 65 µL 100 mM ammonium bicarbonate. Only 45 µL of 100 mM ammonium bicarbonate was added to the LCM samples, as 20 µL was already present from the collection process. Samples were incubated at 37°C for 14 hours, dried using a centrifugal vacuum concentrator and then reconstituted in 0.1% TFA. Extracts were desalted and purified using $C_{18}$ ZipTips and analytes were eluted into new low-retention microcentrifuge

tubes. Samples were dried down and reconstituted in 10 µL 0.1% formic acid for LC-MS/MS analysis.

*Hydrogel Workflow*

Fabrication: Gels were cast as previously described by Nicklay et al.,[66] with modifications made to the manufacturer's gel formulation guidelines in order to achieve 7.5%, 10%, 12%, 15%, and 18% polyacrylamide gels. Briefly, 30% acrylamide/bis-acrylamide, 1.5M Tris (pH 8.7), and ddH$_2$O were combined in a vacuum flask and degassed under vacuum for 30 minutes with constant stirring. The solution was poured into a 60 x 15 mm polystyrene Petri dish and 10% ammonium persulfate and TEMED were added. The Petri dish was covered and gently swirled to ensure even mixing, then left to polymerize overnight. The resulting polymer had a measured thickness of ~1.7 mm. Biopsy punches of varying sizes (4, 3, 2, 1.5, 1, 0.75, and 0.5 mm) were used to fabricate hydrogels of different diameters. Individual hydrogels were collected in Eppendorf tubes and dried in a centrifugal vacuum concentrator for long-term storage at -80°C.

Placement and incubation: Tissue sections were brought to room temperature in a desiccator prior to hydrogel placement. Porcine trypsin was dissolved in 100 mM ammonium bicarbonate (pH 7.8) to produce concentrations of 0.01, 0.025, 0.1 or 1 µg/µL. Hydrogels were reswelled for 15 min in these trypsin solutions, except for the tissue blanks, which consisted of 7.5% and 18% polyacrylamide hydrogels swelled with 100 mM ammonium bicarbonate alone prior to placement. Hydrogels were placed on the tissue sections, ensuring minimal excess liquid and good contact with the tissue surface. Each experimental condition was repeated a minimum of three times to allow for statistical analysis. A subset of the trypsin-swelled 7.5% and 18% polyacrylamide hydrogels were placed directly on the microscope slide surface with no tissue

present to serve as trypsin blanks. All samples were placed in an incubation chamber[39, 96] containing 1 mL of 100 mM ammonium bicarbonate, sealed with lab tape, and incubated at 37°C for 14 hrs. Samples were removed from the incubation chamber and hydrogels were placed in Eppendorf tubes for analyte extraction.

Extraction from the hydrogels: Analytes were extracted using a modified version of a previous hydrogel extraction protocol,[66, 152] utilizing increasing organic solutions (50%, 60%, 80%, and 3x 95% ACN containing 5% formic acid) alternating with 100 mM ammonium bicarbonate. The organic solutions aided in solubilizing the extracted peptides as well as dehydrating the gels. Conversely, the ammonium bicarbonate rehydrated the gels, reswelling them in between organic steps. Each step had a 5 min incubation followed by centrifugation for 5 min at 6,610xg. The supernatants from each step were pooled into siliconized low-retention microcentrifuge tubes. Once the extraction process was completed, the combined supernatants were dried down using a centrifugal vacuum concentrator and reconstituted in 0.1% TFA. Extracts were desalted and purified using $C_{18}$ ZipTips and analytes were eluted into new low-retention microcentrifuge tubes. The samples were again dried and reconstituted in 10 µL 0.1% formic acid for LC-MS/MS analysis. For instrument reproducibility experiments, three hydrogel extracts (post ZipTip purification) were combined into one tube, dried down, and then reconstituted in 30 µL 0.1% formic acid for LC-MS/MS analysis.

*LC-Coupled Tandem Mass Spectrometry (HCD)*

Bottom-up analysis was performed using an Orbitrap Fusion Tribrid Mass Spectrometer (Thermo Scientific) coupled to an Easy-nLC 1000 (Thermo Fisher Scientific) ultrahigh pressure liquid chromatography (UHPLC) system. Peptides separation was achieved using a 75 µm inner

diameter, 25 cm long PepMap RSLC C18 column (2 µm, 100 Å, Acclaim) with a flow rate of 300 nL/min (mobile phase solvent A: 0.1% formic acid, 99.9% water; mobile phase solvent B: 0.1% formic acid, 99.9% acetonitrile). The LC gradient ran from 2-20%B in 100 min, 20-32%B in 20 min, 32-95%B in 1 min, 95%B for 4 min, 95-2%B for 2 min, and the column equilibrated at 2%B for 3 min. Following gradient-elution, peptides were ionized using nanoelectrospray ionization on a Nanospray Flex ion source (Thermo Fisher Scientific). The Orbitrap mass spectrometer was operated in a 3 second top speed data-dependent acquisition (DDA) mode. Fourier transform mass spectra (FTMS) were acquired at 120,000 resolution with an automated gain control (AGC) target of 200,000 and a maximum injection time of 50 ms. Precursor ions were filtered according to monoisotopic precursor assignment and charge state ($9 > z > 1$ required). Previously interrogated precursor ions were omitted using a dynamic exclusion window (30 s ± 10 ppm). Precursor ions for MS/MS analysis were isolated using a 1.5 *m/z* quadrupole mass filter isolation window and were fragmented with higher energy dissociation (HCD) using a normalized collision energy of 35%. Ion trap MS/MS spectra were collected using an AGC target of 1,000 and maximum injection time of 40 ms.

*Data Analysis*

Raw data files were converted to .mgf format by msConvert (ProteoWizard). Files were then searched against the Uniprot *Rattus norvegicus* proteome and processed using X! Tandem's GPM Cyclone web interface using the predefined Orbitrap (20 ppm) method. Methionine oxidations were included as potential modifications. Confident protein identifications were made with a 2 unique peptide threshold as well as an FDR of less than 2%. Statistical tests were subsequently performed on the data using Graphpad Prism software, including one-way

ANOVAs and Tukey's multiple comparison tests to assess significance at α=0.05 (95% confidence).
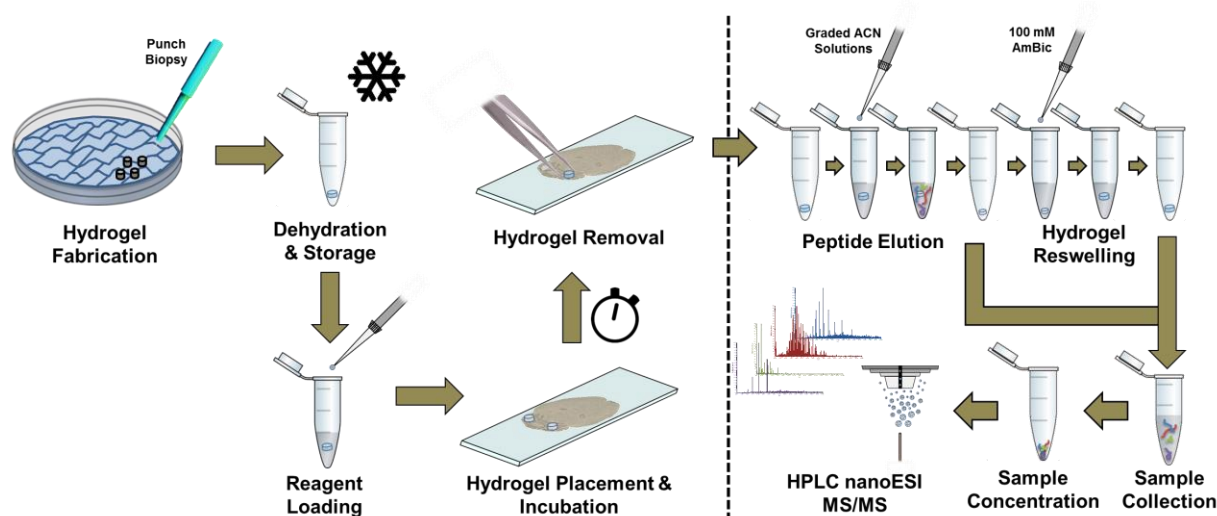


**Figure 4.1:** General hydrogel fabrication, usage, and extraction workflow. Hydrogels were fabricated in advance in large quantities and stored in cold temperatures to ensure minimal contamination or bacterial growth.

### Optimizing Trypsin Concentration for Efficient On-Tissue Digestion

Previous reports have used 1 µg/µL trypsin concentrations in hydrogels for successful digestion for proteomics experiments.[66, 154] This moderately high concentration of enzyme can be cost-prohibitive when performing many hydrogel experiments using proteomics-grade trypsin. Additionally, even with reductive methylation[155] and TPCK treatment[156] to reduce autolysis and non-specific cleavages, trypsin autolytic peaks are still present in concentration-dependent quantities as seen in Table 4.1 and Figure 4.2. These values encompass all tryptic peptide identifications, including multiple charge states of the same peptide, modified and unmodified forms of individual peptides, as well as peptides containing missed cleavages. Statistical

comparisons were performed to highlight the significant concentration dependence for autolytic peaks (Tables 4.2 & 4.3). Loading of the hydrogels with trypsin concentrations which maximize digestion yet minimize enzyme consumption and interference is important to the broad-scale adoption of this methodology.

| Trypsin Autolytic Peptides from Hydrogels with Different Trypsin Concentrations | | | | |
|---|---|---|---|---|
| *Trypsin Concentration (μg/μL)* | *n* | *Average* | *Variance* | *Std Deviation* |
| 0.01 | 3 | 19 | 16 | 4 |
| 0.025 | 3 | 19 | 17 | 4 |
| 0.1 | 3 | 51 | 49 | 7 |
| 1 | 3 | 199 | 247 | 16 |

**Table 4.1.** Average numbers of identified trypsin autolytic peptides from hydrogels with different trypsin concentrations. Hydrogels containing 1 μg/μL trypsin produced the highest number of autolytic trypsin peptide identifications.

| ANOVA for Trypsin Autolytic Peptides from Hydrogels with Different Trypsin Concentrations | | | | | | |
|---|---|---|---|---|---|---|
| *Source of Variation* | *Sum of Squares* | *df* | *Mean Square* | *F* | *P-value* | *F crit* |
| Between Groups | 6.68E+04 | 3 | 2.23E+04 | 270.0762 | 2.24E-08 | 4.0662 |
| Within Groups | 6.59E+02 | 8 | 8.24E+01 | | | |
| Total | 6.74E+04 | 11 | | | | |

**Table 4.2.** Analysis of variance (ANOVA) for numbers of identified trypsin autolytic peptides from hydrogels with different trypsin concentrations, confirming a statistically significant difference among the concentrations (F>F crit).

| Tukey's Multiple Comparison Test for Trypsin Autolytic Peptides from Hydrogels with Different Trypsin Concentrations | | | | | |
|---|---|---|---|---|---|
| *Trypsin Concentration (µg/µL)* | *Mean Diff.* | *q* | *Significant? P < 0.05?* | *Summary* | *95% CI of diff* |
| 0.01 vs 0.025 | 0.00E+00 | 0.000 | No | ns | -23.74 to 23.74 |
| 0.01 vs 0.1 | -3.23E+01 | 6.169 | Yes | * | -56.07 to -8.595 |
| 0.01 vs 1 | -1.80E+02 | 34.410 | Yes | *** | -204.1 to -156.6 |
| 0.025 vs 0.1 | -3.23E+01 | 6.169 | Yes | * | -56.07 to -8.595 |
| 0.025 vs 1 | -1.80E+02 | 34.410 | Yes | *** | -204.1 to -156.6 |
| 0.1 vs 1 | -1.48E+02 | 28.240 | Yes | *** | -171.7 to -124.3 |

**Table 4.3.** Tukey's multiple comparison test for numbers of identified trypsin autolytic peptides from hydrogels with different trypsin concentrations at the 0.05 significance level. ns: not significant; *: p≤0.05; **: p≤0.01; ***: p≤0.001
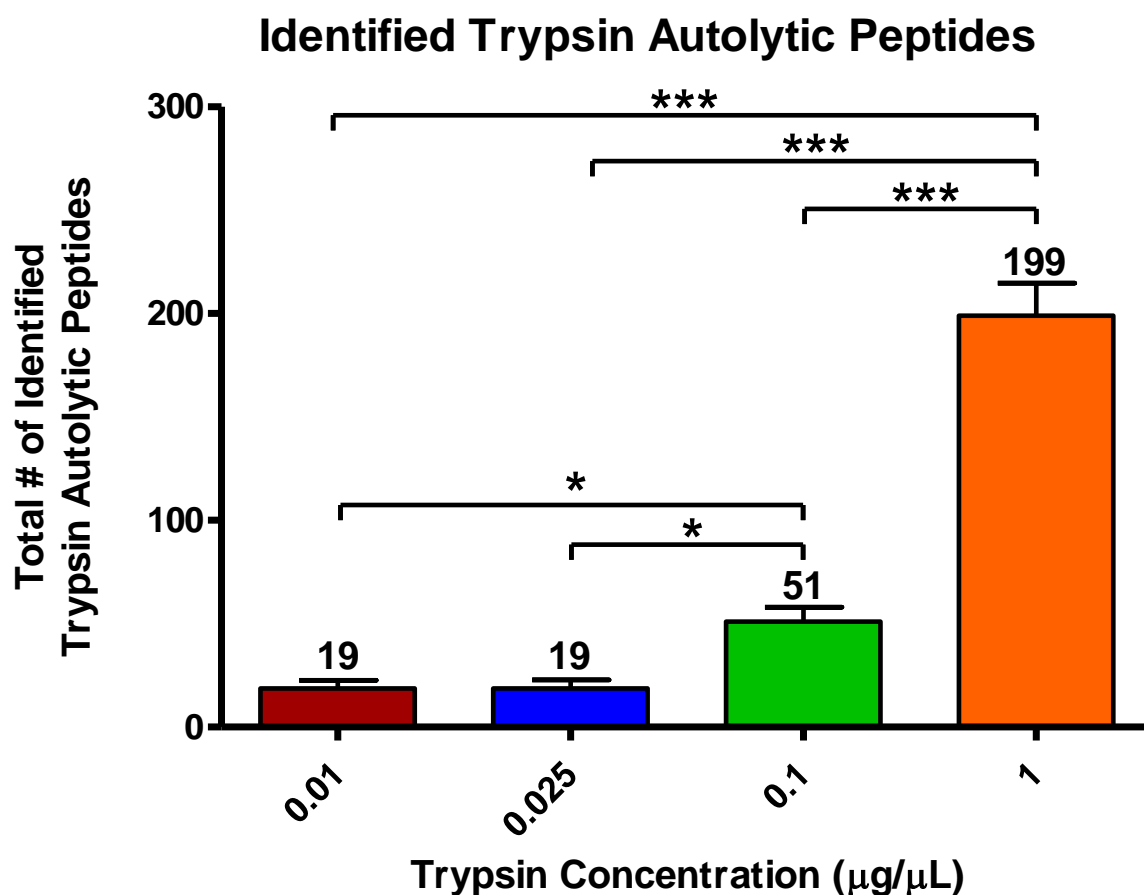


**Figure 4.2.** Average numbers of identified trypsin autolytic peptides from hydrogels with different trypsin concentrations. n=3 for each concentration of trypsin. *: p≤0.05; **: p≤0.01; ***: p≤0.001

When comparing the number of non-trypsin protein identifications and variances between the concentrations of trypsin (Tables 4.4 and 4.5), there are observed differences in the total number of protein identifications. However, they are not statistically significant for hydrogels containing 0.025, 0.1, and 1 µg/µL trypsin (1107 ± 10, 1114 ± 8, and 1075 ± 14 protein identifications, respectively) as seen in Table 4.6 and Figure 4.3. There was a significant decline in the number of identified proteins when the concentration was decreased to 0.01 µg/µL, with a total of 892 ± 84 protein identifications. This is most likely due to a non-optimal trypsin:analyte ratio, with decreased enzymatic efficiency experienced with both too much and too little enzyme.[157] Trypsin concentrations that are too low relative to the analyte concentration will result in incomplete digestion or missed cleavages, while too high of a ratio of trypsin could lead to non-specific digestion.[132] Hydrogels containing 0.1 µg/µL trypsin had the highest number of identified proteins with the lowest variances, and were used for all subsequent experiments.

| Protein Identifications from Hydrogels with Different Trypsin Concentrations | | | | |
|---|---|---|---|---|
| Trypsin Concentration (µg/µL) | n | Average | Variance | Std Deviation |
| 0.01 | 3 | 892 | 7077 | 84 |
| 0.025 | 3 | 1107 | 91 | 10 |
| 0.1 | 3 | 1114 | 69 | 8 |
| 1 | 3 | 1075 | 184 | 14 |

**Table 4.4.** Average numbers of protein identifications detected from hydrogels with different trypsin concentrations. Hydrogels containing 0.1 µg/µL trypsin produced the highest number of identifications with the lowest standard deviation.

| ANOVA for Protein Identifications from Hydrogels with Different Trypsin Concentrations | | | | | | |
|---|---|---|---|---|---|---|
| Source of Variation | Sum of Squares | df | Mean Square | F | P-value | F crit |
| Between Groups | 9.86E+04 | 3 | 3.29E+04 | 17.7085 | 6.83E-04 | 4.0662 |
| Within Groups | 1.48E+04 | 8 | 1.86E+03 | | | |
| Total | 1.13E+05 | 11 | | | | |

**Table 4.5.** Analysis of variance (ANOVA) for numbers of identified proteins from hydrogels with different trypsin concentrations, confirming a statistically significant difference among the concentrations (F>F crit).

| Tukey's Multiple Comparison Test for Protein Identifications from Hydrogels with Different Trypsin Concentrations | | | | | |
|---|---|---|---|---|---|
| Trypsin Concentration (µg/µL) | Mean Diff. | q | Significant? P < 0.05? | Summary | 95% CI of diff |
| 0.01 vs 0.025 | -2.15E+02 | 8.632 | Yes | ** | -327.3 to -102.0 |
| 0.01 vs 0.1 | -2.22E+02 | 8.927 | Yes | ** | -334.6 to -109.4 |
| 0.01 vs 1 | -1.83E+02 | 7.358 | Yes | ** | -295.6 to -70.37 |
| 0.025 vs 0.1 | -7.33E+00 | 0.295 | No | ns | -120.0 to 105.3 |
| 0.025 vs 1 | 3.17E+01 | 1.273 | No | ns | -80.97 to 144.3 |
| 0.1 vs 1 | 3.90E+01 | 1.568 | No | ns | -73.63 to 151.6 |

**Table 4.6.** Tukey's multiple comparison test for differences in identified proteins from hydrogels with different trypsin concentrations at the 0.05 significance level. ns: not significant; *: p≤0.05; **: p≤0.01; ***: p≤0.001
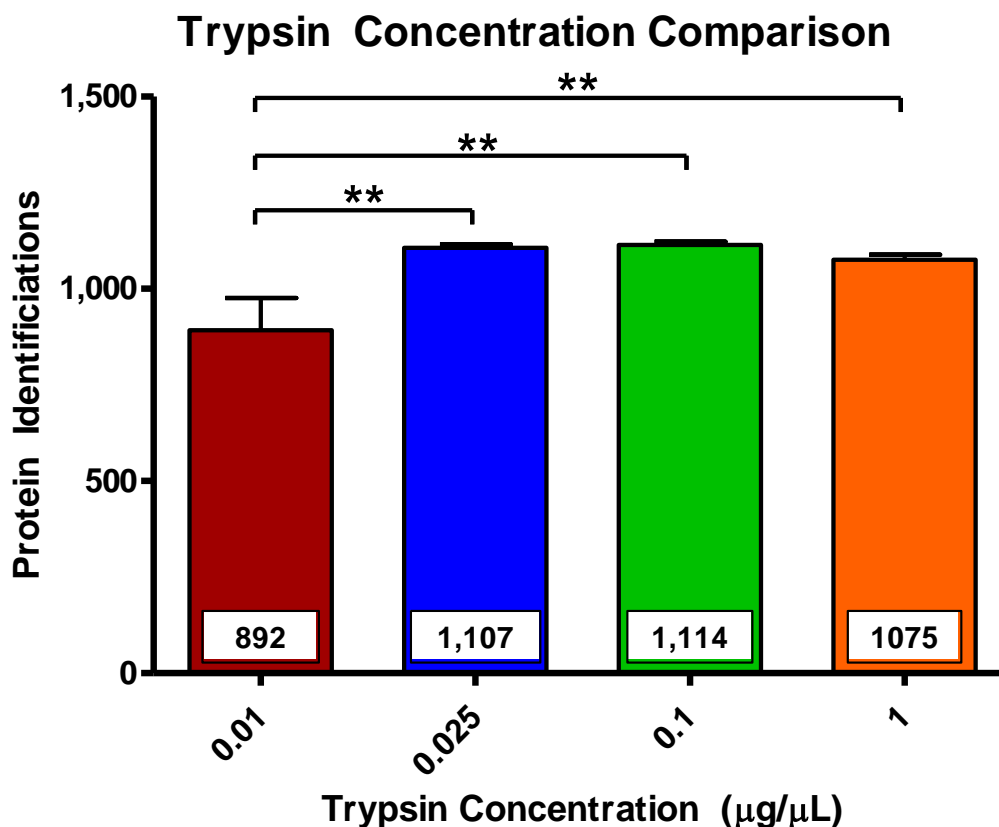


**Figure 4.3.** Average numbers of protein identifications from hydrogels containing different concentrations of trypsin. n=3 for each concentration of trypsin. *: p≤0.05; **: p≤0.01; ***: p≤0.001

### Increasing Polyacrylamide Percentages for Improved Hydrogel Rigidity

The percentage of polyacrylamide in a polymer solution can dictate many physical attributes, such as porosity, rigidity, and elasticity.[158] Of particular interest is how these factors affect the production and functionality of hydrogels in a proteomics workflow. Previous reports of hydrogel fabrications have utilized 7.5% polyacrylamide (37.5:1 monomer:crosslinker) to fabricate hydrogels, due mainly to its prevalence in the field of proteomic separations. Increasing

69

this percentage of polyacrylamide results in more rigid polymers, which are, in turn, more amenable to perforating individual hydrogels using punch biopsies. However, at higher percentages of polyacrylamide, analyte mobility may be hindered, preventing optimal extraction of proteins and peptides into the gel.[159]

Altering the percentage of polyacrylamide within the hydrogels according to Table 4.7 led to no statistical differences between the resulting numbers of protein identifications (Tables 4.8-4.10). All five percentages had approximately 1,200 confident identifications within the respective standard deviations, as seen in Figure 4.4.

| *% Acrylamide* | **7.5%** | **10%** | **12%** | **15%** | **18%** |
|---|---|---|---|---|---|
| 30% Acrylamide/Bis (mL) | 1.25 | 1.67 | 2.00 | 2.50 | 3.00 |
| 1.5 M Tris, pH 8.7 (mL) | 1.25 | 1.25 | 1.25 | 1.25 | 1.25 |
| ddH$_2$O (mL) | 2.48 | 2.06 | 1.73 | 1.23 | 0.73 |

**Table 4.7.** Gel formulation protocols for each polyacrylamide percentage. These solutions were degassed prior to polymerization with 50 μL 10% ammonium persulfate and 10 μL TEMED.

| **Protein Identifications from Hydrogels with Different Polyacrylamide Percentages** | | | | |
|---|---|---|---|---|
| *Percent Polyacrylamide* | *n* | *Average* | *Variance* | *Std Deviation* |
| 7.5% | 5 | 1195 | 748 | 27 |
| 10% | 3 | 1193 | 3634 | 60 |
| 12% | 4 | 1214 | 2185 | 47 |
| 15% | 3 | 1203 | 1010 | 32 |
| 18% | 5 | 1234 | 883 | 30 |

**Table 4.8.** Average numbers of protein identifications from hydrogels with different polyacrylamide percentages.

| ANOVA for Hydrogels with Different Polyacrylamide Percentages | | | | | | |
|---|---|---|---|---|---|---|
| *Source of Variation* | *Sum of Squares* | *df* | *Mean Square* | *F* | *P-value* | *F crit* |
| Between Groups | 5.01E+03 | 4 | 1.25E+03 | 0.8399 | 5.21E-01 | 3.0556 |
| Within Groups | 2.24E+04 | 15 | 1.49E+03 | | | |
| Total | 2.74E+04 | 19 | | | | |

**Table 4.9.** Analysis of variance (ANOVA) for numbers of protein identifications from hydrogels with different polyacrylamide percentages, confirming no statistically significant difference among the percentages (F<F crit).

| Tukey's Multiple Comparison Test for Hydrogels with Different Polyacrylamide Percentages | | | | | |
|---|---|---|---|---|---|
| *Percent Polyacrylamide (%)* | *Mean Diff.* | *q* | *Significant? P < 0.05?* | *Summary* | *95% CI of diff* |
| 7.5% vs 10% | 2.07E+00 | 0.104 | No | ns | -85.02 to 89.15 |
| 7.5% vs 12% | -1.89E+01 | 1.029 | No | ns | -98.84 to 61.14 |
| 7.5% vs 15% | -7.27E+00 | 0.364 | No | ns | -94.35 to 79.82 |
| 7.5% vs 18% | -3.86E+01 | 2.235 | No | ns | -114.0 to 36.82 |
| 10% vs 12% | -2.09E+01 | 1.003 | No | ns | -112.0 to 70.16 |
| 10% vs 15% | -9.33E+00 | 0.419 | No | ns | -106.7 to 88.03 |
| 10% vs 18% | -4.07E+01 | 2.039 | No | ns | -127.7 to 46.42 |
| 12% vs 15% | 1.16E+01 | 0.555 | No | ns | -79.49 to 102.7 |
| 12% vs 18% | -1.98E+01 | 1.078 | No | ns | -99.74 to 60.24 |
| 15% vs 18% | -3.13E+01 | 1.571 | No | ns | -118.4 to 55.75 |

**Table 4.10.** Tukey's multiple comparison test for differences in numbers of protein identifications from hydrogels with different polyacrylamide percentages at the 0.05 significance level. ns: not significant; *: $p \leq 0.05$; **: $p \leq 0.01$; ***: $p \leq 0.001$

## Percent Polyacrylamide Comparison
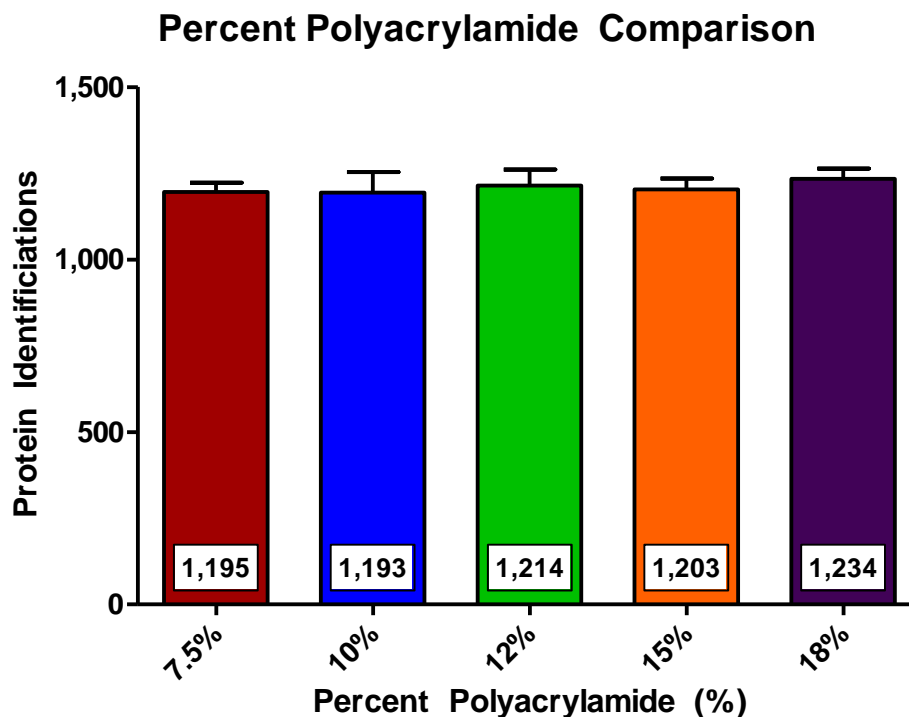


**Figure 4.4.** Average numbers of protein identifications from hydrogels with different polyacrylamide percentages. Each hydrogel was swelled with 0.1 µg/µL trypsin prior to placement. n≥3 for each concentration. No statistically significant differences were observed between the percentages of polyacrylamide hydrogels.

The molecular weight distributions of identified proteins were consistent for both the 7.5 and 18% polyacrylamide, with no observable mass bias as the percentage of polyacrylamide was increased (Table 4.11 and Figure 4.5). This supports the hypothesis that even though the porosity of the hydrogel decreases with increasing percentages of polyacrylamide, the resulting analyte extraction of peptides is unhindered. These distributions closely mirror that of the rat proteome, confirming relatively even proteomic sampling from the tissue. Since the 18% polyacrylamide hydrogels yielded similar numbers of protein identifications when compared to the traditional 7.5% polyacrylamide hydrogels, the 18% gels were chosen to fabricate all subsequent hydrogels because of the ability to more easily and reproducibly prepare the hydrogels.

| Molecular Weight | 7.5% Polyacrylamide | | | 18% Polyacrylamide | | | Rat Proteome |
|---|---|---|---|---|---|---|---|
| Bins (Da) | *Average* | *Variance* | *Std Deviation* | *Average* | *Variance* | *Std Deviation* | |
| <1,000 | 0.00% | 0.0000% | 0.00% | 0.00% | 0.0000% | 0.00% | 0.00% |
| 1,000 | 0.00% | 0.0000% | 0.00% | 0.00% | 0.0000% | 0.00% | 0.01% |
| 5,000 | 0.03% | 0.0001% | 0.08% | 0.03% | 0.0000% | 0.05% | 0.53% |
| 10,000 | 1.27% | 0.0001% | 0.12% | 1.25% | 0.0005% | 0.23% | 2.14% |
| 15,000 | 4.67% | 0.0003% | 0.18% | 4.64% | 0.0002% | 0.15% | 6.03% |
| 20,000 | 5.59% | 0.0002% | 0.14% | 5.67% | 0.0001% | 0.11% | 6.57% |
| 40,000 | 32.85% | 0.0050% | 0.71% | 33.00% | 0.0017% | 0.41% | 31.46% |
| 60,000 | 27.11% | 0.0036% | 0.60% | 27.10% | 0.0005% | 0.23% | 20.67% |
| 75,000 | 10.22% | 0.0007% | 0.27% | 10.16% | 0.0004% | 0.19% | 9.21% |
| 100,000 | 7.91% | 0.0012% | 0.35% | 7.97% | 0.0004% | 0.19% | 9.70% |
| 150,000 | 6.51% | 0.0012% | 0.35% | 6.35% | 0.0005% | 0.21% | 8.24% |
| 200,000 | 1.68% | 0.0010% | 0.32% | 1.86% | 0.0009% | 0.31% | 2.73% |
| 500,000 | 1.94% | 0.0004% | 0.21% | 1.72% | 0.0012% | 0.34% | 2.53% |
| >500,000 | 0.22% | 0.0000% | 0.05% | 0.24% | 0.0000% | 0.06% | 0.17% |

**Table 4.11.** Molecular weight bins of protein identifications from 7.5% and 18% polyacrylamide hydrogels and the Uniprot Rat Proteome. Both 7.5% and 18% polyacrylamide hydrogels were used to ensure there was no bias among polyacrylamide percentages.
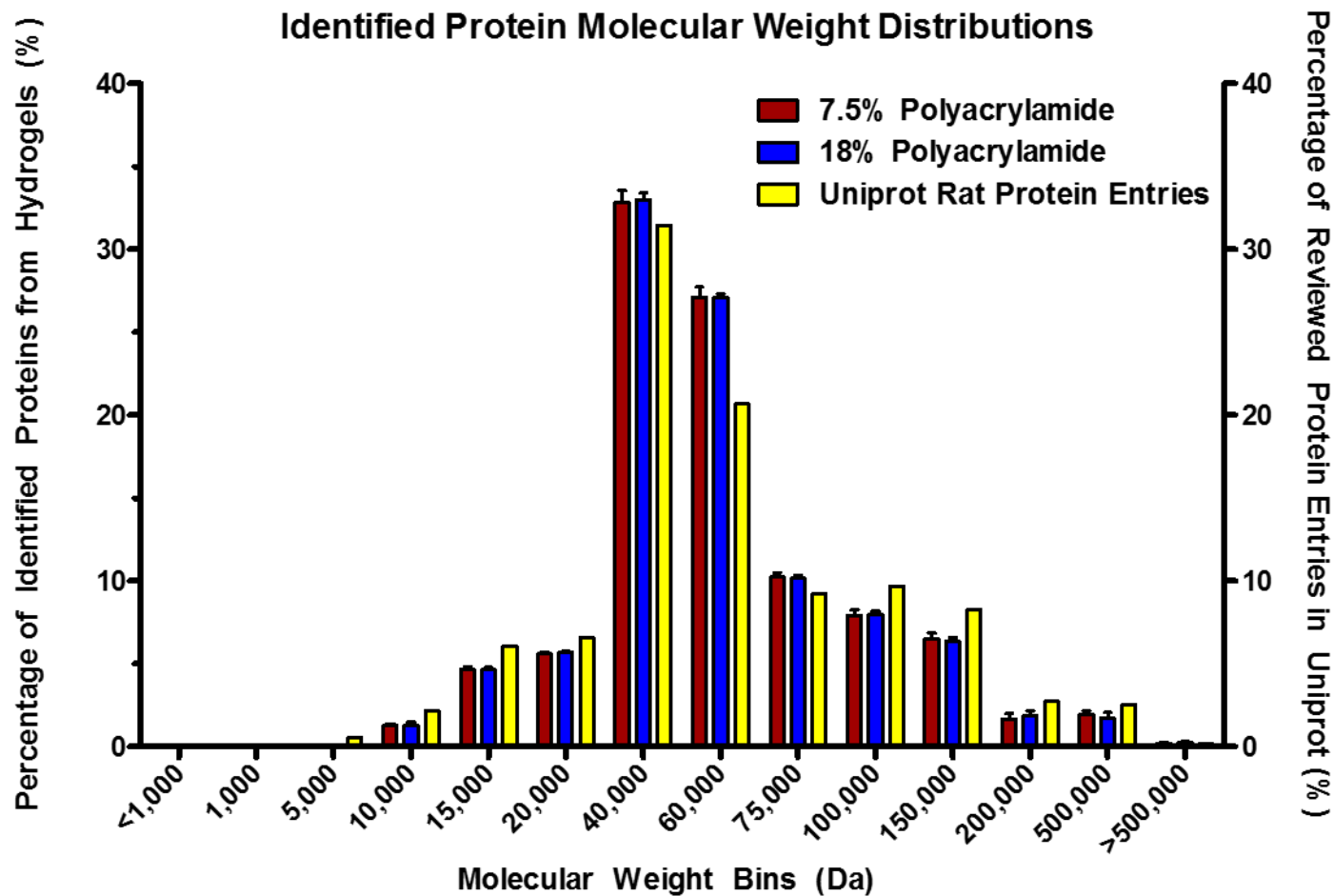
**Figure 4.5.** Molecular weight distributions of protein identifications from 7.5% and 18% polyacrylamide hydrogels and the reviewed protein identifications in the Uniprot rat protein database. Masses of identified proteins were binned for the 7.5% (red) and 18% (blue) polyacrylamide hydrogels (left axis), as well as the UniProt rat proteome (yellow – right axis). n=5 for both of the hydrogel conditions.

In order to ensure that the variability in protein identifications were not due to background interferences, a series of controls were investigated (Table 4.12). Five replicates of 7.5% and 18% polyacrylamide hydrogels containing no trypsin (tissue blanks) were examined to assess endogenous peptide extraction from tissue. No confident identifications were consistently made for the 7.5% polyacrylamide hydrogels, while the 18% polyacrylamide hydrogels produced statistically insignificant numbers of identifications ($74 \pm 84$ confident proteins).  Additionally, hydrogels swelled with trypsin and placed directly onto the microscope slide were used to gauge sample preparation contamination, such as analyte delocalization caused by tissue washes. The 7.5% polyacrylamide hydrogels did produce a number of protein identifications, though largely inconsistent. Conversely, the 18% polyacrylamide hydrogels resulted in negligible identifications. No over-arching trends were observed for either set of blanks, supporting the hypothesis that variations in protein identifications were due to the experimental conditions rather than any background interferences.

| Protein Identifications from Control (Blank) Hydrogels | | | | |
|---|---|---|---|---|
| Control (Blank) | n | Average | Variance | Std Deviation |
| 7.5%  Polyacrylamide - No Tissue | 3 | 148 | 3884 | 62 |
| 18% Polyacrylamide - No Tissue | 3 | 0 | 0 | 1 |
| 7.5%  Polyacrylamide - No Trypsin | 5 | 0 | 0.3 | 1 |
| 18% Polyacrylamide - No Trypsin | 5 | 74 | 6986.7 | 84 |

**Table 4.12.** Average numbers of protein identifications from control (blank) hydrogels. Both 7.5% and 18% polyacrylamide hydrogels were used to ensure there was no bias among polyacrylamide percentages. Tissue blanks were hydrogels swelled in 100 mM ammonium bicarbonate and incubated on tissue (no trypsin). Trypsin blanks were hydrogels swelled in trypsin solutions, but placed directly onto the microscope slide (no tissue).
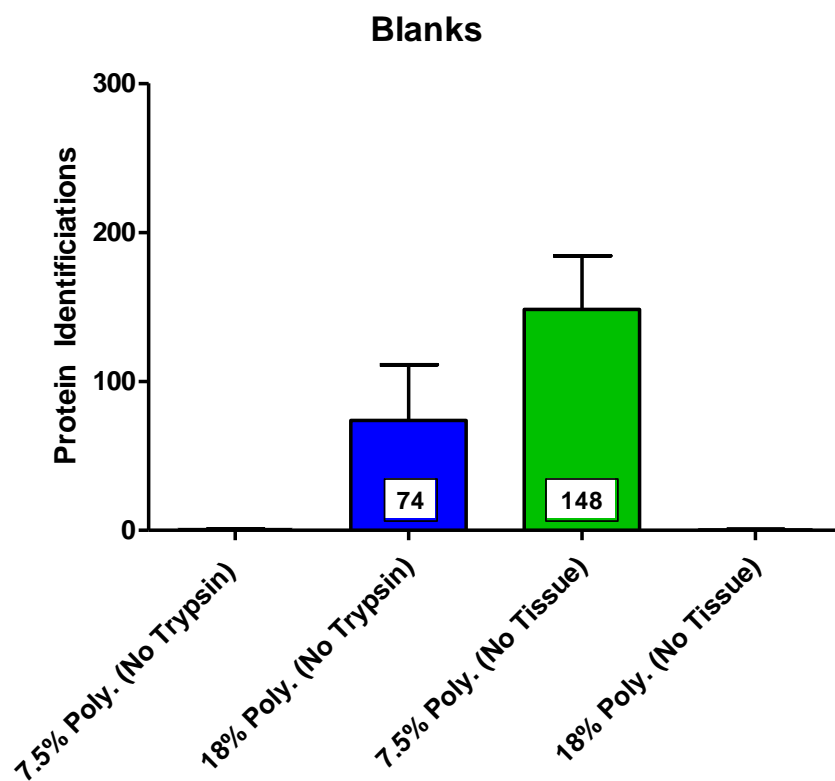


**Figure 4.6.** Average numbers of protein identifications from control (blank) hydrogels. Both 7.5% and 18% polyacrylamide hydrogels were used to ensure there was no bias among polyacrylamide percentages. Tissue blanks were hydrogels swelled in 100 mM ammonium bicarbonate and incubated on tissue (no trypsin). Trypsin blanks were hydrogels swelled in 0.1 μg/μL trypsin solutions, but placed directly onto the microscope slide (no tissue). n=5 for tissue blanks (no trypsin) and n=3 for trypsin blanks (no tissue).

Instrument reproducibility was also assessed to confirm minimal instrument bias between analytical runs. Any discrepancies in liquid chromatographic separation or mass spectrometric acquisition would be observed from technical replicates of a single sample. The number of protein identifications from this triplicate analysis was highly reproducible, resulting in an average of 1,072 confident identifications with a standard deviation of only five proteins, as seen in Table 4.13 and Figure 4.7. When comparing the actual protein identifications, there was a great deal of overlap between the replicates, again highlighting the reproducibility of the analysis (Figure 4.8). A total of 860 proteins were identified in the three replicate runs, which accounts for 63.9% of all protein identifications. An additional 149 proteins were identified in any two of the three runs, or 11% of the protein identifications. This meant that only 25% of the identifications were only observed in a single replicate run.

| Protein Identifications from Technical Replicate Runs of a Hydrogel Extract | | | | | |
|---|---|---|---|---|---|
| Replicate 1 | Replicate 2 | Replicate 3 | *Average* | *Variance* | *Std Deviation* |
| 1071 | 1077 | 1067 | 1072 | 25 | 5 |

**Table 4.13.** Average number of protein identifications from the analysis of a technical replicate experiment repeated three times. Three hydrogel extracts (18% polyacrylamide, 3 mm biopsy punch) were pooled together and diluted three-fold to achieve a total concentration comparable to a single hydrogel experiment. This solution was analyzed three times and the protein identification numbers were compared. The methods appear to be highly reproducible, with an average of $1072 \pm 5$ identified proteins.

**Technical Replicate Comparison**
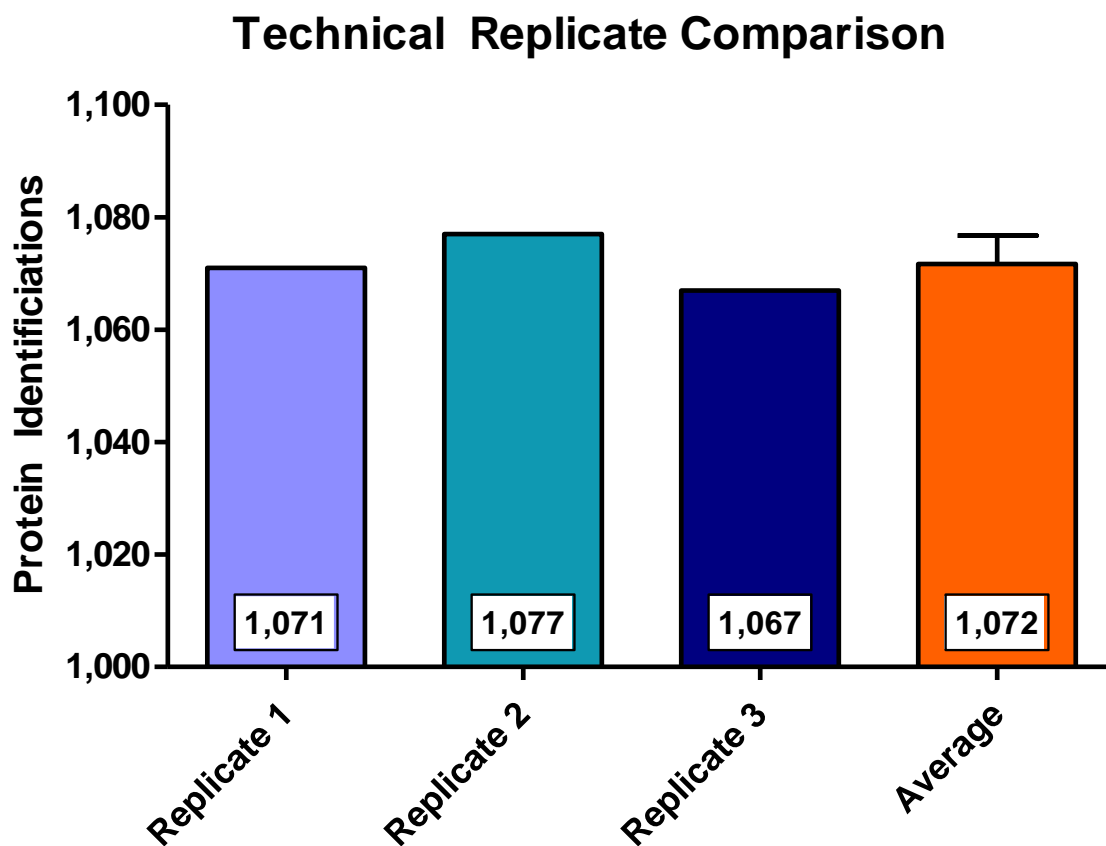
**Figure 4.7.** Average number of protein identifications from the analysis of a technical replicate experiment repeated three times. Reproducibility of the HPLC-MS/MS methods and instrumentation were assessed. Three hydrogel extracts (18% polyacrylamide, 3 mm biopsy punch) were pooled together and diluted three-fold to achieve a total concentration comparable to a single hydrogel experiment. This solution was analyzed three times and the protein identification numbers were compared. The methods appear to be highly reproducible, with an average of $1072 \pm 5$ identified proteins.
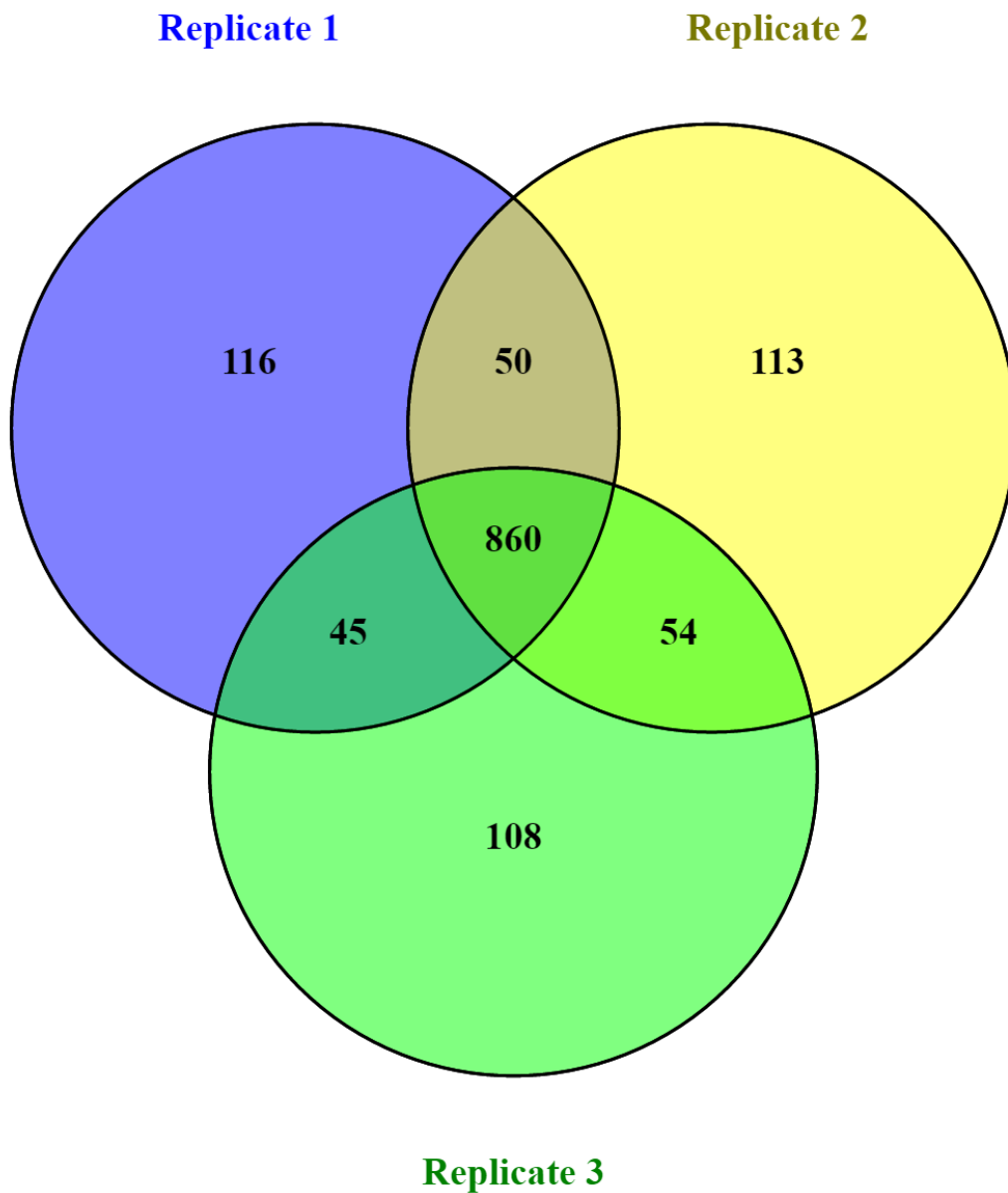
**Figure 4.8.** Venn diagram of protein identifications from the three hydrogel replicates. Over 60% of the identified proteins were found in all three hydrogels (860 protein identifications), and this number increases to ~75% if proteins identified in any two out of the three runs are considered (1,009 protein identifications). Only ~8% of the identifications from each replicate run were unique and not found in the other runs.

**Fabricating Smaller Hydrogels for More Localized Analyte Extraction**

Ten hydrogels were fabricated using 4, 3, 2, 1.5, 1, 0.75, and 0.5 mm biopsy punches, and the resulting hydrogel diameters were measured using a microscope (Table 4.14 and Figure 4.9). Although the hydrogels did not have the same diameter as the biopsy punches used to fabricate them, the standard deviations were <250 μm for each measurement group. The discrepancy between the punch diameter and the hydrogel diameter can be attributed to the ductile properties of the gel, causing distortion during the perforation process. This was only minimally observed at larger dimensions, with hydrogel diameters measuring >75% of the punch diameter for the 4, 3, 2, 1.5, and 1 mm biopsy punches. However, utilizing the 0.75 and 0.5 mm biopsy punches resulted in reproducible hydrogel diameters of 357 and 259 μm respectively, which is ~50% of the biopsy punch diameters.

| Diameter Measurements of Hydrogels Fabricated with Different Biopsy Punch Diameters | | | | | | | |
|---|---|---|---|---|---|---|---|
| Punch Biopsy Diameter (mm) | 4 | 3 | 2 | 1.5 | 1 | 0.75 | 0.5 |
| Hydrogel Diameter Measurement 1 (μm) | 3841.82 | 2377.81 | 1691.71 | 1306.00 | 793.98 | 335.54 | 350.67 |
| Hydrogel Diameter Measurement 2 (μm) | 3828.62 | 2337.26 | 1833.46 | 1353.32 | 811.13 | 388.52 | 397.20 |
| Hydrogel Diameter Measurement 3 (μm) | 3863.37 | 2477.06 | 1293.73 | 1284.28 | 876.03 | 374.44 | 275.60 |
| Hydrogel Diameter Measurement 4 (μm) | 4042.53 | 2577.23 | 1443.58 | 1251.36 | 781.31 | 397.98 | 303.59 |
| Hydrogel Diameter Measurement 5 (μm) | 4013.39 | 2517.99 | 1554.02 | 1317.16 | 737.70 | 341.40 | 267.69 |
| Hydrogel Diameter Measurement 6 (μm) | 3934.26 | 2393.63 | 1764.33 | 1135.85 | 765.36 | 271.01 | 204.14 |
| Hydrogel Diameter Measurement 7 (μm) | 3704.35 | 2860.60 | 1583.74 | 1133.80 | 700.42 | 343.89 | 219.31 |
| Hydrogel Diameter Measurement 8 (μm) | 3939.23 | 2715.70 | 1764.33 | 955.47 | 674.80 | 390.22 | 217.87 |
| Hydrogel Diameter Measurement 9 (μm) | 3990.17 | 2932.39 | 1919.14 | 1013.83 | 808.63 | 335.54 | 177.98 |
| Hydrogel Diameter Measurement 10 (μm) | 3994.13 | 2928.34 | 1813.09 | 1281.62 | 812.09 | 388.52 | 180.12 |
| *Average* | 3915.19 | 2611.80 | 1666.11 | 1203.27 | 776.15 | 356.71 | 259.42 |
| *Variance* | 10963.26 | 53505.39 | 37902.15 | 18635.68 | 3498.97 | 1533.67 | 5433.66 |
| *Std Deviation* | 104.71 | 231.31 | 194.68 | 136.51 | 59.15 | 39.16 | 73.71 |

**Table 4.14.** Average diameter measurements of hydrogels fabricated with different diameters biopsy punches. Ten measurements were recorded for each biopsy punch diameter.

**(a)**

**Hydrogel Diameter Reproducibility**

**(b)**

| Hydrogel Image (4x) | Average Hydrogel Size (± Std. Dev.) n=10 |
|---|---|
| | 3,915 ± 105 µm |
| | 2,612 ± 231 µm |
| | 1,666 ± 195 µm |
| | 1,203 ± 137 µm |
| | 776 ± 59 µm |
| | 357 ± 39 µm |
| 1 mm | 259 ± 73 µm |
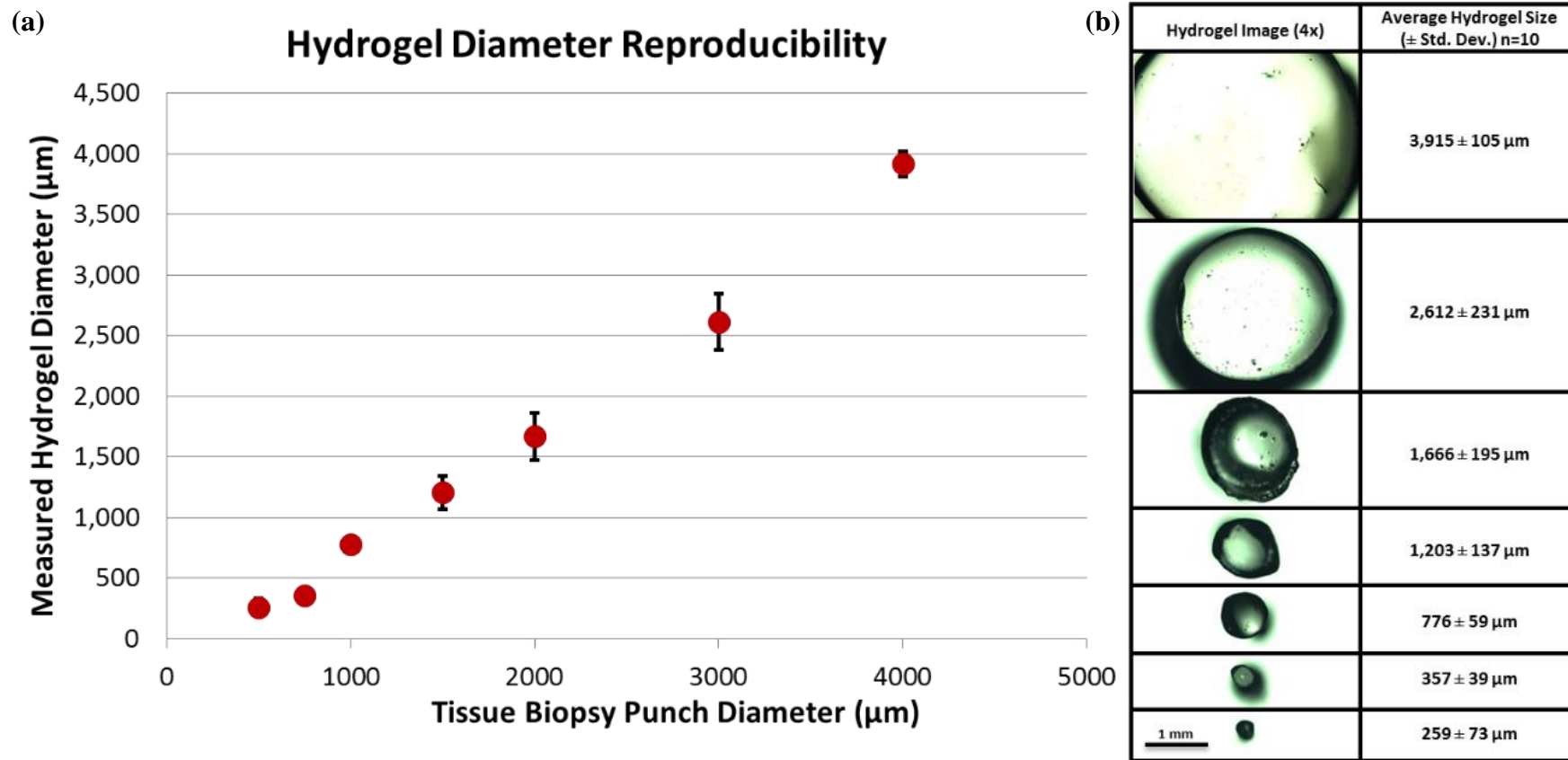
**Figure 4.9.** Measured diameters of 18% polyacrylamide hydrogels fabricated with different diameter biopsy punches. (a) A graph of the biopsy punch diameters vs. measured hydrogel diameters. n=10 for each measurement and the standard deviation is plotted. (b) Optical images of each hydrogel size as well as the measured diameters and standard deviation for each measurement. Scale bar: 1 mm.

In order to test the utility of these smaller diameter hydrogels, hydrogels fabricated from biopsy punches with diameters of 2, 1.5, 1, 0.75, and 0.5 mm were investigated. As the diameter of the biopsy punch decreased, ultimately decreasing the fabricated hydrogel diameter, the number of protein identifications showed a similar trend (Table 4.15-4.17). The 2 mm biopsy punch hydrogels resulted in 1,052 identifications with a standard deviation of only 7 identifications. The standard deviations for the 1.5, 1, 0.75, and 0.5 mm biopsy punches were higher, with standard deviations of 77, 56, 78, and 56 identifications, respectively. However, even the smallest diameter hydrogels still provided 671 confident protein identifications. (Figure 4.10a). To ensure the hydrogels were only sampling from the tissue directly beneath them, the tissue sections were H&E stained post-hydrogel removal. Figure 4.10b shows the result of a 259 μm diameter hydrogel digestion on a rat liver section with the surrounding tissue largely undisturbed from the digestion and extraction process. The vast majority of the signal is therefore derived only from cells being sampled under the hydrogels.

| Protein Identifications from Hydrogels Fabricated with Different Biopsy Punch Diameters | | | | |
|---|---|---|---|---|
| *Biopsy Punch Diameter (mm)* | *Count* | *Average* | *Variance* | *Std Deviation* |
| 0.5 | 3 | 671 | 3163 | 56 |
| 0.75 | 4 | 708 | 6065 | 78 |
| 1 | 3 | 827 | 3082 | 56 |
| 1.5 | 3 | 902 | 5869 | 77 |
| 2 | 3 | 1052 | 43 | 7 |

**Table 4.15.** Average numbers of protein identifications from hydrogels fabricated with different diameter biopsy punches. Hydrogels containing 0.1 μg/μL trypsin produced the highest number of identifications with the lowest standard deviation.

| ANOVA for Hydrogels Fabricated with Different Biopsy Punch Diameters | | | | | | |
|---|---|---|---|---|---|---|
| *Source of Variation* | *Sum of Squares* | *df* | *Mean Square* | *F* | *P-value* | *F crit* |
| Between Groups | 2.98E+05 | 4 | 7.46E+04 | 19.2963 | 6.20E-05 | 3.3567 |
| Within Groups | 4.25E+04 | 11 | 3.86E+03 | | | |
| Total | 3.41E+05 | 15 | | | | |

**Table 4.16.** Analysis of variance (ANOVA) for numbers of protein identifications from hydrogels fabricated with different diameter biopsy punches, confirming a statistically significant difference among the diameters (F>F crit).

| Tukey's Multiple Comparison Test for Hydrogels Fabricated with Different Biopsy Punch Diameters | | | | | |
|---|---|---|---|---|---|
| *Biopsy Punch Diameter (mm)* | *Mean Diff.* | *q* | *Significant? P < 0.05?* | *Summary* | *95% CI of diff* |
| 0.5 vs 0.75 | -3.70E+01 | 1.102 | No | ns | -190.6 to 116.6 |
| 0.5 vs 1 | -1.56E+02 | 4.337 | No | ns | -319.8 to 8.497 |
| 0.5 vs 1.5 | -2.31E+02 | 6.436 | Yes | ** | -395.2 to -66.84 |
| 0.5 vs 2 | -3.81E+02 | 10.620 | Yes | *** | -545.2 to -216.8 |
| 0.75 vs 1 | -1.19E+02 | 3.535 | No | ns | -272.2 to 34.89 |
| 0.75 vs 1.5 | -1.94E+02 | 5.779 | Yes | * | -347.6 to -40.44 |
| 0.75 vs 2 | -3.44E+02 | 10.250 | Yes | *** | -497.6 to -190.4 |
| 1 vs 1.5 | -7.53E+01 | 2.099 | No | ns | -239.5 to 88.83 |
| 1 vs 2 | -2.25E+02 | 6.278 | Yes | ** | -389.5 to -61.17 |
| 1.5 vs 2 | -1.50E+02 | 4.179 | No | ns | -314.2 to 14.16 |

**Table 4.17.** Tukey's multiple comparison test for differences in numbers of protein identifications from hydrogels fabricated with different diameter biopsy punches at the 0.05 significance level. ns: not significant; *: p≤0.05; **: p≤0.01; ***: p≤0.001
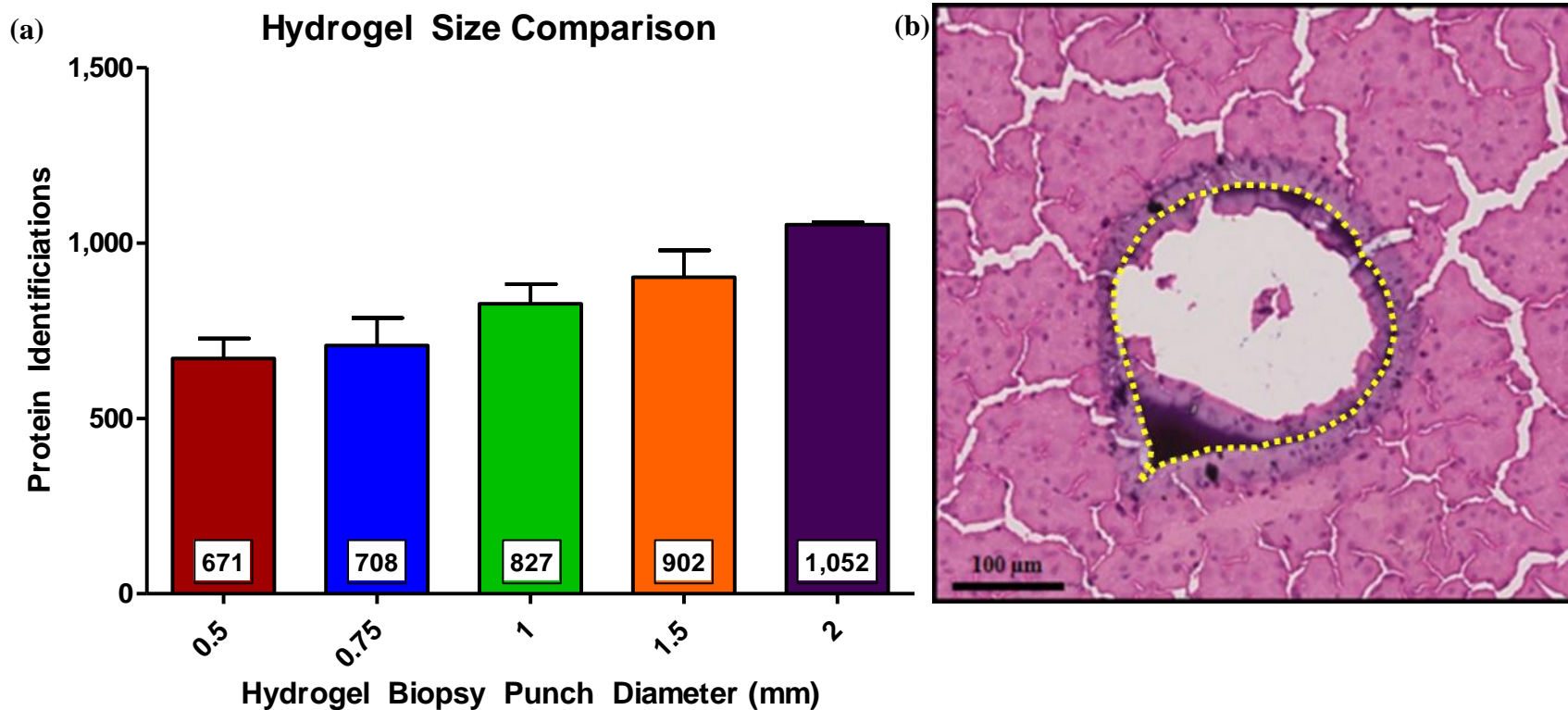
**Figure 4.10.** Evaluating the utility and effectiveness of smaller diameter hydrogels in a proteomics workflow. (a) Average number of protein identifications detected from 18% polyacrylamide hydrogels fabricated with different diameter biopsy punches all containing 0.1 µg/µL trypsin. n≥3 for each size. (b) H&E-stained tissue section after a 260 µm diameter hydrogel (0.5 mm biopsy punch) was removed. The outline of the hydrogel is represented by the yellow dotted line. Scale bar: 100 µm.

An approximate calculation was performed to assess the number of cells beneath a 259 μm diameter hydrogel, defined by the ratio of the surface area of the hydrogel to the surface area of a eukaryotic cell (conservatively estimated to be 10 μm in diameter[160]):

$$\pi r^2 = A$$
$$\pi(\frac{259\mu m}{2})^2 = 5.27x\ 10^4 \mu m^2$$

$$\pi r^2 = A$$
$$\pi(\frac{10\mu m}{2})^2 = 78.5\ \mu m^2$$

$$\frac{5.27x\ 10^4\ \mu m^2\ hydrogel\ area}{78.5\ \mu m^2\ cell\ area} = 671\ cells$$

Though this calculation makes assumptions about the circular shape of both hydrogels and cells, the approximation provides general context for the protein yields from such small sample areas. Comparatively, LCM-based protocols traditionally recommend cell counts at least an order of magnitude higher for robust protein-based analyses.[57]

### Comparison of Sample Collection Methods

A direct comparison of hydrogel-mediated protein identifications to both LCM and tissue homogenization methodologies was performed to validate the hydrogel approaches against existing methods. A biopsy punch with a diameter of 1.5 mm was used to fabricate hydrogels with a resulting diameter of ~1.2 mm. The same diameter biopsy punch was used to perforate 12 μm-thick tissue sections and place the 1.5 mm tissue punches into individual Eppendorf tubes. To account for the discrepancy between the diameters of the hydrogel and the tissue punches,

LCM was used to collect circular regions at diameters of both 1.2 and 1.5 mm. The hydrogels were incubated on-tissue, while the LCM and tissue punch digestions were incubated for the same amount of time in-solution.

| Protein Identifications from Different Sample Collection Methods | | | | |
|---|---|---|---|---|
| Sample Collection Methods | Count | Average | Variance | Std Deviation |
| 1.2mm LCM | 3 | 708 | 272 | 17 |
| 1.5mm LCM | 3 | 764 | 4033 | 64 |
| 1.2mm Hydrogel | 3 | 902 | 5869 | 77 |
| 1.5mm Tissue Punch | 3 | 889 | 320 | 18 |

**Table 4.18.** Average numbers of protein identifications from different sample collection methods. The 1.2 mm diameter hydrogel and 1.5 mm diameter tissue punch yielded the highest number of identifications.

| ANOVA for Different Sample Collection Methods | | | | | | |
|---|---|---|---|---|---|---|
| Source of Variation | Sum of Squares | df | Mean Square | F | P-value | F crit |
| Between Groups | 8.13E+04 | 3 | 2.71E+04 | 10.3305 | 3.99E-03 | 4.0662 |
| Within Groups | 2.10E+04 | 8 | 2.62E+03 | | | |
| Total | 1.02E+05 | 11 | | | | |

**Table 4.19.** Analysis of variance (ANOVA) for numbers of protein identifications from different sample collection methods, confirming a statistically significant difference among the methods (F>F crit).

| Tukey's Multiple Comparison Test for Different Sample Collection Methods | | | | | |
|---|---|---|---|---|---|
| Sample Collection Method | Mean Diff. | q | Significant? P < 0.05? | Summary | 95% CI of diff |
| 1.2mm LCM vs 1.5mm LCM | -5.53E+01 | 1.871 | No | ns | -189.3 to 78.60 |
| 1.2mm LCM vs 1.2mm Hydrogel | -1.94E+02 | 6.549 | Yes | ** | -327.6 to -59.73 |
| 1.2mm LCM vs 1.5mm Tissue Punch | -1.81E+02 | 6.120 | Yes | * | -314.9 to -47.06 |
| 1.5mm LCM vs 1.2mm Hydrogel | -1.38E+02 | 4.678 | Yes | * | -272.3 to -4.396 |
| 1.5mm LCM vs 1.5mm Tissue Punch | -1.26E+02 | 4.249 | No | ns | -259.6 to 8.271 |
| 1.2mm Hydrogel vs 1.5mm Tissue Punch | 1.27E+01 | 0.428 | No | ns | -121.3 to 146.6 |

**Table 4.20.** Tukey's multiple comparison test for differences in numbers of protein identifications from different sample collection methods at the 0.05 significance level. ns: not significant; *: p≤0.05; **: p≤0.01; ***: p≤0.001
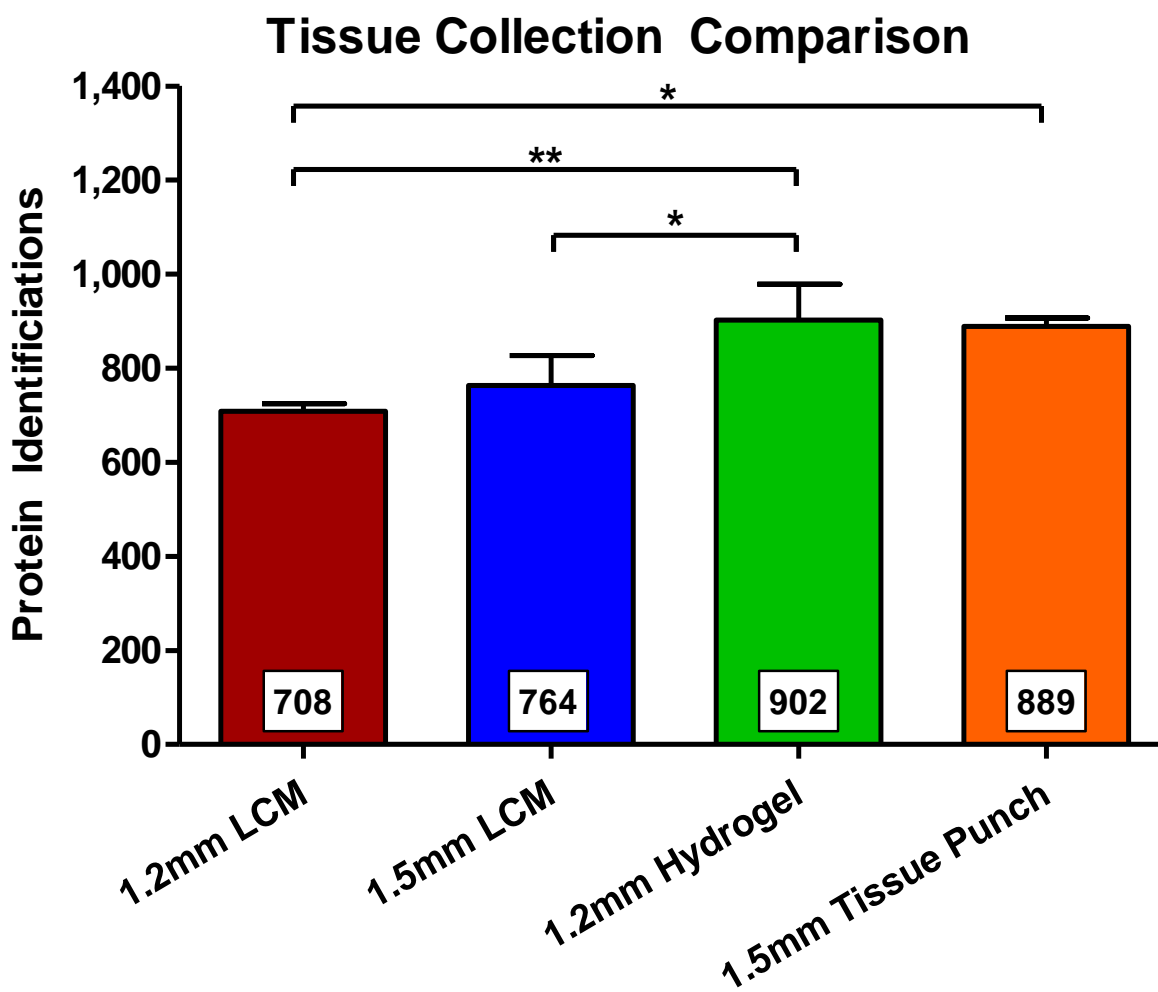
**Figure 4.11.** Average numbers of protein identifications from different sample collection methods. Circular tissue regions with diameters of 1.2 and 1.5 mm were collected by LCM. A 1.5 mm biopsy punch was used to collect circular regions of tissue and perform in-solution digests in parallel to LCM experiments. Hydrogels with diameters of 1.2 mm were placed on serial tissue sections and incubated for the same period of time as the in-solution digests. n=3 for each method. ns: not significant; *: p≤0.05; **: p≤0.01; ***: p≤0.001

Compared to the tissue punch method, which requires separate collection and incubation steps, the hydrogel digestion/extraction process yielded statistically similar results as seen in Tables 4.18-4.20 and Figure 4.11 (889 ± 18 and 902 ± 77 protein identifications, respectively). Though manual manipulation of hydrogels may prove challenging with smaller diameter gels, a tissue punch of the same diameter would inherently prove to be more difficult.

The 1.2 mm hydrogel outperformed both the 1.2 mm and 1.5 mm LCM experiments, which had 708 ± 17 and 764 ± 64 identifications. The decreased number of protein identifications from the LCM process relative to the other methods is most likely due to sample loss during the catapulting process of the sample into the collection apparatus. Though robust, this transfer method is not 100% efficient, as seen by particulates falling back down onto the sample between laser pulses. This, compounded by the high cost of equipment, potentially long collection times, and separate digestion steps, highlights an advantage of the hydrogel technologies.

### Differential Proteomic Analysis of Rat Cerebellum Substructures

The need for spatially-directed proteomic analyses is particularly useful for spatially heterogeneous tissue samples with many different cell types. These can include organ substructures,[31, 161] the interface between a host and infectious agents,[146, 162] or the infiltration of diseased tissue, such as a cancerous growth, into surrounding healthy tissue.[71, 94, 163, 164] The rat cerebellum is a simple example that has many distinct layers comprising the tissue, including the white matter, granule layer, and molecular layer.

Hydrogels were fabricated with a 1 mm diameter biopsy punch and placed on either the white matter or the molecular layer, designated by the circles in Figure 4.12a. These hydrogels

were placed less than 1 mm away from each other to highlight the ability of hydrogel technologies to perform independent experiments in close spatial proximity. LC-MS/MS experiments showed that while there was a great deal of overlap between the identified proteins from each region, the white matter had 272 unique proteins and the molecular layer had 174 unique proteins (Figure 4.12b). The top ten unique protein identifications based on X! Tandem rankings for each hydrogel are listed in Table 4.21.

| | Accession | Description |
|---|---|---|
| **White Matter** | TBA1_RAT | Tubulin alpha-1A chain |
| | MAG_RAT | Myelin-associated glycoprotein |
| | NOTC3_RAT | Neurogenic locus notch homolog protein 3 |
| | MOG_RAT | Myelin-oligodendrocyte glycoprotein |
| | HNRPD_RAT | Heterogeneous nuclear ribonucleoprotein D0 |
| | CXA1_RAT | Gap junction alpha-1 protein |
| | H2A4_RAT | Histone H2A type 4 |
| | PIMT_RAT | Protein-L-isoaspartate(D-aspartate) O-methyltransferase |
| | CDC5L_RAT | Cell division cycle 5-like protein |
| | NOVA1_RAT | RNA-binding protein Nova-1 |
| **Molecular Layer** | TBA2_RAT | Tubulin alpha-1B chain |
| | CAC1G_RAT | Voltage-dependent T-type calcium channel subunit alpha-1G |
| | MYH11_RAT | Myosin-11 |
| | NDKB_RAT | Nucleoside diphosphate kinase B |
| | UN13A_RAT | Protein unc-13 homolog A |
| | HD_RAT | Huntingtin |
| | NRX2A_RAT | Neurexin-2 |
| | THIKA_RAT | 3-ketoacyl-CoA thiolase A, peroxisomal |
| | ITB1_RAT | Integrin beta-1 |
| | CO3A1_RAT | Collagen alpha-1(III) chain |

**Table 4.21.** The 10 highest-ranked hydrogel-mediated protein identifications unique to the white matter or molecular layer of the rat cerebellum.
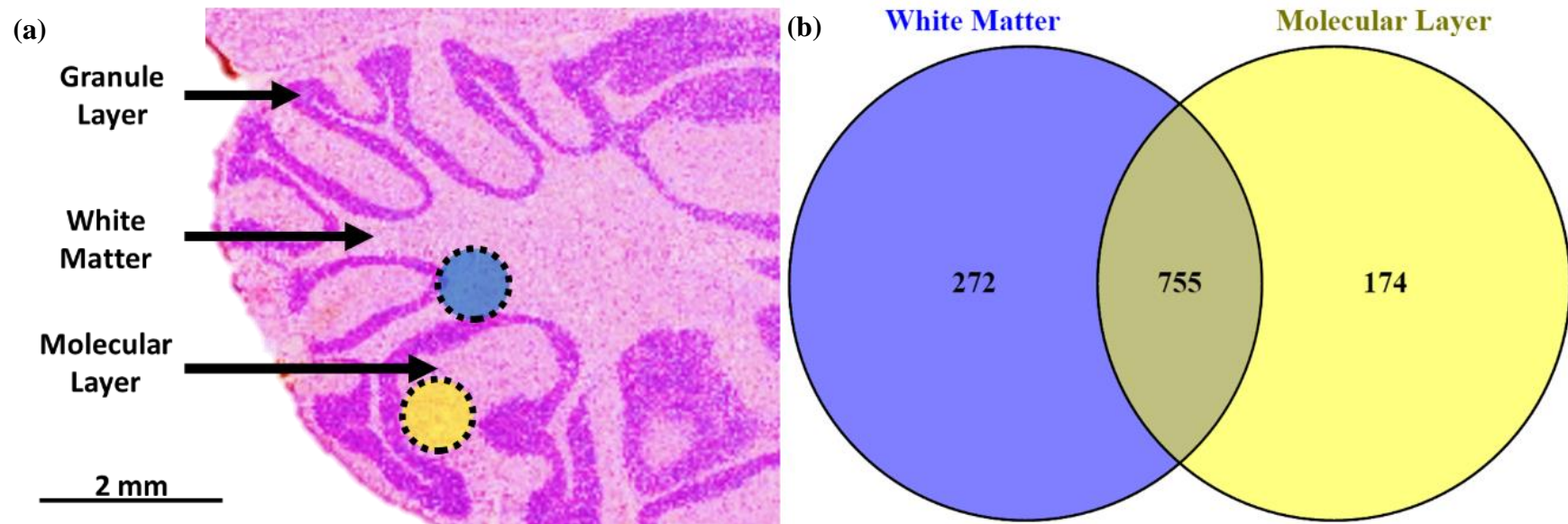
**Figure 4.12.** Differential proteomic analysis of rat cerebellum substructures. (a) H&E section of 12 µm thick rat cerebellum tissue after two hydrogels with diameters of ~777 µm were placed on either the white matter or molecular layer. The regions have been denoted by the circles overlaid on the H&E. Scale bar: 2 mm. (b) Venn diagram of protein identifications from the two cerebellum regions. The diagram is color-coded to match the circles shown in (a).

These identifications within the rat cerebellum are supported by previous literature reports.[165] For example, myelin-associated glycoprotein and myelin-oligodendrocyte glycoprotein are highly expressed in white matter regions within the central nervous system and are found to diminish with age, leading to disorders such as Alzheimer's and Parkinson's disease.[166-168] Conversely, neurexin-2 and voltage-dependent T-type calcium channel subunit alpha-1G, found in the molecular layer, mediate neuronal signaling and electrophysiological activity, respectively.[169, 170] A complete list of identified proteins can be found in Appendix A-C. One potential explanation for the high overlap is due to the granule layer, seen as dark purple in the H&E stained section, and the Purkinje layer, which is a one-cell thick layer between the white matter and the granule layer. Both hydrogels were tangential to these layers, with small portions present within the digestion/extraction regions underneath the hydrogels. It stands to reason that proteins are relatively homogeneous within specific layers, so both hydrogels would extract similar analytes from these interfering regions of tissue.

## Conclusions

The current methodologies for hydrogel-mediated analysis have been improved to allow for more efficient analyte:trypsin ratios and the use of more rigid polymers. Trypsin concentrations were reduced 10-fold while still maintaining the detection of over 1,000 proteins. The use of 18% polyacrylamide to cast hydrogels led to more reproducible hydrogel diameters as well as the ability to fabricate smaller hydrogels down to 260 µm. Even these narrow hydrogels provided robust proteomics data, with over 670 proteins confidently identified. The tissue adjacent to these small hydrogels does not appear to be altered in any way, as seen by H&E

staining post-hydrogel removal. This means that the hydrogels are truly sampling the tissue directly below them, not delocalizing into the surrounding areas.

On-tissue hydrogel digestion and extractions performed statistically better than in-solution digests from LCM and were comparable to tissue punch workflows, supporting this methodology as an easy to use and cost-effective alternative for many biological studies. When applying the newly optimized hydrogels to a rat cerebellum tissue, close to 1,000 proteins were identified from the white matter and molecular layer. Though there was a great deal of overlap between the identified proteins between the two substructures, 272 identifications were unique to the white matter and 174 identifications were unique to the molecular layer. Upon closer inspection, the top-ranked proteins that were unique to each region made biological sense, and were supported by previous literature reports.

# CHAPTER V

## CONCLUSIONS & PERSPECTIVES

### MALDI FTICR IMS of Intact Proteins: Using Mass Accuracy to Link Protein Images with Proteomics Data

Next-generation MALDI imaging platforms can provide unprecedented performance in terms of mass resolution for spatial proteomics experiments. The advantages of performing imaging experiments of intact proteins using MALDI FTICR IMS have been shown with vastly different tissue types. In the analysis of rat brain tissue, the ability to detect proteins with good sensitivity up to $m/z$ ~17,000 and proteins as large as ~20 kDa was achieved. This is an $m/z$ increase of almost 5,000 over previously reported results. IMS of rat brain tissue and clear cell renal cell carcinoma tissue from a human patient using MALDI FTICR IMS produced ion images with high mass resolution (~75,000 at $m/z$ 5,000) and accuracy (< 5 ppm). The analysis of ccRCC tissue elucidated proteins that were observed to be at greater abundance in the healthy tissue regions of the tissue (HH4-AC/2Me, $[M+2H]^{2+}$, -4.4 ppm), within the tumor (Thyβ10-AC, $[M+H]^{1+}$, 3.1 ppm), and also localized to areas of increased vascularization around the tumor (HBB, $[M+2H]^{2+}$, 4.7 ppm). These data showed the capabilities of MALDI FTICR IMS to provide the molecular specificity needed to overcome the challenges associated with direct tissue analysis. Improving spectral performance criteria such as mass resolving power and accuracy are critical for next-generation molecular imaging experiments. Specifically, direct tissue analysis provides unique challenges associated with overcoming bimolecular complexity and protein identification. For example, only 15 confident IMS identifications were made using this approach, due in large part to differences in observed peaks between the MALDI IMS and LC-

ESI MS/MS experiments. Although many more peaks were observed in each data set, the focus of this study was on the ions observed in both sets. Continued work must focus on addressing the inherent differences between these two ionization techniques in order to increase the number of identifications.

**Spatially-Targeted Extractions to Improve Peptide Identifications from MALDI FTICR IMS Experiments**

MALDI FTICR IMS can be an extremely useful tool for not only protein imaging, but peptide imaging as well. High mass resolution and mass accuracy aids in differentiating near isobaric peptide signals, many of which have overlapping isotopic envelopes. Though matrices such as CHCA have been used previously for peptide IMS experiments, the incorporation of a DHA method has greatly improved the signal intensities and peak abundances. This volatile matrix can rapidly sublime off of samples in high vacuum sources, such as those found on TOFs, but the reduced pressure source of the FTICR makes it perfectly amenable to DHA imaging. Sample preparation optimization also included the investigation of incubation conditions to ensure sufficient digestion while still minimizing delocalization. Volumes of ammonium bicarbonate were reduced to 50-100 μL for over-night digests, but still maintained robust peptide signals detected on the FTICR.

Integrating spatially-driven proteomic identification approaches, such as microextractions, into the imaging workflow provided rich peptide and protein datasets. This method is favored over homogenization because it maintains spatial information while remaining relatively easy to perform. Additionally, approximately 70 proteins were identified from the microextract that were not observed in the homogenate analysis. Microextracts have been used to

extract proteins prior to in-solution digestion, but extracting peptides from a tissue that has undergone the same *in situ* digestion as is used for imaging mass spectrometry experiments increases the chance that the peptides will be observed in both datasets. It reduces a major variable that could interfere with the confident identifications of peptides and proteins from tissue.

## Advanced Hydrogel Technologies For Enhanced On-Tissue Protein Digestion and Improved Spatial Localization

Although previous iterations of hydrogels have successfully performed spatially-directed proteomics analyses from tissue, improvements could still be made to all aspects of their use. The reduction of trypsin concentrations from 1 µg/µL to 0.1 µg/µL produced no statistical different in the number of protein identifications. This can be beneficial to make the technology even more cost-effective, especially if many hydrogel experiments are being performed simultaneously. Further experiments revealed that increasing the percentage of polyacrylamide from 7.5% to 18% formed a more rigid polymer. The rigidity allowed for hydrogels to be fabricated from smaller diameter punch biopsies, reproducibly creating the first hydrogels of this type with diameters of 260 µm. Alterations to the percentage of polyacrylamide showed no decrease in protein identifications, or in the molecular weight ranges of proteins identified. Reducing the diameter of the hydrogels did decrease the number of protein identifications, which is to be expected as less tissue is being sampled. However, even the smallest diameter hydrogels yielded ~670 confident identifications. Hydrogels performed as well as or better than LCM and tissue punches of the same area, which shows the power of performing digestions and extractions in one incubation step. When applied to the white matter and molecular layer within rat

cerebellum tissue sections, rich datasets were observed for each hydrogel. This again highlights the technology, providing around 1,000 protein identifications while maintaining their localization within the tissue.

## Future Research Directions

Detection of proteins from tissue with masses >17kDa using MALDI FTICR IMS represents a significant advancement in molecular imaging technologies; however, a vast number of endogenous proteins have even larger molecular weights. Diminished sensitivity for larger proteins is likely due to the difficulty in desorbing higher molecular weight analytes from tissue and limited ion transfer efficiencies of these analytes for many commercial source components (e.g., multipoles and ion funnels). This issue is not unique to MALDI FTICR IMS experiments, as the majority of proteins detected from tissue using MALDI-TOF platforms are typically <30kDa. Continuing to develop new methods for detecting and identifying proteins is critical to exposing the underlying biology that drives the images we collect. High mass accuracy and resolving power instrumentation enables such identifications to be made with high confidence.

Additionally, the detectable mass range can be extended by *in situ* tryptic digestion and imaging of tryptic peptides. Many hurdles still remain to be overcome, such as reduction and alkylation steps which are routinely used in in-solution digestion protocols. By breaking the cysteine bonds and allowing the protein to unfold, enzymes have better access to internal cleavage sites, improving overall sequence coverage. Heat-denaturing the tissue prior to digestion could provide a solution-free alternative, and has begun to be incorporated as an antigen retrieval step for FFPE IMS workflows. Additionally, more standard rehydration conditions would allow for better reproducibility from day to day and from person to person.

Modified trypsin able to withstand high temperatures would allow for more rapid digestion times, minimizing the chance of delocalization from the moisture in the incubation chamber.

Hydrogels have become highly useful tools for histology-driven analyses on a wide range of biological specimens, where specific anatomical features are targeted for direct profiling or identifications. However, as the targets of such analyses continue to become smaller and smaller, the hydrogel diameters will also need to decrease. Accurate placement of such hydrogels is important in experiments with very small spatial features. Manual manipulation is likely not feasible at these dimensions and the introduction of more precise equipment, such as micromanipulators, will improve this facet. Robotic manipulation would improve placement accuracy and precision, especially when used in conjunction with microscopy-directed targets. Alternatively, incorporating an array of hydrogels would allow for a multiplexed approach where hydrogels of interest within the array can be excised and subsequently analyzed. By incorporating the hydrogel technologies into proteomic workflows, robust and reproducible results can now be achieved at smaller dimensions, opening the door for targeting smaller anatomical features, such as specific substructures within tissues, or future clinical applications.

## Conclusions

In summary, high resolution MALDI IMS and spatially-directed proteomics experiments were used to improve protein identification confidence as well as provide alternatives to basic homogenization strategies. Methods have been developed to routinely image proteins on an FTICR, achieving *m/z* measurements of 17,000 and above. When comparing to top-down ETD fragmentation identifications, proteins were able to be matched to IMS ions with accuracies of less than 5 ppm. Peptide imaging was also improved, with similar sample preparation conditions

yielding robust peptide imaging datasets. Optimizing the incubation conditions resulted in better localization within the tissue section. Hydrogel technologies have also been advanced to target smaller biological regions, while still providing over 670 confident protein identifications. Hydrogels outperformed analogous LCM experiments and were comparable to traditional tissue homogenization approaches on the same amount of tissue.

These approaches can be incorporated into almost any protein-driven investigation to yield confident identifications with distinct imaging mass spectrometry patterns representative of the natural distributions within the tissue. High mass accuracy and resolution can be used to parse apart protein variations, such as isoforms, splice variants, or post-translationally modified forms. As hydrogel dimensions continue to decrease, smaller features within tissue can be targeted for unambiguous protein identifications. Scientific communities that study heterogeneous tissues, such as infectious disease and cancer research, would greatly benefit from these technological advancements to detect protein changes quickly, efficiently, and confidently. Understanding proteomic changes within complex systems is paramount to understanding biological processes like disease pathogenesis and progression.

# APPENDIX A: Protein Identifications Unique to the "White Matter" Hydrogel

| | | | | **272 Protein Identifications Unique to the "White Matter" Hydrogel** | | | | | |
|---|---|---|---|---|---|---|---|---|---|
| *X! Tandem Rank* | *log(e)* | *log(I)* | *Accession* | *Description* | *Mr* | *Unique Peptides* | *Total Peptides* | *% (measured)* | *% (corrected)* |
| 22 | -364.1 | 6.68 | TBA1_RAT | Tubulin alpha-1A chain | 50.1 | 41 | 82 | 43 | 63 |
| 72 | -165.6 | 6.34 | AT1A4_RAT | Sodium/potassium-transporting ATPase subunit alpha-4 | 113.9 | 2 | 2 | 3.6 | 6 |
| 151 | -90.7 | 5.82 | MAG_RAT | Myelin-associated glycoprotein | 69.3 | 11 | 18 | 16 | 36 |
| 195 | -75.5 | 5.68 | HSP71_RAT | no protein information available | 8.6 | 9 | 26 | 46 | 57 |
| 233 | -65.6 | 4.93 | NOTC3_RAT | Neurogenic locus notch homolog protein 3 | 244.1 | 10 | 10 | 8.9 | 17 |
| 236 | -64.7 | 5.41 | MOG_RAT | Myelin-oligodendrocyte glycoprotein | 27.9 | 9 | 12 | 34 | 66 |
| 242 | -63.3 | 5.4 | HNRPD_RAT | Heterogeneous nuclear ribonucleoprotein D0 | 38.2 | 9 | 15 | 23 | 58 |
| 269 | -57.8 | 5.41 | CXA1_RAT | Gap junction alpha-1 protein | 42.9 | 8 | 10 | 22 | 32 |
| 287 | -55.4 | 6.34 | H2A4_RAT | Histone H2A type 4 | 14.1 | 8 | 14 | 32 | 73 |
| 319 | -51.8 | 4.95 | CDC5L_RAT | Cell division cycle 5-like protein | 92.2 | 7 | 7 | 12 | 19 |
| 321 | -51.2 | 5.4 | PIMT_RAT | Protein-L-isoaspartate(D-aspartate) O-methyltransferase | 24.5 | 8 | 9 | 33 | 45 |
| 327 | -50.1 | 5.22 | NOVA1_RAT | RNA-binding protein Nova-1 | 48.4 | 7 | 7 | 15 | 31 |
| 329 | -50 | 5.13 | TR150_RAT | Thyroid hormone receptor-associated protein 3 | 108.2 | 7 | 7 | 9.7 | 17 |
| 335 | -48.8 | 5.61 | NDKA_RAT | Nucleoside diphosphate kinase A | 17.2 | 6 | 8 | 26 | 29 |
| 372 | -43.6 | 5.2 | MYO1D_RAT | Unconventional myosin-Id | 116 | 7 | 7 | 5.7 | 8 |
| 378 | -42.8 | 4.67 | MAST1_RAT | Microtubule-associated serine/threonine-protein kinase 1 | 170.9 | 7 | 7 | 5.1 | 7 |
| 394 | -40.6 | 5.37 | PP2AB_RAT | Serine/threonine-protein phosphatase 2A catalytic subunit beta isoform | 35.6 | 5 | 8 | 12 | 16 |
| 403 | -39.4 | 5.43 | RAB10_RAT | Ras-related protein Rab-10 | 22.8 | 5 | 7 | 24 | 35 |
| 425 | -37.5 | 5.2 | S6A11_RAT | Sodium- and chloride-dependent GABA transporter 3 | 69.9 | 5 | 7 | 6.1 | 19 |
| 431 | -36.4 | 5.2 | NUCKS_RAT | Nuclear ubiquitous casein and cyclin-dependent kinase substrate 1 | 27.1 | 5 | 6 | 21 | 30 |
| 449 | -34.7 | 5.51 | PRDX1_RAT | Peroxiredoxin-1 | 22.1 | 2 | 3 | 5 | 6 |
| 451 | -34.4 | 5.38 | RAB3B_RAT | Ras-related protein Rab-3B | 24.8 | 3 | 3 | 11 | 15 |
| 458 | -34 | 5.09 | LAT1_RAT | Large neutral amino acids transporter small subunit 1 | 55.9 | 4 | 4 | 5.3 | 19 |
| 473 | -32.7 | 5.17 | GBB1_RAT | Guanine nucleotide-binding protein G(I)/G(S)/G(T) subunit beta-1 | 37.2 | 2 | 2 | 11 | 16 |
| 488 | -31.5 | 5 | FPPS_RAT | Farnesyl pyrophosphate synthase | 40.8 | 5 | 6 | 12 | 17 |
| 500 | -30.8 | 5.06 | TOP1_RAT | DNA topoisomerase 1 | 90.7 | 5 | 5 | 7.3 | 14 |
| 506 | -30.3 | 4.58 | ABCF1_RAT | ATP-binding cassette sub-family F member 1 | 95.2 | 5 | 5 | 8.3 | 11 |
| 507 | -30.3 | 4.83 | CELR3_RAT | Cadherin EGF LAG seven-pass G-type receptor 3 | 359.1 | 5 | 5 | 2.6 | 4 |
| 519 | -29.3 | 5.05 | TCEA1_RAT | Transcription elongation factor A protein 1 | 33.9 | 5 | 5 | 15 | 22 |
| 527 | -28.6 | 5.25 | KAP2_RAT | cAMP-dependent protein kinase type II-alpha regulatory subunit | 45.4 | 3 | 4 | 6.3 | 9 |
| 535 | -28.3 | 4.85 | AL3A2_RAT | Fatty aldehyde dehydrogenase | 54 | 4 | 4 | 8.5 | 15 |
| 541 | -28.1 | 5.01 | CTL1_RAT | Choline transporter-like protein 1 | 73 | 4 | 5 | 7.2 | 17 |
| 542 | -28.1 | 4.52 | B3A3_RAT | Anion exchange protein 3 | 135.3 | 5 | 5 | 9.6 | 17 |
| 553 | -27.6 | 5.5 | MYPR_RAT | Myelin proteolipid protein | 29.9 | 4 | 6 | 8 | 22 |
| 557 | -27 | 4.89 | DNJA2_RAT | DnaJ homolog subfamily A member 2 | 45.7 | 4 | 6 | 22 | 33 |
| 559 | -26.9 | 5.02 | GCP_RAT | Probable tRNA N6-adenosine threonylcarbamoyltransferase | 34.6 | 4 | 5 | 14 | 14 |
| 564 | -26.8 | 5.14 | RS9_RAT | 40S ribosomal protein S9 | 22.4 | 4 | 4 | 19 | 30 |
| 565 | -26.6 | 4.77 | NUP53_RAT | Nucleoporin NUP53 | 34.8 | 4 | 5 | 17 | 34 |

# APPENDIX A: Protein Identifications Unique to the "White Matter" Hydrogel (Cont'd)

| X! Tandem Rank | log(e) | log(I) | Accession | Description | Mr | Unique Peptides | Total Peptides | % (measured) | % (corrected) |
|---|---|---|---|---|---|---|---|---|---|
| | | | | **272 Protein Identifications Unique to the "White Matter" Hydrogel** | | | | | |
| 573 | -26 | 4.9 | ERC2_RAT | ERC protein 2 | 110.5 | 2 | 2 | 4.2 | 6 |
| 576 | -25.8 | 4.63 | NCBP1_RAT | Nuclear cap-binding protein subunit 1 | 91.9 | 4 | 4 | 5.1 | 8 |
| 578 | -25.6 | 4.84 | CADH2_RAT | Cadherin-2 | 365.2 | 2 | 2 | 0.8 | 2 |
| 585 | -25.4 | 5.03 | ZN238_RAT | Zinc finger and BTB domain-containing protein 18 | 58.3 | 4 | 5 | 11 | 13 |
| 591 | -25.2 | 5.29 | ACBP_RAT | Acyl-CoA-binding protein | 9.9 | 4 | 9 | 44 | 72 |
| 592 | -25.2 | 4.7 | OX2G_RAT | OX-2 membrane glycoprotein | 31.1 | 4 | 4 | 15 | 55 |
| 597 | -24.9 | 4.82 | WBP11_RAT | WW domain-binding protein 11 | 70 | 4 | 4 | 8.4 | 15 |
| 600 | -24.7 | 5.08 | PERI_RAT | Peripherin | 53.5 | 3 | 3 | 6.2 | 8 |
| 605 | -24.5 | 4.9 | SMC1A_RAT | Structural maintenance of chromosomes protein 1A | 143.1 | 4 | 6 | 3.2 | 5 |
| 608 | -24.1 | 5 | HMOX2_RAT | Heme oxygenase 2 | 35.7 | 4 | 4 | 16 | 24 |
| 609 | -24 | 4.91 | NEUA_RAT | N-acylneuraminate cytidylyltransferase | 48.1 | 4 | 4 | 12 | 18 |
| 611 | -23.7 | 4.39 | SCG2_RAT | Secretogranin-2 | 71 | 4 | 4 | 8.9 | 11 |
| 612 | -23.7 | 4.41 | DBPA_RAT | Y-box-binding protein 3 | 38.8 | 3 | 4 | 12 | 18 |
| 616 | -23.6 | 4.94 | GAK_RAT | Cyclin-G-associated kinase | 143.6 | 4 | 4 | 2.6 | 5 |
| 617 | -23.6 | 4.91 | NUPL_RAT | Arf-GAP domain and FG repeat-containing protein 1 | 58.1 | 3 | 4 | 8.9 | 22 |
| 619 | -23.5 | 5.33 | PSA2_RAT | Proteasome subunit alpha type-2 | 25.8 | 4 | 6 | 21 | 34 |
| 623 | -23.4 | 5 | PRS6B_RAT | 26S protease regulatory subunit 6B | 47.4 | 4 | 5 | 9.8 | 14 |
| 624 | -23.4 | 4.11 | DKC1_RAT | H/ACA ribonucleoprotein complex subunit 4 | 56.4 | 3 | 3 | 10 | 13 |
| 625 | -23.3 | 5.11 | RAP2B_RAT | Ras-related protein Rap-2b | 20.5 | 3 | 3 | 16 | 18 |
| 627 | -23.1 | 4.96 | PCNP_RAT | PEST proteolytic signal-containing nuclear protein | 20.2 | 4 | 4 | 24 | 28 |
| 630 | -23 | 4.71 | PTN23_RAT | Tyrosine-protein phosphatase non-receptor type 23 | 163.4 | 3 | 3 | 2.3 | 4 |
| 632 | -22.8 | 5.24 | SEP10_RAT | Septin-10 | 53 | 3 | 3 | 9.2 | 12 |
| 636 | -22.7 | 4.75 | ERG19_RAT | Diphosphomevalonate decarboxylase | 43.9 | 3 | 3 | 8.5 | 11 |
| 639 | -22.7 | 4.95 | SFRS5_RAT | Serine/arginine-rich splicing factor 5 | 30.9 | 3 | 3 | 13 | 30 |
| 640 | -22.7 | 5.22 | HMGA1_RAT | High mobility group protein HMG-I/HMG-Y | 11.6 | 3 | 6 | 22 | 37 |
| 641 | -22.7 | 5.37 | RS7_RAT | 40S ribosomal protein S7 | 22.1 | 4 | 4 | 14 | 22 |
| 643 | -22.6 | 5.39 | ARL8B_RAT | ADP-ribosylation factor-like protein 8B | 21.5 | 4 | 5 | 24 | 33 |
| 644 | -22.6 | 5.3 | RAB4A_RAT | Ras-related protein Rab-4A | 23.9 | 2 | 2 | 12 | 14 |
| 645 | -22.5 | 4.72 | MRP1_RAT | Multidrug resistance-associated protein 1 | 171.4 | 4 | 4 | 3.8 | 6 |
| 647 | -22.4 | 5.04 | ENSA_RAT | Alpha-endosulfine | 13.3 | 3 | 6 | 32 | 41 |
| 651 | -22.1 | 5.07 | CYTC_RAT | Cystatin-C | 15.4 | 3 | 5 | 19 | 30 |
| 655 | -22 | 4.51 | S4A7_RAT | Sodium bicarbonate cotransporter 3 | 135.9 | 4 | 4 | 6.9 | 14 |
| 656 | -22 | 5.31 | RL18_RAT | 60S ribosomal protein L18 | 21.5 | 3 | 3 | 17 | 41 |
| 667 | -21.4 | 5.36 | HDGR3_RAT | Hepatoma-derived growth factor-related protein 3 | 22.4 | 3 | 5 | 14 | 22 |
| 672 | -20.9 | 4.57 | PDLI5_RAT | PDZ and LIM domain protein 5 | 63.2 | 4 | 4 | 11 | 17 |
| 678 | -20.6 | 4.77 | DNMT1_RAT | DNA (cytosine-5)-methyltransferase 1 | 182.7 | 4 | 4 | 4.4 | 6 |
| 679 | -20.5 | 4.74 | HMCS1_RAT | Hydroxymethylglutaryl-CoA synthase, cytoplasmic | 57.4 | 3 | 3 | 7.3 | 12 |
| 680 | -20.5 | 4.81 | MOT1_RAT | Monocarboxylate transporter 1 | 53.2 | 3 | 3 | 10 | 21 |

# APPENDIX A: Protein Identifications Unique to the "White Matter" Hydrogel (Cont'd)

| X! Tandem Rank | log(e) | log(I) | Accession | Description | Mr | Unique Peptides | Total Peptides | % (measured) | % (corrected) |
|---|---|---|---|---|---|---|---|---|---|
| | | | | **272 Protein Identifications Unique to the "White Matter" Hydrogel** | | | | | |
| 682 | -20.4 | 4.88 | NOLC1_RAT | Nucleolar and coiled-body phosphoprotein 1 | 73.5 | 4 | 4 | 6.7 | 9 |
| 685 | -20.3 | 5.15 | RL13_RAT | 60S ribosomal protein L13 | 24.2 | 3 | 3 | 10 | 17 |
| 693 | -19.8 | 4.75 | FAHD1_RAT | Acylpyruvase FAHD1, mitochondrial | 24.5 | 3 | 3 | 17 | 19 |
| 694 | -19.8 | 5.03 | ILF2_RAT | Interleukin enhancer-binding factor 2 | 51.3 | 3 | 4 | 7.1 | 8 |
| 696 | -19.7 | 4.75 | NCLN_RAT | Nicalin | 63 | 3 | 4 | 6.2 | 13 |
| 702 | -19.4 | 5.25 | RL14_RAT | 60S ribosomal protein L14 | 23.2 | 3 | 3 | 9.4 | 21 |
| 703 | -19.4 | 4.31 | MBB1A_RAT | Myb-binding protein 1A | 152.2 | 3 | 3 | 3.7 | 5 |
| 705 | -19.3 | 4.62 | NFIA_RAT | Nuclear factor 1 A-type | 55.9 | 3 | 3 | 8.4 | 15 |
| 708 | -19.2 | 5 | RS24_RAT | 40S ribosomal protein S24 | 15.4 | 3 | 4 | 23 | 48 |
| 709 | -19.2 | 4.09 | CSPG4_RAT | Chondroitin sulfate proteoglycan 4 | 251.8 | 3 | 3 | 1.8 | 3 |
| 710 | -19.1 | 4.94 | GPSN2_RAT | Very-long-chain enoyl-CoA reductase | 36.1 | 3 | 4 | 8.8 | 20 |
| 714 | -19 | 5.16 | CSN2_RAT | COP9 signalosome complex subunit 2 | 51.6 | 3 | 3 | 14 | 20 |
| 717 | -18.9 | 4.66 | ADRM1_RAT | Proteasomal ubiquitin receptor ADRM1 | 42.1 | 3 | 3 | 9.1 | 27 |
| 719 | -18.8 | 5.27 | PRP19_RAT | Pre-mRNA-processing factor 19 | 55.2 | 3 | 4 | 8.5 | 13 |
| 721 | -18.8 | 4.9 | OAT_RAT | Ornithine aminotransferase, mitochondrial | 48.3 | 3 | 3 | 6.8 | 10 |
| 725 | -18.6 | 4.78 | PP2CB_RAT | Protein phosphatase 1B | 42.9 | 2 | 2 | 10 | 12 |
| 730 | -18.3 | 4.66 | SFR12_RAT | Splicing regulatory glutamine/lysine-rich protein 1 | 56.8 | 3 | 3 | 8.3 | 28 |
| 734 | -18.2 | 4.63 | RABE2_RAT | Rab GTPase-binding effector protein 2 | 61.9 | 3 | 3 | 6.1 | 9 |
| 742 | -17.8 | 4.79 | SNP23_RAT | Synaptosomal-associated protein 23 | 23.2 | 2 | 2 | 14 | 18 |
| 744 | -17.7 | 4.75 | PEX19_RAT | Peroxisomal biogenesis factor 19 | 32.5 | 3 | 3 | 14 | 18 |
| 745 | -17.7 | 4.98 | MPPB_RAT | Mitochondrial-processing peptidase subunit beta | 54.3 | 3 | 3 | 5.9 | 9 |
| 746 | -17.7 | 4.55 | COPB2_RAT | Coatomer subunit beta' | 102.4 | 3 | 3 | 3.2 | 4 |
| 755 | -17.5 | 4.89 | SCPDH_RAT | Saccharopine dehydrogenase-like oxidoreductase | 47.1 | 3 | 3 | 14 | 20 |
| 763 | -17.3 | 5.98 | H33_RAT | Histone H3.3 | 15.2 | 3 | 4 | 16 | 23 |
| 770 | -17.1 | 4.58 | PCYOX_RAT | Prenylcysteine oxidase | 56.3 | 3 | 3 | 9.3 | 11 |
| 771 | -17.1 | 4.92 | SYUG_RAT | Gamma-synuclein | 12.9 | 3 | 4 | 23 | 41 |
| 772 | -17.1 | 4.39 | PP1RB_RAT | Protein phosphatase 1 regulatory subunit 11 | 13.9 | 2 | 2 | 41 | 50 |
| 773 | -17.1 | 4.72 | DPP2_RAT | Dipeptidyl peptidase 2 | 55.1 | 3 | 3 | 4.6 | 8 |
| 774 | -17 | 4.64 | CNN3_RAT | Calponin-3 | 36.4 | 3 | 3 | 12 | 22 |
| 776 | -17 | 4.89 | BLMH_RAT | Bleomycin hydrolase | 52.3 | 3 | 3 | 6.4 | 7 |
| 782 | -16.9 | 4.58 | NP1L1_RAT | Nucleosome assembly protein 1-like 1 | 45.3 | 2 | 2 | 7.9 | 14 |
| 785 | -16.6 | 4.95 | CREB1_RAT | Cyclic AMP-responsive element-binding protein 1 | 36.6 | 3 | 3 | 4.1 | 15 |
| 787 | -16.5 | 4.6 | MYO5B_RAT | Unconventional myosin-Vb | 213.6 | 2 | 2 | 1.3 | 2 |
| 793 | -16.4 | 4.49 | NRX2B_RAT | Neurexin-2-beta | 70.5 | 3 | 3 | 5.7 | 10 |
| 794 | -16.4 | 5 | HMCS2_RAT | Hydroxymethylglutaryl-CoA synthase, mitochondrial | 56.9 | 2 | 2 | 3.3 | 5 |
| 800 | -16.3 | 4.61 | AL1A1_RAT | Retinal dehydrogenase 1 | 54.3 | 3 | 3 | 8 | 10 |
| 801 | -16.2 | 4.67 | RL10_RAT | 60S ribosomal protein L10 | 24.5 | 3 | 3 | 13 | 20 |
| 802 | -16.2 | 4.89 | CACB2_RAT | Voltage-dependent L-type calcium channel subunit beta-2 | 73.2 | 3 | 3 | 6.4 | 9 |

| X! Tandem Rank | log(e) | log(I) | Accession | Description | Mr | Unique Peptides | Total Peptides | % (measured) | % (corrected) |
|---|---|---|---|---|---|---|---|---|---|
| | | | | **272 Protein Identifications Unique to the "White Matter" Hydrogel** | | | | | |
| 803 | -16.2 | 4.58 | HCN1_RAT | Potassium/sodium hyperpolarization-activated cyclic nucleotide-gated channel 1 | 102.4 | 3 | 3 | 4.6 | 9 |
| 807 | -16 | 5 | SEPT9_RAT | Septin-9 | 63.8 | 3 | 3 | 4.4 | 6 |
| 808 | -15.9 | 4.64 | GBRA6_RAT | Gamma-aminobutyric acid receptor subunit alpha-6 | 51.2 | 3 | 3 | 8.2 | 12 |
| 809 | -15.9 | 5.28 | RS26_RAT | 40S ribosomal protein S26 | 12.9 | 3 | 3 | 20 | 36 |
| 814 | -15.7 | 4.95 | FIS1_RAT | Mitochondrial fission 1 protein | 17 | 3 | 4 | 17 | 26 |
| 817 | -15.6 | 5.05 | RL23A_RAT | 60S ribosomal protein L23a | 17.7 | 3 | 4 | 17 | 37 |
| 818 | -15.5 | 4.65 | GCYB1_RAT | Guanylate cyclase soluble subunit beta-1 | 70.4 | 3 | 3 | 4.4 | 6 |
| 819 | -15.5 | 4.6 | MYPT1_RAT | Protein phosphatase 1 regulatory subunit 12A | 115.2 | 3 | 5 | 3.6 | 6 |
| 821 | -15.5 | 4.52 | CPSM_RAT | Carbamoyl-phosphate synthase [ammonia], mitochondrial | 164.5 | 3 | 3 | 3 | 5 |
| 823 | -15.4 | 4.82 | PDC6I_RAT | Programmed cell death 6-interacting protein | 44 | 3 | 3 | 6.5 | 11 |
| 825 | -15.3 | 4.84 | BPNT1_RAT | 3'(2'),5'-bisphosphate nucleotidase 1 | 33.2 | 3 | 3 | 9.7 | 11 |
| 828 | -15.1 | 4.62 | DLC2A_RAT | Dynein light chain roadblock-type 1 | 10.9 | 2 | 2 | 12 | 13 |
| 831 | -14.8 | 5 | XKR4_RAT | XK-related protein 4 | 72.7 | 3 | 3 | 5.7 | 11 |
| 833 | -14.7 | 5.04 | PTBP2_RAT | Polypyrimidine tract-binding protein 2 | 57.5 | 3 | 3 | 5.8 | 11 |
| 834 | -14.7 | 4.58 | FAAA_RAT | Fumarylacetoacetase | 45.9 | 2 | 2 | 6 | 9 |
| 837 | -14.5 | 4.8 | NMDZ1_RAT | Glutamate receptor ionotropic, NMDA 1 | 105.4 | 3 | 3 | 4.5 | 8 |
| 839 | -14.4 | 5.06 | NPM_RAT | Nucleophosmin | 32.5 | 3 | 3 | 14 | 17 |
| 842 | -14.3 | 4.53 | CORO7_RAT | Coronin-7 | 48.9 | 2 | 3 | 5.6 | 8 |
| 844 | -14.3 | 4.36 | HBS1L_RAT | HBS1-like protein | 74.7 | 3 | 3 | 7.7 | 10 |
| 845 | -14.2 | 4.37 | CLD11_RAT | Claudin-11 | 22 | 2 | 2 | 6.3 | 15 |
| 847 | -14 | 4.58 | CO1A2_RAT | Collagen alpha-2(I) chain | 129.5 | 3 | 3 | 4.2 | 5 |
| 848 | -14 | 4.82 | CSPG2_RAT | Versican core protein | 299.8 | 2 | 2 | 0.7 | 1 |
| 850 | -13.8 | 4.57 | IF5A1_RAT | Eukaryotic translation initiation factor 5A-1 | 16.7 | 2 | 2 | 22 | 27 |
| 851 | -13.7 | 3.74 | LAT2_RAT | Large neutral amino acids transporter small subunit 2 | 58.2 | 2 | 2 | 7.5 | 23 |
| 856 | -13.3 | 4.35 | TSC2_RAT | Tuberin | 201.2 | 2 | 2 | 1.7 | 2 |
| 857 | -13.2 | 4.39 | PTBP1_RAT | Polypyrimidine tract-binding protein 1 | 59.3 | 2 | 3 | 6.7 | 11 |
| 858 | -13.2 | 4.28 | PHLPP_RAT | PH domain leucine-rich repeat protein phosphatase 1 | 183.2 | 2 | 2 | 1.2 | 2 |
| 859 | -13.2 | 4.51 | UCHL3_RAT | Ubiquitin carboxyl-terminal hydrolase isozyme L3 | 26.1 | 2 | 2 | 11 | 15 |
| 861 | -13.1 | 4.39 | NMT1_RAT | Glycylpeptide N-tetradecanoyltransferase 1 | 56.8 | 2 | 2 | 8.1 | 11 |
| 863 | -13 | 4.27 | CP2D1_RAT | Cytochrome P450 2D1 | 57.1 | 2 | 2 | 9.1 | 12 |
| 866 | -12.8 | 4.73 | SIRT2_RAT | NAD-dependent protein deacetylase sirtuin-2 | 39.5 | 2 | 2 | 5.1 | 6 |
| 870 | -12.5 | 4.43 | SQSTM_RAT | Sequestosome-1 | 47.7 | 2 | 2 | 6.4 | 9 |
| 871 | -12.5 | 4.25 | CPNS1_RAT | Calpain small subunit 1 | 28.6 | 2 | 2 | 8.5 | 14 |
| 875 | -12.2 | 4.99 | DOCK9_RAT | Dedicator of cytokinesis protein 9 | 82.4 | 2 | 2 | 2.5 | 3 |
| 877 | -12.1 | 4.61 | S61A1_RAT | Protein transport protein Sec61 subunit alpha isoform 1 | 52.1 | 2 | 2 | 4.6 | 10 |
| 878 | -12.1 | 4.23 | ADCY2_RAT | Adenylate cyclase type 2 | 123.2 | 2 | 2 | 2.1 | 4 |
| 879 | -12.1 | 4.91 | RL38_RAT | 60S ribosomal protein L38 | 8.1 | 2 | 3 | 26 | 55 |
| 885 | -12 | 4.36 | PA1B3_RAT | Platelet-activating factor acetylhydrolase IB subunit gamma | 25.8 | 2 | 2 | 12 | 14 |

# APPENDIX A: Protein Identifications Unique to the "White Matter" Hydrogel (Cont'd)

| X! Tandem Rank | log(e) | log(I) | Accession | Description | Mr | Unique Peptides | Total Peptides | % (measured) | % (corrected) |
|---|---|---|---|---|---|---|---|---|---|
| | | | | **272 Protein Identifications Unique to the "White Matter" Hydrogel** | | | | | |
| 887 | -12 | 4.7 | ELOB_RAT | Transcription elongation factor B polypeptide 2 | 13.2 | 2 | 2 | 12 | 12 |
| 888 | -12 | 4.45 | CD81_RAT | CD81 antigen | 25.9 | 2 | 3 | 8.1 | 23 |
| 890 | -11.9 | 4.35 | FBX6_RAT | F-box only protein 6 | 32.8 | 2 | 2 | 6.3 | 9 |
| 891 | -11.9 | 4.38 | CCD16_RAT | Zinc finger protein 830 | 41.6 | 2 | 2 | 5.9 | 8 |
| 892 | -11.9 | 4.75 | TCP4_RAT | Activated RNA polymerase II transcriptional coactivator p15 | 14.3 | 2 | 2 | 14 | 17 |
| 895 | -11.8 | 4.34 | A1I3_RAT | Alpha-1-inhibitor 3 | 163.7 | 2 | 2 | 1.8 | 3 |
| 898 | -11.7 | 4.73 | CPSF5_RAT | Cleavage and polyadenylation specificity factor subunit 5 | 26.2 | 2 | 2 | 11 | 16 |
| 901 | -11.7 | 4.41 | PGTB_RAT | Geranylgeranyl transferase type-2 subunit beta | 36.8 | 2 | 2 | 13 | 27 |
| 902 | -11.6 | 4.77 | RL17_RAT | 60S ribosomal protein L17 | 21.3 | 2 | 2 | 12 | 20 |
| 904 | -11.5 | 3.94 | ATF2_RAT | Cyclic AMP-dependent transcription factor ATF-2 | 52.3 | 2 | 2 | 10 | 22 |
| 905 | -11.5 | 4.67 | TBAP_RAT | Protein Dr1 | 19.4 | 2 | 2 | 11 | 18 |
| 908 | -11.4 | 4.4 | AMPD3_RAT | AMP deaminase 3 | 88.4 | 2 | 2 | 2.6 | 4 |
| 911 | -11.3 | 4.29 | NOP5_RAT | Nucleolar protein 58 | 60 | 2 | 2 | 5.2 | 8 |
| 912 | -11.3 | 4.5 | RL15_RAT | 60S ribosomal protein L15 | 24 | 2 | 2 | 10 | 15 |
| 913 | -11.3 | 4.42 | NDE1_RAT | Nuclear distribution protein nudE homolog 1 | 38.5 | 2 | 2 | 6.4 | 8 |
| 917 | -11.2 | 4.61 | LMAN1_RAT | Protein ERGIC-53 | 57.9 | 2 | 2 | 4.1 | 7 |
| 918 | -11.1 | 4.55 | SVIP_RAT | Small VCP/p97-interacting protein | 8.2 | 2 | 2 | 29 | 42 |
| 922 | -11.1 | 4.59 | SCN2B_RAT | Sodium channel subunit beta-2 | 24.1 | 2 | 3 | 11 | 21 |
| 923 | -11.1 | 4.21 | GCP60_RAT | Golgi resident protein GCP60 | 60.3 | 2 | 2 | 4.6 | 7 |
| 924 | -11 | 4.59 | NUDC2_RAT | NudC domain-containing protein 2 | 17.7 | 2 | 2 | 17 | 22 |
| 925 | -11 | 4.37 | UBE4A_RAT | Ubiquitin conjugation factor E4 A | 122.3 | 2 | 3 | 2.4 | 4 |
| 927 | -10.9 | 4.79 | RS4X_RAT | 40S ribosomal protein S4, X isoform | 29.4 | 2 | 3 | 8 | 11 |
| 928 | -10.9 | 4.65 | RL9_RAT | 60S ribosomal protein L9 | 21.9 | 2 | 2 | 14 | 26 |
| 929 | -10.9 | 4.79 | RBM4B_RAT | RNA-binding protein 4B | 40 | 2 | 2 | 4.8 | 7 |
| 930 | -10.8 | 4.28 | TOP2A_RAT | DNA topoisomerase 2-alpha | 173.1 | 2 | 2 | 1.9 | 3 |
| 931 | -10.8 | 4.23 | UBQL1_RAT | Ubiquilin-1 | 62 | 2 | 2 | 4.3 | 10 |
| 932 | -10.8 | 4.18 | CLIC4_RAT | Chloride intracellular channel protein 4 | 28.5 | 2 | 2 | 16 | 20 |
| 933 | -10.8 | 4.41 | PSB3_RAT | Proteasome subunit beta type-3 | 22.9 | 2 | 2 | 14 | 23 |
| 935 | -10.8 | 4.73 | UB2D4_RAT | Ubiquitin-conjugating enzyme E2 D2B | 16.6 | 2 | 2 | 17 | 57 |
| 937 | -10.7 | 4.96 | CYTB_RAT | Cystatin-B | 11.2 | 2 | 3 | 31 | 40 |
| 939 | -10.7 | 4.76 | FHL1_RAT | Four and a half LIM domains protein 1 | 31.9 | 2 | 2 | 6.4 | 9 |
| 941 | -10.7 | 5.03 | BAF_RAT | Barrier-to-autointegration factor | 10 | 2 | 3 | 42 | 52 |
| 942 | -10.7 | 4.48 | SH3K1_RAT | SH3 domain-containing kinase-binding protein 1 | 78 | 2 | 2 | 3.8 | 5 |
| 943 | -10.7 | 4.65 | TCTP_RAT | Translationally-controlled tumor protein | 19.4 | 2 | 2 | 5.2 | 9 |
| 944 | -10.7 | 4.09 | ABCA2_RAT | ATP-binding cassette sub-family A member 2 | 270.8 | 2 | 2 | 1.7 | 3 |
| 945 | -10.7 | 3.91 | GMPR1_RAT | GMP reductase 1 | 37.5 | 2 | 2 | 8.1 | 11 |
| 946 | -10.6 | 4.15 | CDK9_RAT | Cyclin-dependent kinase 9 | 42.7 | 2 | 2 | 6.2 | 8 |
| 947 | -10.6 | 4.46 | HSPB1_RAT | Heat shock protein beta-1 | 22.9 | 2 | 2 | 11 | 16 |

# APPENDIX A: Protein Identifications Unique to the "White Matter" Hydrogel (Cont'd)

| X! Tandem Rank | log(e) | log(I) | Accession | Description | Mr | Unique Peptides | Total Peptides | % (measured) | % (corrected) |
|---|---|---|---|---|---|---|---|---|---|
| | | | | **272 Protein Identifications Unique to the "White Matter" Hydrogel** | | | | | |
| 951 | -10.5 | 4.68 | CYH1_RAT | Cytohesin-1 | 46.2 | 2 | 2 | 8 | 11 |
| 953 | -10.4 | 4.55 | D2HDH_RAT | D-2-hydroxyglutarate dehydrogenase, mitochondrial | 58.8 | 2 | 2 | 5 | 8 |
| 956 | -10.3 | 4.44 | RS27_RAT | 40S ribosomal protein S27 | 9.3 | 2 | 2 | 27 | 33 |
| 957 | -10.3 | 4.47 | B2MG_RAT | Beta-2-microglobulin | 13.7 | 2 | 2 | 17 | 25 |
| 959 | -10.2 | 4.56 | RL35A_RAT | 60S ribosomal protein L35a | 12.5 | 2 | 2 | 17 | 32 |
| 964 | -10.1 | 4.3 | TSNAX_RAT | Translin-associated protein X | 33 | 2 | 2 | 8.3 | 10 |
| 965 | -10.1 | 4.4 | HMGB2_RAT | High mobility group protein B2 | 24 | 2 | 2 | 11 | 17 |
| 968 | -10 | 4.32 | MA2C1_RAT | Alpha-mannosidase 2C1 | 115.9 | 2 | 2 | 2.3 | 3 |
| 970 | -9.9 | 4.51 | SCFD1_RAT | Sec1 family domain-containing protein 1 | 72.2 | 2 | 2 | 4.9 | 7 |
| 972 | -9.9 | 4.44 | SUMO2_RAT | Small ubiquitin-related modifier 2 | 10.9 | 2 | 2 | 21 | 48 |
| 973 | -9.9 | 4.71 | CYB5_RAT | Cytochrome b5 | 34 | 2 | 2 | 9 | 13 |
| 975 | -9.9 | 4.57 | KPCA_RAT | Protein kinase C alpha type | 76.6 | 2 | 2 | 5.1 | 8 |
| 982 | -9.8 | 4.47 | LCAP_RAT | Leucyl-cystinyl aminopeptidase | 117.1 | 2 | 2 | 1.6 | 3 |
| 983 | -9.8 | 4.68 | GCS1_RAT | Mannosyl-oligosaccharide glucosidase | 91.8 | 2 | 2 | 3.4 | 5 |
| 984 | -9.7 | 3.98 | GLRB_RAT | Glycine receptor subunit beta | 55.9 | 2 | 2 | 3 | 4 |
| 985 | -9.7 | 4.42 | RNPS1_RAT | RNA-binding protein with serine-rich domain 1 | 34.2 | 2 | 2 | 6.9 | 12 |
| 987 | -9.7 | 4.01 | ADNP_RAT | Activity-dependent neuroprotector homeobox protein | 91.3 | 2 | 3 | 4 | 6 |
| 990 | -9.6 | 4.67 | CB032_RAT | CB1 cannabinoid receptor-interacting protein 1 | 18.6 | 2 | 2 | 13 | 24 |
| 991 | -9.6 | 4.82 | ATOX1_RAT | Copper transport protein ATOX1 | 7.3 | 2 | 2 | 49 | 57 |
| 994 | -9.6 | 4.64 | NCB5R_RAT | NADH-cytochrome b5 reductase 3 | 34 | 2 | 2 | 9 | 13 |
| 995 | -9.5 | 4.88 | ATP5E_RAT | ATP synthase subunit epsilon, mitochondrial | 5.6 | 2 | 2 | 32 | 73 |
| 998 | -9.4 | 4.49 | FBRL_RAT | rRNA 2'-O-methyltransferase fibrillarin | 34.2 | 2 | 2 | 8.6 | 10 |
| 999 | -9.4 | 3.75 | RCOR2_RAT | REST corepressor 2 | 57.9 | 2 | 2 | 6.1 | 8 |
| 1000 | -9.4 | 4.07 | CA077_RAT | Chromatin target of PRMT1 protein | 26.5 | 2 | 2 | 12 | 20 |
| 1002 | -9.4 | 4.47 | ZN265_RAT | Zinc finger Ran-binding domain-containing protein 2 | 37.8 | 2 | 2 | 6.3 | 10 |
| 1005 | -9.3 | 4.33 | SMU1_RAT | WD40 repeat-containing protein SMU1 | 57.5 | 2 | 2 | 4.3 | 6 |
| 1006 | -9.3 | 4.51 | ELOA1_RAT | Transcription elongation factor B polypeptide 3 | 87.1 | 2 | 2 | 4 | 6 |
| 1008 | -9.3 | 4.56 | CIRBP_RAT | Cold-inducible RNA-binding protein | 18.6 | 2 | 2 | 10 | 15 |
| 1009 | -9.3 | 4.1 | STX4_RAT | Syntaxin-4 | 34.2 | 2 | 2 | 11 | 17 |
| 1010 | -9.3 | 4.25 | PTPRN_RAT | Receptor-type tyrosine-protein phosphatase-like N | 106.2 | 2 | 2 | 3.1 | 6 |
| 1012 | -9.2 | 4.41 | XPO1_RAT | Exportin-1 | 123 | 2 | 2 | 2.1 | 3 |
| 1014 | -9.1 | 4.31 | GGABP_RAT | Coiled-coil domain-containing protein 91 | 50.1 | 2 | 2 | 5.4 | 9 |
| 1015 | -9.1 | 4.32 | DUOX2_RAT | Dual oxidase 2 | 171.4 | 2 | 2 | 2.2 | 3 |
| 1016 | -9.1 | 4.99 | FABPE_RAT | Fatty acid-binding protein, epidermal | 14.9 | 2 | 2 | 12 | 19 |
| 1017 | -9.1 | 4.23 | GUC2F_RAT | Retinal guanylyl cyclase 2 | 124.3 | 2 | 2 | 2.3 | 3 |
| 1018 | -9.1 | 4.85 | MT1_RAT | Metallothionein-1 | 6 | 2 | 2 | 39 | 100+ |
| 1019 | -9 | 4.71 | KCNA2_RAT | Potassium voltage-gated channel subfamily A member 2 | 56.7 | 2 | 2 | 5.4 | 11 |
| 1020 | -9 | 4.21 | CENG1_RAT | Arf-GAP with GTPase, ANK repeat and PH domain-containing protein 2 | 124.4 | 2 | 2 | 1.9 | 3 |

# APPENDIX A: Protein Identifications Unique to the "White Matter" Hydrogel (Cont'd)

| X! Tandem Rank | log(e) | log(I) | Accession | Description | Mr | Unique Peptides | Total Peptides | % (measured) | % (corrected) |
|---|---|---|---|---|---|---|---|---|---|
| | | | | **272 Protein Identifications Unique to the "White Matter" Hydrogel** | | | | | |
| 1022 | -9 | 4.37 | KIF5C_RAT | Kinesin heavy chain isoform 5C | 27 | 2 | 2 | 11 | 16 |
| 1023 | -9 | 4.77 | GSTT2_RAT | Glutathione S-transferase theta-2 | 27.3 | 2 | 2 | 8.6 | 12 |
| 1024 | -8.9 | 4.66 | FZD1_RAT | Frizzled-1 | 71 | 2 | 2 | 3.3 | 6 |
| 1026 | -8.9 | 4.67 | TS101_RAT | Tumor susceptibility gene 101 protein | 44 | 2 | 2 | 5.1 | 9 |
| 1027 | -8.9 | 4.53 | TM55A_RAT | Type 2 phosphatidylinositol 4,5-bisphosphate 4-phosphatase | 28 | 2 | 3 | 12 | 16 |
| 1028 | -8.9 | 4.23 | PHLB1_RAT | Pleckstrin homology-like domain family B member 1 | 93.5 | 2 | 2 | 2.3 | 3 |
| 1029 | -8.9 | 4.7 | ACY2_RAT | Aspartoacylase | 35.6 | 2 | 2 | 5.7 | 9 |
| 1030 | -8.9 | 4.32 | SAM68_RAT | KH domain-containing, RNA-binding, signal transduction-associated protein 1 | 48.3 | 2 | 2 | 3.8 | 7 |
| 1031 | -8.8 | 4.6 | RINI_RAT | Ribonuclease inhibitor | 49.9 | 2 | 2 | 6.8 | 8 |
| 1032 | -8.8 | 4.43 | DHI1_RAT | Corticosteroid 11-beta-dehydrogenase isozyme 1 | 31.9 | 2 | 2 | 8.3 | 10 |
| 1033 | -8.8 | 4.38 | KEAP1_RAT | Kelch-like ECH-associated protein 1 | 69.4 | 2 | 2 | 3 | 4 |
| 1034 | -8.8 | 4.86 | CHSP1_RAT | Calcium-regulated heat stable protein 1 | 15.9 | 2 | 2 | 17 | 27 |
| 1035 | -8.7 | 4.08 | SYPM_RAT | Probable proline--tRNA ligase, mitochondrial | 53.3 | 2 | 2 | 5.9 | 7 |
| 1036 | -8.7 | 4.69 | I2C2_RAT | Protein argonaute-2 | 97.3 | 2 | 2 | 3 | 4 |
| 1037 | -8.7 | 4.75 | DNJC8_RAT | DnaJ homolog subfamily C member 8 | 29.8 | 2 | 2 | 6.7 | 10 |
| 1040 | -8.6 | 4.82 | COPB_RAT | Coatomer subunit beta | 106.9 | 2 | 3 | 2.8 | 4 |
| 1041 | -8.6 | 4.52 | RABP1_RAT | Cellular retinoic acid-binding protein 1 | 3.7 | 2 | 2 | 58 | 70 |
| 1042 | -8.6 | 4.99 | PDZK3_RAT | PDZ domain-containing protein 2 | 293.7 | 2 | 2 | 0.9 | 1 |
| 1043 | -8.6 | 4.41 | THYG_RAT | Thyroglobulin | 304.4 | 2 | 2 | 0.9 | 2 |
| 1044 | -8.5 | 4.05 | LRP2_RAT | Low-density lipoprotein receptor-related protein 2 | 518.9 | 2 | 2 | 1.1 | 2 |
| 1046 | -8.5 | 4.63 | CAD23_RAT | Cadherin-23 | 365.2 | 2 | 2 | 0.8 | 2 |
| 1047 | -8.5 | 3.99 | NEO1_RAT | Neogenin | 150.5 | 2 | 2 | 2.6 | 4 |
| 1048 | -8.5 | 4.45 | MRP5_RAT | Multidrug resistance-associated protein 5 | 160.8 | 2 | 2 | 1.5 | 3 |
| 1049 | -8.5 | 4.41 | DLP1_RAT | Decaprenyl-diphosphate synthase subunit 2 | 44.3 | 2 | 2 | 5.7 | 8 |
| 1050 | -8.5 | 4.33 | PRGR_RAT | Progesterone receptor | 99.3 | 2 | 2 | 3.8 | 5 |
| 1051 | -8.5 | 4.57 | CABIN_RAT | Calcineurin-binding protein cabin-1 | 242.7 | 2 | 2 | 1.6 | 2 |
| 1052 | -8.4 | 4.02 | ORML3_RAT | ORM1-like protein 3 | 17.5 | 2 | 2 | 17 | 27 |
| 1053 | -8.4 | 4.84 | SLIT3_RAT | Slit homolog 3 protein | 167.7 | 2 | 2 | 1.4 | 2 |
| 1054 | -8.4 | 4.65 | RNF39_RAT | RING finger protein 39 | 38.3 | 2 | 2 | 6.8 | 8 |
| 1057 | -8.4 | 4.36 | HRH1_RAT | Histamine H1 receptor | 55.7 | 2 | 2 | 6.4 | 14 |
| 1059 | -8.3 | 4.76 | R4RL1_RAT | Reticulon-4 receptor-like 1 | 49.7 | 2 | 2 | 4.7 | 10 |
| 1060 | -8.3 | 4.6 | SSBP3_RAT | Single-stranded DNA-binding protein 3 | 37.7 | 2 | 2 | 7.5 | 28 |
| 1063 | -8.3 | 4.68 | MYO9B_RAT | Unconventional myosin-IXb | 224.9 | 2 | 2 | 1.1 | 1 |
| 1064 | -8.3 | 3.83 | CRBN_RAT | Protein cereblon | 50.8 | 2 | 2 | 13 | 19 |
| 1066 | -8.2 | 4.08 | K1C19_RAT | Keratin, type I cytoskeletal 19 | 44.6 | 2 | 2 | 5.7 | 6 |
| 1070 | -8.2 | 4.35 | BRE1B_RAT | E3 ubiquitin-protein ligase BRE1B | 113.8 | 2 | 2 | 2.4 | 3 |
| 1071 | -8.1 | 3.97 | ZEP2_RAT | Human immunodeficiency virus type I enhancer-binding protein 2 homolog | 267.3 | 2 | 2 | 2 | 3 |
| 1072 | -8.1 | 4.38 | MPPA_RAT | Mitochondrial-processing peptidase subunit alpha | 58.6 | 2 | 2 | 3.8 | 5 |

APPENDIX A: Protein Identifications Unique to the "White Matter" Hydrogel (Cont'd)

| X! Tandem Rank | log(e) | log(I) | Accession | Description | Mr | Unique Peptides | Total Peptides | % (measured) | % (corrected) |
|---|---|---|---|---|---|---|---|---|---|
| 272 Protein Identifications Unique to the "White Matter" Hydrogel | | | | | | | | | |
| 1073 | -8.1 | 4.55 | KLH10_RAT | Kelch-like protein 10 | 68.9 | 2 | 2 | 4.1 | 5 |
| 1074 | -8.1 | 4.7 | ROCK1_RAT | Rho-associated protein kinase 1 | 159.5 | 2 | 2 | 1.2 | 2 |
| 1076 | -8 | 4.37 | P5CR2_RAT | Pyrroline-5-carboxylate reductase 2 | 33.7 | 2 | 2 | 5.6 | 8 |
| 1077 | -8 | 4.09 | UN13B_RAT | Protein unc-13 homolog B | 183.9 | 2 | 2 | 1.4 | 2 |
| 1078 | -8 | 4.73 | SPEG_RAT | Striated muscle-specific serine/threonine-protein kinase | 353.9 | 2 | 2 | 0.6 | 1 |
| 1079 | -7.9 | 5.03 | TEP1_RAT | Telomerase protein component 1 | 291.5 | 2 | 2 | 0.7 | 1 |

# APPENDIX B: Protein Identifications Unique to the "Molecular Layer" Hydrogel

| | | | | **174 Protein Identifications Unique to the "Molecular Layer" Hydrogel** | | | | | |
|---|---|---|---|---|---|---|---|---|---|
| *X! Tandem Rank* | *log(e)* | *log(I)* | *Accession* | *Description* | *Mr* | *Unique Peptides* | *Total Peptides* | *% (measured)* | *% (corrected)* |
| 17 | -321.7 | 6.61 | TBA2_RAT | Tubulin alpha-1B chain | 50.1 | 35 | 69 | 44 | 64 |
| 118 | -99.1 | 5.39 | MYH11_RAT | Myosin-11 | 152.4 | 11 | 12 | 8.5 | 15 |
| 149 | -80.4 | 4.97 | CAC1G_RAT | Voltage-dependent T-type calcium channel subunit alpha-1G | 250.2 | 12 | 12 | 7 | 13 |
| 225 | -58.5 | 5.18 | K6PL_RAT | ATP-dependent 6-phosphofructokinase, liver type | 85.2 | 4 | 4 | 5 | 9 |
| 231 | -56.7 | 5.65 | GNA11_RAT | Guanine nucleotide-binding protein subunit alpha-11 | 42 | 3 | 3 | 11 | 15 |
| 261 | -49.6 | 5.36 | HXK2_RAT | Hexokinase-2 | 102.5 | 2 | 2 | 3.1 | 4 |
| 273 | -47.8 | 5.64 | NDKB_RAT | Nucleoside diphosphate kinase B | 17.3 | 6 | 10 | 32 | 37 |
| 298 | -45 | 5.67 | GNAI3_RAT | Guanine nucleotide-binding protein G(k) subunit alpha | 40.4 | 2 | 2 | 5.9 | 10 |
| 305 | -43.6 | 5.11 | GRIA3_RAT | Glutamate receptor 3 | 100.3 | 2 | 2 | 3.6 | 6 |
| 317 | -41.6 | 5.34 | ITPR2_RAT | Inositol 1,4,5-trisphosphate receptor type 2 | 306.9 | 2 | 2 | 1.1 | 2 |
| 362 | -36.8 | 5.11 | UN13A_RAT | Protein unc-13 homolog A | 196.2 | 6 | 7 | 3.4 | 6 |
| 406 | -32.8 | 5.07 | K2C8_RAT | Keratin, type II cytoskeletal 8 | 53.9 | 3 | 3 | 9.8 | 15 |
| 416 | -32.3 | 4.58 | HD_RAT | Huntingtin | 343.5 | 5 | 6 | 3.1 | 5 |
| 421 | -32 | 4.9 | NRX2A_RAT | Neurexin-2 | 185.2 | 5 | 7 | 5.1 | 8 |
| 445 | -30 | 4.91 | THIKA_RAT | 3-ketoacyl-CoA thiolase A, peroxisomal | 43.8 | 5 | 6 | 11 | 15 |
| 451 | -29 | 4.71 | ITB1_RAT | Integrin beta-1 | 88.4 | 5 | 5 | 11 | 21 |
| 453 | -28.9 | 4.54 | CLIC6_RAT | Chloride intracellular channel protein 6 | 64.6 | 4 | 4 | 11 | 17 |
| 477 | -26.9 | 4.61 | CO3A1_RAT | Collagen alpha-1(III) chain | 138.9 | 5 | 5 | 5.3 | 8 |
| 492 | -25.6 | 4.33 | LPP_RAT | no protein information available | 68.2 | 4 | 4 | 16 | 24 |
| 494 | -25.6 | 5.16 | ITPR3_RAT | Inositol 1,4,5-trisphosphate receptor type 3 | 304.1 | 2 | 2 | 1.5 | 2 |
| 521 | -23.9 | 4.97 | ARBK1_RAT | Beta-adrenergic receptor kinase 1 | 79.7 | 4 | 5 | 6.8 | 8 |
| 524 | -23.9 | 5.06 | NRX1A_RAT | Neurexin-1 | 166.1 | 3 | 3 | 2.6 | 4 |
| 527 | -23.9 | 4.67 | FIBB_RAT | Fibrinogen beta chain | 54.3 | 4 | 4 | 11 | 12 |
| 529 | -23.7 | 4.53 | PHAR2_RAT | Phosphatase and actin regulator 2 | 62.2 | 4 | 5 | 10 | 18 |
| 536 | -23.4 | 5.12 | ARF4_RAT | ADP-ribosylation factor 4 | 20.3 | 2 | 2 | 13 | 16 |
| 542 | -23.2 | 4.84 | UN13C_RAT | Protein unc-13 homolog C | 249 | 4 | 5 | 2.3 | 4 |
| 543 | -23.1 | 4.74 | STRN_RAT | Striatin | 86.2 | 4 | 4 | 7.9 | 13 |
| 547 | -23 | 4.34 | CO2A1_RAT | Collagen alpha-1(II) chain | 134.5 | 4 | 4 | 5.1 | 6 |
| 550 | -22.8 | 4.82 | L2GL1_RAT | Lethal(2) giant larvae protein homolog 1 | 112.4 | 3 | 3 | 3.1 | 6 |
| 551 | -22.7 | 5.08 | RAC1_RAT | Ras-related C3 botulinum toxin substrate 1 | 21.4 | 3 | 3 | 19 | 34 |
| 556 | -22.5 | 4.94 | TAGL_RAT | Transgelin | 22.5 | 4 | 4 | 20 | 22 |
| 573 | -21.7 | 5.14 | CYH3_RAT | Cytohesin-3 | 46.3 | 4 | 5 | 9.8 | 15 |
| 577 | -21.5 | 4.51 | APBA1_RAT | Amyloid beta A4 precursor protein-binding family A member 1 | 92.6 | 4 | 5 | 6.4 | 10 |
| 595 | -20.2 | 4.99 | GNAZ_RAT | Guanine nucleotide-binding protein G(z) subunit alpha | 40.7 | 2 | 2 | 6.8 | 9 |
| 605 | -19.9 | 5.24 | RAB4B_RAT | Ras-related protein Rab-4B | 23.6 | 2 | 2 | 12 | 15 |
| 608 | -19.8 | 4.54 | SYGP1_RAT | Ras/Rap GTPase-activating protein SynGAP | 143 | 3 | 3 | 3.1 | 5 |
| 609 | -19.6 | 4.47 | BCAR1_RAT | Breast cancer anti-estrogen resistance protein 1 | 104.2 | 3 | 3 | 3.2 | 5 |
| 617 | -19.4 | 4.93 | RHEB_RAT | GTP-binding protein Rheb | 20.5 | 3 | 4 | 18 | 30 |

107

APPENDIX B: Protein Identifications Unique to the "Molecular Layer" Hydrogel (Cont'd)

| | | | | 174 Protein Identifications Unique to the "Molecular Layer" Hydrogel | | | | | | |
|---|---|---|---|---|---|---|---|---|---|
| X! Tandem Rank | log(e) | log(I) | Accession | Description | Mr | Unique Peptides | Total Peptides | % (measured) | % (corrected) |
| 628 | -18.9 | 4.57 | CANB1_RAT | Calcineurin subunit B type 1 | 19.2 | 3 | 3 | 22 | 26 |
| 631 | -18.8 | 4.88 | PP1B_RAT | Serine/threonine-protein phosphatase PP1-beta catalytic subunit | 37 | 2 | 2 | 5.5 | 8 |
| 633 | -18.8 | 4.45 | ZN148_RAT | Zinc finger protein 148 | 88.7 | 3 | 3 | 9.3 | 15 |
| 634 | -18.7 | 4.7 | CACB3_RAT | Voltage-dependent L-type calcium channel subunit beta-3 | 54.5 | 3 | 3 | 6.4 | 9 |
| 637 | -18.7 | 4.54 | TM109_RAT | Transmembrane protein 109 | 26.2 | 3 | 3 | 19 | 55 |
| 639 | -18.5 | 4.62 | CSN8_RAT | COP9 signalosome complex subunit 8 | 23.2 | 3 | 4 | 22 | 31 |
| 641 | -18.5 | 4.73 | KACA_RAT | Ig kappa chain C region, A allele | 11.7 | 3 | 4 | 24 | 29 |
| 643 | -18.5 | 4.81 | RALB_RAT | Ras-related protein Ral-B | 23.3 | 3 | 3 | 16 | 24 |
| 648 | -18.4 | 4.86 | FIBG_RAT | Fibrinogen gamma chain | 50.6 | 3 | 3 | 7.6 | 9 |
| 655 | -18.1 | 4.72 | PI52A_RAT | Phosphatidylinositol 5-phosphate 4-kinase type-2 alpha | 46.2 | 2 | 2 | 7.9 | 14 |
| 656 | -18 | 4.8 | DDAH1_RAT | N(G),N(G)-dimethylarginine dimethylaminohydrolase 1 | 31.3 | 3 | 5 | 12 | 17 |
| 666 | -17.7 | 4.44 | CYB5M_RAT | Cytochrome b5 type B | 16.3 | 3 | 3 | 15 | 21 |
| 667 | -17.7 | 4.73 | GLPK_RAT | Glycerol kinase | 57.4 | 3 | 4 | 5.9 | 8 |
| 670 | -17.5 | 4.42 | LAMP1_RAT | Lysosome-associated membrane glycoprotein 1 | 43.9 | 3 | 3 | 13 | 42 |
| 674 | -17.2 | 4.73 | ALAT_RAT | Alanine aminotransferase 1 | 54.9 | 3 | 3 | 5.9 | 8 |
| 678 | -17.1 | 4.92 | ARF6_RAT | ADP-ribosylation factor 6 | 19.9 | 3 | 3 | 17 | 25 |
| 679 | -17 | 4.54 | MGR4_RAT | Metabotropic glutamate receptor 4 | 101.8 | 3 | 3 | 3.5 | 5 |
| 680 | -17 | 4.34 | SNX17_RAT | Sorting nexin-17 | 52.8 | 2 | 2 | 5.7 | 7 |
| 684 | -16.7 | 4.85 | ADHX_RAT | Alcohol dehydrogenase class-3 | 39.4 | 3 | 3 | 8.3 | 11 |
| 687 | -16.7 | 4.81 | SCN4A_RAT | Sodium channel protein type 4 subunit alpha | 208.7 | 2 | 2 | 2.2 | 6 |
| 695 | -16.4 | 4.64 | PTPRA_RAT | Receptor-type tyrosine-protein phosphatase alpha | 90.2 | 3 | 3 | 4.1 | 7 |
| 699 | -16.2 | 3.9 | A2MG_RAT | Alpha-2-macroglobulin | 163.6 | 3 | 3 | 3.8 | 6 |
| 700 | -16.2 | 5.39 | MLP3B_RAT | Microtubule-associated proteins 1A/1B light chain 3B | 16.3 | 3 | 3 | 18 | 38 |
| 705 | -15.9 | 4.71 | ACTN1_RAT | Alpha-actinin-1 | 102.9 | 3 | 4 | 3.4 | 4 |
| 708 | -15.8 | 4.62 | KC1D_RAT | Casein kinase I isoform delta | 47.3 | 3 | 3 | 7 | 11 |
| 709 | -15.8 | 4.76 | TMM33_RAT | Transmembrane protein 33 | 28 | 2 | 2 | 7.7 | 10 |
| 712 | -15.7 | 4.81 | TRXR1_RAT | Thioredoxin reductase 1, cytoplasmic | 54.3 | 3 | 3 | 8.4 | 10 |
| 714 | -15.7 | 4.43 | NF1_RAT | Neurofibromin | 316.9 | 3 | 4 | 1.8 | 3 |
| 719 | -15.4 | 4.9 | PSB2_RAT | Proteasome subunit beta type-2 | 22.9 | 3 | 4 | 16 | 22 |
| 720 | -15.4 | 3.82 | TAOK1_RAT | no protein information available | 115.9 | 3 | 3 | 7.8 | 14 |
| 731 | -15.2 | 4.52 | PDLI4_RAT | PDZ and LIM domain protein 4 | 35.5 | 3 | 3 | 9.7 | 14 |
| 733 | -15.1 | 4.7 | PUR6_RAT | Multifunctional protein ADE2 | 46.9 | 3 | 3 | 7.3 | 10 |
| 734 | -15.1 | 4.37 | RBBP7_RAT | Histone-binding protein RBBP7 | 47.8 | 3 | 3 | 7.5 | 13 |
| 737 | -14.9 | 5.09 | UCRH_RAT | Cytochrome b-c1 complex subunit 6, mitochondrial | 10.4 | 2 | 4 | 20 | 25 |
| 738 | -14.9 | 4.33 | ARHGB_RAT | Rho guanine nucleotide exchange factor 11 | 168.4 | 3 | 4 | 3.5 | 5 |
| 743 | -14.7 | 4.49 | HSP47_RAT | Serpin H1 | 46.5 | 2 | 2 | 6 | 9 |
| 745 | -14.7 | 4.23 | PLCG1_RAT | 1-phosphatidylinositol 4,5-bisphosphate phosphodiesterase gamma-1 | 148.5 | 3 | 3 | 2.4 | 3 |
| 748 | -14.5 | 4.89 | MARK1_RAT | Serine/threonine-protein kinase MARK1 | 88.2 | 2 | 2 | 3.7 | 5 |

108

# APPENDIX B: Protein Identifications Unique to the "Molecular Layer" Hydrogel (Cont'd)

| X! Tandem Rank | log(e) | log(I) | Accession | Description | Mr | Unique Peptides | Total Peptides | % (measured) | % (corrected) |
|---|---|---|---|---|---|---|---|---|---|
| | | | | **174 Protein Identifications Unique to the "Molecular Layer" Hydrogel** | | | | | |
| 753 | -14.1 | 5.05 | RS13_RAT | 40S ribosomal protein S13 | 17.1 | 2 | 2 | 13 | 19 |
| 759 | -13.9 | 4.61 | ARHG7_RAT | Rho guanine nucleotide exchange factor 7 | 73.1 | 2 | 2 | 3.3 | 5 |
| 760 | -13.7 | 4.19 | XKR7_RAT | no protein information available | 64.3 | 2 | 2 | 5.5 | 9 |
| 766 | -13.4 | 4.91 | PP2AA_RAT | Serine/threonine-protein phosphatase 2A catalytic subunit alpha isoform | 35.6 | 2 | 2 | 5.5 | 7 |
| 772 | -13.2 | 4.42 | ICAL_RAT | Calpastatin | 71.3 | 2 | 2 | 4.9 | 8 |
| 774 | -12.8 | 5.12 | CDIPT_RAT | CDP-diacylglycerol--inositol 3-phosphatidyltransferase | 23.6 | 2 | 5 | 8.9 | 15 |
| 780 | -12.4 | 4.47 | PSMF1_RAT | Proteasome inhibitor PI31 subunit | 29.8 | 2 | 2 | 8.1 | 15 |
| 790 | -12 | 4.23 | TRIM9_RAT | E3 ubiquitin-protein ligase TRIM9 | 79.2 | 2 | 2 | 3.7 | 5 |
| 796 | -11.7 | 4.71 | DHSB_RAT | Succinate dehydrogenase [ubiquinone] iron-sulfur subunit, mitochondrial | 16.8 | 2 | 2 | 13 | 18 |
| 800 | -11.6 | 4.67 | PSA3_RAT | Proteasome subunit alpha type-3 | 28.3 | 2 | 2 | 7.9 | 15 |
| 803 | -11.5 | 4.38 | GBRG2_RAT | Gamma-aminobutyric acid receptor subunit gamma-2 | 54 | 2 | 2 | 4.7 | 8 |
| 805 | -11.4 | 4.46 | CCD93_RAT | Coiled-coil domain-containing protein 93 | 72.6 | 2 | 2 | 3.3 | 5 |
| 806 | -11.4 | 4.2 | ELOC_RAT | Transcription elongation factor B polypeptide 1 | 12.5 | 2 | 2 | 25 | 47 |
| 812 | -11.2 | 4.37 | KPRB_RAT | Phosphoribosyl pyrophosphate synthase-associated protein 2 | 40.8 | 2 | 2 | 5.7 | 7 |
| 814 | -11.1 | 4.37 | PLAK_RAT | Junction plakoglobin | 81.7 | 2 | 2 | 3.8 | 5 |
| 815 | -11.1 | 4.24 | SL9A1_RAT | Sodium/hydrogen exchanger 1 | 91.6 | 2 | 2 | 5.4 | 12 |
| 817 | -11.1 | 4.53 | STX7_RAT | Syntaxin-7 | 29.6 | 2 | 2 | 9.6 | 17 |
| 818 | -11.1 | 4.29 | CREL1_RAT | Cysteine-rich with EGF-like domain protein 1 | 45.7 | 2 | 2 | 5 | 6 |
| 820 | -11.1 | 4.39 | RL13A_RAT | 60S ribosomal protein L13a | 23.3 | 2 | 2 | 13 | 21 |
| 821 | -11 | 4.76 | PPAC_RAT | Low molecular weight phosphotyrosine protein phosphatase | 18 | 2 | 2 | 27 | 44 |
| 827 | -10.9 | 4.46 | FAAH_RAT | Fatty-acid amide hydrolase 1 | 63.3 | 2 | 2 | 7.1 | 9 |
| 829 | -10.9 | 4.81 | UK14_RAT | Ribonuclease UK114 | 14.2 | 2 | 2 | 26 | 28 |
| 831 | -10.9 | 4.63 | MIRO2_RAT | Mitochondrial Rho GTPase 2 | 69.1 | 2 | 2 | 3.4 | 6 |
| 832 | -10.8 | 3.65 | VGFR2_RAT | no protein information available | 150.3 | 2 | 2 | 4.5 | 8 |
| 838 | -10.7 | 5.11 | ARC1A_RAT | Actin-related protein 2/3 complex subunit 1A | 41.6 | 2 | 2 | 6.2 | 7 |
| 842 | -10.7 | 5.02 | TF2B_RAT | Transcription initiation factor IIB | 34.8 | 2 | 2 | 2.8 | 4 |
| 848 | -10.5 | 4.43 | GFPT2_RAT | Glutamine--fructose-6-phosphate aminotransferase [isomerizing] 2 | 76.8 | 2 | 2 | 4.8 | 6 |
| 854 | -10.4 | 4.15 | CAC1B_RAT | Voltage-dependent N-type calcium channel subunit alpha-1B | 262.1 | 2 | 2 | 1.5 | 3 |
| 855 | -10.4 | 4.72 | GABR1_RAT | Gamma-aminobutyric acid type B receptor subunit 1 | 111.5 | 2 | 2 | 2.5 | 4 |
| 857 | -10.3 | 4.91 | NQO1_RAT | NAD(P)H dehydrogenase [quinone] 1 | 30.8 | 2 | 2 | 7 | 9 |
| 859 | -10.3 | 4.71 | HCFC2_RAT | Host cell factor 2 | 79.1 | 2 | 2 | 1.2 | 2 |
| 860 | -10.3 | 4.2 | CSTN3_RAT | Calsyntenin-3 | 105.9 | 2 | 2 | 2.6 | 5 |
| 861 | -10.3 | 4.25 | KCNH7_RAT | Potassium voltage-gated channel subfamily H member 7 | 134.8 | 2 | 2 | 3 | 5 |
| 862 | -10.2 | 4.57 | CD166_RAT | CD166 antigen | 65 | 2 | 2 | 3.8 | 7 |
| 863 | -10.2 | 4.01 | PDPK1_RAT | 3-phosphoinositide-dependent protein kinase 1 | 63.6 | 2 | 2 | 4.8 | 6 |
| 865 | -10.2 | 4.66 | VPS45_RAT | Vacuolar protein sorting-associated protein 45 | 64.9 | 2 | 2 | 3 | 4 |
| 866 | -10.2 | 4.77 | GCA_RAT | Ig gamma-2A chain C region | 35.2 | 2 | 2 | 6.2 | 9 |
| 867 | -10.1 | 4.47 | APT_RAT | Adenine phosphoribosyltransferase | 19.5 | 2 | 2 | 20 | 22 |

| X! Tandem Rank | log(e) | log(I) | Accession | Description | Mr | Unique Peptides | Total Peptides | % (measured) | % (corrected) |
|---|---|---|---|---|---|---|---|---|---|
| 870 | -10.1 | 4.41 | AP4A_RAT | Bis(5'-nucleosyl)-tetraphosphatase [asymmetrical] | 16.8 | 2 | 2 | 15 | 19 |
| 872 | -10.1 | 4.26 | COR1B_RAT | Coronin-1B | 53.8 | 2 | 2 | 7.4 | 15 |
| 876 | -10 | 4.75 | D3D2_RAT | Enoyl-CoA delta isomerase 1, mitochondrial | 32.2 | 2 | 2 | 7.6 | 12 |
| 878 | -10 | 4.62 | MT2_RAT | Metallothionein-2 | 6.1 | 2 | 3 | 48 | 100+ |
| 885 | -9.9 | 4.26 | S20A1_RAT | Sodium-dependent phosphate transporter 1 | 74.1 | 2 | 2 | 5.9 | 12 |
| 888 | -9.8 | 4.6 | COMT_RAT | Catechol O-methyltransferase | 29.6 | 2 | 2 | 9.1 | 11 |
| 889 | -9.8 | 4.48 | ROBO1_RAT | no protein information available | 180.6 | 2 | 2 | 1.2 | 2 |
| 891 | -9.8 | 4.58 | NEDD4_RAT | E3 ubiquitin-protein ligase NEDD4 | 102.3 | 2 | 2 | 5.2 | 7 |
| 892 | -9.8 | 4.51 | TIMP4_RAT | no protein information available | 25.6 | 2 | 2 | 7.6 | 11 |
| 895 | -9.7 | 4.02 | GDF15_RAT | no protein information available | 33.4 | 2 | 2 | 9.2 | 12 |
| 896 | -9.7 | 4.58 | CP4F4_RAT | Cytochrome P450 4F4 | 60 | 2 | 2 | 3.3 | 4 |
| 897 | -9.7 | 4.11 | TBX3_RAT | no protein information available | 79.3 | 2 | 2 | 3.9 | 8 |
| 898 | -9.7 | 4.28 | WNK4_RAT | no protein information available | 132.8 | 2 | 2 | 3.7 | 6 |
| 899 | -9.7 | 4.55 | NTRK3_RAT | no protein information available | 97 | 2 | 2 | 2.1 | 4 |
| 903 | -9.6 | 4.77 | SERB_RAT | Phosphoserine phosphatase | 25 | 2 | 2 | 8 | 9 |
| 906 | -9.6 | 4.49 | ASB2_RAT | Ankyrin repeat and SOCS box protein 2 | 70.2 | 2 | 2 | 4.1 | 5 |
| 908 | -9.6 | 4.41 | NDST1_RAT | no protein information available | 100.7 | 2 | 2 | 2.5 | 4 |
| 910 | -9.5 | 4.39 | FAM5A_RAT | BMP/retinoic acid-inducible neural-specific protein 1 | 88.6 | 2 | 2 | 3.2 | 5 |
| 911 | -9.5 | 4.68 | EXOC3_RAT | Exocyst complex component 3 | 86.4 | 2 | 3 | 2.3 | 3 |
| 914 | -9.4 | 4.56 | HAPIP_RAT | Kalirin | 218.7 | 2 | 2 | 1.1 | 2 |
| 915 | -9.3 | 4.48 | DSRAD_RAT | Double-stranded RNA-specific adenosine deaminase | 129.8 | 2 | 2 | 2.3 | 3 |
| 917 | -9.3 | 4.67 | CACP_RAT | Carnitine O-acetyltransferase | 70.8 | 2 | 3 | 3.2 | 6 |
| 920 | -9.2 | 4.42 | MGR7_RAT | no protein information available | 102.2 | 2 | 2 | 3.1 | 5 |
| 926 | -9.1 | 4.23 | PANK4_RAT | Pantothenate kinase 4 | 86.2 | 2 | 2 | 3 | 3 |
| 927 | -9.1 | 4.43 | COA1_RAT | Acetyl-CoA carboxylase 1 | 265 | 2 | 2 | 1 | 1 |
| 929 | -9 | 4.45 | RBBP9_RAT | Putative hydrolase RBBP9 | 21 | 2 | 2 | 8.1 | 10 |
| 930 | -9 | 4.52 | NRX3A_RAT | Neurexin-3 | 173.9 | 2 | 2 | 1.3 | 2 |
| 932 | -9 | 4.46 | CP2DA_RAT | Cytochrome P450 2D10 | 57 | 2 | 2 | 4.2 | 6 |
| 933 | -9 | 3.79 | GAS6_RAT | no protein information available | 74.6 | 2 | 2 | 7.9 | 10 |
| 934 | -9 | 4.24 | MFN2_RAT | Mitofusin-2 | 86.1 | 2 | 2 | 3.6 | 5 |
| 936 | -8.9 | 4 | DAK_RAT | Triokinase/FMN cyclase | 59.4 | 2 | 2 | 6.1 | 8 |
| 939 | -8.9 | 3.98 | PGCA_RAT | Aggrecan core protein | 221 | 2 | 2 | 1.9 | 5 |
| 940 | -8.9 | 4.63 | SCAM5_RAT | Secretory carrier-associated membrane protein 5 | 26.1 | 2 | 2 | 7.7 | 34 |
| 942 | -8.9 | 4.41 | ITM2B_RAT | no protein information available | 30.3 | 2 | 2 | 8.6 | 12 |
| 943 | -8.9 | 4.56 | STXB5_RAT | Syntaxin-binding protein 5 | 127.6 | 2 | 2 | 1.9 | 3 |
| 944 | -8.8 | 4.83 | TBX5_RAT | no protein information available | 57.7 | 2 | 2 | 3.1 | 4 |
| 946 | -8.7 | 4.42 | STA5A_RAT | Signal transducer and activator of transcription 5A | 90.8 | 2 | 2 | 2.1 | 3 |
| 947 | -8.7 | 4.1 | MVP_RAT | Major vault protein | 95.6 | 2 | 2 | 2.9 | 3 |
| 867 | -10.1 | 4.47 | APT_RAT | Adenine phosphoribosyltransferase | 19.5 | 2 | 2 | 20 | 22 |

| X! Tandem Rank | log(e) | log(I) | Accession | Description | Mr | Unique Peptides | Total Peptides | % (measured) | % (corrected) |
|---|---|---|---|---|---|---|---|---|---|
| | | | | **174 Protein Identifications Unique to the "Molecular Layer" Hydrogel** | | | | | |
| 948 | -8.7 | 5.01 | GBRL2_RAT | Gamma-aminobutyric acid receptor-associated protein-like 2 | 13.7 | 2 | 2 | 9.4 | 11 |
| 949 | -8.7 | 4.36 | RTKN_RAT | no protein information available | 61.1 | 2 | 2 | 5.8 | 7 |
| 950 | -8.7 | 4.76 | GSH1_RAT | Glutamate--cysteine ligase catalytic subunit | 72.4 | 2 | 2 | 3.9 | 6 |
| 953 | -8.6 | 4.28 | TIM8B_RAT | Mitochondrial import inner membrane translocase subunit Tim8 B | 9.3 | 2 | 3 | 16 | 17 |
| 955 | -8.6 | 3.77 | FINC_RAT | Fibronectin | 272.3 | 2 | 2 | 1.8 | 3 |
| 956 | -8.6 | 4.68 | GSHB_RAT | Glutathione synthetase | 52.3 | 2 | 2 | 5.1 | 7 |
| 959 | -8.5 | 4.35 | EXOC7_RAT | Exocyst complex component 7 | 75 | 2 | 2 | 3.8 | 6 |
| 960 | -8.4 | 4.49 | ANKS3_RAT | no protein information available | 73 | 2 | 2 | 6.8 | 8 |
| 964 | -8.4 | 4.61 | SYCP2_RAT | Synaptonemal complex protein 2 | 172.5 | 2 | 2 | 1.5 | 2 |
| 966 | -8.3 | 4.62 | LRC57_RAT | no protein information available | 26.7 | 2 | 2 | 9.2 | 11 |
| 968 | -8.3 | 3.66 | AKAP6_RAT | A-kinase anchor protein 6 | 254.2 | 2 | 2 | 1.8 | 3 |
| 969 | -8.3 | 4.71 | TGM1_RAT | Protein-glutamine gamma-glutamyltransferase K | 90.7 | 2 | 2 | 3.4 | 5 |
| 970 | -8.3 | 4.8 | PAFA2_RAT | Platelet-activating factor acetylhydrolase 2, cytoplasmic | 43.5 | 2 | 2 | 6.2 | 7 |
| 971 | -8.2 | 4.66 | TIM_RAT | no protein information available | 138.5 | 2 | 2 | 1.6 | 2 |
| 973 | -8.2 | 4.63 | ULA1_RAT | NEDD8-activating enzyme E1 regulatory subunit | 60.3 | 2 | 2 | 2.4 | 4 |
| 976 | -8.1 | 4.36 | MRS2L_RAT | no protein information available | 49.3 | 2 | 2 | 6 | 7 |
| 977 | -8.1 | 4.32 | PTN9_RAT | Tyrosine-protein phosphatase non-receptor type 9 | 67.9 | 2 | 2 | 4 | 5 |
| 978 | -8.1 | 3.75 | CAN10_RAT | no protein information available | 74.5 | 2 | 2 | 6.3 | 8 |
| 980 | -8.1 | 4.54 | HCN3_RAT | Potassium/sodium hyperpolarization-activated cyclic nucleotide-gated channel 3 | 86.8 | 2 | 2 | 3.7 | 5 |
| 981 | -8.1 | 4.77 | HGS_RAT | Hepatocyte growth factor-regulated tyrosine kinase substrate | 86.2 | 2 | 2 | 1.7 | 4 |
| 982 | -8 | 4.5 | HCN4_RAT | no protein information available | 128.7 | 2 | 2 | 1.9 | 3 |
| 983 | -7.9 | 4.17 | MK12_RAT | no protein information available | 42 | 2 | 2 | 6.5 | 10 |

# APPENDIX C: Protein Identifications Common to both the "White Matter" and "Molecular Layer" Hydrogels

| Accession | Description | Mr | X! Tandem Rank (White Matter) | X! Tandem Rank (Molecular Layer) | Unique Peptides (White Matter) | Unique Peptides (Molecular Layer) | Total Peptides (White Matter) | Total Peptides (Molecular Layer) |
|---|---|---|---|---|---|---|---|---|
| | **755 Protein Identifications Common to the "White Matter" and "Molecular Layer" Hydrogels** | | | | | | | |
| 1433B_RAT | 14-3-3 protein beta/alpha | 27.9 | 148 | 139 | 6 | 7 | 11 | 11 |
| 1433E_RAT | 14-3-3 protein epsilon | 29.2 | 55 | 54 | 25 | 22 | 41 | 42 |
| 1433F_RAT | 14-3-3 protein eta | 28.1 | 69 | 74 | 16 | 9 | 24 | 16 |
| 1433G_RAT | 14-3-3 protein gamma | 28.2 | 91 | 70 | 9 | 14 | 15 | 18 |
| 1433T_RAT | 14-3-3 protein theta | 27.8 | 82 | 92 | 6 | 5 | 14 | 13 |
| 1433Z_RAT | 14-3-3 protein zeta/delta | 27.8 | 58 | 62 | 17 | 15 | 28 | 24 |
| 2AAB_RAT | Serine/threonine-protein phosphatase 2A 65 kDa regulatory subunit A beta isoform | 66 | 940 | 713 | 2 | 3 | 2 | 3 |
| 2ABA_RAT | Serine/threonine-protein phosphatase 2A 55 kDa regulatory subunit B alpha isoform | 51.6 | 881 | 811 | 2 | 2 | 2 | 2 |
| 3HIDH_RAT | 3-hydroxyisobutyrate dehydrogenase, mitochondrial | 35.3 | 286 | 456 | 8 | 5 | 9 | 5 |
| A1AT_RAT | Alpha-1-antiproteinase | 46.1 | 712 | 773 | 3 | 2 | 3 | 2 |
| A4_RAT | Amyloid beta A4 protein | 86.6 | 752 | 717 | 3 | 3 | 3 | 3 |
| AATC_RAT | Aspartate aminotransferase, cytoplasmic | 46.2 | 180 | 191 | 11 | 10 | 12 | 11 |
| AATM_RAT | Aspartate aminotransferase, mitochondrial | 47.3 | 93 | 108 | 17 | 14 | 26 | 22 |
| ABI1_RAT | Abl interactor 1 | 51.5 | 841 | 807 | 2 | 2 | 2 | 3 |
| ABLM2_RAT | Actin-binding LIM protein 2 | 68 | 427 | 240 | 5 | 8 | 5 | 8 |
| ACADL_RAT | Long-chain specific acyl-CoA dehydrogenase, mitochondrial | 47.8 | 579 | 704 | 4 | 2 | 4 | 2 |
| ACADV_RAT | Very long-chain specific acyl-CoA dehydrogenase, mitochondrial | 70.7 | 554 | 286 | 4 | 7 | 4 | 7 |
| ACLY_RAT | ATP-citrate synthase | 120.6 | 176 | 328 | 11 | 6 | 11 | 7 |
| ACON_RAT | Aconitate hydratase, mitochondrial | 85.4 | 31 | 47 | 37 | 24 | 57 | 35 |
| ACOT2_RAT | Acyl-coenzyme A thioesterase 2, mitochondrial | 49.7 | 806 | 783 | 3 | 2 | 3 | 2 |
| ACPH_RAT | Acylamino-acid-releasing enzyme | 81.3 | 936 | 664 | 2 | 3 | 2 | 3 |
| ACSL6_RAT | Long-chain-fatty-acid--CoA ligase 6 | 78.1 | 593 | 533 | 4 | 4 | 5 | 4 |
| ACTA_RAT | Actin, aortic smooth muscle | 42 | 87 | 63 | 2 | 3 | 2 | 5 |
| ACTG_RAT | Actin, cytoplasmic 2 | 41.8 | 32 | 23 | 34 | 33 | 76 | 75 |
| ACTN4_RAT | Alpha-actinin-4 | 104.7 | 411 | 498 | 6 | 4 | 7 | 4 |
| ADDA_RAT | Alpha-adducin | 80.3 | 84 | 83 | 18 | 15 | 23 | 19 |
| ADDB_RAT | Beta-adducin | 80.4 | 182 | 188 | 10 | 10 | 10 | 12 |
| ADDG_RAT | Gamma-adducin | 78.8 | 171 | 172 | 11 | 10 | 13 | 13 |
| ADT1_RAT | ADP/ATP translocase 1 | 32.8 | 197 | 156 | 11 | 11 | 15 | 14 |
| ADT2_RAT | ADP/ATP translocase 2 | 32.7 | 215 | 196 | 5 | 5 | 5 | 5 |
| AFAD_RAT | Afadin | 207.5 | 375 | 636 | 6 | 3 | 6 | 3 |
| AGRN_RAT | Agrin | 208.5 | 1039 | 640 | 2 | 3 | 2 | 3 |
| AINX_RAT | Alpha-internexin | 56.1 | 26 | 82 | 31 | 17 | 52 | 21 |
| AK1A1_RAT | Alcohol dehydrogenase [NADP(+)] | 36.4 | 262 | 297 | 8 | 6 | 11 | 6 |
| AL9A1_RAT | 4-trimethylaminobutyraldehyde dehydrogenase | 53.6 | 210 | 403 | 9 | 4 | 10 | 5 |
| ALBU_RAT | Serum albumin | 68.7 | 340 | 226 | 6 | 8 | 8 | 10 |
| ALDH2_RAT | Aldehyde dehydrogenase, mitochondrial | 56.5 | 282 | 361 | 8 | 5 | 8 | 6 |
| ALDOA_RAT | Fructose-bisphosphate aldolase A | 39.2 | 53 | 55 | 23 | 18 | 42 | 36 |

# APPENDIX C: Protein Identifications Common to both the "White Matter" and "Molecular Layer" Hydrogels (Cont'd)

| | | | | | | | | |
|---|---|---|---|---|---|---|---|---|
| | **755 Protein Identifications Common to the "White Matter" and "Molecular Layer" Hydrogels** | | | | | | | |
| Accession | Description | Mr | X! Tandem Rank (White Matter) | X! Tandem Rank (Molecular Layer) | Unique Peptides (White Matter) | Unique Peptides (Molecular Layer) | Total Peptides (White Matter) | Total Peptides (Molecular Layer) |
| ALDOC_RAT | Fructose-bisphosphate aldolase C | 39.1 | 33 | 37 | 33 | 25 | 63 | 64 |
| ALDR_RAT | Aldose reductase | 35.6 | 305 | 279 | 7 | 6 | 7 | 8 |
| AMPB_RAT | Aminopeptidase B | 72.6 | 589 | 589 | 4 | 3 | 4 | 4 |
| AMPH_RAT | Amphiphysin | 74.8 | 94 | 115 | 16 | 14 | 19 | 15 |
| AMPM2_RAT | Methionine aminopeptidase 2 | 53 | 868 | 852 | 2 | 2 | 2 | 2 |
| AN32A_RAT | Acidic leucine-rich nuclear phosphoprotein 32 family member A | 28.5 | 273 | 638 | 9 | 3 | 9 | 4 |
| ANGT_RAT | Angiotensinogen | 51.9 | 792 | 710 | 3 | 3 | 3 | 3 |
| ANM1_RAT | Protein arginine N-methyltransferase 1 | 40.5 | 1025 | 877 | 2 | 2 | 2 | 2 |
| ANXA1_RAT | Annexin A1 | 38.7 | 849 | 622 | 2 | 3 | 2 | 4 |
| ANXA2_RAT | Annexin A2 | 38.5 | 444 | 399 | 5 | 5 | 5 | 5 |
| ANXA3_RAT | Annexin A3 | 36.2 | 267 | 285 | 8 | 6 | 11 | 7 |
| ANXA5_RAT | Annexin A5 | 35.6 | 405 | 346 | 6 | 6 | 6 | 6 |
| ANXA6_RAT | Annexin A6 | 75.6 | 123 | 223 | 15 | 9 | 20 | 9 |
| AOFA_RAT | Amine oxidase [flavin-containing] A | 59.5 | 547 | 396 | 4 | 5 | 4 | 5 |
| AOFB_RAT | Amine oxidase [flavin-containing] B | 58.2 | 455 | 765 | 5 | 2 | 8 | 4 |
| AP180_RAT | Clathrin coat assembly protein AP180 | 93.5 | 164 | 162 | 10 | 10 | 11 | 14 |
| AP1B1_RAT | AP-1 complex subunit beta-1 | 104.5 | 185 | 105 | 3 | 15 | 4 | 16 |
| AP2A2_RAT | AP-2 complex subunit alpha-2 | 103.8 | 144 | 94 | 14 | 16 | 16 | 20 |
| AP2B1_RAT | AP-2 complex subunit beta | 104.5 | 109 | 110 | 14 | 7 | 19 | 10 |
| AP2M1_RAT | AP-2 complex subunit mu | 49.6 | 539 | 561 | 5 | 4 | 5 | 4 |
| APC_RAT | Adenomatous polyposis coli protein | 310.3 | 681 | 588 | 4 | 4 | 4 | 4 |
| APEX1_RAT | DNA-(apurinic or apyrimidinic site) lyase | 35.4 | 367 | 819 | 6 | 2 | 9 | 2 |
| APLP2_RAT | Amyloid-like protein 2 | 86.8 | 1007 | 762 | 2 | 2 | 2 | 2 |
| APOE_RAT | Apolipoprotein E | 35.7 | 238 | 142 | 8 | 11 | 9 | 15 |
| AQP4_RAT | Aquaporin-4 | 34.5 | 737 | 787 | 3 | 2 | 7 | 3 |
| ARAF_RAT | Serine/threonine-protein kinase A-Raf | 67.5 | 659 | 853 | 4 | 2 | 5 | 2 |
| ARF1_RAT | ADP-ribosylation factor 1 | 20.6 | 311 | 282 | 7 | 6 | 9 | 13 |
| ARF5_RAT | ADP-ribosylation factor 5 | 20.4 | 459 | 407 | 2 | 2 | 4 | 2 |
| ARK72_RAT | Aflatoxin B1 aldehyde reductase member 2 | 40.6 | 723 | 620 | 3 | 3 | 3 | 4 |
| ARL3_RAT | ADP-ribosylation factor-like protein 3 | 20.4 | 805 | 465 | 3 | 4 | 3 | 4 |
| ARP2_RAT | Actin-related protein 2 | 44.7 | 460 | 304 | 5 | 6 | 5 | 6 |
| AT1A1_RAT | Sodium/potassium-transporting ATPase subunit alpha-1 | 113 | 2 | 5 | 61 | 49 | 130 | 123 |
| AT1A2_RAT | Sodium/potassium-transporting ATPase subunit alpha-2 | 112.1 | 3 | 6 | 27 | 25 | 48 | 46 |
| AT1A3_RAT | Sodium/potassium-transporting ATPase subunit alpha-3 | 111.6 | 4 | 7 | 17 | 15 | 37 | 25 |
| AT1B1_RAT | Sodium/potassium-transporting ATPase subunit beta-1 | 35.2 | 213 | 252 | 8 | 7 | 10 | 9 |
| AT1B2_RAT | Sodium/potassium-transporting ATPase subunit beta-2 | 33.4 | 230 | 174 | 8 | 9 | 17 | 23 |
| AT2A2_RAT | Sarcoplasmic/endoplasmic reticulum calcium ATPase 2 | 114.7 | 80 | 57 | 19 | 22 | 20 | 29 |
| AT2A3_RAT | Sarcoplasmic/endoplasmic reticulum calcium ATPase 3 | 109.3 | 88 | 89 | 17 | 14 | 19 | 17 |

# APPENDIX C: Protein Identifications Common to both the "White Matter" and "Molecular Layer" Hydrogels (Cont'd)

| Accession | Description | Mr | X! Tandem Rank (White Matter) | X! Tandem Rank (Molecular Layer) | Unique Peptides (White Matter) | Unique Peptides (Molecular Layer) | Total Peptides (White Matter) | Total Peptides (Molecular Layer) |
|---|---|---|---|---|---|---|---|---|
| AT2B1_RAT | Plasma membrane calcium-transporting ATPase 1 | 138.6 | 41 | 48 | 14 | 8 | 14 | 9 |
| AT2B2_RAT | Plasma membrane calcium-transporting ATPase 2 | 136.7 | 19 | 15 | 42 | 38 | 65 | 57 |
| AT2B3_RAT | Plasma membrane calcium-transporting ATPase 3 | 138.5 | 34 | 36 | 19 | 15 | 22 | 16 |
| AT2B4_RAT | Plasma membrane calcium-transporting ATPase 4 | 133 | 65 | 106 | 3 | 2 | 3 | 2 |
| AT5F1_RAT | ATP synthase F(0) complex subunit B1, mitochondrial | 28.9 | 377 | 400 | 6 | 5 | 7 | 6 |
| ATG3_RAT | Ubiquitin-like-conjugating enzyme ATG3 | 35.8 | 689 | 893 | 3 | 2 | 3 | 2 |
| ATP5H_RAT | ATP synthase subunit d, mitochondrial | 18.6 | 433 | 315 | 5 | 6 | 5 | 9 |
| ATP5I_RAT | ATP synthase subunit e, mitochondrial | 8.1 | 443 | 512 | 5 | 3 | 8 | 5 |
| ATP5J_RAT | ATP synthase-coupling factor 6, mitochondrial | 12.5 | 217 | 259 | 8 | 6 | 10 | 7 |
| ATPA_RAT | ATP synthase subunit alpha, mitochondrial | 59.7 | 17 | 16 | 42 | 35 | 73 | 67 |
| ATPB_RAT | ATP synthase subunit beta, mitochondrial | 56.3 | 11 | 25 | 45 | 30 | 75 | 55 |
| ATPD_RAT | ATP synthase subunit delta, mitochondrial | 17.6 | 398 | 294 | 5 | 5 | 5 | 7 |
| ATPG_RAT | ATP synthase subunit gamma, mitochondrial | 30.2 | 218 | 293 | 10 | 7 | 11 | 10 |
| ATPO_RAT | ATP synthase subunit O, mitochondrial | 23.4 | 172 | 200 | 10 | 9 | 15 | 12 |
| ATX10_RAT | Ataxin-10 | 53.7 | 786 | 871 | 3 | 2 | 4 | 2 |
| BACH_RAT | Cytosolic acyl coenzyme A thioester hydrolase | 42.7 | 205 | 423 | 9 | 5 | 13 | 5 |
| BAIP2_RAT | Brain-specific angiogenesis inhibitor 1-associated protein 2 | 59.1 | 429 | 245 | 5 | 8 | 5 | 8 |
| BASI_RAT | Basigin | 42.4 | 461 | 390 | 5 | 5 | 5 | 5 |
| BASP_RAT | Brain acid soluble protein 1 | 21.6 | 70 | 66 | 19 | 16 | 34 | 30 |
| BAT2_RAT | Protein PRRC2A | 228.9 | 199 | 433 | 12 | 5 | 12 | 6 |
| BAT3_RAT | Large proline-rich protein BAG6 | 114.6 | 312 | 729 | 7 | 3 | 11 | 4 |
| BCAS1_RAT | Breast carcinoma-amplified sequence 1 homolog | 58.6 | 125 | 490 | 13 | 4 | 17 | 4 |
| BCAT1_RAT | Branched-chain-amino-acid aminotransferase, cytosolic | 46 | 480 | 544 | 5 | 4 | 7 | 6 |
| BDH_RAT | D-beta-hydroxybutyrate dehydrogenase, mitochondrial | 38.2 | 810 | 559 | 3 | 3 | 4 | 5 |
| BIEA_RAT | Biliverdin reductase A | 33.5 | 893 | 440 | 2 | 5 | 2 | 5 |
| BIN1_RAT | Myc box-dependent-interacting protein 1 | 64.5 | 174 | 141 | 9 | 10 | 15 | 13 |
| BSN_RAT | Protein bassoon | 418 | 8 | 3 | 54 | 72 | 68 | 87 |
| C1QBP_RAT | Complement component 1 Q subcomponent-binding protein, mitochondrial | 30.7 | 489 | 388 | 4 | 4 | 5 | 5 |
| C1TC_RAT | C-1-tetrahydrofolate synthase, cytoplasmic | 100.8 | 259 | 155 | 8 | 10 | 8 | 10 |
| CAC1A_RAT | Voltage-dependent P/Q-type calcium channel subunit alpha-1A | 251.4 | 271 | 207 | 8 | 10 | 9 | 12 |
| CAC1H_RAT | Voltage-dependent T-type calcium channel subunit alpha-1H | 260.9 | 1038 | 557 | 2 | 4 | 2 | 4 |
| CAC2D_RAT | Voltage-dependent calcium channel subunit alpha-2/delta-1 | 123.7 | 756 | 497 | 3 | 4 | 3 | 4 |
| CAH2_RAT | Carbonic anhydrase 2 | 29 | 572 | 777 | 4 | 2 | 7 | 3 |
| CAH8_RAT | Carbonic anhydrase-related protein | 32.8 | 333 | 267 | 6 | 6 | 7 | 7 |
| CALB1_RAT | Calbindin | 29.8 | 187 | 138 | 10 | 11 | 14 | 19 |
| CALB2_RAT | Calretinin | 31.4 | 124 | 126 | 14 | 13 | 24 | 20 |
| CALD1_RAT | Non-muscle caldesmon | 60.5 | 604 | 652 | 4 | 3 | 4 | 3 |
| CALM_RAT | Calmodulin | 16.7 | 322 | 243 | 7 | 8 | 14 | 17 |

APPENDIX C: Protein Identifications Common to both the "White Matter" and "Molecular Layer" Hydrogels (Cont'd)

| | | | | | | | | |
|---|---|---|---|---|---|---|---|---|
| **755 Protein Identifications Common to the "White Matter" and "Molecular Layer" Hydrogels** | | | | | | | | |
| Accession | Description | Mr | X! Tandem Rank (White Matter) | X! Tandem Rank (Molecular Layer) | Unique Peptides (White Matter) | Unique Peptides (Molecular Layer) | Total Peptides (White Matter) | Total Peptides (Molecular Layer) |
| CALX_RAT | Calnexin | 67.2 | 188 | 280 | 11 | 6 | 14 | 8 |
| CAN2_RAT | Calpain-2 catalytic subunit | 79.7 | 490 | 519 | 5 | 4 | 5 | 6 |
| CAND1_RAT | Cullin-associated NEDD8-dissociated protein 1 | 136.3 | 143 | 199 | 12 | 9 | 13 | 11 |
| CAP1_RAT | Adenylyl cyclase-associated protein 1 | 51.4 | 347 | 331 | 7 | 6 | 7 | 7 |
| CAP2_RAT | Adenylyl cyclase-associated protein 2 | 52.9 | 353 | 383 | 6 | 6 | 7 | 6 |
| CAPS1_RAT | Calcium-dependent secretion activator 1 | 146.2 | 193 | 125 | 10 | 13 | 14 | 13 |
| CATA_RAT | Catalase | 59.6 | 521 | 446 | 4 | 5 | 5 | 5 |
| CATD_RAT | Cathepsin D | 44.7 | 736 | 958 | 3 | 2 | 5 | 2 |
| CCDC8_RAT | Coiled-coil domain-containing protein 8 | 69.5 | 1021 | 974 | 2 | 2 | 4 | 2 |
| CDC37_RAT | Hsp90 co-chaperone Cdc37 | 44.5 | 354 | 537 | 7 | 4 | 8 | 4 |
| CDK5_RAT | Cyclin-dependent-like kinase 5 | 33.2 | 981 | 707 | 2 | 3 | 3 | 3 |
| CDS2_RAT | Phosphatidate cytidylyltransferase 2 | 51.3 | 509 | 571 | 4 | 3 | 7 | 4 |
| CH10_RAT | 10 kDa heat shock protein, mitochondrial | 10.8 | 279 | 255 | 7 | 7 | 10 | 10 |
| CH60_RAT | 60 kDa heat shock protein, mitochondrial | 60.9 | 120 | 81 | 14 | 17 | 25 | 23 |
| CJ058_RAT | Redox-regulatory protein FAM213A | 25.7 | 894 | 514 | 2 | 4 | 2 | 4 |
| CLAP2_RAT | CLIP-associating protein 2 | 140.6 | 75 | 61 | 21 | 20 | 22 | 22 |
| CLCA_RAT | Clathrin light chain A | 27 | 626 | 686 | 4 | 3 | 4 | 4 |
| CLCB_RAT | Clathrin light chain B | 25.1 | 784 | 437 | 3 | 5 | 3 | 6 |
| CLH_RAT | Clathrin heavy chain 1 | 191.5 | 20 | 10 | 43 | 40 | 60 | 55 |
| CLUS_RAT | Clusterin | 51.3 | 1013 | 726 | 2 | 3 | 2 | 3 |
| CN37_RAT | 2',3'-cyclic-nucleotide 3'-phosphodiesterase | 47.2 | 50 | 134 | 26 | 12 | 53 | 16 |
| CNKR2_RAT | Connector enhancer of kinase suppressor of ras 2 | 117.3 | 751 | 513 | 3 | 4 | 3 | 4 |
| CNTN1_RAT | Contactin-1 | 113.4 | 40 | 29 | 31 | 31 | 47 | 47 |
| CNTN2_RAT | Contactin-2 | 113 | 219 | 176 | 10 | 10 | 12 | 11 |
| CNTP1_RAT | Contactin-associated protein 1 | 155.8 | 477 | 194 | 5 | 9 | 6 | 10 |
| CO1A1_RAT | Collagen alpha-1(I) chain | 137.8 | 368 | 752 | 7 | 3 | 7 | 3 |
| CO3_RAT | Complement C3 | 186.3 | 247 | 224 | 9 | 8 | 12 | 10 |
| CO5A1_RAT | Collagen alpha-1(V) chain | 183.9 | 1069 | 967 | 2 | 2 | 2 | 2 |
| COF1_RAT | Cofilin-1 | 18.4 | 232 | 233 | 9 | 8 | 11 | 9 |
| COPD_RAT | Coatomer subunit delta | 57.2 | 764 | 912 | 3 | 2 | 3 | 2 |
| COX2_RAT | Cytochrome c oxidase subunit 2 | 25.9 | 562 | 386 | 4 | 5 | 5 | 7 |
| COX41_RAT | Cytochrome c oxidase subunit 4 isoform 1, mitochondrial | 19.5 | 348 | 389 | 7 | 5 | 12 | 8 |
| COX5A_RAT | Cytochrome c oxidase subunit 5A, mitochondrial | 16.1 | 718 | 775 | 3 | 2 | 5 | 3 |
| COX5B_RAT | Cytochrome c oxidase subunit 5B, mitochondrial | 13.9 | 161 | 215 | 10 | 7 | 23 | 18 |
| CPLX1_RAT | Complexin-1 | 15.1 | 245 | 374 | 8 | 4 | 15 | 9 |
| CPSF7_RAT | Cleavage and polyadenylation specificity factor subunit 7 | 51 | 760 | 873 | 3 | 2 | 4 | 2 |
| CPT2_RAT | Carnitine O-palmitoyltransferase 2, mitochondrial | 74.1 | 954 | 651 | 2 | 3 | 2 | 3 |
| CRK_RAT | Adapter molecule crk | 33.8 | 570 | 594 | 4 | 3 | 4 | 5 |

APPENDIX C: Protein Identifications Common to both the "White Matter" and "Molecular Layer" Hydrogels (Cont'd)

| Accession | Description | Mr | X! Tandem Rank (White Matter) | X! Tandem Rank (Molecular Layer) | Unique Peptides (White Matter) | Unique Peptides (Molecular Layer) | Total Peptides (White Matter) | Total Peptides (Molecular Layer) |
|---|---|---|---|---|---|---|---|---|
| | 755 Protein Identifications Common to the "White Matter" and "Molecular Layer" Hydrogels | | | | | | | |
| CRTC_RAT | Calreticulin | 48 | 355 | 409 | 7 | 5 | 8 | 5 |
| CSAD_RAT | Cysteine sulfinic acid decarboxylase | 55.2 | 978 | 894 | 2 | 2 | 3 | 2 |
| CSDE1_RAT | Cold shock domain-containing protein E1 | 88.8 | 903 | 808 | 2 | 2 | 3 | 2 |
| CSK21_RAT | Casein kinase II subunit alpha | 45 | 843 | 913 | 3 | 2 | 3 | 2 |
| CSKI1_RAT | Caskin-1 | 150.3 | 297 | 148 | 7 | 12 | 10 | 12 |
| CSKP_RAT | Peripheral plasma membrane protein CASK | 103.2 | 889 | 336 | 2 | 6 | 2 | 6 |
| CSN1_RAT | COP9 signalosome complex subunit 1 | 53.4 | 631 | 698 | 4 | 3 | 4 | 3 |
| CSN4_RAT | COP9 signalosome complex subunit 4 | 46.3 | 556 | 647 | 4 | 3 | 5 | 4 |
| CSPG3_RAT | Neurocan core protein | 135.5 | 976 | 900 | 2 | 2 | 2 | 2 |
| CSRP1_RAT | Cysteine and glycine-rich protein 1 | 20.5 | 729 | 798 | 3 | 2 | 3 | 2 |
| CTBP1_RAT | C-terminal-binding protein 1 | 46.6 | 587 | 471 | 4 | 4 | 4 | 4 |
| CTNB1_RAT | Catenin beta-1 | 85.4 | 486 | 302 | 5 | 7 | 6 | 8 |
| CUL5_RAT | Cullin-5 | 90.8 | 406 | 644 | 6 | 3 | 6 | 3 |
| CYC_RAT | Cytochrome c, somatic | 11.5 | 401 | 864 | 4 | 2 | 5 | 2 |
| CYLN2_RAT | CAP-Gly domain-containing linker protein 2 | 115.4 | 523 | 340 | 4 | 6 | 5 | 7 |
| DBNL_RAT | Drebrin-like protein | 48.6 | 531 | 401 | 4 | 5 | 4 | 6 |
| DC1I1_RAT | Cytoplasmic dynein 1 intermediate chain 1 | 72.7 | 323 | 392 | 7 | 5 | 7 | 6 |
| DC1I2_RAT | Cytoplasmic dynein 1 intermediate chain 2 | 71.1 | 426 | 750 | 4 | 2 | 8 | 5 |
| DC1L1_RAT | Cytoplasmic dynein 1 light intermediate chain 1 | 56.8 | 561 | 846 | 4 | 2 | 6 | 2 |
| DC1L2_RAT | Cytoplasmic dynein 1 light intermediate chain 2 | 54.7 | 727 | 412 | 3 | 5 | 3 | 5 |
| DCAK1_RAT | Serine/threonine-protein kinase DCLK1 | 47.7 | 648 | 635 | 4 | 3 | 5 | 3 |
| DCE1_RAT | Glutamate decarboxylase 1 | 66.6 | 790 | 816 | 3 | 2 | 3 | 3 |
| DCE2_RAT | Glutamate decarboxylase 2 | 65.4 | 606 | 823 | 4 | 2 | 4 | 2 |
| DCTN4_RAT | Dynactin subunit 4 | 53.1 | 650 | 464 | 4 | 5 | 4 | 6 |
| DCXR_RAT | L-xylulose reductase | 25.7 | 720 | 682 | 3 | 3 | 3 | 3 |
| DDX1_RAT | ATP-dependent RNA helicase DDX1 | 82.4 | 257 | 703 | 9 | 3 | 9 | 4 |
| DDX46_RAT | Probable ATP-dependent RNA helicase DDX46 | 117.3 | 362 | 722 | 7 | 3 | 7 | 3 |
| DEK_RAT | Protein DEK | 42.9 | 697 | 965 | 3 | 2 | 3 | 2 |
| DEST_RAT | Destrin | 18.4 | 826 | 688 | 2 | 3 | 4 | 5 |
| DGKZ_RAT | Diacylglycerol kinase zeta | 103.9 | 783 | 357 | 2 | 5 | 2 | 5 |
| DHB4_RAT | Peroxisomal multifunctional enzyme type 2 | 79.2 | 326 | 234 | 7 | 8 | 8 | 8 |
| DHCA_RAT | Carbonyl reductase [NADPH] 1 | 30.4 | 955 | 782 | 2 | 2 | 2 | 2 |
| DHE3_RAT | Glutamate dehydrogenase 1, mitochondrial | 61.4 | 60 | 80 | 22 | 16 | 37 | 26 |
| DHPR_RAT | Dihydropteridine reductase | 25.5 | 275 | 598 | 7 | 3 | 9 | 3 |
| DHSA_RAT | Succinate dehydrogenase [ubiquinone] flavoprotein subunit, mitochondrial | 71.6 | 198 | 262 | 10 | 7 | 13 | 10 |
| DHSO_RAT | Sorbitol dehydrogenase | 42.8 | 869 | 902 | 2 | 2 | 2 | 2 |
| DLG1_RAT | Disks large homolog 1 | 100.5 | 272 | 160 | 7 | 9 | 10 | 9 |
| DLG2_RAT | Disks large homolog 2 | 94.9 | 186 | 135 | 11 | 12 | 11 | 13 |

116

| | | | | | | | |
|---|---|---|---|---|---|---|---|
| | | | 755 Protein Identifications Common to the "White Matter" and "Molecular Layer" Hydrogels | | | | |
| Accession | Description | Mr | X! Tandem Rank (White Matter) | X! Tandem Rank (Molecular Layer) | Unique Peptides (White Matter) | Unique Peptides (Molecular Layer) | Total Peptides (White Matter) | Total Peptides (Molecular Layer) |
| DLG3_RAT | Disks large homolog 3 | 93.5 | 596 | 429 | 4 | 3 | 4 | 5 |
| DLG4_RAT | Disks large homolog 4 | 80.4 | 569 | 309 | 3 | 5 | 4 | 5 |
| DLGP1_RAT | Disks large-associated protein 1 | 110.1 | 478 | 303 | 5 | 7 | 6 | 7 |
| DLGP3_RAT | Disks large-associated protein 3 | 105.9 | 853 | 756 | 2 | 2 | 2 | 2 |
| DLGP4_RAT | Disks large-associated protein 4 | 108 | 791 | 356 | 2 | 6 | 4 | 6 |
| DNJC5_RAT | DnaJ homolog subfamily C member 5 | 22.1 | 909 | 511 | 2 | 4 | 3 | 5 |
| DNM1L_RAT | Dynamin-1-like protein | 83.9 | 108 | 98 | 15 | 15 | 15 | 17 |
| DOPD_RAT | D-dopachrome decarboxylase | 13 | 574 | 586 | 4 | 3 | 6 | 5 |
| DPP3_RAT | Dipeptidyl peptidase 3 | 83 | 470 | 430 | 5 | 5 | 5 | 5 |
| DPP6_RAT | Dipeptidyl aminopeptidase-like protein 6 | 97.2 | 463 | 485 | 4 | 4 | 7 | 5 |
| DPYL1_RAT | Dihydropyrimidinase-related protein 1 | 62.2 | 68 | 49 | 15 | 19 | 18 | 24 |
| DPYL2_RAT | Dihydropyrimidinase-related protein 2 | 62.2 | 21 | 34 | 40 | 28 | 72 | 56 |
| DPYL3_RAT | Dihydropyrimidinase-related protein 3 | 61.9 | 168 | 107 | 6 | 10 | 10 | 16 |
| DPYL4_RAT | Dihydropyrimidinase-related protein 4 | 61 | 101 | 93 | 16 | 15 | 27 | 27 |
| DPYL5_RAT | Dihydropyrimidinase-related protein 5 | 61.5 | 261 | 272 | 9 | 7 | 9 | 7 |
| DREB_RAT | Drebrin | 77.3 | 435 | 349 | 5 | 6 | 6 | 6 |
| DYHC_RAT | Cytoplasmic dynein 1 heavy chain 1 | 531.9 | 5 | 8 | 66 | 47 | 74 | 53 |
| DYN1_RAT | Dynamin-1 | 95.9 | 18 | 26 | 45 | 34 | 60 | 50 |
| DYN2_RAT | Dynamin-2 | 98.2 | 140 | 264 | 3 | 2 | 3 | 2 |
| DYN3_RAT | Dynamin-3 | 95.5 | 103 | 131 | 9 | 8 | 9 | 9 |
| DYNA_RAT | Dynactin subunit 1 | 141.8 | 116 | 73 | 15 | 19 | 17 | 19 |
| EAA1_RAT | Excitatory amino acid transporter 1 | 59.7 | 177 | 91 | 10 | 14 | 24 | 36 |
| EAA2_RAT | Excitatory amino acid transporter 2 | 62.1 | 250 | 348 | 9 | 6 | 14 | 7 |
| EAA4_RAT | Excitatory amino acid transporter 4 | 60.7 | 577 | 268 | 4 | 6 | 4 | 8 |
| ECHA_RAT | Trifunctional enzyme subunit alpha, mitochondrial | 82.5 | 387 | 288 | 6 | 7 | 6 | 8 |
| ECHB_RAT | Trifunctional enzyme subunit beta, mitochondrial | 51.4 | 352 | 343 | 7 | 6 | 7 | 6 |
| ECHM_RAT | Enoyl-CoA hydratase, mitochondrial | 31.5 | 549 | 770 | 4 | 2 | 4 | 4 |
| EDF1_RAT | Endothelial differentiation-related factor 1 | 16.4 | 757 | 904 | 3 | 2 | 3 | 3 |
| EF1A1_RAT | Elongation factor 1-alpha 1 | 50.1 | 150 | 193 | 12 | 5 | 15 | 11 |
| EF1A2_RAT | Elongation factor 1-alpha 2 | 50.4 | 154 | 175 | 3 | 10 | 5 | 12 |
| EF1G_RAT | Elongation factor 1-gamma | 49.9 | 229 | 385 | 9 | 5 | 10 | 6 |
| EF2_RAT | Elongation factor 2 | 95.1 | 225 | 157 | 10 | 12 | 13 | 13 |
| EFG1_RAT | Elongation factor G, mitochondrial | 83.7 | 765 | 963 | 3 | 2 | 3 | 2 |
| EI2BD_RAT | Translation initiation factor eIF-2B subunit delta | 57.8 | 733 | 486 | 3 | 4 | 3 | 4 |
| ELAV4_RAT | ELAV-like protein 4 | 40.9 | 446 | 801 | 5 | 2 | 5 | 2 |
| ENOA_RAT | Alpha-enolase | 47 | 49 | 58 | 23 | 18 | 39 | 35 |
| ENOG_RAT | Gamma-enolase | 47 | 78 | 76 | 13 | 12 | 20 | 16 |
| EPN1_RAT | Epsin-1 | 60.1 | 654 | 528 | 3 | 4 | 5 | 6 |

# APPENDIX C: Protein Identifications Common to both the "White Matter" and "Molecular Layer" Hydrogels (Cont'd)

| Accession | Description | Mr | X! Tandem Rank (White Matter) | X! Tandem Rank (Molecular Layer) | Unique Peptides (White Matter) | Unique Peptides (Molecular Layer) | Total Peptides (White Matter) | Total Peptides (Molecular Layer) |
|---|---|---|---|---|---|---|---|---|
| | **755 Protein Identifications Common to the "White Matter" and "Molecular Layer" Hydrogels** | | | | | | | |
| EPN2_RAT | Epsin-2 | 62.3 | 767 | 565 | 2 | 4 | 2 | 4 |
| ERP29_RAT | Endoplasmic reticulum resident protein 29 | 28.6 | 417 | 232 | 6 | 8 | 8 | 10 |
| ES1_RAT | ES1 protein homolog, mitochondrial | 28.2 | 278 | 381 | 7 | 4 | 9 | 5 |
| ETFA_RAT | Electron transfer flavoprotein subunit alpha, mitochondrial | 35 | 412 | 925 | 6 | 2 | 6 | 2 |
| ETFB_RAT | Electron transfer flavoprotein subunit beta | 27.5 | 351 | 275 | 6 | 6 | 7 | 6 |
| ETFD_RAT | Electron transfer flavoprotein-ubiquinone oxidoreductase, mitochondrial | 68.2 | 967 | 461 | 2 | 5 | 2 | 5 |
| EXOC4_RAT | Exocyst complex component 4 | 110.5 | 768 | 483 | 3 | 4 | 3 | 4 |
| EXOC8_RAT | Exocyst complex component 8 | 81 | 741 | 657 | 3 | 3 | 3 | 3 |
| EZRI_RAT | Ezrin | 69.2 | 475 | 534 | 2 | 2 | 2 | 3 |
| F107B_RAT | Protein FAM107B | 15.6 | 629 | 619 | 4 | 3 | 4 | 4 |
| F10A1_RAT | Hsc70-interacting protein | 41.3 | 613 | 642 | 4 | 3 | 5 | 3 |
| FABPB_RAT | Fatty acid-binding protein, brain | 14.7 | 657 | 538 | 3 | 3 | 4 | 3 |
| FABPH_RAT | Fatty acid-binding protein, heart | 14.6 | 436 | 443 | 5 | 5 | 6 | 5 |
| FAS_RAT | Fatty acid synthase | 272.5 | 71 | 65 | 21 | 19 | 29 | 22 |
| FAT2_RAT | Protocadherin Fat 2 | 480.4 | 338 | 79 | 8 | 19 | 8 | 20 |
| FIBA_RAT | Fibrinogen alpha chain | 86.6 | 290 | 711 | 7 | 3 | 7 | 3 |
| FKB1A_RAT | Peptidyl-prolyl cis-trans isomerase FKBP1A | 11.8 | 666 | 742 | 3 | 2 | 5 | 2 |
| FLOT1_RAT | Flotillin-1 | 47.5 | 439 | 337 | 6 | 6 | 6 | 7 |
| FLOT2_RAT | Flotillin-2 | 47 | 740 | 333 | 3 | 6 | 3 | 6 |
| FOLH1_RAT | Glutamate carboxypeptidase 2 | 84.5 | 615 | 789 | 4 | 2 | 4 | 2 |
| FTHFD_RAT | Cytosolic 10-formyltetrahydrofolate dehydrogenase | 99.1 | 264 | 145 | 7 | 11 | 8 | 11 |
| FUBP2_RAT | Far upstream element-binding protein 2 | 74.2 | 67 | 277 | 22 | 7 | 27 | 9 |
| FUMH_RAT | Fumarate hydratase, mitochondrial | 54.4 | 129 | 212 | 13 | 8 | 18 | 10 |
| G3P_RAT | Glyceraldehyde-3-phosphate dehydrogenase | 35.7 | 47 | 96 | 28 | 15 | 63 | 40 |
| G6PD_RAT | Glucose-6-phosphate 1-dehydrogenase | 59.2 | 274 | 417 | 8 | 5 | 9 | 6 |
| GABR2_RAT | Gamma-aminobutyric acid type B receptor subunit 2 | 105.7 | 599 | 382 | 4 | 5 | 4 | 6 |
| GABT_RAT | 4-aminobutyrate aminotransferase, mitochondrial | 56.4 | 223 | 216 | 9 | 8 | 9 | 11 |
| GBB2_RAT | Guanine nucleotide-binding protein G(I)/G(S)/G(T) subunit beta-2 | 37.2 | 440 | 230 | 5 | 8 | 8 | 12 |
| GBLP_RAT | Receptor of activated protein C kinase 1 | 34.9 | 382 | 690 | 6 | 3 | 7 | 4 |
| GBRA1_RAT | Gamma-aminobutyric acid receptor subunit alpha-1 | 51.7 | 919 | 685 | 2 | 3 | 2 | 3 |
| GBRB2_RAT | Gamma-aminobutyric acid receptor subunit beta-2 | 54.6 | 598 | 345 | 4 | 6 | 4 | 6 |
| GCB_RAT | Ig gamma-2B chain C region | 36.5 | 780 | 804 | 3 | 2 | 3 | 2 |
| GDIA_RAT | Rab GDP dissociation inhibitor alpha | 50.5 | 115 | 67 | 16 | 18 | 24 | 26 |
| GDIB_RAT | Rab GDP dissociation inhibitor beta | 50.7 | 216 | 169 | 8 | 7 | 9 | 8 |
| GEPH_RAT | Gephyrin | 83.2 | 358 | 263 | 7 | 7 | 7 | 7 |
| GFAP_RAT | Glial fibrillary acidic protein | 49.9 | 36 | 32 | 34 | 30 | 55 | 52 |
| GGT4_RAT | Gamma-glutamyltransferase 7 | 70.3 | 779 | 669 | 2 | 3 | 2 | 3 |
| GHC2_RAT | Mitochondrial glutamate carrier 2 | 33.6 | 778 | 931 | 3 | 2 | 3 | 2 |

| | | | | | | | | |
|---|---|---|---|---|---|---|---|---|
| **755 Protein Identifications Common to the "White Matter" and "Molecular Layer" Hydrogels** | | | | | | | | |
| *Accession* | *Description* | *Mr* | *X! Tandem Rank (White Matter)* | *X! Tandem Rank (Molecular Layer)* | *Unique Peptides (White Matter)* | *Unique Peptides (Molecular Layer)* | *Total Peptides (White Matter)* | *Total Peptides (Molecular Layer)* |
| GIPC1_RAT | PDZ domain-containing protein GIPC1 | 36.1 | 670 | 764 | 3 | 2 | 3 | 2 |
| GIT1_RAT | ARF GTPase-activating protein GIT1 | 85.2 | 865 | 952 | 2 | 2 | 3 | 2 |
| GLNA_RAT | Glutamine synthetase | 42.1 | 179 | 260 | 10 | 6 | 19 | 12 |
| GLO2_RAT | Hydroxyacylglutathione hydrolase, mitochondrial | 28.9 | 706 | 681 | 3 | 3 | 4 | 3 |
| GLSK_RAT | Glutaminase kidney isoform, mitochondrial | 74 | 153 | 195 | 11 | 9 | 20 | 13 |
| GMFB_RAT | Glia maturation factor beta | 16.6 | 860 | 506 | 2 | 4 | 2 | 5 |
| GNAI1_RAT | Guanine nucleotide-binding protein G(i) subunit alpha-1 | 40.2 | 318 | 173 | 2 | 5 | 2 | 6 |
| GNAI2_RAT | Guanine nucleotide-binding protein G(i) subunit alpha-2 | 40.3 | 160 | 163 | 8 | 8 | 10 | 9 |
| GNAO1_RAT | Guanine nucleotide-binding protein G(o) subunit alpha | 39.9 | 62 | 78 | 22 | 17 | 29 | 23 |
| GNAQ_RAT | Guanine nucleotide-binding protein G(q) subunit alpha | 41.4 | 234 | 198 | 9 | 9 | 11 | 12 |
| GNAS_RAT | Guanine nucleotide-binding protein G(s) subunit alpha isoforms short | 45.6 | 293 | 532 | 6 | 3 | 7 | 3 |
| GPDA_RAT | Glycerol-3-phosphate dehydrogenase [NAD(+)], cytoplasmic | 37.2 | 380 | 404 | 7 | 5 | 9 | 6 |
| GPDM_RAT | Glycerol-3-phosphate dehydrogenase, mitochondrial | 80.9 | 268 | 673 | 9 | 3 | 9 | 3 |
| GRAP1_RAT | GRIP1-associated protein 1 | 96 | 294 | 152 | 8 | 12 | 8 | 12 |
| GRB2_RAT | Growth factor receptor-bound protein 2 | 25.2 | 603 | 916 | 4 | 2 | 4 | 2 |
| GRIA1_RAT | Glutamate receptor 1 | 101.5 | 546 | 244 | 5 | 7 | 5 | 8 |
| GRIA2_RAT | Glutamate receptor 2 | 98.6 | 722 | 249 | 2 | 5 | 2 | 6 |
| GRIA4_RAT | Glutamate receptor 4 | 100.7 | 485 | 300 | 5 | 3 | 7 | 4 |
| GRID2_RAT | Glutamate receptor ionotropic, delta-2 | 113.2 | 119 | 84 | 15 | 16 | 18 | 22 |
| GRP75_RAT | Stress-70 protein, mitochondrial | 73.8 | 48 | 71 | 22 | 16 | 31 | 18 |
| GRP78_RAT | 78 kDa glucose-regulated protein | 72.3 | 44 | 56 | 25 | 18 | 30 | 25 |
| GSK3A_RAT | Glycogen synthase kinase-3 alpha | 51 | 701 | 306 | 3 | 6 | 3 | 6 |
| GSK3B_RAT | Glycogen synthase kinase-3 beta | 46.7 | 916 | 858 | 2 | 2 | 3 | 2 |
| GSTM1_RAT | Glutathione S-transferase Mu 1 | 25.8 | 434 | 553 | 5 | 3 | 5 | 5 |
| GSTM4_RAT | Glutathione S-transferase Yb-3 | 25.5 | 536 | 601 | 3 | 3 | 3 | 3 |
| GSTO1_RAT | Glutathione S-transferase omega-1 | 27.7 | 529 | 484 | 4 | 4 | 8 | 5 |
| GSTP1_RAT | Glutathione S-transferase P | 23.3 | 530 | 763 | 4 | 2 | 4 | 2 |
| GTR3_RAT | Solute carrier family 2, facilitated glucose transporter member 3 | 53.5 | 743 | 781 | 3 | 2 | 3 | 3 |
| H10_RAT | Histone H1.0 | 20.7 | 476 | 624 | 4 | 3 | 7 | 4 |
| H12_RAT | Histone H1.4 | 21.8 | 156 | 137 | 11 | 10 | 19 | 13 |
| H2AY_RAT | Core histone macro-H2A.1 | 39.3 | 349 | 502 | 6 | 4 | 14 | 5 |
| H2AZ_RAT | Histone H2A.Z | 13.4 | 652 | 725 | 2 | 3 | 3 | 3 |
| H2B_RAT | Histone H2B type 1 | 13.9 | 122 | 147 | 12 | 10 | 51 | 18 |
| H4_RAT | Histone H4 | 11.2 | 162 | 354 | 11 | 5 | 29 | 10 |
| HAP28_RAT | 28 kDa heat- and acid-stable phosphoprotein | 20.6 | 437 | 935 | 5 | 2 | 5 | 2 |
| HBA_RAT | Hemoglobin subunit alpha-1/2 | 15.2 | 74 | 151 | 19 | 10 | 46 | 26 |
| HBB1_RAT | Hemoglobin subunit beta-1 | 15.8 | 64 | 72 | 20 | 16 | 37 | 34 |
| HBB2_RAT | Hemoglobin subunit beta-2 | 15.8 | 128 | 130 | 4 | 3 | 7 | 3 |

119

# APPENDIX C: Protein Identifications Common to both the "White Matter" and "Molecular Layer" Hydrogels (Cont'd)

| Accession | Description | Mr | X! Tandem Rank (White Matter) | X! Tandem Rank (Molecular Layer) | Unique Peptides (White Matter) | Unique Peptides (Molecular Layer) | Total Peptides (White Matter) | Total Peptides (Molecular Layer) |
|---|---|---|---|---|---|---|---|---|
| HCC1_RAT | SAP domain-containing ribonucleoprotein | 23.5 | 668 | 539 | 3 | 4 | 3 | 4 |
| HCD2_RAT | 3-hydroxyacyl-CoA dehydrogenase type-2 | 27.1 | 363 | 359 | 6 | 5 | 8 | 8 |
| HDGF_RAT | Hepatoma-derived growth factor | 26.5 | 418 | 694 | 5 | 3 | 7 | 3 |
| HMGB1_RAT | High mobility group protein B1 | 24.7 | 317 | 779 | 8 | 2 | 11 | 2 |
| HMGN2_RAT | Non-histone chromosomal protein HMG-17 | 9.2 | 481 | 665 | 4 | 3 | 14 | 4 |
| HNRPG_RAT | RNA-binding motif protein, X chromosome | 42.2 | 149 | 599 | 13 | 4 | 15 | 5 |
| HNRPK_RAT | Heterogeneous nuclear ribonucleoprotein K | 50.9 | 54 | 100 | 23 | 14 | 52 | 27 |
| HNRPM_RAT | Heterogeneous nuclear ribonucleoprotein M | 73.6 | 57 | 179 | 25 | 10 | 30 | 10 |
| HNRPQ_RAT | Heterogeneous nuclear ribonucleoprotein Q | 59.7 | 695 | 663 | 3 | 3 | 4 | 4 |
| HOME3_RAT | Homer protein homolog 3 | 39.9 | 131 | 60 | 13 | 18 | 15 | 26 |
| HPCL1_RAT | Hippocalcin-like protein 1 | 22.2 | 246 | 209 | 8 | 8 | 15 | 12 |
| HPRT_RAT | Hypoxanthine-guanine phosphoribosyltransferase | 24.5 | 687 | 426 | 3 | 4 | 5 | 6 |
| HS105_RAT | Heat shock protein 105 kDa | 96.4 | 479 | 269 | 4 | 7 | 6 | 8 |
| HS70L_RAT | Heat shock 70 kDa protein 1-like | 70.5 | 130 | 186 | 3 | 3 | 3 | 3 |
| HS90B_RAT | Heat shock protein HSP 90-beta | 83.1 | 37 | 41 | 34 | 26 | 44 | 35 |
| HSP7C_RAT | Heat shock cognate 71 kDa protein | 70.8 | 15 | 24 | 44 | 33 | 92 | 67 |
| HXK1_RAT | Hexokinase-1 | 102.3 | 63 | 50 | 23 | 24 | 25 | 29 |
| ICLN_RAT | Methylosome subunit pICln | 26.1 | 692 | 875 | 3 | 2 | 3 | 2 |
| IDH3A_RAT | Isocitrate dehydrogenase [NAD] subunit alpha, mitochondrial | 39.6 | 239 | 228 | 9 | 8 | 13 | 9 |
| IDH3B_RAT | Isocitrate dehydrogenase [NAD] subunit beta, mitochondrial | 42.3 | 183 | 153 | 10 | 11 | 10 | 12 |
| IDH3G_RAT | Isocitrate dehydrogenase [NAD] subunit gamma 1, mitochondrial | 42.8 | 594 | 587 | 4 | 3 | 6 | 4 |
| IDHC_RAT | Isocitrate dehydrogenase [NADP] cytoplasmic | 46.7 | 525 | 520 | 5 | 4 | 6 | 6 |
| IF2A_RAT | Eukaryotic translation initiation factor 2 subunit 1 | 36 | 855 | 489 | 2 | 4 | 2 | 4 |
| IF39_RAT | Eukaryotic translation initiation factor 3 subunit B | 90.9 | 214 | 505 | 8 | 4 | 11 | 5 |
| IF5_RAT | Eukaryotic translation initiation factor 5 | 48.9 | 950 | 691 | 2 | 3 | 2 | 3 |
| ILF3_RAT | Interleukin enhancer-binding factor 3 | 95.9 | 248 | 744 | 9 | 2 | 10 | 2 |
| IMB1_RAT | Importin subunit beta-1 | 97.1 | 277 | 435 | 8 | 5 | 8 | 6 |
| IMPA1_RAT | Inositol monophosphatase 1 | 30.5 | 283 | 311 | 7 | 6 | 7 | 6 |
| INP4A_RAT | Type I inositol 3,4-bisphosphate 4-phosphatase | 105.5 | 308 | 210 | 7 | 10 | 7 | 10 |
| IP3KA_RAT | Inositol-trisphosphate 3-kinase A | 50.8 | 673 | 227 | 3 | 8 | 3 | 9 |
| IPP2_RAT | Protein phosphatase inhibitor 2 | 22.9 | 484 | 516 | 5 | 4 | 5 | 4 |
| IREB1_RAT | Cytoplasmic aconitate hydratase | 98.1 | 545 | 480 | 5 | 5 | 5 | 6 |
| ITPR1_RAT | Inositol 1,4,5-trisphosphate receptor type 1 | 313.1 | 6 | 4 | 60 | 55 | 80 | 75 |
| ITSN1_RAT | Intersectin-1 | 137.1 | 961 | 610 | 2 | 3 | 2 | 4 |
| IVD_RAT | Isovaleryl-CoA dehydrogenase, mitochondrial | 46.4 | 452 | 574 | 5 | 3 | 5 | 4 |
| K0152_RAT | Malectin | 32.4 | 707 | 675 | 3 | 3 | 3 | 3 |
| K6PF_RAT | ATP-dependent 6-phosphofructokinase, muscle type | 85.4 | 189 | 197 | 10 | 7 | 12 | 9 |
| K6PP_RAT | ATP-dependent 6-phosphofructokinase, platelet type | 85.7 | 181 | 113 | 10 | 14 | 15 | 17 |

755 Protein Identifications Common to the "White Matter" and "Molecular Layer" Hydrogels

120

APPENDIX C: Protein Identifications Common to both the "White Matter" and "Molecular Layer" Hydrogels (Cont'd)

| | | | | | | | | |
|---|---|---|---|---|---|---|---|---|
| **755 Protein Identifications Common to the "White Matter" and "Molecular Layer" Hydrogels** | | | | | | | | |
| Accession | Description | Mr | X! Tandem Rank (White Matter) | X! Tandem Rank (Molecular Layer) | Unique Peptides (White Matter) | Unique Peptides (Molecular Layer) | Total Peptides (White Matter) | Total Peptides (Molecular Layer) |
| KAD1_RAT | Adenylate kinase isoenzyme 1 | 21.6 | 258 | 258 | 8 | 7 | 10 | 9 |
| KAD2_RAT | Adenylate kinase 2, mitochondrial | 26.2 | 607 | 928 | 4 | 2 | 4 | 2 |
| KAD4_RAT | Adenylate kinase 4, mitochondrial | 25.2 | 513 | 630 | 5 | 3 | 6 | 4 |
| KAP0_RAT | cAMP-dependent protein kinase type I-alpha regulatory subunit | 42.9 | 361 | 444 | 6 | 4 | 8 | 4 |
| KAP3_RAT | cAMP-dependent protein kinase type II-beta regulatory subunit | 46 | 514 | 692 | 5 | 3 | 5 | 3 |
| KAPCA_RAT | cAMP-dependent protein kinase catalytic subunit alpha | 40.5 | 958 | 545 | 2 | 4 | 2 | 5 |
| KAT1_RAT | Kynurenine--oxoglutarate transaminase 1, mitochondrial | 51.6 | 907 | 460 | 2 | 5 | 2 | 5 |
| KCAB2_RAT | Voltage-gated potassium channel subunit beta-2 | 41 | 543 | 751 | 4 | 2 | 6 | 3 |
| KCC2A_RAT | Calcium/calmodulin-dependent protein kinase type II subunit alpha | 54.1 | 346 | 366 | 3 | 3 | 3 | 3 |
| KCC2B_RAT | Calcium/calmodulin-dependent protein kinase type II subunit beta | 60.4 | 107 | 140 | 15 | 9 | 24 | 15 |
| KCC2D_RAT | Calcium/calmodulin-dependent protein kinase type II subunit delta | 60 | 206 | 133 | 6 | 12 | 9 | 15 |
| KCC2G_RAT | Calcium/calmodulin-dependent protein kinase type II subunit gamma | 59 | 224 | 325 | 2 | 2 | 2 | 2 |
| KCC4_RAT | Calcium/calmodulin-dependent protein kinase type IV | 53.1 | 155 | 312 | 12 | 7 | 15 | 9 |
| KCNA1_RAT | Potassium voltage-gated channel subfamily A member 1 | 56.3 | 571 | 924 | 4 | 2 | 5 | 2 |
| KCNC1_RAT | Potassium voltage-gated channel subfamily C member 1 | 65.8 | 824 | 799 | 3 | 2 | 3 | 2 |
| KCNC3_RAT | Potassium voltage-gated channel subfamily C member 3 | 94.3 | 989 | 909 | 2 | 2 | 2 | 2 |
| KCND2_RAT | Potassium voltage-gated channel subfamily D member 2 | 70.5 | 753 | 828 | 3 | 2 | 3 | 2 |
| KCRB_RAT | Creatine kinase B-type | 42.7 | 14 | 14 | 41 | 37 | 93 | 109 |
| KCRU_RAT | Creatine kinase U-type, mitochondrial | 47 | 441 | 562 | 5 | 3 | 8 | 5 |
| KIF1B_RAT | Kinesin-like protein KIF1B | 204 | 423 | 418 | 6 | 5 | 6 | 5 |
| KIF3C_RAT | Kinesin-like protein KIF3C | 89.8 | 996 | 662 | 2 | 3 | 2 | 3 |
| KKCC2_RAT | Calcium/calmodulin-dependent protein kinase kinase 2 | 64.4 | 884 | 554 | 2 | 4 | 2 | 4 |
| KLC1_RAT | Kinesin light chain 1 | 63.2 | 350 | 458 | 7 | 4 | 8 | 4 |
| KPCE_RAT | Protein kinase C epsilon type | 83.4 | 550 | 476 | 4 | 4 | 6 | 6 |
| KPCG_RAT | Protein kinase C gamma type | 78.3 | 192 | 242 | 10 | 7 | 11 | 10 |
| KPYM_RAT | Pyruvate kinase PKM | 57.6 | 35 | 31 | 32 | 29 | 53 | 42 |
| KS6A1_RAT | Ribosomal protein S6 kinase alpha-1 | 82.8 | 830 | 290 | 2 | 6 | 2 | 6 |
| L1CAM_RAT | Neural cell adhesion molecule L1 | 140.8 | 867 | 405 | 2 | 5 | 2 | 5 |
| LA_RAT | Lupus La protein homolog | 47.7 | 457 | 845 | 5 | 2 | 6 | 2 |
| LAMB2_RAT | Laminin subunit beta-2 | 196.3 | 266 | 168 | 9 | 11 | 9 | 12 |
| LANC1_RAT | LanC-like protein 1 | 45.2 | 910 | 616 | 2 | 3 | 2 | 5 |
| LAP2_RAT | Lamina-associated polypeptide 2, isoform beta | 50.1 | 141 | 475 | 11 | 4 | 15 | 4 |
| LASP1_RAT | LIM and SH3 domain protein 1 | 30 | 126 | 167 | 13 | 9 | 16 | 16 |
| LDHA_RAT | L-lactate dehydrogenase A chain | 36.4 | 173 | 466 | 6 | 3 | 7 | 3 |
| LDHB_RAT | L-lactate dehydrogenase B chain | 36.5 | 83 | 247 | 18 | 8 | 27 | 12 |
| LETM1_RAT | LETM1 and EF-hand domain-containing protein 1, mitochondrial | 83 | 132 | 221 | 13 | 9 | 14 | 9 |
| LGI1_RAT | Leucine-rich glioma-inactivated protein 1 | 63.7 | 534 | 758 | 4 | 2 | 4 | 2 |
| LIN7A_RAT | Protein lin-7 homolog A | 25.8 | 464 | 493 | 5 | 2 | 5 | 3 |

| | | | | | | | |
|---|---|---|---|---|---|---|---|
| | **755 Protein Identifications Common to the "White Matter" and "Molecular Layer" Hydrogels** | | | | | | |
| *Accession* | *Description* | *Mr* | *X! Tandem Rank (White Matter)* | *X! Tandem Rank (Molecular Layer)* | *Unique Peptides (White Matter)* | *Unique Peptides (Molecular Layer)* | *Total Peptides (White Matter)* | *Total Peptides (Molecular Layer)* |
| LIN7C_RAT | Protein lin-7 homolog C | 21.8 | 638 | 320 | 2 | 6 | 2 | 7 |
| LIPA3_RAT | Liprin-alpha-3 | 133.3 | 300 | 122 | 8 | 14 | 8 | 19 |
| LIPA4_RAT | Liprin-alpha-4 | 117.9 | 508 | 393 | 5 | 4 | 5 | 4 |
| LIS1_RAT | Platelet-activating factor acetylhydrolase IB subunit alpha | 46.5 | 341 | 415 | 7 | 5 | 7 | 5 |
| LKHA4_RAT | Leukotriene A-4 hydrolase | 69 | 512 | 576 | 5 | 4 | 5 | 4 |
| LMNA_RAT | Prelamin-A/C | 74.3 | 86 | 69 | 15 | 17 | 19 | 19 |
| LMNB1_RAT | Lamin-B1 | 66.4 | 56 | 85 | 24 | 14 | 34 | 16 |
| LPP3_RAT | Phospholipid phosphatase 3 | 35.3 | 660 | 347 | 3 | 5 | 6 | 9 |
| LRC59_RAT | Leucine-rich repeat-containing protein 59 | 34.8 | 1075 | 886 | 2 | 2 | 2 | 2 |
| LSAMP_RAT | Limbic system-associated membrane protein | 37.3 | 575 | 441 | 4 | 5 | 6 | 8 |
| LUZP1_RAT | Leucine zipper protein 1 | 117.1 | 256 | 724 | 10 | 3 | 11 | 3 |
| LXN_RAT | Latexin | 25.6 | 688 | 629 | 3 | 3 | 6 | 9 |
| LYPA1_RAT | Acyl-protein thioesterase 1 | 24.7 | 777 | 868 | 3 | 2 | 3 | 2 |
| LYRIC_RAT | Protein LYRIC | 63.9 | 620 | 809 | 4 | 2 | 4 | 2 |
| M2OM_RAT | Mitochondrial 2-oxoglutarate/malate carrier protein | 34.1 | 376 | 289 | 6 | 6 | 7 | 7 |
| MAOX_RAT | NADP-dependent malic enzyme | 64 | 482 | 371 | 5 | 5 | 6 | 5 |
| MAP1A_RAT | Microtubule-associated protein 1A | 299.3 | 13 | 27 | 52 | 36 | 73 | 45 |
| MAP1B_RAT | Microtubule-associated protein 1B | 269.3 | 10 | 9 | 50 | 43 | 65 | 54 |
| MAP2_RAT | Methionine aminopeptidase 2 | 202.3 | 30 | 35 | 39 | 29 | 44 | 34 |
| MARCS_RAT | Myristoylated alanine-rich C-kinase substrate | 29.6 | 28 | 22 | 34 | 30 | 65 | 65 |
| MARE1_RAT | Microtubule-associated protein RP/EB family member 1 | 29.9 | 748 | 531 | 2 | 4 | 2 | 5 |
| MARE2_RAT | Microtubule-associated protein RP/EB family member 2 | 37 | 430 | 530 | 6 | 4 | 8 | 4 |
| MARE3_RAT | Microtubule-associated protein RP/EB family member 3 | 31.9 | 447 | 570 | 5 | 3 | 7 | 3 |
| MARK2_RAT | Serine/threonine-protein kinase MARK2 | 80.8 | 492 | 413 | 5 | 5 | 5 | 6 |
| MARK3_RAT | MAP/microtubule affinity-regulating kinase 3 | 88.7 | 816 | 723 | 3 | 2 | 3 | 2 |
| MATR3_RAT | Matrin-3 | 94.4 | 104 | 143 | 15 | 11 | 22 | 16 |
| MAVS_RAT | Mitochondrial antiviral-signaling protein | 53.8 | 798 | 747 | 3 | 3 | 3 | 3 |
| MBP_RAT | Myelin basic protein | 21.4 | 45 | 222 | 28 | 8 | 111 | 13 |
| MDHC_RAT | Malate dehydrogenase, cytoplasmic | 36.3 | 111 | 192 | 15 | 9 | 19 | 13 |
| MDHM_RAT | Malate dehydrogenase, mitochondrial | 35.6 | 106 | 136 | 14 | 11 | 18 | 13 |
| MDR1_RAT | Multidrug resistance protein 1 | 141.3 | 728 | 884 | 3 | 2 | 3 | 3 |
| MECP2_RAT | Methyl-CpG-binding protein 2 | 53 | 142 | 645 | 12 | 3 | 16 | 4 |
| MEPD_RAT | Thimet oligopeptidase | 78.1 | 390 | 824 | 6 | 2 | 7 | 2 |
| MGR1_RAT | Metabotropic glutamate receptor 1 | 133.2 | 797 | 178 | 3 | 10 | 3 | 11 |
| MK01_RAT | Mitogen-activated protein kinase 1 | 41.1 | 637 | 439 | 4 | 3 | 4 | 3 |
| MK03_RAT | Mitogen-activated protein kinase 3 | 43 | 739 | 281 | 2 | 7 | 2 | 8 |
| MLRA_RAT | Myosin regulatory light chain RLC-A | 19.8 | 675 | 438 | 3 | 4 | 4 | 7 |
| MMSA_RAT | Methylmalonate-semialdehyde dehydrogenase [acylating], mitochondrial | 57.8 | 520 | 380 | 4 | 5 | 4 | 5 |

# APPENDIX C: Protein Identifications Common to both the "White Matter" and "Molecular Layer" Hydrogels (Cont'd)

| Accession | Description | Mr | X! Tandem Rank (White Matter) | X! Tandem Rank (Molecular Layer) | Unique Peptides (White Matter) | Unique Peptides (Molecular Layer) | Total Peptides (White Matter) | Total Peptides (Molecular Layer) |
|---|---|---|---|---|---|---|---|---|
| | **755 Protein Identifications Common to the "White Matter" and "Molecular Layer" Hydrogels** | | | | | | | |
| MOES_RAT | Moesin | 67.6 | 392 | 500 | 6 | 4 | 6 | 5 |
| MP2K1_RAT | Dual specificity mitogen-activated protein kinase kinase 1 | 43.3 | 502 | 425 | 5 | 5 | 7 | 6 |
| MPCP_RAT | Phosphate carrier protein, mitochondrial | 39.4 | 289 | 266 | 8 | 7 | 13 | 9 |
| MRCKA_RAT | Serine/threonine-protein kinase MRCK alpha | 196.9 | 516 | 961 | 5 | 2 | 5 | 2 |
| MRCKB_RAT | Serine/threonine-protein kinase MRCK beta | 194.8 | 664 | 353 | 3 | 6 | 4 | 6 |
| MRIP_RAT | Myosin phosphatase Rho-interacting protein | 117 | 548 | 276 | 5 | 7 | 5 | 7 |
| MRP_RAT | MARCKS-related protein | 19.7 | 749 | 702 | 3 | 3 | 4 | 5 |
| MTPN_RAT | Myotrophin | 12.7 | 832 | 771 | 2 | 2 | 2 | 3 |
| MYH10_RAT | Myosin-10 | 228.8 | 29 | 11 | 39 | 43 | 52 | 52 |
| MYH9_RAT | Myosin-9 | 226.1 | 96 | 68 | 12 | 15 | 15 | 19 |
| MYL6_RAT | Myosin light polypeptide 6 | 16.8 | 241 | 472 | 8 | 4 | 11 | 5 |
| MYO5A_RAT | Unconventional myosin-Va | 211.6 | 51 | 43 | 26 | 25 | 34 | 30 |
| NAC2_RAT | Sodium/calcium exchanger 2 | 100.5 | 235 | 185 | 8 | 9 | 9 | 13 |
| NCAM1_RAT | Neural cell adhesion molecule 1 | 94.6 | 42 | 38 | 30 | 26 | 36 | 49 |
| NCKP1_RAT | Nck-associated protein 1 | 128.8 | 400 | 937 | 6 | 2 | 6 | 2 |
| NCPR_RAT | NADPH--cytochrome P450 reductase | 76.8 | 969 | 901 | 2 | 2 | 2 | 2 |
| NDRG2_RAT | Protein NDRG2 | 40.8 | 136 | 164 | 11 | 9 | 13 | 17 |
| NEB2_RAT | Neurabin-2 | 89.6 | 284 | 201 | 8 | 9 | 10 | 11 |
| NECP1_RAT | Adaptin ear-binding coat-associated protein 1 | 29.8 | 551 | 434 | 4 | 4 | 5 | 6 |
| NEDD8_RAT | NEDD8 | 9 | 661 | 715 | 3 | 3 | 3 | 3 |
| NEGR1_RAT | Neuronal growth regulator 1 | 37.8 | 505 | 503 | 4 | 4 | 4 | 5 |
| NEUM_RAT | Neuromodulin | 23.6 | 77 | 51 | 19 | 20 | 34 | 42 |
| NFASC_RAT | Neurofascin | 137.9 | 66 | 87 | 20 | 15 | 25 | 20 |
| NFH_RAT | Neurofilament heavy polypeptide | 115.3 | 38 | 218 | 30 | 8 | 36 | 9 |
| NFL_RAT | Neurofilament light polypeptide | 61.2 | 25 | 150 | 35 | 9 | 49 | 9 |
| NFM_RAT | Neurofilament medium polypeptide | 95.6 | 12 | 166 | 50 | 7 | 74 | 9 |
| NHERF_RAT | Na(+)/H(+) exchange regulatory cofactor NHE-RF1 | 38.7 | 170 | 239 | 11 | 8 | 12 | 10 |
| NHRF2_RAT | Na(+)/H(+) exchange regulatory cofactor NHE-RF2 | 37.3 | 683 | 585 | 3 | 3 | 4 | 3 |
| NLGN2_RAT | Neuroligin-2 | 90.9 | 407 | 508 | 6 | 4 | 7 | 4 |
| NLGN3_RAT | Neuroligin-3 | 93.8 | 646 | 835 | 3 | 2 | 4 | 2 |
| NLTP_RAT | Non-specific lipid-transfer protein | 58.8 | 761 | 736 | 3 | 3 | 4 | 3 |
| NONO_RAT | Non-POU domain-containing octamer-binding protein | 54.9 | 313 | 701 | 8 | 3 | 11 | 3 |
| NOS1_RAT | Nitric oxide synthase, brain | 160.5 | 410 | 190 | 6 | 9 | 7 | 10 |
| NP1L4_RAT | Nucleosome assembly protein 1-like 4 | 43.9 | 408 | 376 | 5 | 5 | 6 | 6 |
| NPTN_RAT | Neuroplastin | 31.3 | 862 | 611 | 2 | 3 | 3 | 3 |
| NPTX1_RAT | Neuronal pentraxin-1 | 47.2 | 789 | 874 | 3 | 2 | 3 | 2 |
| NPTXR_RAT | Neuronal pentraxin receptor | 52.3 | 649 | 402 | 4 | 5 | 4 | 5 |
| NRCAM_RAT | Neuronal cell adhesion molecule | 133.8 | 203 | 154 | 11 | 12 | 11 | 12 |

# APPENDIX C: Protein Identifications Common to both the "White Matter" and "Molecular Layer" Hydrogels (Cont'd)

| | | | | | | | | |
|---|---|---|---|---|---|---|---|---|
| | **755 Protein Identifications Common to the "White Matter" and "Molecular Layer" Hydrogels** | | | | | | | |
| Accession | Description | Mr | X! Tandem Rank (White Matter) | X! Tandem Rank (Molecular Layer) | Unique Peptides (White Matter) | Unique Peptides (Molecular Layer) | Total Peptides (White Matter) | Total Peptides (Molecular Layer) |
| NRDC_RAT | Nardilysin | 132.9 | 977 | 474 | 2 | 4 | 2 | 4 |
| NSF1C_RAT | NSFL1 cofactor p47 | 40.7 | 118 | 123 | 14 | 13 | 17 | 16 |
| NTRI_RAT | Neurotrimin | 38 | 1001 | 671 | 2 | 3 | 2 | 3 |
| NUCB1_RAT | Nucleobindin-1 | 53.5 | 515 | 830 | 5 | 2 | 5 | 2 |
| NUCL_RAT | Nucleolin | 77 | 252 | 428 | 9 | 5 | 9 | 5 |
| NUDC_RAT | Nuclear migration protein nudC | 38.4 | 373 | 250 | 7 | 8 | 7 | 8 |
| NUDT3_RAT | Diphosphoinositol polyphosphate phosphohydrolase 1 | 19.1 | 915 | 728 | 2 | 2 | 3 | 2 |
| NUHM_RAT | NADH dehydrogenase [ubiquinone] flavoprotein 2, mitochondrial | 27.4 | 324 | 387 | 7 | 5 | 7 | 6 |
| ODO2_RAT | Dihydrolipoyllysine-residue succinyltransferase component of 2-oxoglutarate dehydrogenase complex, | 48.9 | 365 | 284 | 6 | 6 | 8 | 8 |
| ODP2_RAT | Dihydrolipoyllysine-residue acetyltransferase component of pyruvate dehydrogenase complex, mitoch | 58.7 | 212 | 202 | 9 | 7 | 11 | 9 |
| ODPA_RAT | Pyruvate dehydrogenase E1 component subunit alpha, somatic form, mitochondrial | 43.2 | 135 | 211 | 12 | 8 | 14 | 11 |
| ODPB_RAT | Pyruvate dehydrogenase E1 component subunit beta, mitochondrial | 38.8 | 134 | 159 | 12 | 10 | 18 | 12 |
| OGT1_RAT | UDP-N-acetylglucosamine--peptide N-acetylglucosaminyltransferase 110 kDa subunit | 115.5 | 663 | 572 | 3 | 4 | 5 | 4 |
| OPLA_RAT | 5-oxoprolinase | 137.6 | 840 | 509 | 3 | 4 | 4 | 4 |
| OSBL1_RAT | Oxysterol-binding protein-related protein 1 | 107.7 | 1058 | 740 | 2 | 3 | 2 | 3 |
| OXR1_RAT | Oxidation resistance protein 1 | 84.1 | 138 | 217 | 11 | 8 | 11 | 10 |
| OXRP_RAT | Hypoxia up-regulated protein 1 | 111.2 | 201 | 251 | 11 | 8 | 14 | 10 |
| PA1B2_RAT | Platelet-activating factor acetylhydrolase IB subunit beta | 25.6 | 634 | 398 | 3 | 5 | 4 | 5 |
| PABP1_RAT | Polyadenylate-binding protein 1 | 70.7 | 249 | 291 | 9 | 7 | 9 | 8 |
| PACN1_RAT | Protein kinase C and casein kinase substrate in neurons protein 1 | 50.4 | 194 | 189 | 10 | 9 | 19 | 16 |
| PACN2_RAT | Protein kinase C and casein kinase substrate in neurons 2 protein | 55.9 | 583 | 869 | 3 | 2 | 3 | 2 |
| PACS1_RAT | Phosphofurin acidic cluster sorting protein 1 | 104.6 | 540 | 447 | 4 | 4 | 5 | 4 |
| PADI2_RAT | Protein-arginine deiminase type-2 | 75.3 | 330 | 649 | 7 | 3 | 8 | 3 |
| PAIRB_RAT | Plasminogen activator inhibitor 1 RNA-binding protein | 44.7 | 518 | 646 | 3 | 3 | 7 | 3 |
| PAK1_RAT | Serine/threonine-protein kinase PAK 1 | 60.5 | 331 | 338 | 7 | 6 | 10 | 7 |
| PAK2_RAT | Serine/threonine-protein kinase PAK 2 | 57.9 | 339 | 375 | 5 | 3 | 10 | 7 |
| PARK7_RAT | Protein deglycase DJ-1 | 20 | 555 | 549 | 4 | 4 | 7 | 4 |
| PCCA_RAT | Propionyl-CoA carboxylase alpha chain, mitochondrial | 77.7 | 754 | 422 | 2 | 4 | 2 | 4 |
| PCCB_RAT | Propionyl-CoA carboxylase beta chain, mitochondrial | 58.6 | 522 | 602 | 4 | 3 | 4 | 3 |
| PCLO_RAT | Protein piccolo | 552.4 | 46 | 21 | 30 | 36 | 32 | 45 |
| PDCD8_RAT | Apoptosis-inducing factor 1, mitochondrial | 66.7 | 402 | 579 | 6 | 3 | 6 | 3 |
| PDE4B_RAT | cAMP-specific 3',5'-cyclic phosphodiesterase 4B | 82 | 993 | 677 | 2 | 3 | 2 | 3 |
| PDIA1_RAT | Protein disulfide-isomerase | 56.9 | 292 | 334 | 8 | 6 | 12 | 6 |
| PDIA3_RAT | Protein disulfide-isomerase A3 | 56.6 | 90 | 103 | 17 | 15 | 21 | 18 |
| PDIA4_RAT | Protein disulfide-isomerase A4 | 72.7 | 325 | 851 | 8 | 2 | 8 | 3 |
| PDIA6_RAT | Protein disulfide-isomerase A6 | 48.1 | 356 | 257 | 5 | 6 | 6 | 7 |
| PDK2_RAT | [Pyruvate dehydrogenase (acetyl-transferring)] kinase isozyme 2, mitochondrial | 46.1 | 926 | 951 | 2 | 2 | 2 | 2 |
| PDXK_RAT | Pyridoxal kinase | 34.9 | 280 | 323 | 8 | 6 | 10 | 8 |

124

| | | | | | | | |
|---|---|---|---|---|---|---|---|
| **755 Protein Identifications Common to the "White Matter" and "Molecular Layer" Hydrogels** | | | | | | |
| *Accession* | *Description* | *Mr* | *X! Tandem Rank (White Matter)* | *X! Tandem Rank (Molecular Layer)* | *Unique Peptides (White Matter)* | *Unique Peptides (Molecular Layer)* | *Total Peptides (White Matter)* | *Total Peptides (Molecular Layer)* |
| PEBP1_RAT | Phosphatidylethanolamine-binding protein 1 | 20.7 | 145 | 214 | 11 | 8 | 16 | 11 |
| PEP19_RAT | Purkinje cell protein 4 | 6.7 | 306 | 575 | 7 | 2 | 12 | 5 |
| PGAM1_RAT | Phosphoglycerate mutase 1 | 28.5 | 337 | 326 | 7 | 6 | 8 | 9 |
| PGAM2_RAT | Phosphoglycerate mutase 2 | 28.6 | 558 | 368 | 3 | 2 | 3 | 2 |
| PGCB_RAT | Brevican core protein | 96 | 314 | 834 | 8 | 2 | 8 | 2 |
| PGK1_RAT | Phosphoglycerate kinase 1 | 44.4 | 61 | 117 | 21 | 11 | 33 | 18 |
| PGM1_RAT | Phosphoglucomutase-1 | 61.2 | 165 | 254 | 11 | 7 | 17 | 8 |
| PGRC1_RAT | Membrane-associated progesterone receptor component 1 | 21.5 | 395 | 373 | 5 | 5 | 5 | 5 |
| PHB_RAT | Prohibitin | 29.8 | 209 | 274 | 9 | 7 | 11 | 8 |
| PHB2_RAT | Prohibitin-2 | 33.3 | 220 | 205 | 9 | 9 | 10 | 11 |
| PI51C_RAT | Phosphatidylinositol 4-phosphate 5-kinase type-1 gamma | 75.5 | 566 | 367 | 4 | 5 | 4 | 5 |
| PI52B_RAT | Phosphatidylinositol 5-phosphate 4-kinase type-2 beta | 47.2 | 462 | 394 | 5 | 5 | 5 | 6 |
| PICA_RAT | Phosphatidylinositol-binding clathrin assembly protein | 69.2 | 796 | 372 | 2 | 5 | 2 | 5 |
| PIPNA_RAT | Phosphatidylinositol transfer protein alpha isoform | 31.8 | 601 | 546 | 4 | 4 | 4 | 4 |
| PIPNB_RAT | Phosphatidylinositol transfer protein beta isoform | 31.3 | 952 | 945 | 2 | 2 | 2 | 2 |
| PITM1_RAT | Membrane-associated phosphatidylinositol transfer protein 1 | 134.9 | 445 | 319 | 5 | 6 | 6 | 7 |
| PLAP_RAT | Phospholipase A-2-activating protein | 87 | 472 | 365 | 5 | 5 | 5 | 5 |
| PLCB1_RAT | 1-phosphatidylinositol 4,5-bisphosphate phosphodiesterase beta-1 | 138.3 | 414 | 314 | 5 | 7 | 5 | 7 |
| PLCB3_RAT | 1-phosphatidylinositol 4,5-bisphosphate phosphodiesterase beta-3 | 139.4 | 882 | 650 | 2 | 3 | 2 | 3 |
| PLCB4_RAT | 1-phosphatidylinositol 4,5-bisphosphate phosphodiesterase beta-4 | 134.4 | 677 | 321 | 4 | 6 | 4 | 6 |
| PLEC1_RAT | Plectin | 533.2 | 9 | 28 | 55 | 37 | 64 | 40 |
| PLM_RAT | Phospholemman | 10.4 | 671 | 473 | 3 | 4 | 5 | 4 |
| PLPP_RAT | Pyridoxal phosphate phosphatase | 33.1 | 454 | 467 | 4 | 4 | 7 | 5 |
| PLST_RAT | Plastin-3 | 70.3 | 296 | 355 | 7 | 6 | 8 | 6 |
| PP1A_RAT | Serine/threonine-protein phosphatase PP1-alpha catalytic subunit | 37.5 | 448 | 468 | 5 | 4 | 5 | 4 |
| PP1G_RAT | Serine/threonine-protein phosphatase PP1-gamma catalytic subunit | 37 | 979 | 501 | 2 | 3 | 2 | 3 |
| PP1R7_RAT | Protein phosphatase 1 regulatory subunit 7 | 41.3 | 1068 | 463 | 2 | 5 | 2 | 6 |
| PP2BA_RAT | Serine/threonine-protein phosphatase 2B catalytic subunit alpha isoform | 58.6 | 89 | 97 | 15 | 15 | 22 | 21 |
| PP2BB_RAT | Serine/threonine-protein phosphatase 2B catalytic subunit beta isoform | 59.1 | 191 | 208 | 4 | 3 | 4 | 4 |
| PP2CA_RAT | Protein phosphatase 1A | 42.4 | 581 | 591 | 4 | 3 | 6 | 3 |
| PPIA_RAT | Peptidyl-prolyl cis-trans isomerase A | 17.7 | 422 | 342 | 5 | 5 | 7 | 10 |
| PPIB_RAT | Peptidyl-prolyl cis-trans isomerase B | 22.8 | 533 | 613 | 5 | 3 | 5 | 3 |
| PPID_RAT | Peptidyl-prolyl cis-trans isomerase D | 40.6 | 822 | 457 | 3 | 5 | 3 | 5 |
| PPT1_RAT | Palmitoyl-protein thioesterase 1 | 34.4 | 880 | 786 | 2 | 2 | 3 | 2 |
| PRDX2_RAT | Peroxiredoxin-2 | 21.6 | 200 | 330 | 8 | 6 | 12 | 9 |
| PRDX5_RAT | Peroxiredoxin-5, mitochondrial | 22.2 | 276 | 350 | 7 | 6 | 10 | 9 |
| PRDX6_RAT | Peroxiredoxin-6 | 24.7 | 167 | 183 | 10 | 9 | 13 | 10 |
| PRIO_RAT | Major prion protein | 27.8 | 726 | 788 | 3 | 2 | 4 | 3 |

| Accession | Description | Mr | X! Tandem Rank (White Matter) | X! Tandem Rank (Molecular Layer) | Unique Peptides (White Matter) | Unique Peptides (Molecular Layer) | Total Peptides (White Matter) | Total Peptides (Molecular Layer) |
|---|---|---|---|---|---|---|---|---|
| | **755 Protein Identifications Common to the "White Matter" and "Molecular Layer" Hydrogels** | | | | | | | |
| PROF1_RAT | Profilin-1 | 14.8 | 315 | 470 | 7 | 4 | 9 | 5 |
| PROF2_RAT | Profilin-2 | 14.9 | 815 | 592 | 2 | 3 | 2 | 3 |
| PRS4_RAT | 26S protease regulatory subunit 4 | 49.2 | 450 | 496 | 5 | 4 | 7 | 4 |
| PRS6A_RAT | 26S protease regulatory subunit 6A | 49.1 | 595 | 462 | 4 | 4 | 4 | 4 |
| PRS7_RAT | 26S protease regulatory subunit 7 | 48.4 | 370 | 358 | 6 | 5 | 6 | 6 |
| PRS8_RAT | 26S protease regulatory subunit 8 | 45.6 | 467 | 659 | 4 | 3 | 5 | 3 |
| PRVA_RAT | Parvalbumin alpha | 11.8 | 590 | 436 | 4 | 5 | 4 | 5 |
| PSA1_RAT | Proteasome subunit alpha type-1 | 29.5 | 526 | 397 | 4 | 5 | 4 | 6 |
| PSA4_RAT | Proteasome subunit alpha type-4 | 29.5 | 938 | 836 | 2 | 2 | 2 | 2 |
| PSA5_RAT | Proteasome subunit alpha type-5 | 26.4 | 610 | 593 | 4 | 3 | 4 | 3 |
| PSA6_RAT | Proteasome subunit alpha type-6 | 27.4 | 580 | 850 | 4 | 2 | 4 | 2 |
| PSA7_RAT | Proteasome subunit alpha type-7 | 28.3 | 731 | 632 | 3 | 3 | 3 | 3 |
| PSB1_RAT | Proteasome subunit beta type-1 | 26.5 | 704 | 606 | 3 | 3 | 4 | 3 |
| PSB4_RAT | Proteasome subunit beta type-4 | 29.2 | 781 | 603 | 3 | 3 | 3 | 3 |
| PSB6_RAT | Proteasome subunit beta type-6 | 25.3 | 622 | 668 | 4 | 3 | 4 | 3 |
| PSD9_RAT | Disks large homolog 4 | 24.8 | 495 | 683 | 5 | 3 | 6 | 3 |
| PSIP1_RAT | PC4 and SFRS1-interacting protein | 59.6 | 133 | 612 | 13 | 3 | 15 | 4 |
| PTMA_RAT | Prothymosin alpha | 12.2 | 304 | 442 | 7 | 4 | 15 | 8 |
| PTMS_RAT | Parathymosin | 11.4 | 669 | 564 | 3 | 4 | 5 | 5 |
| PTN11_RAT | Tyrosine-protein phosphatase non-receptor type 11 | 68.4 | 665 | 754 | 4 | 2 | 4 | 2 |
| PTPRZ_RAT | Receptor-type tyrosine-protein phosphatase zeta | 255.2 | 237 | 161 | 8 | 9 | 12 | 12 |
| PURB_RAT | Transcriptional activator protein Pur-beta | 33.3 | 320 | 313 | 7 | 6 | 8 | 6 |
| PYC_RAT | Pyruvate carboxylase, mitochondrial | 129.6 | 113 | 95 | 15 | 17 | 18 | 18 |
| PYGB_RAT | Glycogen phosphorylase, brain form | 96 | 95 | 116 | 16 | 13 | 18 | 15 |
| PYGM_RAT | Glycogen phosphorylase, muscle form | 97.1 | 243 | 124 | 7 | 11 | 8 | 11 |
| QKI_RAT | Protein quaking | 37.6 | 442 | 697 | 5 | 3 | 5 | 3 |
| RAB14_RAT | Ras-related protein Rab-14 | 23.8 | 301 | 335 | 6 | 4 | 7 | 4 |
| RAB18_RAT | Ras-related protein Rab-18 | 23 | 795 | 555 | 3 | 4 | 4 | 4 |
| RAB1A_RAT | Ras-related protein Rab-1A | 22.5 | 416 | 308 | 3 | 5 | 4 | 6 |
| RAB1B_RAT | Ras-related protein Rab-1B | 22.1 | 537 | 482 | 2 | 2 | 2 | 2 |
| RAB2A_RAT | Ras-related protein Rab-2A | 23.5 | 465 | 295 | 5 | 5 | 7 | 10 |
| RAB35_RAT | Ras-related protein Rab-35 | 23 | 491 | 395 | 2 | 3 | 3 | 3 |
| RAB3A_RAT | Ras-related protein Rab-3A | 25 | 270 | 170 | 7 | 8 | 16 | 20 |
| RAB3C_RAT | Ras-related protein Rab-3C | 25.9 | 471 | 324 | 3 | 4 | 3 | 5 |
| RAB6A_RAT | Ras-related protein Rab-6A | 15.8 | 501 | 329 | 5 | 6 | 8 | 8 |
| RAB7_RAT | Ras-related protein Rab-7a | 23.5 | 251 | 180 | 8 | 9 | 11 | 10 |
| RABE1_RAT | Rab GTPase-binding effector protein 1 | 99.4 | 496 | 672 | 5 | 3 | 5 | 3 |
| RALA_RAT | Ras-related protein Ral-A | 23.5 | 674 | 839 | 3 | 2 | 3 | 2 |

| | 755 Protein Identifications Common to the "White Matter" and "Molecular Layer" Hydrogels | | | | | | | |
|---|---|---|---|---|---|---|---|---|
| Accession | Description | Mr | X! Tandem Rank (White Matter) | X! Tandem Rank (Molecular Layer) | Unique Peptides (White Matter) | Unique Peptides (Molecular Layer) | Total Peptides (White Matter) | Total Peptides (Molecular Layer) |
| RANT_RAT | GTP-binding nuclear protein Ran, testis-specific isoform | 24.4 | 567 | 716 | 4 | 3 | 5 | 3 |
| RAP1A_RAT | Ras-related protein Rap-1A | 21 | 299 | 377 | 7 | 5 | 10 | 5 |
| RASN_RAT | GTPase NRas | 21.2 | 686 | 414 | 3 | 5 | 6 | 7 |
| RB11B_RAT | Ras-related protein Rab-11B | 24.3 | 389 | 241 | 6 | 8 | 6 | 8 |
| RB6I2_RAT | ELKS/Rab6-interacting/CAST family member 1 | 108.8 | 196 | 42 | 10 | 26 | 11 | 29 |
| RCN2_RAT | Reticulocalbin-2 | 37.4 | 872 | 580 | 2 | 4 | 3 | 5 |
| RGS3_RAT | Regulator of G-protein signaling 3 | 106.3 | 1067 | 658 | 2 | 3 | 2 | 3 |
| RGS7_RAT | Regulator of G-protein signaling 7 | 55.7 | 602 | 341 | 4 | 6 | 4 | 6 |
| RGS8_RAT | Regulator of G-protein signaling 8 | 20.9 | 971 | 615 | 2 | 3 | 3 | 3 |
| RHOA_RAT | Transforming protein RhoA | 21.8 | 517 | 563 | 4 | 3 | 7 | 4 |
| RIB1_RAT | Dolichyl-diphosphooligosaccharide--protein glycosyltransferase subunit 1 | 68.3 | 222 | 307 | 9 | 6 | 9 | 7 |
| RIB2_RAT | Dolichyl-diphosphooligosaccharide--protein glycosyltransferase subunit 2 | 69 | 584 | 560 | 4 | 3 | 5 | 4 |
| RIC8A_RAT | Synembryn-A | 59.8 | 835 | 767 | 2 | 2 | 2 | 2 |
| RIMS1_RAT | Regulating synaptic membrane exocytosis protein 1 | 179.5 | 344 | 119 | 7 | 13 | 7 | 13 |
| RIMS2_RAT | Regulating synaptic membrane exocytosis protein 2 | 175.8 | 846 | 363 | 3 | 6 | 3 | 6 |
| RL19_RAT | 60S ribosomal protein L19 | 23.5 | 820 | 794 | 2 | 2 | 3 | 3 |
| RL24_RAT | 60S ribosomal protein L24 | 17.8 | 716 | 844 | 3 | 2 | 3 | 2 |
| RL26_RAT | 60S ribosomal protein L26 | 17.3 | 804 | 802 | 3 | 2 | 3 | 2 |
| RL27_RAT | 60S ribosomal protein L27 | 15.7 | 711 | 795 | 3 | 2 | 3 | 2 |
| RL3_RAT | 60S ribosomal protein L3 | 46 | 466 | 923 | 5 | 2 | 8 | 2 |
| RL31_RAT | 60S ribosomal protein L31 | 14.5 | 992 | 938 | 2 | 2 | 2 | 2 |
| RL4_RAT | 60S ribosomal protein L4 | 47.1 | 221 | 792 | 8 | 2 | 9 | 2 |
| RL5_RAT | 60S ribosomal protein L5 | 34.3 | 628 | 793 | 4 | 2 | 5 | 2 |
| RL6_RAT | 60S ribosomal protein L6 | 33.4 | 438 | 661 | 5 | 3 | 6 | 5 |
| RL7_RAT | 60S ribosomal protein L7 | 30.3 | 369 | 499 | 7 | 4 | 7 | 4 |
| RL7A_RAT | 60S ribosomal protein L7a | 29.8 | 691 | 558 | 3 | 3 | 3 | 4 |
| RL8_RAT | 60S ribosomal protein L8 | 27.9 | 642 | 883 | 4 | 2 | 4 | 2 |
| RLA0_RAT | 60S acidic ribosomal protein P0 | 34.2 | 538 | 621 | 4 | 3 | 6 | 4 |
| RLA2_RAT | 60S acidic ribosomal protein P2 | 11.7 | 409 | 525 | 5 | 3 | 8 | 4 |
| ROA1_RAT | Heterogeneous nuclear ribonucleoprotein A1 | 34.1 | 102 | 219 | 14 | 7 | 18 | 8 |
| ROA3_RAT | Heterogeneous nuclear ribonucleoprotein A3 | 39.6 | 114 | 182 | 13 | 10 | 21 | 13 |
| ROCK2_RAT | Rho-associated protein kinase 2 | 159.3 | 231 | 86 | 9 | 17 | 9 | 17 |
| RP3A_RAT | Rabphilin-3A | 75.8 | 169 | 101 | 11 | 14 | 11 | 18 |
| RPGF4_RAT | Rap guanine nucleotide exchange factor 4 | 50.1 | 836 | 746 | 2 | 3 | 2 | 3 |
| RS14_RAT | 40S ribosomal protein S14 | 16.1 | 494 | 523 | 4 | 3 | 4 | 3 |
| RS16_RAT | 40S ribosomal protein S16 | 16.3 | 732 | 785 | 3 | 2 | 3 | 2 |
| RS18_RAT | 40S ribosomal protein S18 | 17.7 | 483 | 623 | 5 | 3 | 7 | 6 |
| RS19_RAT | 40S ribosomal protein S19 | 15.9 | 419 | 487 | 6 | 4 | 8 | 4 |

## APPENDIX C: Protein Identifications Common to both the "White Matter" and "Molecular Layer" Hydrogels (Cont'd)

| Accession | Description | Mr | X! Tandem Rank (White Matter) | X! Tandem Rank (Molecular Layer) | Unique Peptides (White Matter) | Unique Peptides (Molecular Layer) | Total Peptides (White Matter) | Total Peptides (Molecular Layer) |
|---|---|---|---|---|---|---|---|---|
| | | | **755 Protein Identifications Common to the "White Matter" and "Molecular Layer" Hydrogels** | | | | | |
| RS21_RAT | 40S ribosomal protein S21 | 9.1 | 813 | 566 | 2 | 3 | 2 | 3 |
| RS23_RAT | 40S ribosomal protein S23 | 15.7 | 921 | 840 | 2 | 2 | 3 | 2 |
| RS25_RAT | 40S ribosomal protein S25 | 13.7 | 503 | 882 | 5 | 2 | 5 | 2 |
| RS28_RAT | 40S ribosomal protein S28 | 7.8 | 621 | 706 | 3 | 2 | 4 | 3 |
| RS3_RAT | 40S ribosomal protein S3 | 26.7 | 263 | 488 | 8 | 4 | 8 | 4 |
| RS3A_RAT | 40S ribosomal protein S3a | 29.8 | 614 | 590 | 3 | 4 | 5 | 4 |
| RS6_RAT | 40S ribosomal protein S6 | 28.7 | 381 | 769 | 5 | 2 | 5 | 2 |
| RS8_RAT | 40S ribosomal protein S8 | 24.1 | 497 | 578 | 4 | 4 | 5 | 4 |
| RSSA_RAT | 40S ribosomal protein SA | 32.7 | 397 | 379 | 5 | 4 | 6 | 5 |
| RTN1_RAT | Reticulon-1 | 83 | 97 | 75 | 15 | 17 | 20 | 21 |
| RTN4_RAT | Reticulon-4 | 126.3 | 76 | 112 | 20 | 14 | 26 | 19 |
| RUVB1_RAT | RuvB-like 1 | 50.2 | 775 | 581 | 3 | 4 | 3 | 4 |
| S12A5_RAT | Solute carrier family 12 member 5 | 123.5 | 175 | 213 | 11 | 9 | 13 | 10 |
| S14L2_RAT | SEC14-like protein 2 | 46.1 | 700 | 972 | 3 | 2 | 3 | 2 |
| S27A1_RAT | Long-chain fatty acid transport protein 1 | 71.2 | 532 | 481 | 4 | 4 | 5 | 4 |
| S4A4_RAT | Electrogenic sodium bicarbonate cotransporter 1 | 121.3 | 139 | 104 | 13 | 15 | 18 | 26 |
| S6A17_RAT | Sodium-dependent neutral amino acid transporter SLC6A17 | 81 | 421 | 596 | 5 | 3 | 6 | 3 |
| SAFB1_RAT | Scaffold attachment factor B1 | 104.5 | 190 | 301 | 10 | 6 | 14 | 7 |
| SAHH_RAT | Adenosylhomocysteinase | 47.4 | 240 | 344 | 9 | 6 | 12 | 6 |
| SC6A1_RAT | Sodium- and chloride-dependent GABA transporter 1 | 67 | 618 | 797 | 4 | 2 | 5 | 3 |
| SC6A9_RAT | Sodium- and chloride-dependent glycine transporter 1 | 70.5 | 788 | 757 | 2 | 2 | 4 | 2 |
| SCAM1_RAT | Secretory carrier-associated membrane protein 1 | 38 | 563 | 253 | 4 | 8 | 5 | 11 |
| SCN2A_RAT | Sodium channel protein type 2 subunit alpha | 227.7 | 166 | 121 | 11 | 12 | 13 | 15 |
| SEPT5_RAT | Septin-5 | 42.8 | 838 | 360 | 3 | 5 | 3 | 6 |
| SEPT7_RAT | Septin-7 | 50.5 | 112 | 88 | 15 | 15 | 21 | 28 |
| SERA_RAT | D-3-phosphoglycerate dehydrogenase | 56.3 | 228 | 238 | 9 | 8 | 10 | 8 |
| SET_RAT | Protein SET | 33.4 | 586 | 689 | 4 | 3 | 4 | 3 |
| SFRS2_RAT | Serine/arginine-rich splicing factor 2 | 25.3 | 386 | 491 | 6 | 4 | 8 | 6 |
| SFXN1_RAT | Sideroflexin-1 | 35.4 | 413 | 410 | 4 | 4 | 5 | 5 |
| SFXN3_RAT | Sideroflexin-3 | 35.4 | 364 | 256 | 6 | 7 | 8 | 10 |
| SFXN5_RAT | Sideroflexin-5 | 37.3 | 399 | 431 | 5 | 4 | 5 | 4 |
| SGTA_RAT | Small glutamine-rich tetratricopeptide repeat-containing protein alpha | 34.1 | 493 | 567 | 4 | 3 | 6 | 4 |
| SH3G1_RAT | Endophilin-A2 | 41.5 | 385 | 332 | 5 | 5 | 5 | 6 |
| SH3G2_RAT | Endophilin-A1 | 28.4 | 211 | 283 | 9 | 6 | 12 | 13 |
| SHAN1_RAT | SH3 and multiple ankyrin repeat domains protein 1 | 226.2 | 158 | 46 | 12 | 24 | 14 | 29 |
| SHAN2_RAT | SH3 and multiple ankyrin repeat domains protein 2 | 158.6 | 424 | 59 | 6 | 19 | 6 | 23 |
| SHAN3_RAT | SH3 and multiple ankyrin repeat domains protein 3 | 193.1 | 504 | 292 | 5 | 6 | 6 | 7 |
| SHPS1_RAT | Tyrosine-protein phosphatase non-receptor type substrate 1 | 55.7 | 253 | 165 | 8 | 10 | 12 | 11 |

128

| Accession | Description | Mr | X! Tandem Rank (White Matter) | X! Tandem Rank (Molecular Layer) | Unique Peptides (White Matter) | Unique Peptides (Molecular Layer) | Total Peptides (White Matter) | Total Peptides (Molecular Layer) |
|---|---|---|---|---|---|---|---|---|
| | **755 Protein Identifications Common to the "White Matter" and "Molecular Layer" Hydrogels** | | | | | | | |
| SKP1_RAT | S-phase kinase-associated protein 1 | 18.5 | 699 | 749 | 3 | 2 | 5 | 3 |
| SLK_RAT | STE20-like serine/threonine-protein kinase | 137.8 | 560 | 448 | 4 | 5 | 4 | 5 |
| SMC3_RAT | Structural maintenance of chromosomes protein 3 | 138.4 | 384 | 735 | 7 | 3 | 7 | 3 |
| SNAA_RAT | Alpha-soluble NSF attachment protein | 33.2 | 227 | 220 | 9 | 8 | 10 | 12 |
| SND1_RAT | Staphylococcal nuclease domain-containing protein 1 | 101.9 | 117 | 271 | 15 | 7 | 15 | 8 |
| SNG1_RAT | Synaptogyrin-1 | 25.7 | 658 | 270 | 3 | 6 | 3 | 7 |
| SNIP_RAT | SRC kinase signaling inhibitor 1 | 129.7 | 81 | 40 | 20 | 27 | 23 | 31 |
| SNP25_RAT | Synaptosomal-associated protein 25 | 23.3 | 99 | 45 | 14 | 23 | 31 | 48 |
| SNX1_RAT | Sorting nexin-1 | 59 | 653 | 626 | 3 | 3 | 3 | 3 |
| SODC_RAT | Superoxide dismutase [Cu-Zn] | 15.8 | 552 | 600 | 4 | 3 | 6 | 3 |
| SPRE_RAT | Sepiapterin reductase | 28.1 | 914 | 778 | 2 | 2 | 2 | 2 |
| SPRL1_RAT | SPARC-like protein 1 | 70.6 | 428 | 299 | 5 | 7 | 6 | 7 |
| SPTA2_RAT | Spectrin alpha chain, non-erythrocytic 1 | 284.5 | 1 | 1 | 118 | 120 | 154 | 165 |
| SPTN2_RAT | Spectrin beta chain, non-erythrocytic 2 | 270.9 | 7 | 2 | 57 | 70 | 72 | 96 |
| SRC_RAT | Proto-oncogene tyrosine-protein kinase Src | 59.9 | 684 | 278 | 3 | 7 | 4 | 7 |
| SSDH_RAT | Succinate-semialdehyde dehydrogenase, mitochondrial | 52.2 | 343 | 427 | 7 | 5 | 8 | 6 |
| STIP1_RAT | Stress-induced-phosphoprotein 1 | 62.5 | 85 | 144 | 19 | 12 | 21 | 14 |
| STMN1_RAT | Stathmin | 17.1 | 291 | 604 | 8 | 3 | 9 | 3 |
| STRN3_RAT | Striatin-3 | 50.4 | 1004 | 495 | 2 | 4 | 2 | 5 |
| STTP1_RAT | Elongator complex protein 2 | 91.7 | 876 | 847 | 2 | 2 | 2 | 2 |
| STX1A_RAT | Syntaxin-1A | 33 | 371 | 181 | 3 | 6 | 3 | 8 |
| STX1C_RAT | Syntaxin-1B | 33.2 | 73 | 52 | 19 | 21 | 37 | 44 |
| STX6_RAT | Syntaxin-6 | 29 | 568 | 541 | 3 | 3 | 4 | 3 |
| STXB1_RAT | Syntaxin-binding protein 1 | 67.5 | 39 | 18 | 29 | 34 | 39 | 55 |
| SUCA_RAT | Succinyl-CoA ligase [ADP/GDP-forming] subunit alpha, mitochondrial | 35 | 360 | 518 | 5 | 4 | 7 | 4 |
| SUOX_RAT | Sulfite oxidase, mitochondrial | 54.3 | 920 | 721 | 2 | 3 | 2 | 3 |
| SV2A_RAT | Synaptic vesicle glycoprotein 2A | 82.6 | 456 | 204 | 5 | 8 | 7 | 14 |
| SV2B_RAT | Synaptic vesicle glycoprotein 2B | 77.5 | 766 | 411 | 2 | 4 | 3 | 5 |
| SYD_RAT | Aspartate--tRNA ligase, cytoplasmic | 57.1 | 309 | 384 | 8 | 6 | 9 | 6 |
| SYN1_RAT | Synapsin-1 | 73.9 | 43 | 20 | 26 | 32 | 63 | 65 |
| SYN2_RAT | Synapsin-2 | 63.4 | 110 | 53 | 12 | 18 | 18 | 29 |
| SYN3_RAT | Synapsin-3 | 63.3 | 1056 | 825 | 2 | 2 | 3 | 2 |
| SYNG_RAT | Synergin gamma | 74 | 960 | 826 | 2 | 2 | 2 | 2 |
| SYNJ1_RAT | Synaptojanin-1 | 172.8 | 59 | 77 | 23 | 17 | 27 | 21 |
| SYPH_RAT | Synaptophysin | 33.3 | 432 | 568 | 4 | 3 | 7 | 8 |
| SYT1_RAT | Synaptotagmin-1 | 47.4 | 285 | 246 | 6 | 4 | 6 | 6 |
| SYT12_RAT | Synaptotagmin-12 | 46.6 | 357 | 158 | 7 | 10 | 7 | 10 |
| SYT2_RAT | Synaptotagmin-2 | 47.2 | 159 | 109 | 11 | 13 | 11 | 17 |

| Accession | Description | Mr | X! Tandem Rank (White Matter) | X! Tandem Rank (Molecular Layer) | Unique Peptides (White Matter) | Unique Peptides (Molecular Layer) | Total Peptides (White Matter) | Total Peptides (Molecular Layer) |
|---|---|---|---|---|---|---|---|---|
| | **755 Protein Identifications Common to the "White Matter" and "Molecular Layer" Hydrogels** | | | | | | | |
| SYTC_RAT | Threonine--tRNA ligase, cytoplasmic | 80.5 | 769 | 627 | 3 | 3 | 3 | 3 |
| SYUA_RAT | Alpha-synuclein | 14.5 | 255 | 171 | 6 | 8 | 7 | 12 |
| SYUB_RAT | Beta-synuclein | 14.5 | 146 | 132 | 11 | 11 | 18 | 14 |
| SYV_RAT | Valine--tRNA ligase | 140.3 | 383 | 391 | 6 | 5 | 7 | 5 |
| SYYC_RAT | Tyrosine--tRNA ligase, cytoplasmic | 58.9 | 676 | 316 | 3 | 7 | 4 | 7 |
| TAGL3_RAT | Transgelin-3 | 24.7 | 393 | 318 | 6 | 6 | 11 | 10 |
| TALDO_RAT | Transaldolase | 37.4 | 453 | 784 | 5 | 2 | 5 | 2 |
| TAU_RAT | Microtubule-associated protein tau | 78.4 | 105 | 99 | 14 | 14 | 24 | 23 |
| TBA8_RAT | Tubulin alpha-8 chain | 50 | 52 | 44 | 3 | 4 | 5 | 5 |
| TBB1_RAT | Tubulin beta-2B chain | 49.9 | 16 | 12 | 43 | 40 | 89 | 82 |
| TBB3_RAT | Tubulin beta-3 chain | 50.4 | 27 | 30 | 11 | 6 | 18 | 10 |
| TBB5_RAT | Tubulin beta-5 chain | 49.6 | 23 | 13 | 10 | 9 | 21 | 17 |
| TCPA_RAT | T-complex protein 1 subunit alpha | 60.3 | 152 | 184 | 11 | 9 | 12 | 10 |
| TCPD_RAT | T-complex protein 1 subunit delta | 57.9 | 157 | 128 | 11 | 12 | 14 | 13 |
| TENR_RAT | Tenascin-R | 149.3 | 163 | 129 | 11 | 12 | 11 | 12 |
| TERA_RAT | Transitional endoplasmic reticulum ATPase | 89.2 | 79 | 64 | 20 | 20 | 29 | 27 |
| THIL_RAT | Acetyl-CoA acetyltransferase, mitochondrial | 44.7 | 207 | 287 | 9 | 6 | 14 | 8 |
| THIM_RAT | 3-ketoacyl-CoA thiolase, mitochondrial | 41.8 | 738 | 515 | 3 | 4 | 4 | 4 |
| THIO_RAT | Thioredoxin | 11.5 | 896 | 618 | 2 | 3 | 2 | 3 |
| THTM_RAT | 3-mercaptopyruvate sulfurtransferase | 32.8 | 511 | 507 | 4 | 4 | 6 | 5 |
| THTR_RAT | Thiosulfate sulfurtransferase | 33.3 | 374 | 730 | 6 | 2 | 6 | 3 |
| TIM13_RAT | Mitochondrial import inner membrane translocase subunit Tim13 | 10.5 | 524 | 449 | 5 | 4 | 5 | 5 |
| TIM44_RAT | Mitochondrial import inner membrane translocase subunit TIM44 | 51 | 980 | 833 | 2 | 2 | 2 | 2 |
| TKT_RAT | Transketolase | 67.6 | 92 | 187 | 16 | 9 | 26 | 11 |
| TMOD2_RAT | Tropomodulin-2 | 39.5 | 295 | 229 | 8 | 8 | 11 | 12 |
| TOIP1_RAT | Torsin-1A-interacting protein 1 | 65.6 | 758 | 918 | 3 | 2 | 3 | 2 |
| TPD54_RAT | Tumor protein D54 | 24 | 510 | 454 | 4 | 4 | 6 | 5 |
| TPIS_RAT | Triosephosphate isomerase | 26.8 | 316 | 351 | 6 | 5 | 18 | 14 |
| TPM1_RAT | Tropomyosin alpha-1 chain | 32.7 | 342 | 206 | 5 | 9 | 6 | 9 |
| TPM4_RAT | Tropomyosin alpha-4 chain | 28.4 | 336 | 248 | 7 | 6 | 7 | 6 |
| TPP2_RAT | Tripeptidyl-peptidase 2 | 138.1 | 635 | 582 | 4 | 4 | 5 | 4 |
| TRA2B_RAT | Transformer-2 protein homolog beta | 33.6 | 391 | 890 | 5 | 2 | 9 | 2 |
| TRFE_RAT | Serotransferrin | 76.3 | 1003 | 810 | 2 | 2 | 2 | 2 |
| TRIM3_RAT | Tripartite motif-containing protein 3 | 80.7 | 328 | 369 | 7 | 5 | 7 | 5 |
| TRXR2_RAT | Thioredoxin reductase 2, mitochondrial | 56.5 | 900 | 654 | 2 | 3 | 4 | 4 |
| TWF1_RAT | Twinfilin-1 | 40.1 | 724 | 370 | 3 | 5 | 3 | 5 |
| TXNL1_RAT | Thioredoxin-like protein 1 | 32.1 | 334 | 352 | 7 | 6 | 9 | 6 |
| UAP56_RAT | Spliceosome RNA helicase Ddx39b | 49 | 137 | 522 | 13 | 4 | 18 | 5 |

| Accession | Description | Mr | X! Tandem Rank (White Matter) | X! Tandem Rank (Molecular Layer) | Unique Peptides (White Matter) | Unique Peptides (Molecular Layer) | Total Peptides (White Matter) | Total Peptides (Molecular Layer) |
|---|---|---|---|---|---|---|---|---|
| UB2V2_RAT | Ubiquitin-conjugating enzyme E2 variant 2 | 16.2 | 499 | 856 | 5 | 2 | 6 | 2 |
| UBA3_RAT | NEDD8-activating enzyme E1 catalytic subunit | 51.7 | 854 | 761 | 2 | 2 | 2 | 2 |
| UBE2N_RAT | Ubiquitin-conjugating enzyme E2 N | 17.1 | 415 | 776 | 6 | 2 | 7 | 3 |
| UBIQ_RAT | no protein information available | 8.6 | 226 | 265 | 9 | 7 | 26 | 13 |
| UCHL1_RAT | Ubiquitin carboxyl-terminal hydrolase isozyme L1 | 24.8 | 469 | 791 | 5 | 2 | 8 | 3 |
| UCRI_RAT | Cytochrome b-c1 complex subunit Rieske, mitochondrial | 29.4 | 178 | 127 | 11 | 12 | 12 | 13 |
| UE1D1_RAT | Ubiquitin-like modifier-activating enzyme 5 | 44.9 | 873 | 768 | 2 | 2 | 2 | 2 |
| UGGG1_RAT | UDP-glucose:glycoprotein glucosyltransferase 1 | 173.9 | 474 | 424 | 5 | 5 | 5 | 5 |
| UQCR2_RAT | Cytochrome b-c1 complex subunit 2, mitochondrial | 48.3 | 121 | 203 | 14 | 9 | 17 | 12 |
| USMG5_RAT | Up-regulated during skeletal muscle growth protein 5 | 6.4 | 588 | 552 | 3 | 3 | 6 | 4 |
| VAMP1_RAT | Vesicle-associated membrane protein 1 | 12.8 | 345 | 419 | 5 | 4 | 8 | 9 |
| VAMP3_RAT | Vesicle-associated membrane protein 3 | 11.5 | 388 | 510 | 5 | 2 | 6 | 3 |
| VAPA_RAT | Vesicle-associated membrane protein-associated protein A | 27.2 | 281 | 378 | 8 | 5 | 11 | 5 |
| VAPB_RAT | Vesicle-associated membrane protein-associated protein B | 26.8 | 582 | 526 | 3 | 3 | 4 | 3 |
| VATB2_RAT | V-type proton ATPase subunit B, brain isoform | 56.5 | 100 | 90 | 16 | 14 | 30 | 23 |
| VATF_RAT | V-type proton ATPase subunit F | 13.4 | 498 | 548 | 4 | 3 | 5 | 3 |
| VCIP1_RAT | Deubiquitinating protein VCIP135 | 134.5 | 897 | 432 | 2 | 5 | 2 | 5 |
| VDAC1_RAT | Voltage-dependent anion-selective channel protein 1 | 30.6 | 147 | 120 | 11 | 12 | 20 | 19 |
| VDAC2_RAT | Voltage-dependent anion-selective channel protein 2 | 31.7 | 307 | 455 | 6 | 4 | 13 | 6 |
| VDAC3_RAT | Voltage-dependent anion-selective channel protein 3 | 30.8 | 404 | 607 | 4 | 3 | 6 | 4 |
| VDP_RAT | General vesicular transport factor p115 | 107.1 | 303 | 420 | 8 | 5 | 8 | 5 |
| VIAAT_RAT | Vesicular inhibitory amino acid transporter | 57.4 | 966 | 907 | 2 | 2 | 2 | 2 |
| VIGLN_RAT | Vigilin | 141.5 | 265 | 540 | 8 | 3 | 10 | 4 |
| VIME_RAT | Vimentin | 53.6 | 184 | 39 | 11 | 27 | 12 | 36 |
| VISL1_RAT | Visinin-like protein 1 | 22 | 204 | 327 | 10 | 6 | 14 | 7 |
| VPP1_RAT | V-type proton ATPase 116 kDa subunit a isoform 1 | 96.3 | 98 | 114 | 16 | 13 | 23 | 19 |
| VTI1A_RAT | Vesicle transport through interaction with t-SNAREs homolog 1A | 26 | 544 | 727 | 5 | 3 | 5 | 3 |
| WBP2_RAT | WW domain-binding protein 2 | 28.1 | 974 | 813 | 2 | 2 | 2 | 2 |
| WDR7_RAT | WD repeat-containing protein 7 | 163.1 | 396 | 177 | 6 | 9 | 6 | 9 |
| WNK1_RAT | Serine/threonine-protein kinase WNK1 | 225.1 | 963 | 696 | 2 | 3 | 2 | 3 |
| XAB2_RAT | Pre-mRNA-splicing factor SYF1 | 99.9 | 759 | 755 | 3 | 3 | 3 | 3 |
| XPP1_RAT | Xaa-Pro aminopeptidase 1 | 69.6 | 528 | 469 | 5 | 5 | 5 | 5 |
| YBOX1_RAT | Nuclease-sensitive element-binding protein 1 | 35.6 | 468 | 459 | 5 | 4 | 7 | 4 |

REFERENCES

[1] Tanaka, K., Waki, H., Ido, Y., Akita, S., Yoshida, Y., Yoshida, T., and Matsuo, T. (1988) Protein and polymer analyses up to m/z 100 000 by laser ionization time-of-flight mass spectrometry, *Rapid Communications in Mass Spectrometry 2*, 151-153.

[2] Karas, M., Bachmann, D., Bahr, U., and Hillenkamp, F. (1987) Matrix-assisted ultraviolet laser desorption of non-volatile compounds, *International Journal of Mass Spectrometry and Ion Processes 78*, 53-68.

[3] Karas, M., and Hillenkamp, F. (1988) Laser desorption ionization of proteins with molecular masses exceeding 10,000 daltons, *Analytical Chemistry 60*, 2299-2301.

[4] Kampmeier, J., Dreisewerd, K., Schürenberg, M., and Strupat, K. (1997) Investigations of 2, 5-DHB and succinic acid as matrices for IR and UV MALDI. Part: I UV and IR laser ablation in the MALDI process, *International journal of mass spectrometry and ion processes 169*, 31-41.

[5] Kirpekar, F., Berkenkamp, S., and Hillenkamp, F. (1999) Detection of double-stranded DNA by IR-and UV-MALDI mass spectrometry, *Analytical chemistry 71*, 2334-2339.

[6] Jaskolla, T. W., and Karas, M. (2011) Compelling evidence for Lucky Survivor and gas phase protonation: the unified MALDI analyte protonation mechanism, *J Am Soc Mass Spectrom 22*, 976-988.

[7] Karas, M., and Kruger, R. (2003) Ion formation in MALDI: the cluster ionization mechanism, *Chem Rev 103*, 427-440.

[8] Schiller, J., Süss, R., Fuchs, B., Müller, M., Petković, M., Zschörnig, O., and Waschipky, H. (2007) The suitability of different DHB isomers as matrices for the MALDI-TOF MS analysis of phospholipids: which isomer for what purpose?, *Eur Biophys J 36*, 517-527.

[9] Hankin, J. A., Barkley, R. M., and Murphy, R. C. (2007) Sublimation as a Method of Matrix Application for Mass Spectrometric Imaging, *Journal of the American Society for Mass Spectrometry 18*, 1646-1652.

[10] Li, L., Garden, R. W., Romanova, E. V., and Sweedler, J. V. (1999) In Situ Sequencing of Peptides from Biological Tissues and Single Cells Using MALDI–PSD/CID Analysis, *Analytical Chemistry 71*, 5451-5458.

[11] Groseclose, M. R., Andersson, M., Hardesty, W. M., and Caprioli, R. M. (2007) Identification of proteins directly from tissue: in situ tryptic digestions coupled with imaging mass spectrometry, *Journal of Mass Spectrometry 42*, 254-262.

[12] Chaurand, P., and Caprioli, R. M. (2002) Direct profiling and imaging of peptides and proteins from mammalian cells and tissue sections by mass spectrometry, *Electrophoresis 23*, 3125-3135.

[13] Fitzgerald, M. C., Parr, G. R., and Smith, L. M. (1993) Basic matrixes for the matrix-assisted laser desorption/ionization mass spectrometry of proteins and oligonucleotides, *Analytical Chemistry 65*, 3204-3211.

[14] Li, J., Inutan, E., Wang, B., Lietz, C., Green, D., Manly, C., Richards, A., Marshall, D., Lingenfelter, S., Ren, Y., and Trimpin, S. Matrix Assisted Ionization: New Aromatic and Nonaromatic Matrix Compounds Producing Multiply Charged Lipid, Peptide,

and Protein Ions in the Positive and Negative Mode Observed Directly from Surfaces, *Journal of The American Society for Mass Spectrometry*, 1-19.

[15] Francese, S., Bradshaw, R., Flinders, B., Mitchell, C., Bleay, S., Cicero, L., and Clench, M. R. (2013) Curcumin: A Multipurpose Matrix for MALDI Mass Spectrometry Imaging Applications, *Analytical Chemistry 85*, 5240-5248.

[16] Calvano, C. D., van der Werf, I. D., Sabbatini, L., and Palmisano, F. (2015) On plate graphite supported sample processing for simultaneous lipid and protein identification by matrix assisted laser desorption ionization mass spectrometry, *Talanta 137*, 161-166.

[17] Arakawa, R., and Kawasaki, H. (2010) Functionalized Nanoparticles and Nanostructured Surfaces for Surface-Assisted Laser Desorption/Ionization Mass Spectrometry, *Analytical Sciences 26*, 1229-1240.

[18] McLean, J. A., Stumpo, K. A., and Russell, D. H. (2005) Size-selected (2-10 nm) gold nanoparticles for matrix assisted laser desorption ionization of peptides, *Journal of the American Chemical Society 127*, 5304-5305.

[19] Armstrong, D. W., Zhang, L. K., He, L. F., and Gross, M. L. (2001) Ionic liquids as matrixes for matrix-assisted laser desorption/ionization mass spectrometry, *Analytical Chemistry 73*, 3679-3686.

[20] Gimenez, E., Benavente, F., Barbosa, J., and Sanz-Nebot, V. (2010) Ionic liquid matrices for MALDI-TOF-MS analysis of intact glycoproteins, *Analytical and Bioanalytical Chemistry 398*, 357-365.

[21] Jones, J. J., Batoy, S., Wilkins, C. L., Liyanage, R., and Lay, J. O. (2005) Ionic liquid matrix-induced metastable decay of peptides and oligonucleotides and stabilization of phospholipids in MALDI FTMS analyses, *Journal of the American Society for Mass Spectrometry 16*, 2000-2008.

[22] Caprioli, R. M., Farmer, T. B., and Gile, J. (1997) Molecular imaging of biological samples: Localization of peptides and proteins using MALDI-TOF MS, *Analytical Chemistry 69*, 4751-4760.

[23] Huang, J. T., Hannah-Qiuhua, L., Szyszka, R., Veselov, V., Reed, G., Wang, X., Price, S., Alquier, L., and Vas, G. (2012) Molecular imaging of drug-eluting coronary stents: method development, optimization and selected applications, *J Mass Spectrom 47*, 155-162.

[24] Nilsson, A., Goodwin, R. J. A., Shariatgorji, M., Vallianatou, T., Webborn, P. J. H., and Andren, P. E. (2015) Mass Spectrometry Imaging in Drug Development, *Analytical Chemistry 87*, 1437-1455.

[25] Bhandari, D. R., Schott, M., Roempp, A., Vilcinskas, A., and Spengler, B. (2015) Metabolite localization by atmospheric pressure high-resolution scanning microprobe matrix-assisted laser desorption/ionization mass spectrometry imaging in whole-body sections and individual organs of the rove beetle Paederus riparius, *Analytical and Bioanalytical Chemistry 407*, 2189-2201.

[26] Berry, K. A. Z., Hankin, J. A., Barkley, R. M., Spraggins, J. M., Caprioli, R. M., and Murphy, R. C. (2011) MALDI Imaging of Lipid Biochemistry in Tissues by Mass Spectrometry, *Chemical Reviews 111*, 6491-6512.

[27] Schober, Y., Guenther, S., Spengler, B., and Roempp, A. (2012) High-resolution matrix-assisted laser desorption/ionization imaging of tryptic peptides from tissue, *Rapid Communications in Mass Spectrometry 26*, 1141-1146.

[28] Deutskens, F., Yang, J., and Caprioli, R. M. (2011) High spatial resolution imaging mass spectrometry and classical histology on a single tissue section, *Journal of Mass Spectrometry 46*, 568-571.

[29] Seeley, E. H., Schwamborn, K., and Caprioli, R. M. (2011) Imaging of intact tissue sections: moving beyond the microscope, *J Biol Chem 286*, 25459-25466.

[30] Aerni, H. R., Cornett, D. S., and Caprioli, R. M. (2006) Automated acoustic matrix deposition for MALDI sample preparation, *Analytical Chemistry 78*, 827-834.

[31] Grey, A. C., Chaurand, P., Caprioli, R. M., and Schey, K. L. (2009) MALDI Imaging Mass Spectrometry of Integral Membrane Proteins from Ocular Lens and Retinal Tissue, *Journal of Proteome Research 8*, 3278-3283.

[32] Reyzer, M. L., Hsieh, Y. S., Ng, K., Korfmacher, W. A., and Caprioli, R. M. (2003) Direct analysis of drug candidates in tissue by matrix-assisted laser desorption/ionization mass spectrometry, *Journal of Mass Spectrometry 38*, 1081-1092.

[33] Angel, P. M., Spraggins, J. M., Baldwin, H. S., and Caprioli, R. (2012) Enhanced sensitivity for high spatial resolution lipid analysis by negative ion mode matrix assisted laser desorption ionization imaging mass spectrometry, *Anal Chem 84*, 1557-1564.

[34] Schwamborn, K., and Caprioli, R. M. (2010) INNOVATION Molecular imaging by mass spectrometry - looking beyond classical histology, *Nature Reviews Cancer 10*, 639-646.

[35] Smith, L. M., Kelleher, N. L., and Consortium Top Down, P. (2013) Proteoform: a single term describing protein complexity, *Nature Methods 10*, 186-187.

[36] Marshall, A. G., and Hendrickson, C. L. (2008) High-resolution mass spectrometers, *Annu Rev Anal Chem (Palo Alto Calif) 1*, 579-599.

[37] Cornett, D. S., Frappier, S. L., and Caprioli, R. M. (2008) MALDI-FTICR imaging mass spectrometry of drugs and metabolites in tissue, *Analytical Chemistry 80*, 5648-5653.

[38] Wang, X., Han, J., Pan, J., and Borchers, C. H. (2014) Comprehensive imaging of porcine adrenal gland lipids by MALDI-FTMS using quercetin as a matrix, *Anal Chem 86*, 638-646.

[39] Wenke, J. L., Rose, K. L., Spraggins, J. M., and Schey, K. L. (2015) MALDI Imaging Mass Spectrometry Spatially Maps Age-Related Deamidation and Truncation of Human Lens Aquaporin-0, *Invest Ophthalmol Vis Sci 56*, 7398-7405.

[40] G Marshall, A., T Blakney, G., Chen, T., K Kaiser, N., M McKenna, A., P Rodgers, R., M Ruddy, B., and Xian, F. (2013) Mass resolution and mass accuracy: how much is enough?, *Mass Spectrom (Tokyo) 2*, S0009.

[41] Williams Jr, D. K., Hawkridge, A. M., and Muddiman, D. C. (2007) Sub Parts-Per-Million Mass Measurement Accuracy of Intact Proteins and Product Ions Achieved Using a Dual Electrospray Ionization Quadrupole Fourier Transform Ion Cyclotron Resonance Mass Spectrometer, *Journal of the American Society for Mass Spectrometry 18*, 1-7.

[42] Flora, J. W., Hannis, J. C., and Muddiman, D. C. (2001) High-Mass Accuracy of Product Ions Produced by SORI-CID Using a Dual Electrospray Ionization Source Coupled with FTICR Mass Spectrometry, *Analytical Chemistry 73*, 1247-1251.

[43] Cimino, J., Calligaris, D., Far, J., Debois, D., Blacher, S., Sounni, N. E., Noel, A., and De Pauw, E. (2013) Towards lipidomics of low-abundant species for exploring tumor

heterogeneity guided by high-resolution mass spectrometry imaging, *Int J Mol Sci 14*, 24560-24580.

[44] Jones, E. E., Dworski, S., Canals, D., Casas, J., Fabrias, G., Schoenling, D., Levade, T., Denlinger, C., Hannun, Y. A., Medin, J. A., and Drake, R. R. (2014) On-tissue localization of ceramides and other sphingolipids by MALDI mass spectrometry imaging, *Anal Chem 86*, 8303-8311.

[45] Sun, N., Fernandez, I. E., Wei, M., Wu, Y., Aichler, M., Eickelberg, O., and Walch, A. (2016) Pharmacokinetic and pharmacometabolomic study of pirfenidone in normal mouse tissues using high mass resolution MALDI-FTICR-mass spectrometry imaging, *Histochem Cell Biol 145*, 201-211.

[46] Amster, I. J. (1996) Fourier Transform Mass Spectrometry, *Journal of Mass Spectrometry 31*, 1325-1337.

[47] Marshall, A. G., Hendrickson, C. L., and Jackson, G. S. (1998) Fourier transform ion cyclotron resonance mass spectrometry: A primer, *Mass Spectrometry Reviews 17*, 1-35.

[48] Schweikhard, L., and Marshall, A. G. (1993) Excitation modes for Fourier transform-ion cyclotron resonance mass spectrometry, *Journal of the American Society for Mass Spectrometry 4*, 433-452.

[49] Peng, Y., Gregorich, Z. R., Valeja, S. G., Zhang, H., Cai, W., Chen, Y. C., Guner, H., Chen, A. J., Schwahn, D. J., Hacker, T. A., Liu, X., and Ge, Y. (2014) Top-down proteomics reveals concerted reductions in myofilament and Z-disc protein phosphorylation after acute myocardial infarction, *Mol Cell Proteomics 13*, 2752-2764.

[50] Wisniewski, J. R., Zougman, A., Nagaraj, N., and Mann, M. (2009) Universal sample preparation method for proteome analysis, *Nature methods 6*, 359.

[51] Caldwell, R. L., and Caprioli, R. M. (2005) Tissue profiling by mass spectrometry: a review of methodology and applications, *Mol Cell Proteomics 4*, 394-401.

[52] Zubarev, R. A. (2013) The challenge of the proteome dynamic range and its implications for in-depth proteomics, *Proteomics 13*, 723-726.

[53] Banks, R. E., Dunn, M. J., Forbes, M. A., Stanley, A., Pappin, D., Naven, T., Gough, M., Harnden, P., and Selby, P. J. (1999) The potential use of laser capture microdissection to selectively obtain distinct populations of cells for proteomic analysis--preliminary findings, *Electrophoresis 20*, 689-700.

[54] Fend, F., and Raffeld, M. (2000) Laser capture microdissection in pathology, *J Clin Pathol 53*, 666-672.

[55] Castro, N. P., Merchant, A. S., Saylor, K. L., Anver, M. R., Salomon, D. S., and Golubeva, Y. G. (2016) Adaptation of Laser Microdissection Technique for the Study of a Spontaneous Metastatic Mammary Carcinoma Mouse Model by NanoString Technologies, *PLoS One 11*, e0153270.

[56] Gross, A., Schoendube, J., Zimmermann, S., Steeb, M., Zengerle, R., and Koltay, P. (2015) Technologies for Single-Cell Isolation, *Int J Mol Sci 16*, 16897-16919.

[57] Espina, V., Wulfkuhle, J. D., Calvert, V. S., VanMeter, A., Zhou, W., Coukos, G., Geho, D. H., Petricoin, E. F., and Liotta, L. A. (2006) Laser-capture microdissection, *Nat Protoc 1*, 586-603.

[58] Schey, K. L., Anderson, D. M., and Rose, K. L. (2013) Spatially-Directed Protein Identification from Tissue Sections by Top-Down LC-MS/MS with Electron Transfer Dissociation, *Anal Chem*.

[59] Turiák, L., Shao, C., Meng, L., Khatri, K., Leymarie, N., Wang, Q., Pantazopoulos, H., Leon, D. R., and Zaia, J. (2014) Workflow for combined proteomics and glycomics profiling from histological tissues, *Anal Chem 86*, 9670-9678.

[60] Van Berkel, G. J., Kertesz, V., Koeplinger, K. A., Vavrek, M., and Kong, A. N. (2008) Liquid microjunction surface sampling probe electrospray mass spectrometry for detection of drugs and metabolites in thin tissue sections, *J Mass Spectrom 43*, 500-508.

[61] Kertesz, V., and Van Berkel, G. J. (2010) Liquid microjunction surface sampling coupled with high-pressure liquid chromatography-electrospray ionization-mass spectrometry for analysis of drugs and metabolites in whole-body thin tissue sections, *Anal Chem 82*, 5917-5921.

[62] Sarsby, J., Martin, N. J., Lalor, P. F., Bunch, J., and Cooper, H. J. (2014) Top-down and bottom-up identification of proteins by liquid extraction surface analysis mass spectrometry of healthy and diseased human liver tissue, *J Am Soc Mass Spectrom 25*, 1953-1961.

[63] Wisztorski, M., Desmons, A., Quanico, J., Fatou, B., Gimeno, J. P., Franck, J., Salzet, M., and Fournier, I. (2016) Spatially-resolved protein surface microsampling from tissue sections using liquid extraction surface analysis, *Proteomics*.

[64] Harris, G. A., Nicklay, J. J., and Caprioli, R. M. (2013) Localized in situ hydrogel-mediated protein digestion and extraction technique for on-tissue analysis, *Anal Chem 85*, 2717-2723.

[65] Taverna, D., Pollins, A. C., Nanney, L. B., Sindona, G., and Caprioli, R. M. (2015) Histology-guided protein digestion/extraction from FFPE pressure ulcer biopsies, *Exp Dermatol*.

[66] Nicklay, J. J., Harris, G. A., Schey, K. L., and Caprioli, R. M. (2013) MALDI imaging and in situ identification of integral membrane proteins from rat brain tissue sections, *Anal Chem 85*, 7191-7196.

[67] Taverna, D., Norris, J. L., and Caprioli, R. M. (2015) Histology-directed microwave assisted enzymatic protein digestion for MALDI MS analysis of mammalian tissue, *Anal Chem 87*, 670-676.

[68] Scherperel, G., and Reid, G. E. (2007) Emerging methods in proteomics: top-down protein characterization by multistage tandem mass spectrometry, *Analyst 132*, 500-506.

[69] Zhang, Y., Fonslow, B. R., Shan, B., Baek, M.-C., and Yates, J. R., III. (2013) Protein Analysis by Shotgun/Bottom-up Proteomics, *Chemical Reviews 113*, 2343-2394.

[70] Schwartz, S. A., Weil, R. J., Johnson, M. D., Toms, S. A., and Caprioli, R. M. (2004) Protein profiling in brain tumors using mass spectrometry: Feasibility of a new technique for the analysis of protein expression, *Clinical Cancer Research 10*, 981-987.

[71] Balluff, B., Rauser, S., Meding, S., Elsner, M., Schoene, C., Feuchtinger, A., Schuhmacher, C., Novotny, A., Juetting, U., Maccarrone, G., Sarioglu, H., Ueffing, M., Braselmann, H., Zitzelsberger, H., Schmid, R. M., Hoefler, H., Ebert, M. P., and Walch, A. (2011) MALDI Imaging Identifies Prognostic Seven-Protein Signature of Novel Tissue Markers in Intestinal-Type Gastric Cancer, *American Journal of Pathology 179*, 2720-2729.

[72] Kelleher, N. L. (2004) Top-down proteomics, *Anal Chem 76*, 197A-203A.

[73] Liu, Z., and Schey, K. L. (2008) Fragmentation of multiply-charged intact protein ions using MALDI TOF-TOF mass spectrometry, *J Am Soc Mass Spectrom 19*, 231-238.

[74] Trimpin, S., Inutan, E. D., Herath, T. N., and McEwen, C. N. (2010) Laserspray Ionization, a New Atmospheric Pressure MALDI Method for Producing Highly Charged Gas-phase Ions of Peptides and Proteins Directly from Solid Solutions, *Molecular & Cellular Proteomics 9*, 362-367.

[75] Inutan, E. D., Richards, A. L., Wager-Miller, J., Mackie, K., McEwen, C. N., and Trimpin, S. (2011) Laserspray ionization, a new method for protein analysis directly from tissue at atmospheric pressure with ultrahigh mass resolution and electron transfer dissociation, *Mol Cell Proteomics 10*, M110.000760.

[76] Takats, Z., Wiseman, J. M., Gologan, B., and Cooks, R. G. (2004) Mass spectrometry sampling under ambient conditions with desorption electrospray ionization, *Science 306*, 471-473.

[77] Nemes, P., and Vertes, A. (2007) Laser ablation electrospray ionization for atmospheric pressure, in vivo, and imaging mass spectrometry, *Analytical Chemistry 79*, 8098-8106.

[78] Robichaud, G., Barry, J. A., Garrard, K. P., and Muddiman, D. C. (2013) Infrared Matrix-Assisted Laser Desorption Electrospray Ionization (IR-MALDESI) Imaging Source Coupled to a FT-ICR Mass Spectrometer, *Journal of the American Society for Mass Spectrometry 24*, 92-100.

[79] Kiss, A., Smith, D. F., Reschke, B. R., Powell, M. J., and Heeren, R. M. A. (2014) Top-down mass spectrometry imaging of intact proteins by laser ablation ESIFT-ICR MS, *Proteomics 14*, 1283-1289.

[80] Robichaud, G., Barry, J. A., and Muddiman, D. C. (2014) IR-MALDESI Mass Spectrometry Imaging of Biological Tissue Sections Using Ice as a Matrix, *Journal of the American Society for Mass Spectrometry 25*, 319-328.

[81] Mascini, N. E., and Heeren, R. M. A. (2012) Protein identification in mass-spectrometry imaging, *Trac-Trends in Analytical Chemistry 40*, 28-37.

[82] Gessel, M. M., Norris, J. L., and Caprioli, R. M. (2014) MALDI imaging mass spectrometry: Spatial molecular analysis to enable a new age of discovery, *Journal of Proteomics 107*, 71-82.

[83] Schey, K. L., Anderson, D. M., and Rose, K. L. (2013) Spatially-Directed Protein Identification from Tissue Sections by Top-Down LC-MS/MS with Electron Transfer Dissociation, *Analytical Chemistry 85*, 6767-6774.

[84] Spraggins, J. M., Rizzo, D. G., Moore, J. L., Rose, K. L., Hammer, N. D., Skaar, E. P., and Caprioli, R. M. (2015) MALDI FTICR IMS of Intact Proteins: Using Mass Accuracy to Link Protein Images with Proteomics Data, *J Am Soc Mass Spectrom 26*, 974-985.

[85] Spraggins, J. M., Rizzo, D. G., Moore, J. L., Noto, M. J., Skaar, E. P., and Caprioli, R. M. (2016) Next-generation technologies for spatial proteomics: Integrating ultra-high speed MALDI-TOF and high mass resolution MALDI FTICR imaging mass spectrometry for protein analysis, *Proteomics*.

[86] Makarov, A. (2000) Electrostatic axially harmonic orbital trapping: A high-performance technique of mass analysis, *Analytical Chemistry 72*, 1156-1162.

[87] Zubarev, R. A., and Makarov, A. (2013) Orbitrap Mass Spectrometry, *Analytical Chemistry 85*, 5288-5296.

[88] Wang, X., Han, J., Pan, J., and Borchers, C. H. (2014) Comprehensive Imaging of Porcine Adrenal Gland Lipids by MALDI-FTMS Using Quercetin as a Matrix, *Analytical Chemistry 86*, 638-646.

[89] Minerva, L., Boonen, K., Menschaert, G., Landuyt, B., Baggerman, G., and Arckens, L. (2011) Linking Mass Spectrometric Imaging and Traditional Peptidomics: A Validation in the Obese Mouse Model, *Analytical Chemistry 83*, 7682-7691.

[90] Schober, Y., Schramm, T., Spengler, B., and Roempp, A. (2011) Protein identification by accurate mass matrix-assisted laser desorption/ionization imaging of tryptic peptides, *Rapid Communications in Mass Spectrometry 25*, 2475-2483.

[91] Manier, M. L., Spraggins, J. M., Reyzer, M. L., Norris, J. L., and Caprioli, R. M. (2014) A derivatization and validation strategy for determining the spatial localization of endogenous amine metabolites in tissues using MALDI imaging mass spectrometry, *Journal of Mass Spectrometry 49*, 665-673.

[92] Groseclose, M. R., Andersson, M., Hardesty, W. M., and Caprioli, R. M. (2007) Identification of proteins directly from tissue: in situ tryptic digestions coupled with imaging mass spectrometry, *Journal of Mass Spectrometry 42*, 254-262.

[93] Seeley, E. H., Oppenheimer, S. R., Mi, D., Chaurand, P., and Caprioli, R. M. (2008) Enhancement of protein sensitivity for MALDI imaging mass spectrometry after chemical treatment of tissue sections, *Journal of the American Society for Mass Spectrometry 19*, 1069-1077.

[94] Oppenheimer, S. R., Mi, D. M., Sanders, M. E., and Caprioli, R. M. (2010) Molecular Analysis of Tumor Margins by MALDI Mass Spectrometry in Renal Carcinoma, *Journal of Proteome Research 9*, 2182-2190.

[95] Jones, E. A., Shyti, R., van Zeijl, R. J., van Heiningen, S. H., Ferrari, M. D., Deelder, A. M., Tolner, E. A., van den Maagdenberg, A. M., and McDonnell, L. A. (2012) Imaging mass spectrometry to visualize biomolecule distributions in mouse brain tissue following hemispheric cortical spreading depression, *J Proteomics 75*, 5027-5035.

[96] Yang, J., and Caprioli, R. M. (2011) Matrix Sublimation/Recrystallization for Imaging Proteins by Mass Spectrometry at High Spatial Resolution, *Analytical Chemistry 83*, 5728-5734.

[97] Yang, J., and Caprioli, R. M. (2011) Matrix sublimation/recrystallization for imaging proteins by mass spectrometry at high spatial resolution, *Anal Chem 83*, 5728-5734.

[98] McDonnell, L. A., Walch, A., Stoeckli, M., and Corthals, G. L. (2014) MSiMass list: a public database of identifications for protein MALDI MS imaging, *J Proteome Res 13*, 1138-1142.

[99] Cornett, D. S., Peschke, M., LaiHing, K., Cheng, P. Y., Willey, K. F., and Duncan, M. A. (1992) Reflectron time-of-flight mass spectrometer for laser photodissociation, *Review of Scientific Instruments 62*, 2177-2186.

[100] Trim, P. J., Djidja, M.-C., Atkinson, S. J., Oakes, K., Cole, L. M., Anderson, D. M. G., Hart, P. J., Francese, S., and Clench, M. R. (2010) Introduction of a 20 kHz Nd:YVO4 laser into a hybrid quadrupole time-of-flight mass spectrometer for MALDI-MS imaging, *Analytical and Bioanalytical Chemistry 397*, 3409-3419.

[101] Spraggins, J. M., and Caprioli, R. M. (2011) High-Speed MALDI-TOF Imaging Mass Spectrometry: Rapid Ion Image Acquisition and Considerations for Next Generation Instrumentation, *Journal of the American Society for Mass Spectrometry 22*, 1022-1031.

[102] Prentice, B. M., Chumbley, C. W., and Caprioli, R. M. (2015) High-speed MALDI MS/MS imaging mass spectrometry using continuous raster sampling, *Journal of Mass Spectrometry 50*, 703-710.

[103] Jones, E. E., Powers, T. W., Neely, B. A., Cazares, L. H., Troyer, D. A., Parker, A. S., and Drake, R. R. (2014) MALDI imaging mass spectrometry profiling of proteins and lipids in clear cell renal cell carcinoma, *Proteomics 14*, 924-935.

[104] Ye, H., Mandal, R., Catherman, A., Thomas, P. M., Kelleher, N. L., Ikonomidou, C., and Li, L. (2014) Top-down proteomics with mass spectrometry imaging: a pilot study towards discovery of biomarkers for neurodevelopmental disorders, *PLoS One 9*, e92831.

[105] Johanson, R. A., Sarau, H. M., Foley, J. J., and Slemmon, J. R. (2000) Calmodulin-binding peptide PEP-19 modulates activation of calmodulin kinase II In situ, *J Neurosci 20*, 2860-2866.

[106] Berridge, M. J., Bootman, M. D., and Roderick, H. L. (2003) Calcium signalling: dynamics, homeostasis and remodelling, *Nat Rev Mol Cell Biol 4*, 517-529.

[107] O'Sullivan, B. P., and Freedman, S. D. (2009) Cystic fibrosis, *Lancet 373*, 1891-1904.

[108] Siripala, A. D., and Welch, M. D. (2007) SnapShot: actin regulators I, *Cell 128*, 626.

[109] Siripala, A. D., and Welch, M. D. (2007) SnapShot: Actin regulators II, *Cell 128*, 1014-1014.

[110] von Ballmoos, C., Wiedenmann, A., and Dimroth, P. (2009) Essentials for ATP Synthesis by F1F0 ATP Synthases, In *Annual Review of Biochemistry*, pp 649-672.

[111] Habersetzer, J., Ziani, W., Larrieu, I., Stines-Chaumeil, C., Giraud, M.-F., Brethes, D., Dautant, A., and Paumard, P. (2013) ATP synthase oligomerization: From the enzyme models to the mitochondrial morphology, *International Journal of Biochemistry & Cell Biology 45*, 99-105.

[112] Sautiere, P., Tyrou, D., Moschetto, Y., and Biserte, G. (1971) [Primary structure of glycine-rich and arginine-rich histone isolated from chloroleukemic tumor of the rat], *Biochimie 53*, 479-483.

[113] Luger, K., Mader, A. W., Richmond, R. K., Sargent, D. F., and Richmond, T. J. (1997) Crystal structure of the nucleosome core particle at 2.8 A resolution, *Nature 389*, 251-260.

[114] Arnaudo, A. M., and Garcia, B. A. (2013) Proteomic characterization of novel histone post-translational modifications, *Epigenetics & Chromatin 6*.

[115] Siegel, R. L., Miller, K. D., and Jemal, A. (2015) Cancer statistics, 2015, *CA Cancer J Clin 65*, 5-29.

[116] Wu, Y., Kwon, Y. S., Labib, M., Foran, D. J., and Singer, E. A. (2015) Magnetic Resonance Imaging as a Biomarker for Renal Cell Carcinoma, *Dis Markers 2015*, 648495.

[117] Hernandez-Yanez, M., Heymach, J. V., and Zurita, A. J. (2012) Circulating biomarkers in advanced renal cell carcinoma: clinical applications, *Curr Oncol Rep 14*, 221-229.

[118] Krabbe, L.-M., Bagrodia, A., Margulis, V., and Wood, C. G. (2014) Surgical Management of Renal Cell Carcinoma, *Semin intervent Radiol 31*, 027-032.

[119] Chow, W. H., Dong, L. M., and Devesa, S. S. (2010) Epidemiology and risk factors for kidney cancer, *Nat Rev Urol 7*, 245-257.

[120] Roesch-Ely, M., Nees, M., Karsai, S., Ruess, A., Bogumil, R., Warnken, U., Schnölzer, M., Dietz, A., Plinkert, P. K., Hofele, C., and Bosch, F. X. (2007) Proteomic analysis reveals successive aberrations in protein expression from healthy mucosa to invasive head and neck cancer, *Oncogene 26*, 54-64.

[121] Hall, A. K. (1991) Differential expression of thymosin genes in human tumors and in the developing human kidney, *Int J Cancer 48*, 672-677.

[122] Hardesty, W. M., and Caprioli, R. M. (2008) In situ molecular imaging of proteins in tissues using mass spectrometry, *Anal Bioanal Chem 391*, 899-903.

[123] Ramakrishnan, S., Ellis, L., and Pili, R. (2013) Histone modifications: implications in renal cell carcinoma, *Epigenomics 5*, 453-462.

[124] LeDuc, R. D., Taylor, G. K., Kim, Y.-B., Januszyk, T. E., Bynum, L. H., Sola, J. V., Garavelli, J. S., and Kelleher, N. L. (2004) ProSight PTM: an integrated environment for protein identification and characterization by top-down mass spectrometry, *Nucleic acids research 32*, W340-W345.

[125] Zamdborg, L., LeDuc, R. D., Glowacz, K. J., Kim, Y.-B., Viswanathan, V., Spaulding, I. T., Early, B. P., Bluhm, E. J., Babai, S., and Kelleher, N. L. (2007) ProSight PTM 2.0: improved protein identification and characterization for top down mass spectrometry, *Nucleic acids research 35*, W701-W706.

[126] Kılıç, S., Sagitova, D. M., Wolfish, S., Bely, B., Courtot, M., Ciufo, S., Tatusova, T., O'Donovan, C., Chibucos, M. C., Martin, M. J., and Erill, I. (2016) From data repositories to submission portals: rethinking the role of domain-specific databases in CollecTF, *Database (Oxford) 2016*.

[127] Consortium, U. (2011) Ongoing and future developments at the Universal Protein Resource, *Nucleic Acids Res 39*, D214-219.

[128] Tran, J. C., Zamdborg, L., Ahlf, D. R., Lee, J. E., Catherman, A. D., Durbin, K. R., Tipton, J. D., Vellaichamy, A., Kellie, J. F., Li, M., Wu, C., Sweet, S. M., Early, B. P., Siuti, N., LeDuc, R. D., Compton, P. D., Thomas, P. M., and Kelleher, N. L. (2011) Mapping intact protein isoforms in discovery mode using top-down proteomics, *Nature 480*, 254-258.

[129] Fox, C. H., Johnson, F. B., Whiting, J., and Roller, P. P. (1985) Formaldehyde fixation, *J Histochem Cytochem 33*, 845-853.

[130] Diehl, H. C., Beine, B., Elm, J., Trede, D., Ahrens, M., Eisenacher, M., Marcus, K., Meyer, H. E., and Henkel, C. (2015) The challenge of on-tissue digestion for MALDI MSI- a comparison of different protocols to improve imaging experiments, *Anal Bioanal Chem 407*, 2223-2243.

[131] Luebker, S. A., Wojtkiewicz, M., and Koepsell, S. A. (2015) Two methods for proteomic analysis of formalin-fixed, paraffin embedded tissue result in differential protein identification, data quality, and cost, *Proteomics 15*, 3744-3753.

[132] Norrgran, J., Williams, T. L., Woolfitt, A. R., Solano, M. I., Pirkle, J. L., and Barr, J. R. (2009) Optimization of digestion parameters for protein quantification, *Anal Biochem 393*, 48-55.

[133] Borner, G. H., and Fielding, A. B. (2014) Using in-solution digestion, peptide fractionation, and a Q exactive mass spectrometer to analyze the proteome of clathrin-coated vesicles, *Cold Spring Harb Protoc 2014*, 1192-1195.

[134] Qiao, J., Kim, J. Y., Wang, Y. Y., Qi, L., Wang, F. Y., and Moon, M. H. (2016) Trypsin immobilization in ordered porous polymer membranes for effective protein digestion, *Anal Chim Acta 906*, 156-164.

[135] Gustafsson, O. J. R., Briggs, M. T., Condina, M. R., Winderbaum, L. J., Pelzing, M., McColl, S. R., Everest-Dass, A. V., Packer, N. H., and Hoffmann, P. (2015) MALDI imaging mass spectrometry of N-linked glycans on formalin-fixed paraffin-embedded murine kidney, *Analytical and Bioanalytical Chemistry 407*, 2127-2139.

[136] Vestal, M. L. (2009) Modern MALDI time-of-flight mass spectrometry, *J Mass Spectrom 44*, 303-317.

[137] Bereman, M. S., Nyadong, L., Fernandez, F. M., and Muddiman, D. C. (2006) Direct high-resolution peptide and protein analysis by desorption electrospray ionization Fourier transform ion cyclotron resonance mass spectrometry, *Rapid communications in mass spectrometry 20*, 3409-3411.

[138] Schober, Y., Schramm, T., Spengler, B., and Rompp, A. (2011) Protein identification by accurate mass matrix-assisted laser desorption/ionization imaging of tryptic peptides, *Rapid Communications in Mass Spectrometry 25*, 2475-2483.

[139] Herring, K. D., Oppenheimer, S. R., and Caprioli, R. M. (2007) Direct Tissue Analysis by Matrix-Assisted Laser Desorption Ionization Mass Spectrometry: Application to Kidney Biology, *Seminars in Nephrology 27*, 597-608.

[140] Groseclose, M. R., Massion, P. P., Chaurand, P., and Caprioli, R. M. (2008) High-throughput proteomic analysis of formalin-fixed paraffin-embedded tissue microarrays using MALDI imaging mass spectrometry, *Proteomics 8*, 3715-3724.

[141] Franck, J., Arafah, K., Barnes, A., Wisztorski, M., Salzet, M., and Fournier, I. (2009) Improving tissue preparation for matrix-assisted laser desorption ionization mass spectrometry imaging. Part 1: using microspotting, *Analytical chemistry 81*, 8193-8202.

[142] Chen, Z., Li, Y., Lin, S., Wei, M., Du, F., and Ruan, G. (2014) Development of continuous microwave-assisted protein digestion with immobilized enzyme, *Biochem Biophys Res Commun 445*, 491-496.

[143] Stauber, J., MacAleese, L., Franck, J., Claude, E., Snel, M., Kaletas, B. K., Wiel, I. M. V. D., Wisztorski, M., Fournier, I., and Heeren, R. M. A. (2010) On-tissue protein identification and imaging by MALDI-ion mobility mass spectrometry, *Journal of the American Society for Mass Spectrometry 21*, 338-347.

[144] Lemaire, R., Menguellet, S. A., Stauber, J., Marchaudon, V., Lucot, J. P., Collinet, P., Farine, M. O., Vinatier, D., Day, R., Ducoroy, P., Salzet, M., and Fournier, I. (2007) Specific MALDI imaging and profiling for biomarker hunting and validation: fragment of the 11S proteasome activator complex, Reg alpha fragment, is a new potential ovary cancer biomarker, *J Proteome Res 6*, 4127-4134.

[145] Lagarrigue, M., Becker, M., Lavigne, R., Deininger, S. O., Walch, A., Aubry, F., Suckau, D., and Pineau, C. (2011) Revisiting rat spermatogenesis with MALDI imaging at 20-microm resolution, *Mol Cell Proteomics 10*, M110.005991.

[146] Moore, J. L., Becker, K. W., Nicklay, J. J., Boyd, K. L., Skaar, E. P., and Caprioli, R. M. (2014) Imaging mass spectrometry for assessing temporal proteomics: Analysis of calprotectin in Acinetobacter baumannii pulmonary infection, *Proteomics 14*, 820-828.

[147] Wang, H. Y. (2007) Laser capture microdissection in comparative proteomic analysis of hepatocellular carcinoma, *Methods Cell Biol 82*, 689-707.

[148] Kaspar, S., Weier, D., Weschke, W., Mock, H. P., and Matros, A. (2010) Protein analysis of laser capture micro-dissected tissues revealed cell-type specific biological functions in developing barley grains, *Anal Bioanal Chem 398*, 2883-2893.

[149] Waanders, L. F., Chwalek, K., Monetti, M., Kumar, C., Lammert, E., and Mann, M. (2009) Quantitative proteomic analysis of single pancreatic islets, *Proc Natl Acad Sci U S A 106*, 18902-18907.

[150] Van Berkel, G. J., and Kertesz, V. (2009) Application of a liquid extraction based sealing surface sampling probe for mass spectrometric analysis of dried blood spots and mouse whole-body thin tissue sections, *Anal Chem 81*, 9146-9152.

[151] Quanico, J., Franck, J., Dauly, C., Strupat, K., Dupuy, J., Day, R., Salzet, M., Fournier, I., and Wisztorski, M. (2013) Development of liquid microjunction extraction strategy for improving protein identification from tissue sections, *J Proteomics 79*, 200-218.

[152] Taverna, D., Pollins, A. C., Sindona, G., Caprioli, R. M., and Nanney, L. B. (2015) Imaging mass spectrometry for assessing cutaneous wound healing: analysis of pressure ulcers, *J Proteome Res 14*, 986-996.

[153] Mathews, T. P., Hill, S., Rose, K. L., Ivanova, P. T., Lindsley, C. W., and Brown, H. A. (2015) Human phospholipase D activity transiently regulates pyrimidine biosynthesis in malignant gliomas, *ACS Chem Biol 10*, 1258-1268.

[154] Taverna, D., Boraldi, F., De Santis, G., Caprioli, R. M., and Quaglino, D. (2015) Histology-directed and imaging mass spectrometry: An emerging technology in ectopic calcification, *Bone 74*, 83-94.

[155] Rice, R. H., Means, G. E., and Brown, W. D. (1977) Stabilization of bovine trypsin by reductive methylation, *Biochim Biophys Acta 492*, 316-321.

[156] Carpenter, F. H. (1967) [26] Treatment of trypsin with TPCK, In *Methods in Enzymology*, p 237, Academic Press.

[157] Hustoft, H. K., Reubsaet, L., Greibrokk, T., Lundanes, E., and Malerod, H. (2011) Critical assessment of accelerating trypsination methods, *J Pharm Biomed Anal 56*, 1069-1078.

[158] Denisin, A. K., and Pruitt, B. L. (2016) Tuning the Range of Polyacrylamide Gel Stiffness for Mechanobiology Applications, *ACS Appl Mater Interfaces*.

[159] Blattler, D. P., Garner, F., van Slyke, K., and Bradley, A. (1972) Quantitative electrophoresis in polyacrylamide gels of 2–40%, *Journal of Chromatography A 64*, 147-155.

[160] Alkhas, A., Hood, B. L., Oliver, K., Teng, P. N., Oliver, J., Mitchell, D., Hamilton, C. A., Maxwell, G. L., and Conrads, T. P. (2011) Standardization of a sample preparation and analytical workflow for proteomics of archival endometrial cancer tissue, *J Proteome Res 10*, 5264-5271.

[161] Velic, A., Macek, B., and Wagner, C. A. (2010) Toward quantitative proteomics of organ substructures: implications for renal physiology, *Semin Nephrol 30*, 487-499.

[162] Dhanwani, R., Khan, M., Alam, S. I., Rao, P. V., and Parida, M. (2011) Differential proteome analysis of Chikungunya virus-infected new-born mice tissues reveal implication of stress, inflammatory and apoptotic pathways in disease pathogenesis, *Proteomics 11*, 1936-1951.

[163] Steurer, S., Borkowski, C., Odinga, S., Buchholz, M., Koop, C., Huland, H., Becker, M., Witt, M., Trede, D., Omidi, M., Kraus, O., Bahar, A. S., Seddiqi, A. S., Singer, J. M., Kwiatkowski, M., Trusch, M., Simon, R., Wurlitzer, M., Minner, S., Schlomm, T., Sauter, G., and Schlüter, H. (2013) MALDI mass spectrometric imaging based identification of clinically relevant signals in prostate cancer using large-scale tissue microarrays, *Int J Cancer 133*, 920-928.

[164] Kondo, T. (2014) Inconvenient truth: cancer biomarker development by using proteomics, *Biochim Biophys Acta 1844*, 861-865.

[165] Maurya, D. K., Sundaram, C. S., and Bhargava, P. (2010) Proteome profile of whole cerebellum of the mature rat, *Proteomics 10*, 4311-4319.

[166] Nguyen, T., Mehta, N. R., Conant, K., Kim, K. J., Jones, M., Calabresi, P. A., Melli, G., Hoke, A., Schnaar, R. L., Ming, G. L., Song, H., Keswani, S. C., and Griffin, J. W. (2009) Axonal protective effects of the myelin-associated glycoprotein, *J Neurosci 29*, 630-637.

[167] Bartzokis, G. (2011) Alzheimer's disease as homeostatic responses to age-related myelin breakdown, *Neurobiol Aging 32*, 1341-1371.

[168] Xie, F., Zhang, J. C., Fu, H., and Chen, J. (2013) Age-related decline of myelin proteins is highly correlated with activation of astrocytes and microglia in the rat CNS, *Int J Mol Med 32*, 1021-1028.

[169] Yunker, A. M., Sharp, A. H., Sundarraj, S., Ranganathan, V., Copeland, T. D., and McEnery, M. W. (2003) Immunological characterization of T-type voltage-dependent calcium channel CaV3.1 (alpha 1G) and CaV3.3 (alpha 1I) isoforms reveal differences in their localization, expression, and neural development, *Neuroscience 117*, 321-335.

[170] Pregno, G., Frola, E., Graziano, S., Patrizi, A., Bussolino, F., Arese, M., and Sassoè-Pognetto, M. (2013) Differential regulation of neurexin at glutamatergic and GABAergic synapses, *Front Cell Neurosci 7*, 35.

# David G. Rizzo

Work: (615) 343-3503

Cell: (404) 578-0354

david.g.rizzo@vanderbilt.edu

---

*Permanent Address*

320 Old Hickory Blvd

Unit 1808

Nashville, TN 37221

*University Address*

Mass Spectrometry Research Center

Vanderbilt University

PMB 407916

Nashville, TN 37240-7916

## Education

**2010-Present**  Vanderbilt University, Nashville, TN
Doctor of Philosophy in Chemistry; Anticipated Graduation: April 2016
Graduate Research Advisor: Dr. Richard M. Caprioli
Graduate Thesis: *High Mass Accuracy Coupled to Spatially Directed Proteomics*
*for Improved Protein Identifications in Imaging Mass Spectrometry Experiments*
GPA: 3.69

**2005-2009**  Georgia Institute of Technology, Atlanta, GA
Bachelor of Science in Chemistry (Research Option) with Honors
Certificate in Social/Personality Psychology
Undergraduate Research Advisor: Dr. Facundo M. Fernández
Undergraduate Thesis: *Amino Acid Profiling by Reactive Desorption Electrospray Ionization Tandem Mass Spectrometry (DESI-MS/MS)*
GPA: 3.23

## Laboratory Experience

**2010-Present**  **Graduate Research Assistant** (Vanderbilt University Department of Chemistry)
- Developed sample preparation and instrumentation methods to perform robust protein IMS on a 15T MALDI FTICR
- Optimized on-tissue digestion methods and incubation procedures to ensure sufficient enzymatic digestion as evaluated by MALDI IMS
- Performed localized microextracts for LC-MS/MS protein and peptide identifications to correlate to ions observed in MALDI FTICR IMS experiments

- Thoroughly investigated functional properties of trypsin-filled polyacrylamide hydrogels to improve reproducibility and reduce the diameter for spatially-targeted proteomics experiments
  - o Evaluated trypsin concentration, polyacrylamide percentages, and hydrogel diameter based on the number of protein identifications
  - o Applied optimized hydrogel technology to rat cerebellum substructures to differentially identify proteins based on hydrogel placement

**2008- Undergraduate Researcher** (Georgia Institute of Technology Department of **2009** Chemistry)

- Developed MS methods for the detection of amino acids by reactive DESI-MS/MS
- Assessed binding efficiencies of reactive DESI additives, such as crown ethers and β-cyclodextrin

## Presentations (Presenting Author Underlined)

**12)** High Mass Accuracy Coupled to Spatially-Directed Proteomics for Improved Protein Identifications in Imaging Mass Spectrometry Experiments (Poster) - **David G. Rizzo**, Jeffrey M. Spraggins, Jessica L. Moore, Kristie L. Rose, Richard M. Caprioli
*The NATO Science for Peace and Security Program - Advanced Study Institute* (Calabria, Italy, 2016)

**11)** Developing and Assessing Polyacrylamide Hydrogel Technologies for Improved Protein Extraction from Targeted Regions of Biological Tissues (Poster) - **David G. Rizzo**, Jessica L. Moore, Boone M. Prentice, Jeremy L. Norris, Richard M. Caprioli
*63rd ASMS Conference on Mass Spectrometry & Allied Topics* (St. Louis, MO, 2015)

**10)** Spatial Extraction and Enrichment of Phosphopeptides from Tissues Using Hydrogels Containing Metal Ion-Functionalized Nanopolymers (Poster) – M. Lisa Manier, Jamie L. Wenke, **David G. Rizzo**, Jeremy L. Norris, Kevin L. Schey, Richard M. Caprioli
*63rd ASMS Conference on Mass Spectrometry & Allied Topics* (St. Louis, MO, 2015)

**9)** Top-Down and Bottom-Up Analyses of Proteins on the *Same Tissue Section* Using High Mass Resolution Imaging Mass Spectrometry (Poster) - **David G. Rizzo**, Jeffrey M. Spraggins, Kristie L. Rose, Richard M. Caprioli
*62nd ASMS Conference on Mass Spectrometry & Allied Topics* (Baltimore, MD, 2014)

**8)** Imaging and Accurate Mass Identifications of Intact Proteins above 10kDa Using Multiply Charged Ions and High Resolution MS (Poster) – **David G. Rizzo**, Jeffrey M. Spraggins, Kristie L. Rose, Richard M. Caprioli
*61st ASMS Conference on Mass Spectrometry & Allied Topics* (Minneapolis, MN, 2013)

**7)** Visualizing Biomolecular Modifications in Tissue: Integrating Mass Difference (Δ-*m/z*) Scanning Algorithms and MALDI FT-ICR Imaging Mass Spectrometry (Oral) - Jeffrey M. Spraggins; Raf Van de Plas; Kerri J. Grove; **David G. Rizzo**; Richard M. Caprioli
*61st ASMS Conference on Mass Spectrometry & Allied Topics* (Minneapolis, MN, 2013)

**6)** Integrating the Spatial Domain and Top-Down Proteomics using Mass Accuracy: Enhancing Protein Mapping for Biological Applications (Oral) – Jeffrey M. Spraggins, **David G. Rizzo**, Jessica L. Moore, Eric P. Skaar, Richard M. Caprioli
*ASMS Annual Sanibel Conference: Top Down Proteomics* (St. Pete Beach, FL, 2013)

**5)** Imaging of Proteins Up to 80kDa in Biological Tissues by MALDI MS (Poster) – **David**

**G. Rizzo**, Erin H. Seeley, Junhai Yang, Richard M. Caprioli
*60th ASMS Conference on Mass Spectrometry & Allied Topics* (Vancouver, BC, Canada, 2012)

4) Amino Acid Profiling in Biological Mixtures by Reactive Desorption Electrospray Ionization Tandem Mass Spectrometry (DESI MS/MS) (Poster) - **David G. Rizzo**, Leonard Nyadong, Facundo M. Fernández
*42nd Annual Southeast Regional ACS Undergraduate Research Conference* (Kennesaw State University, Kennesaw, GA, 2010)

3) Amino Acid Profiling in Serum by On-plate Solid Phase Extraction and Multicapillary Desorption Electrospray Ionization Mass Spectrometry (DESI MS) (Poster) – **David G. Rizzo**, Leonard Nyadong, Facundo M. Fernández
*Undergraduate Research Opportunities Program (UROP) Spring Symposium* (Georgia Institute of Technology, Atlanta, GA, 2009)

2) Amino Acid Profiling in Biological Mixtures by Reactive Desorption Electrospray Ionization Tandem Mass Spectrometry (DESI MS/MS) (Poster) - **David G. Rizzo**, Leonard Nyadong, Facundo M. Fernández
*Georgia Institute of Technology Chemistry REU Summer Program Symposium - Aquatic Chemical Ecology* (Georgia Institute of Technology, Atlanta, GA, 2009)

1) Amino Acid Profiling in Biological Mixtures by Reactive Desorption Electrospray Ionization Tandem Mass Spectrometry (DESI MS/MS) (Poster) - **David G. Rizzo**, Leonard Nyadong, Asiri S. Galhena, Facundo M. Fernández
*Herty Medalist Undergraduate Research Symposium* (Morehouse College, Atlanta, GA, 2009)

## Publications

**2015** Jeffrey M. Spraggins, **David G. Rizzo**, Jessica L. Moore, Kristie L. Rose, Neal D. Hammer, Eric P. Skaar, and Richard M. Caprioli, *Journal of the American Society for Mass Spectrometry,* **2015**, *26* (6), 974-85. "MALDI FTICR IMS of Intact Proteins: Using Mass Accuracy to Link Protein Images with Proteomics Data"

**2016** Jeffrey M. Spraggins, **David G. Rizzo**, Jessica L. Moore, Michael J. Noto, Eric P. Skaar, and Richard M. Caprioli, *Proteomics*, **2016**, "Next-generation Technologies for Spatial Proteomics: Integrating Ultra-high Speed MALDI-TOF and High Mass Resolution MALDI FTICR Imaging Mass Spectrometry for Protein Analysis"

*In Draft* **David G. Rizzo**, Boone M. Prentice, Jessica L. Moore, Jeremy L. Norris, Richard M. Caprioli. "Advanced Hydrogel Technologies for Enhanced On-Tissue Protein Digestion and Improved Spatial Localization"

## Teaching Experience

**2015** Vanderbilt Internal Fundamental Mass Spectrometry Lecture Series Lecturer
   • "Fundamentals of Ion Mobility"

**2015** Vanderbilt Aspirnaut$^{TM}$ HS Summer Internship Program Research Mentor

**2013-2015** Advanced Imaging Mass Spectrometry (AIMS) Laboratory Course – Workshop Leader
   • "Instrumentation: Ion Mobility" 2013-2015

- "Matrix Application: Robotic Spraying" 2013-2015
- "Sample Preparation: Washing and Staining" 2013

2010-2011    Vanderbilt University Chemistry Department Teaching Assistant

- Chem 295: Advanced Integrated Laboratory (Senior Capstone Lab) – Spring 2011
- Chem 104A: General Chemistry Lab – Fall 2010

## Awards

| | |
|---|---|
| **2015-2016** | Aegis Sciences Fellowship in Chemistry at Vanderbilt University |
| **2009** | Herty Medalist Undergraduate Research Symposium Award |
| **2009** | Georgia Institute of Technology Chemistry REU Summer Program Aquatic Chemical Ecology |
| **Fall 2008- Spring 2009; Fall 2005-Spring 2007** | Georgia Institute of Technology Dean's List |

## Leadership Experience/Activities

**2012-2013**   **Vanderbilt University Chemistry Department Warren Lecture Search Committee**

**2012-2013**   **Vanderbilt University Chemistry Graduate Student Association**

- Founding member and analytical chemistry representative
- Liaison to the department of chemistry faculty and administration

**2011-Present**   **American Society for Mass Spectrometry Member**

**2009-2011**   **American Chemical Society Member**

**2008-2009**   **Connect with Tech Host**

- Hosted high school students interested in coming to Georgia Tech, showcasing
  campus, classes, and student life
- Student life Q&A panelist for potential students and parents

**2006-2009**   **Georgia Tech Interfraternity Council** (*Homecoming Events Committee, Fall 2006; Greek Week Events Committee, Spring 2007; Homecoming Events Committee Chair, Fall 2007; Greek Neighborhood Association Chair, Fall 2008-Spring 2009; Earth Day Planning Committee, Spring 2009*)

**2006-2009**   **Phi Sigma Pi National Honor Fraternity – Epsilon Theta Chapter** (*Charter Member, Fall 2006; Initiate Education Officer, Spring 2007-Spring 2008*)

**2005-2009**   **Sigma Nu Fraternity – Gamma Alpha Chapter** (*Campus Involvement Chair, 2006; Kitchen Administrator, Fall 2006-Fall 2007; Honor Council: Member, Spring 2006-Fall 2009; Chair, Fall 2007-Fall 2008; Lieutenant Commander/Vice President, Fall 2007-Fall 2008; Housing Manager, Fall 2008-Fall 2009*)

# David G. Rizzo

<u>**Instrumentation, Skills, and Software**</u>

- Tissue Sectioning and Handling
  - Thermo HM325 Microm Microtome
  - Leica CM 3050S, Leica CM 1900, and Thermo NX70 Cryotomes
  - Leica CM 3600 XP Cryomacrotome
  - Zeiss PALM MicroBeam Laser Capture Microdissection (LCM)
  - FFPE tissue deparaffination and antigen retrieval
  - Tissue washing
  - Histological staining
- MALDI Matrix Application Systems
  - HTX TM-Sprayer robotic sprayer
  - Labcyte Portrait 630 acoustic spotter
  - Home-built sublimation apparatus
  - Thin layer chromatography (TLC) hand sprayer apparatus

- MALDI TOF and TOF/TOF MS
  - Bruker autoflex, ultrafleXtreme, rapifleX MALDI Tissuetyper
- MALDI FTICR MS
  - Bruker SolariX 9.4T & 15T
- Quadrupole-ion mobility-oTOF MS
  - Waters Synapt G2 and G2-S*i*
- HPLC
  - Waters nanoAcquity
  - Waters 2690 HPLC
- Bruker flexControl, flexAnalysis/dataAnalysis, flexImaging, ClinProTools
- Waters MassLynx, Driftscope, HDImaging
- Thermo Xcalibur
- mMass Open Source Mass Spectrometry Tool
- Scaffold Proteomics Viewer Software
- Vulcan Analytical Protalyzer Proteomics Software
- OriginLab Data Analysis and Graphing Software
- ChemDraw
- Microsoft Office